DEFECT CHARACTERIZATION IN CAST STEEL
BALL MILL RING GEARS

by

ALLEN E. KENDRICK

A thesis submitted to the Faculty of Graduate Studies and Research in partial fulfillment of the requirements for the Degree of Master of Engineering.

Department of Mechanical Engineering
McGill University
Montreal, Quebec
Canada

January 1987

ABSTRACT

This thesis is an investigation of the internal casting defects of a ring gear used to drive the cast-iron shell of an ore crushing ball mill. Special attention is focussed on the production of a defect histogram in which the probability of occurrence is presented for the various defects discovered. The character of the casting defects is needed to calculate the stress concentration factor, K_t, as required in a predictive fatigue crack initiation reliability analysis. Furthermore, the principles of the sand casting method are reviewed followed by a description of radiographic and ultrasonic nondestructive inspection techniques.

The experimental procedure used to characterize the casting flaws incorporates an exhaustive mechanical sectioning technique, a two-directional radiographic inspection, and a three-directional ultrasonic inspection of 25 sample blocks cut from a cast ring gear segment. Furthermore, a microscopic inspection of a number of fractured specimens is carried out using a scanning electron microscope. Finally, a chemical analysis is performed at six locations in the gear to determine the variation of the composition of the alloying elements.

In brief, a defect histogram is developed detailing the probability of occurrence of 8 macroscopic and 6 microscopic flaw types discovered in the investigation. Moreover, the results of the nondestructive inspection techniques are compared. Finally, the defect orientation is discussed.

RÉSUMÉ

Le présent travail porte sur l'évaluation des défauts de coulée d'un engrenage entraînant un broyeur de minerai de fer. Une attention particulière est apportée à l'élaboration de l'histogramme des défauts présénts. La caractérisation des défauts est nécessaire afin d'évaluer le facteur de concentration des contraintes à appliquer dans une analyse de fiabilité, portant sur l'initiation des fissures de fatigue. Les methodes de coulage de l'acier seront aussi préséntées, suivies d'une description de techniques de contrôle non desructif, particulièrement les techniques radiographique et par ultra-son.

Le programme expérimental a porté sur la caractérisation des défauts de 25 échantillons cubiques prélevés de l'engrenage. Les défauts ont été détectés et evalués par sectionnement mécanique, par l'inspection radiographique selon deux directions et par l'inpection utrasonique suivant trois directions. Certains échantillons ont ensuite été étudiés en microscopie electronique à balayage. De plus, une analyse chimique en six endroits différents de l'engrenage a permis d'etabler la variation des éléments d'alliage.

A partir de cette analyse expérimentale, l'histogramme des défauts est tracé, mettant en évidence huit types de défauts macroscopiques et six types de défauts microscopiques. Les resultats des différentes techniques de contrôle sont comparés et l'orientation des défauts est discutée.

ACKNOWLEDGEMENTS

TABLE OF CONTENTS

LIST OF FIGURES

LIST OF TABLES

CHAPTER 1

INTRODUCTION

1.1 MOTIVATION

1.1.1 The Development of Low Cycle Fatigue

In the past, the conventional design of engineering components was based upon selecting a member of suitable cross sectional area to ensure that the stresses in the member were kept below the yield strength of the particular material by means of an arbitrary safety factor. Unfortunately, this failure criteria, based upon the material's yield strength, proved to be inadequate in a number of cases. The failure of the Boston molasses tank in 1919 [1] is one of many structural failures that have occurred where this failure criteria was implemented.

In 1948, G.R. Irwin provided a number of conceptual advances [2] and, as a result, formed the foundation of linear elastic fracture mechanics (LEFM). LEFM is a process in which the stress field magnitude and distribution in the neighborhood of a crack (or other defect) is related to the applied nominal stress, to the size, shape, and orientation of the crack (or other defect), and to the material properties.

At the same time, numerous researchers were investigating the phenomenon whereby engineering components would fail under the action of fluctuating stress. Careful investigation would reveal that the maximum stress amplitude of the fluctuating stress would be lower than the ultimate strength and even lower than the yield strength of the failed material. This phenomenon, known as fatigue, has long been recognized as an important cause in failures of engineering structures. As a

result of the ship failures during the 1940's and 1950's, and of the fatigue initiated failures of the pressure cabin of Comet I jetliners in the 1950's [3], the existence of cracks or sharply contoured defects and the initiation of cracks early in a structural component's life was recognized.

Through the work of Coffin, Topper, Wetzel, and Morrow, among others, a different model was developed in which the initiation of a fatigue crack in a defect-containing member could be represented by the rupture of a filament of material as shown in Fig. 1.1. The smooth specimen, assumed to have a mechanical response similar to the filament of material, can be used to reproduce the stress-strain history of the filament as long as appropriate control of the smooth specimen is maintained. As a result, the fatigue life of the filament and the smooth specimen are considered to be the same for identical stress-strain histories. In brief, this local strain approach model coupled with fracture mechanics and a computer based damage analysis provides the basis of a predictive fatigue crack initiation reliability study.

1.1.2 The Motivation for Defect Characterization

The recent increase of manufacturing requirements, as specified by the purchaser, has forced the manufacturers of large cast steel engineering components to provide reliability studies prior to the sale of any such components. In particular, Provan et al. [4] have proposed a fatigue crack initiation reliability procedure whereby the reliability against crack growth initiation is found for a cast steel ring gear used to drive the cast iron shell of an iron ore crushing ball mill. The analysis is based on the following items:

i) the ring gear's geometry,

ii) the nature of operation of the gear,

iii) a stress and strain analysis of the gear under operating conditions,

iv) a statistical evaluation or characterization of the inherent casting flaws in terms of their shape, size, location, and orientation in the stress field, and

v) a statistical evaluation of the gear material's notch sensitivity, cyclic stress-strain properties, and its low cycle fatigue properties.

The interaction between the five preceding items in the process of determining the fatigue crack initiation life is presented in the fatigue crack initiation life diagram of Fig. 1.2. In brief, present-day computing strength allows the development and utilization of a computer algorithm whose final output will be the probabilistic life expectancy of a particular ring gear.

As can be seen from box 2 of Fig. 1.2, determining the stress concentration factor, K_t, is a required step in the life evaluation process. Accordingly, it is essential to know the character, in terms of the size, shape and orientation, of the defects responsible for the stress concentrations. Since heavy cast components undergo no further forming processes after casting such as forging or rolling (operations which tend to close up any defects), the defects occurring in the casting process must be carefully evaluated. Depending on the size and shape of the defect and its location and orientation in the stress field, fatigue cracks can be initiated and propagate through the component until reaching a critical size at which time catastrophic

3

failure occurs. Consequently, to guard against fatigue failure and provide probabilistic life expectancies of cast steel ball mill ring gears through a low cycle fatigue analysis, a thorough understanding of the inherent casting defects is necessary.

1.2 PREVIOUS RESEARCH

In the past, the American Society for Testing and Materials (ASTM) has developed reference standards to categorize the defect indications obtained from liquid penetrant, magnetic particle, radiographic and ultrasonic nondestructive tests. The ASTM Standard Reference Radiographs for Heavy-Walled Steel Castings [5] provides reference radiographs for casting defects which include gas porosity, sand and slag inclusions, shrinkage, cracks, and hot tears. Furthermore, each type of defect is arbitrarily classified into 5 severity levels. The ASTM also provides recommended standards for categorizing ultrasonic indications. In brief, these reference standards are used only to classify defect indications; the quality levels of the standards cannot be used for an acceptance-rejection criteria. Instead, acceptance-rejection criteria for individual castings must be based on a realistic appraisal of service requirements and the normal casting quality [6].

There has been research conducted to determine acceptable levels of casting defects present in particular cast components. For example, in 1970 R.E. Clark of the Westinghouse Electric Corporation conducted an in-depth fracture mechanics study to determine what type and size of defects could be tolerated in various regions of steam turbine castings [7]. In this particular study, it was discovered that many of the previously removed and weld repaired defects could be left in the

4

casting with no adverse decrease in structural integrity.

Unfortunately, the quality of a cast steel engineering component is dependent on numerous factors involved in the casting process. For instance, metal pour temperature, casting cooling rate, and the presence of chill blocks are only 3 of the variables controlled in the casting process; however, varying any one of these can significantly alter the presence of casting defects known as cold shuts. The variables involved in the casting process generally vary from foundry to foundry and from component to component. Consequently, any defect characterization performed on a component cast under dissimilar conditions as the ball mill ring gear of this investigation would have little significance to this particular investigation. Although there exist defect characterizations for other components and processes, their results cannot be directly applied to the cast ball mill ring gears of this investigation.

1.3 THESIS OBJECTIVES

The primary objective of this investigation is to characterize the defects, in terms of their size, shape, location and orientation, of a cast steel ball mill ring gear. Special attention is focused on the production of a defect histogram in which each class of defect discovered is presented along with its probability of occurrence.

The sand casting process used to produce the cast steel ring gears is explained to provide an insight into the causes of typical casting defects. Furthermore, nondestructive testing techniques such as ultrasonic and radiographic inspection, utilized in this investigation, are examined to provide an understanding of their underlying concepts

5

and inherent limitations.

1.4 **THESIS DESCRIPTION**

This thesis begins with a chapter reviewing the method of sand casting; included in this chapter is a summary of the various types of casting defects and their causes.

Next, the nondestructive testing techniques of radiographic and ultrasonic inspection are summarized in Chapter 3.

Chapter 4 provides the experimental processes followed in this investigation. The sectioning operation used on the ring gear segment from which sample blocks were obtained is presented. This is followed by a summary of the machining operations used to prepare the sample blocks for further testing. Finally, the radiographic and ultrasonic tests are described along with the chemical analysis and the method of the microscopic examination.

The results of the experimental investigation are presented and analyzed in Chapter 5.

The final chapter presents the conclusions and proposals for further research.

To lighten the text, detailed test procedures and test results are provided in the appendices.

CHAPTER 2

A REVIEW OF SAND CASTING

There are various casting methods employed in present-day manufacturing processes. However, most large cast components weighing half a ton or more, including the cast steel ball mill ring gears of this investigation, are produced using the sand casting method. As a result, only sand casting and its various aspects will be discussed in this chapter.

2.1 SAND CASTING

The method of sand casting is one of the oldest and widespread manufacturing processes employed in engineering design. In 1970, according to Bownes [8], sand casting was utilized in almost 90% of total annual foundry production. Sand casting can be defined as the production of a desired shape by the introduction of a molten metal into a previously prepared sand mold where it then solidifies. Casting is an important production process because of its ability to make intricate shapes of almost unlimited size. Furthermore, a proper casting procedure enables the placement of metal where needed to best resist the working stress with virtually no directional properties [9].

2.2 THE PROCESS OF SAND CASTING

The general sand casting process, starting with the fabrication of a casting pattern and ending with the casting shake out and upgrading, is detailed in this section. However, no attempt is made to focus on a particular process; as with most manufacturing methods, the particular

7

production details of a sand-cast component vary from foundry to foundry.

2.2.1 The Casting Pattern

The first stage in sand casting is the production of the casting pattern about which the sand mold is formed. The pattern quality is an important factor in the casting process since a casting cannot be more accurate than the pattern equipment from which the mold is formed. The pattern can be constructed of materials such as expanded polystyrene, plaster, hardwood, softwood, aluminum, and cast iron. The selection of the construction material depends mainly on the pattern life desired.

The casting pattern is not an exact full-scale model of the cast component since allowances for shrinkage, draft and machine finish are incorporated into the pattern design. Shrinkage allowance is the correction on the pattern which is made to compensate for the contraction of the casting as it cools in the mold from the metal freezing temperature to room temperature. The pattern is constructed larger than the actual cast component by an amount determined by the shrinkage allowance which varies with the type of steel used and the casting design. The shrinkage allowance also depends on the sand mold since the compacted sand in the mold offers considerable resistance to compression. Depending on the sand's content and quality, compressive stresses up to 44 MPa can be resisted before crumbling occurs [10]. The draft allowance is the taper that is incorporated on all vertical faces of a pattern to permit its removal from the sand mold without tearing the mold walls. Finally, a sufficient amount of excess metal is provided on all surfaces requiring further machining. The actual amount

8

depends on the metal hardness, the shape and condition of the surface to be machined, the casting size, and the tendency to warp during cooling.

2.2.2 The Casting Mold

In the process of sand casting, the casting mold is formed of a sand base refractory material. Using the pattern, the mold is shaped into the desired form so that the liquid metal introduced into it will, after solidification, retain the shape of the mold. There are a number of demands on the casting mold. First, it must be strong enough to sustain the weight of the casting metal and constructed in a manner to permit any gases formed within it to escape into the surrounding environment. Furthermore, the mold must resist the erosive action and the high temperature of the rapidly moving molten metal. Finally, the mold material must be collapsible to permit the steel to contract freely; the material must also cleanly strip away from the casting after cooling.

The most economical material that satisfies these demands is a bonded granulated refractory called silica sand. Silica is the only mineral naturally occurring in the required size range in sufficient world wide abundance. However, other minerals, oxides or silicates such as zircon, olivine, chromite, and sillimanite can be used as the base material in place of silica; but these must usually be crushed, sieved, and even prefired before use. The high expansion inherent in silica-based molds can be counteracted by smaller particle size and distribution of the silica base, and by special additives which increase the hot plasticity of the mold face and prevent it from cracking [11].

The binder is the molding material component used to produce

cohesion between the sand grains in the green or dried state. Substances such as clays, organic oils, organic resins and silicates possess bonding qualities and may be used singly or in combination to produce the required bonding properties. The binder is normally either in a liquid form or as particles with a size much smaller than that of the sand base grains. Ideally, the binder forms a uniform, thin film around each grain. In general, the compressive strength of molding sand increases with increasing binder content until a point is reached, depending on the sand and binder type and moisture content, where the strength will remain constant.

Generally, a mold is produced by placing the required pattern in a metal box, filling the metal box with molding sand, compacting the molding sand, and then removing the pattern leaving the finished mold. In the case of large castings, individual parts of the mold are fabricated separately and then assembled together in a large pit to produce the finished mold. Dry sand is usually used in large castings since a dry sand mold has high strength properties and can withstand the metal weight and pouring erosion inherent in large castings.

2.2.3 Melting and Casting

The melting procedure is used to achieve close control of metal composition and to decrease gas contamination and non-metallic inclusions. The melting process is initiated by introducing a metal charge into a melting furnace. There are basically three types of melting furnaces including the open-hearth, the electric arc, and the electric induction furnace. With the open hearth furnace, the charge is melted by exposure to the action of a flame. The electric arc furnace

consists of three graphite electrodes through which three phase current is passed. Melting of the metal is accomplished by the heat developed from arcing between the electrodes, or the electrodes and the metallic charge which serves as the common conductor between the electrodes. The electric induction furnace is composed of a crucible, encircled by a water cooled copper induction coil, in which the charge is melted by means of a high-frequency or a low-frequency electromagnetic field.

As the furnace melts the charge, the surface of the charge may react with the surrounding atmosphere. The time required to melt steel alloys is usually sufficiently long for compositional changes to occur. Once the furnace charge is melted, fluxing and slagging operations are performed to remove impurities and metallic and non-metallic elements dissolved in the metal or floating at the liquid metal surface. If any compositional adjustments are required, the alloy additions are made towards the end of the process to avoid losses in these elements. Furthermore, procedures such as degassing and grain refinement are carried out just prior to pouring, otherwise their useful effect may be lost.

After sufficient energy has been supplied to raise the charge to its melting temperature, overcome the latent heat of fusion, and further increase the temperature of the now liquid charge to its tapping temperature, the charge is removed from the furnace and poured into the casting mold. The tapping temperature at which the charge is removed from the furnace depends on the temperature at which the molten material is to be poured and the amount of cooling the molten material undergoes as it is moved in the ladle to the pouring site. The pouring temperature depends on the design of the casting and the desired

metallographic structure of the casting.

During the ·pouring process, the flow of metal must be smooth and uninterrupted to prevent the formation of cold shuts and to prevent slag from entering the mold. If the lip pouring technique is used, the slag cover must be skimmed off prior to pouring. The flow rate of the pour is governed by both the need to minimize turbulence and mold erosion and to complete the pour before appreciable cooling has occurred.

2.2.4 Finishing Operations

The finishing operations are carried out once the casting metal has cooled sufficiently so that it can be removed from the mold. After the casting has been removed from the mold, the residual sand is manually removed. Following this, the casting is subjected to a stronger shotblasting, hydraulic, or chemical cleaning process. Shotblasting is accomplished by high velocity streams of abrasive particles energized by compressed air and directed onto the casting surface. The process of hydraulic cleaning uses high pressure water jets, incorporating sand as an abrasive, that are directed onto the casting's surface. Although it is a seldom used method for large castings, chemical cleaning involves baths of molten caustic soda used to break down the surface oxide layer and loosen the adhering sand. Next, the gating and risering systems are cut from the casting through either sawing, abrasive wheel cut off, or flame cutting techniques.

The casting is then subjected to a heat treatment process depending on the desired properties of the finished component. Following this, the quality of the casting is investigated using one or more of the following non-destructive testing techniques: liquid penetrant

inspection, magnetic particle inspection, radiographic inspection, and ultrasonic inspection. If any severe casting defects are discovered the casting is usually subjected to an upgrading process where the defects are gouged out and filled using a submerged arc welding technique. In addition, destructive tests are performed on test samples cut from the casting to verify its chemical composition and microstructure.

2.3 THE STRUCTURE OF CASTINGS

2.3.1 The Solidification Process

Solidification is a relatively fast process as compared to the other steps required to produce a sand casting; however, solidification does not take place suddenly throughout a casting. Instead, the cooling of a cast component from its initial temperature to the final ambient temperature of the surrounding environment is a sequential, highly ordered process. The thinnest sections of a casting solidify first since they experience the highest cooling rate as a result of the high heat transfer to the cooler, surrounding mold. As the thin sections solidify, they contract and draw liquid metal from adjacent heavier sections that have not yet solidified. As heat energy is constantly lost to the mold and surrounding environment, these heavier sections solidify and draw liquid metal from other adjacent parts of the casting. This solidification and contraction process progresses throughout the casting with the heavier sections feeding molten material to the lighter sections; finally, the last sections to solidify draw liquid metal from the risers. This process in which the casting cools progressively from the extremities to the risers is known as directional solidification. Directional solidification is essential to avoid any shrinkage defects

13

occurring in the solidification process.

2.3.2 Crystallization

The actual process of solidification in which crystallization transforms the liquid metal alloy into a solid structure is quite complex and involves various aspects of physical chemistry, thermodynamics, and crystallography. An in-depth investigation of this subject is beyond the aim of this investigation. However, the microstructure of a cast component is heavily dependent on the crystallization process. Consequently, the basic mechanism of crystallization of cast alloys is presented in this section.

The crystallization of liquid metals follows the pattern of crystallization of most other liquids in which the liquid phase of a substance changes into the solid phase as it cools. The cooling liquid metal loses some of its energy in the form of heat to the surrounding mold and, in doing so, becomes structurally unstable in relation to the solid state. When the temperature is lowered, the average distance between the atoms of the liquid decreases. The attractive forces between neighboring atoms become more prominent as the thermal energy which maintains the vibration of the atoms and keeps them apart is lost to the surrounding environment. With further cooling, the attractive forces between the atoms prevent the atoms from moving away from one another and causes crystallization to occur.

2.3.2.1 Nucleation

The formation of the crystal lattice from the liquid state involves the successive stages of nucleation and growth. Nucleation is the

14

appearance of centers-upon which more atoms can be deposited for the growth of solid crystals at random points in the liquid. These nuclei can be produced by homogeneous nucleation or by hetrogeneous nucleation. Homogeneous nucleation is the formation of ordered groups of atoms forming areas of higher than average density during their random movement within the liquid. These embryonic crystals are unstable and shortlived; however, some reach a critical size at which they become stable and grow. General nucleation theory can predict this critical size in terms of the change in free energy resulting from the formation of a particle.

Hetrogeneous nucleation is the process in which initial growth is provided by a foreign particle included or formed in the melt. In foundry practice, hetrogeneous nucleation usually dominates the nucleation process since some foreign nuclei are always present in the form of impurities originating in the metal, the walls of the mold, or the atmosphere. Once the initial nuclei are formed, more solid may be deposited on the initial nuclei or fresh nucleation of the same or different phase may occur in the liquid.

2.3.2.2 The Liquid-Solid Interface

The growth phase of crystallization is instrumental in determining the final crystallographic structure of the solid. In the growth process, there exists an interface which separates the solid from the liquid component of the cast metal. At this liquid-solid interface, freezing occurs when the localized latent heat of crystallization, generated on the solid side of the interface, is insufficient to reverse the direction of heat flow from the liquid adjacent to the interface.

With reference to Fig. 2.1, the heat generated during crystallization maintains the temperature of the surrounding solid T_S equal to the temperature of the liquid T_L adjacent to the interface. Only when this heat is dissipated out through the solid and T_S drops below T_L can further solidification proceed. The typical temperature gradient at the liquid-solid interface is presented in Fig. 2.2. The heat flow from liquid to solid results from the positive temperature gradient across the interface. However, local evolution of the latent heat of crystallization is sometimes sufficient to produce a negative temperature gradient at the interface with the minimum liquid temperature occurring away from the interface. This leads to zones of undercooling as seen in Fig. 2.3.

In addition, undercooling can be caused from the dynamic conditions associated with casting solidification. With respect to the equilibrium phase diagram for the solid solution of Fig. 2.4, the binary alloy with a concentration of B equal to C_o first solidifies at temperature T_1. The first solid formed is a composition C_1 and is deficient in B with respect to the liquid. As crystallization proceeds under non-equilibrium conditions, solute is rejected at the liquid-solid interface. This causes a compositional gradient in the liquid shown in Fig. 2.5. The composition gradient in the liquid introduces a variation in the freezing temperature. This is because for each particular composition of B, there exists a single equilibrium freezing temperature below which crystallization occurs. These points lie on the liquidus line of Fig. 2.4. Thus, with the composition of B increasing in the liquid as the interface is approached there is a corresponding decrease in the equilibrium freezing temperature. The variation of the freezing

temperature due to solute transport, along with the resulting zone of under cooling, is presented in Fig. 2.6.

The conditions are more favorable for crystallization in the zones of undercooling as compared to the solid-liquid interface. The presence and extent of the undercooled zone, which depends on the interface temperature and compositional gradients, play important roles in determining the microstructure of a casting.

2.3.3 Crystal Growth and the Cast Structure

The cast structure is a function of the type of crystal growth which, in turn, depends on the conditions in the solidification interface and the constitution of the alloy. In this section four types of crystal growth are discussed including columnar growth, dendritic growth, independent nucleation, and eutectic freezing. The first three growth processes are characteristic of solid solutions where the metals of the alloy are completely soluble in each other. However, eutectic freezing occurs only in mechanical mixtures where the metal or alloy constituents are insoluble in each other.

2.3.3.1 Columnar Growth

Columnar growth can be found in pure metals and, under favorable conditions, in solid solutions. For columnar growth to be present in solid solutions, slow cooling must be present to allow more time for solute transport. This diminishes the concentration gradient and the corresponding undercooling in the liquid. Columnar growth is also favored by a steep interface temperature gradient. This ensures renewed growth at the interface occurs before undercooling brings about

17

nucleation at areas distant from the interface.

With reference to Fig. 2.7, columnar growth begins with nucleation at the mold wall. This is followed by multi-directional crystal growth at the wall. Growth in the lateral direction (parallel to the mold wall) proceeds until no space exists between the crystals. With lateral constraint present, crystal growth takes place by the edgewise extension of the now columnar crystals. The columnar grains are oriented with their largest dimension parallel to the direction of the heat flow.

2.3.3.2 Dendritic Growth

The type of crystal growth most commonly encountered in the solidification of commercial cast alloys is dendritic growth. Dendritic growth is favored when undercooling occurs in the band of liquid adjacent to the interface. Any existing protuberance on the solid face tends to act as a center for further growth. The general advance of the interface, as a whole, is retarded by localized latent heat; however, local growth centers proceed further into the undercooled zone. This preferred growth from an edge or corner of an existing embryonic crystal results in the formation known as a dendrite as seen in Fig. 2.8. The projection develops into a needle oriented parallel to the direction of heat flow. The growth of the dendrite in the direction perpendicular to the primary stem is restricted by the localized latent heat that inhibited general growth at the original interface [12]. However, secondary and tertiary branches can develop in the same manner as the primary needle. Solidification progresses through the thickening of the branches and primary stems of the dendritic skeleton.

In addition to growing unidirectionally from a major interface to

produce columnar grains, dendrites can also grow as independent crystals alone in the liquid. In this case, the fully developed grain is equiaxed.

2.3.3.3 Independent Nucleation

Independent nucleation occurs when the freezing of a liquid alloy occurs under a small temperature gradient or at a very rapid rate. If the conditions are right, the undercooling ahead of the solid-liquid interface is sufficient to cause nucleation at locations in the liquid ahead of the interface. The solidification structure associated with independent nucleation is equiaxed grains. These are often found in sand cast components as a result of the inherent low temperature gradients of the sand casting.

2.3.3.4 Eutectic Freezing

Casting alloys that are approximately eutectic or contain eutectic components exhibit eutectic freezing. In this mode of growth, each eutectic grain is formed by the growth of two or more separate phases in close association. The resulting structure may consist of alternate plates of the two phases or rod-like globular elements of a seemingly discontinuous phase suspended in a base matrix of the second phase. The growth of a plate eutectic starts with the nucleation of one of its phases. The concentration of the solute of this phase in the liquid increases until nucleation of the second phase starts at the liquid-solid interface. Then, the two solid phases grow simultaneously.

The growth of the eutectic grain proceeds by the simultaneous edgewise extension of the plates of the two phases. In the final

19

structure, each eutectic grain is the product of associated growth from a single center to a microscopically distinct unit [12]. The resulting grain can be equiaxed or columnar in form. As with solid solutions, columnar eutectic structures can be produced by controlled unidirectional freezing.

2.3.3.5 Cast Structure Variation

The grain structure of a cast component is rarely uniform throughout the volume of the casting. Temperature and constituent variations in the casting produce a multitude of grain types. For example, the solidification of a solid solution alloy casting begins with the formation of a thin chill layer adjacent to the mold wall. The chill layer, formed first because of the lower temperature of the mold wall, usually is a fine-grained structure caused by the large number of nuclei formed as a result of the rapid cooling. As the casting cools, dendrites start to grow from the inner boundary of the chill layer towards the highest temperature area of the casting. The resultant crystals are elongated and continue to grow towards the interior of the casting as the thermal gradient is diminished by the transfer of heat through the already solidified metal. Finally, with little thermal gradient remaining, other crystals nucleate at locations remote from the interface to form randomly orientated equiaxed grains. The result of this process can be seen in Fig. 2.9. Although not all cast steel components solidify in this manner, the process provides a unique example of cast structure variation.

2.4 THE GATING AND RISER SYSTEMS

2.4.1. The Gating System

The gating system is a system of channels through which the molten metal flows into the mold cavity. It is usually connected to the drag (bottom half of the mold) and is the principal means to control the metal flow pattern within the mold. The gating system is an important component of the casting mold since it governs the rate and direction of the metal flow to ensure complete filling of the mold before freezing. Also, the gating system is required to provide smooth and uniform flow with minimum turbulence to avoid air entrapment, metal oxidation, and mold erosion. The system must introduce molten metal into the mold cavity in a manner that will produce temperature gradients in the metal and mold surfaces such that solidification will occur in the direction of the risers. Furthermore, the gating system must have built-in traps to remove any non-metallic inclusions dislodged in the gating system or introduced with the metal.

The typical gating system consists of four main parts: the basin, the sprue, the runner, and the gates as shown in Fig. 2.10. The basin enables the pourer to maintain a full system and provide the required metal flow rate; moreover, the basin helps separate any remaining slag from the metal before it flows through the system. If metal is poured directly into the sprue hole, turbulence and vortexing develop leading to an unsound casting. The sprue carries the molten material from the basin down to the runners. It is usually tapered so that its cross sectional area decreases towards the runners to prevent aspiration occurring in the metal. The metal then flows through the runners which must not have any sudden changes in cross section or any sharp corners.

Once through the runners the metal enters the gates. The gates are the passages of various shape and dimension that determine the rate, type of flow, and position at which the metal enters the mold. A properly designed gating system ensures complete and uniform filling of the mold and provides the initial temperature gradients so that solidification occurs in the direction of the risers.

2.4.2 The Riser System

The primary function of the riser system is to feed molten metal to the casting as it solidifies to minimize any internal or external shrinkage which might occur in the casting. The casting mold is designed in such a manner so that the risers, attached directly to the metal casting, solidify last. As a result, solidification shrinkage of the casting is minimized since molten metal from the risers is able to flow into the casting to compensate for the contraction. The risering system also provides passages allowing any mold gases to escape and provides extra metallastatic pressure. This extra pressure forces the molten metal to reproduce the mold details more closely [11]. The risers are always formed into the cope (top side of the mold) so that any slag remaining in the casting can float up into the risers.

The effectiveness of a particular riser depends largely on its size. If the riser is too small, shrinkage cavities occurring in the riser extend into the casting. If the riser is too large, excess metal is melted per casting and the cost is increased. The size and shape of a particular riser must satisfy two requirements. First, it must freeze sufficiently slowly to ensure that liquid metal will be available throughout the solidification of the casting section the riser feeds.

This is required to maintain directional solidification from the casting into the riser. Second, the riser must be capable of supplying a sufficient amount of molten material required to compensate for the solidification shrinkage.

There are two basic types of risers: those that are open to the atmosphere (called open risers) and those that are not open to the atmosphere (called blind risers). The open riser is the simplest and most commonly used type. A valuable feature of the open riser is the function of providing mold venting during the pouring process. However, open risers are subject to heat loss to the surrounding atmosphere.

In contrast, the blind riser is totally enclosed in the mold. The blind riser is easy to position in a mold since it is not open to the atmosphere. Furthermore, the blind riser can be used to promote directional solidification in thin sections. The larger mass of metal material in the blind riser requires a longer time to solidify as compared to the thin section; consequently, solidification ends in the blind riser. A core that is open to the atmosphere can be inserted into a blind riser to relieve the vacuum developed from shrinkage and help push the metal from the riser into the shrinkage area of the casting.

2.5 CASTING DEFECTS - THEIR DESCRIPTION AND CAUSE

There are numerous types of defects inherent in the casting process; some types can seriously affect the structural integrity of the casting while others will only affect the esthetic value of the casting. In this section, typical casting imperfections with the potential of lowering structural integrity will be described. According to McGonnagle [13], casting imperfections can be broadly grouped as

follows: segregation, blowholes, inclusions, pipes, shrinkage, hot
tears, and cracks.

2.5.1 Segregation

Segregation is the non-uniform distribution of the chemical
elements in an alloy. Some regions of a casting may be rich in certain
elements while other regions are impoverished in these same elements.
Segregation occurs in the solidification process and leads to non-
uniform mechanical properties. Moreover, this defect type occurs in
ductile iron, in many nonferrous alloys, and in all metals in which the
composition desired of a particular element is close to, or exceeds, the
maximum solubility of that particular element. Hence, segregation is a
function of metal composition and cooling rate [14]. It can arise from
a large difference in metal sections or from a section of mold or core
that promotes heat retention. Also, the distribution of gates and
risers promoting heat retention in localized areas acts to provide a
cooling rate in some sections which would normally be found in much
heavier sections. Such a situation does not provide sufficient time for
the concentration of a particular chemical element to equalize
throughout the casting; consequently, segregation occurs. Other
factors that can affect the cooling rate causing segregation are
turbulent metal flow when pouring, incorrect use of exothermic molding
materials, and incorrect metal composition.

2.5.2 Blowholes

The class of defects known as blowholes (or gas porosity) are
gaseous cavities that can be spherical, flattened, or elongated in

24

shape. They are caused by localized gas pressure that exceeds the metal pressure as the metal in the casting mold cools. All of the gas that comes out of solution from the metal cannot escape through the vent holes and, as a result, remains entrapped in the casting. Blowholes can occur as a result of the following: insufficient core venting, inadequate metal pressure due to poor design, low feed pressure, turbulence in the gating system, and inadequate riser size. Furthermore, if the molding sand moisture content is high, if foreign material is in the sand, if the sand is poorly mixed, or if there are excessive gas producing materials in the sand coatings, then blowholes can result.

2.5.3 Inclusions

Inclusions are described as impurities either in solution with the metal or as separately held particles. In general, inclusions result from foreign material entering into the mold through carelessness. In addition, inclusions can arise from the breakdown of the sand coating whereby sand falls directly into the mold. This breakdown can be from poor design, careless mold assembly, or defective core-coating materials. Finally, inclusions can result from the pouring practice; a wet lip on a pouring ladle may chill the metal sufficiently to interfere with proper slag separation, careless skimming of the ladle prior to pouring allows the excess slag to enter into the mold, low pouring temperature or slow pouring lowers the effectiveness of the gating system slag trap, and dirty ladles can result in more slag than the gating system can remove from the metal.

25

2.5.4 Piping and Cold Shuts

The phenomenon known as piping is where a rupture or cavity occurs in the casting metal which solidifies last. The metal adjacent to the mold's walls solidifies first and as the liquid metal in the center of the mold begins to solidify, it tends to pull the already rigid outer shell. This leads to rupture and the resulting pipe. A cold shut, similar in appearance to a pipe, is a discontinuity resulting from imperfect fusion where two streams of metal have converged. Some causes of cold shuts are interrupted metal flow from faulty casting design, improper casting cooling, low fluidity of the molten metal, and poor pouring practice.

2.5.5 Shrinkage

Shrinkage defects can be described as a collection of jagged holes or a sponge like area lined with dendrite crystals [14]. Shrinks usually occur in heavier sections, at changes of section, and at internal hot spots. Since these locations are also prone to gas defects and hot tears, it is sometimes difficult to diagnose the presence of shrinkage. There are two broad categories of shrinkage termed as primary shrinkage and secondary shrinkage.

An example of primary shrinkage is the cavity resulting from inadequate feed metal available from the risering system. In this instance a shrinkage cavity occurs in the riser head and extends into the casting. This defect becomes visible on removal of the riser.

Secondary shrinkage is internal and occurs in areas remote from the risers or feeder heads. Depending on the conditions of the mold, casting metal, and pour, secondary shrinkage may be in the form of a

hollow cavity or a network of filaments [12].

Shrinkage can be attributed to changes in sections that are too abrupt, insufficient metal in a heavy section, insufficient quantity or size of risers, movement of the mold wall, and poor pouring conditions.

2.5.6 Hot Tears

Hot tears are casting defects characterized by partial or complete fracture following an irregular intergranular path. Hot tears form as a result of contraction of the metal cooling at high temperatures when it is in a relatively brittle condition due to liquid films [12]. The appearance of hot tears is often very similar to that of shrinkage cavities.

The causes of hot tears include the lack of adequate fillets in the mold, a rigid mold preventing a section of the casting to expand or contract in its normal fashion leading to high internal stresses, and poorly designed risering and gating systems preventing normal metal contraction. Poor collapsibility of the molding sand and the inadequate use of chills, used to induce initial solidification at the mold walls, also contribute to the formation of hot tears. Moreover, the metal composition and the melting, pouring, and cooling techniques of the casting process play important roles in the formation of hot tears.

2.5.7 Cracks

Cracks are the most detrimental casting defect in that they possess the smallest notch radius at the crack tip that radically increases stress in their vicinity. Cracks are formed in a casting when it has cooled below the temperature at which hot tears will occur but still

lies above the temperature for elastic behaviour and the cooling is
rapid enough that the ultimate stress of the metal is exceeded.

If very high stresses are developed in a cast component with-wide
section variations and poor ductility, fracture can occur with the
resulting crack being straight, clean, and of a catastrophic length.

As with the previous defects, the gating and risering systems, the
quality of the molding sand, the metal composition, and the melting and
pouring practice dictate crack formation in a cast component.

CHAPTER 3

RADIOGRAPHIC AND ULTRASONIC INSPECTION TECHNIQUES

3.1 RADIOGRAPHIC INSPECTION

3.1.1 Physical Principles

The nondestructive testing technique of radiography employs penetrating radiation in the form of either X-rays or gamma radiation to produce a radiograph. A radiograph is a two-dimensional picture of the intensity distribution of some form of penetrating radiation that has been projected from a source and has passed through a material test object. Any voids, thickness variations, or regions of different composition attenuate the penetrating radiation by different amounts, thus producing a shadow of themselves in the radiograph, as shown in Fig. 3.1.

3.1.1.1 Penetrating Radiation

Gamma rays and X-rays are electromagnetic radiation; their position in the electromagnetic spectrum is shown in Fig. 3.2. X-rays and gamma rays of the same wavelength are physically identical. Penetrating radiation, like all forms of electromagnetic radiation, transports energy in discrete packets called quanta or photons. The energy of such a photon is directly proportional to the frequency of the electromagnetic radiation and is given by $E = hf$ where E and f are the energy and frequency of the photon respectively, and h is Plank's constant.

X-rays are produced in two ways. The first method is to slowly accelerate a charged particle, usually an electron, to a very high

velocity and then rapidly decelerate it through collision with the atoms of a solid target material. When the electrons strike the target, a transfer of energy occurs and X-rays are produced. The second method is to remove one of the orbital electrons of an atom to produce an ion in an excited state. As the orbital electrons of the excited ions rearrange themselves, an energy transfer occurs and X-rays are emitted. These X-rays occur having particular wavelengths that are characteristic to the atomic number of the ion from which they are emitted; thus, they are called characteristic X-rays. Conversely, X-rays produced by the bombardment of high speed electrons with a solid material target are in a continuous spectrum having a multitude of wavelengths.

Three fundamental requirements must be met for X-ray production with the collision method: a source of electrons, a means of directing and accelerating the electrons, and a target for the electrons to hit. If certain substances are heated sufficiently, some of the substance's electrons will become extremely energized, escape from the material, and surround it in the form of a cloud. The electrons will return to the emitting material unless some external force pulls them away. Since like charges repel each other and unlike charges attract each other, a strong positive charge must be used to pull the electrons away from where they are generated. The location where the electrons are generated is called the cathode, while the positively charged target is called the anode.

An electric potential is connected between the cathode and anode, both of which are in a common vacuum, so that the anode is positively charged with respect to the cathode. The electron movement towards the anode must be in a vacuum so that energy loss due to collisions with gas

molecules is avoided.

The anode, or electron target, is a solid material with a high atomic number. The higher the atomic number, the higher is the efficiency of X-ray production. Unfortunately, only a small amount of the kinetic energy available in the electron beam is converted into X-ray radiation; the remaining energy is converted into heat and must be dissipated by the target material. Furthermore, the efficiency of X-ray production increases with increasing target atomic number and increasing cathode-anode voltage [15].

Gamma rays, on the other hand, are produced from certain radioactive isotopes such as Irridium 192 or Cobalt 60. Whereas X-rays produced by the bombardment method have various energy levels, isotopic gamma rays corresponding to a particular decay process have the same energy. The decay of some isotopes yields several types of gamma rays with different, sharply defined energies. The strength of the source, or isotope, decays exponentially with time; consequently, the source must be replenished periodically.

3.1.1.2 Penetrating Radiation and Matter

The penetration of an X-ray or gamma-ray photon into a material can result in one of three basic processes. First, an atom of the material may absorb the photon and, as a result, eject an orbital electron and change to an excited ion. The ejected electron expends its energy through collision with other atoms. Then the excited ion becomes neutralized and emits its own characteristic radiation. This process is known as the photoelectric effect [16]. Second, the penetrating photon may collide with an outer electron, lose part of its energy to this

31

electron, and continue in a new direction with reduced energy. The electron involved in the collision is ejected from the atom. This is known as Compton scattering. Finally, if the penetrating photon has sufficient energy, part of this energy may be converted into the mass of an electron and a positron upon collision with the atom. The remaining energy will be in the form of kinetic energy of the electron-positron pair. In brief, depending on the energy of the incident photons, all three of the previous processes may contribute to the attenuation of the penetrating radiation.

If a narrow, well-collimated beam of single-energy level X-ray or gamma ray photons is directed against a sheet of material, the intensity (the number of photons per unit area per second) will show an attenuation largely due to the three processes described above. The attenuation will follow the law: $I = I_0 e^{-ux}$ where I is the transmitted intensity, I_0 is the incident intensity, x is the thickness of the attenuator or sheet, and u is the linear attenuation coefficient. The value of u depends on the energy of the incident photons and the composition of the attenuator. The linear attenuation coefficient measures the probability per unit thickness that a photon in the primary beam is removed from that beam. The attenuator does not absorb all of the energy removed from the primary beam; some of this secondary radiation will escape from the attenuator and possibly interfere with the recording film.

The amount of attenuation depends on the material that the primary photon beam is being transmitted through. Any material flaws will attenuate the penetrating radiation differently from that of the material itself; therefore, the radiation transmitted through any flaw

32

will be of different intensity from that transmitted through the material. It is this difference in transmission of the penetrating radiation that indicates the presence of a flaw.

3.1.1.3 Presentation of Test Results

There are a number of methods to use in the presentation of non-destructive radiographic test results.

Film Radiography - In this method, an X-ray sensitive film is used to record the intensity of the X-rays after they have passed through the test specimen. This is the most widely used method and will be further discussed in Section 3.1.2.5.

Fluoroscopy - Fluoroscopy is where X-ray patterns are converted directly to visible light patterns by the use of fluorescent screens. The sensitivity of the results obtained with fluorescent screens is somewhat less than that of film radiography.

Television Radiography - With this method, closed-circuit television systems, sensitive to X-rays, are employed. This technique provides quick, inexpensive results compared to film radiography.

Xeroradiography - This technique is a combination of X-radiography and electrostatics. The X-ray image is recorded in the form of an electrostatic charge distribution on a special plate. The image is then transferred to paper in the same manner as a Xerox copy.

33

3.1.2 Radiographic Inspection Equipment

3.1.2.1 The Coolidge X-Ray Tube

X-rays were produced in gas filled tubes before 1912. This involved splitting the gas molecules into ions and electrons with an applied high voltage. The positive ions were attracted to the negative cathode; the electrons were accelerated towards the positive anode - the target. X-radiation was produced from the electron-target collisions. These gas filled tubes had two major drawbacks; (1) the electron supply, and thus the X-ray emission, was limited by the amount of gas in the tube, and (2), the gas tended to cause arc-over when high voltages were applied. As a result, X-rays of long wavelength were produced and had very little penetrating power.

Around 1912, Coolidge introduced a heated metallic filament, or incandescent, cathode. The new type of cathode greatly increased the number of electrons that could be accelerated towards the target. Furthermore, a gas was not needed; instead, the tube was evacuated. This led to the application of higher voltages and thus more penetrating X-rays. Fig. 3.3 shows a Coolidge type X-ray tube. Most modern X-ray tubes are refinements of the Coolidge tube and have more stable emission; a longer life, and more efficient shaping and focusing of the electron beam.

3.1.2.2 Accelerating Potentials and Electron Targets

The modern X-ray equipment uses a combination of tube rectifier and iron-core transformer to develop accelerating potentials up to 500 kV. High voltage generation (250 to 4000 kV) uses a resonant transformer with an air-core instead of an iron-core transformer. Furthermore,

electrostatic generators can be used for applied voltages between 500 to 6000 kV (6 MV) that provide a smaller source size and a more coherent X-ray spectrum than the transformer types. Above 6 MV, acceleration by means of an applied voltage is no longer efficient. Instead, magnetic induction systems (betatrons) must be used that accelerate the electrons by magnetic induction. Betatrons for industrial radiography operate in the 20 to 30 MV range and emit extremely short wavelength, highly penetrating X-rays.

An essential component in generating X-rays is the target that absorbs high velocity electrons and converts part of their kinetic energy into X-rays. Heat dissipation, shape of emitted beam, and radiation quality must be considered in target design. Modern targets are made of tungsten, gold or platinum, and are usually cooled using a circulating liquid or gas.

As shown in Fig. 3.4, the sharpness of the radiograph is dependent on the target or source size. The best sharpness is obtained when the radiation source is small, the source-specimen distance is great, and the specimen-film distance is small. Furthermore, as shown in Fig. 3.4, image distortion occurs when either the specimen and the film are not parallel or the radiation beam is not perpendicular to the film.

3.1.2.3 X-Ray Tubes and Linear Accelerators

Two X-ray producing machines commonly employed in radiographic inspection are the X-ray tube and the linear accelerator. Although other types of machines such as the electrostatic generator and the betatron are equally important, an X-ray tube and a linear accelerator are utilized in this investigation; consequently, they are briefly

described in this section.

A typical hot cathode, high vacuum industrial X-ray tube is shown in Fig. 3.5. As with the Coolidge X-ray tube, the heated filament (usually tungsten) emits electrons which are accelerated towards the tungsten target embedded in the copper anode as a result of the applied potential. The unwanted radiation is absorbed by lead shields while a plastic radiation window provides a path for the X-rays of the useful beam [17]. The tungsten target is liquid cooled for continuous operation.

The linear-accelerator X-ray unit is another common source of X-ray radiation. A schematic diagram of a typical linear-accelerator X-ray unit is presented in Fig. 3.6. Here, electrons are generated in the electron gun in the same manner as the X-ray tube. Once produced, the electrons move into the accelerator and are further accelerated to their output energy by the axial electrical field produced in the accelerator by the high frequency oscillator. At the output end of the accelerator, the accelerated electrons strike a transmission-type X-ray target and produce high energy X-rays [17].

3.1.2.4 Gamma Ray Equipment

Any gamma ray source undergoes a decay process in which gamma rays are emitted. The strength of a particular gamma ray source is measured by the number of nuclei which decay each second. A 1-curie source undergoes 3.7×10^{10} nuclei disintegrations per second. The sensitivity of gamma radiography depends mainly on the isotope used.

The equipment in which to store the gamma ray source must be radiation safe and provide a system for the remote handling of the

36

radioiostope source. Regardless of the source, a protection container must be used to protect personnel from gamma radiation when a radioisotope is not in use. The radioisotope is usually stored in the geometric centre of a heavy metal (lead or uranium) container.

There are a number of ways to move the radioisotope in and out of its protective container. They include manual pole handling, cable drive handling, and pneumatic drive handling. Some gamma ray equipment does not require the removal of the source from its container; instead, a section of the container is designed to swing away, permitting an unobstructed escape of radiation. Opening and closing of the container is accomplished from a shielded, safe position.

There are two basic types of gamma-ray beam configurations. The first is when the radiation beam is emitted spherically and is known as panoramic projection. It is used for making many simultaneous exposures. The second type of beam configuration is known as conical or directional projection and is when gamma rays escape through an opening in the container. This method is used with extremely active sources and when the radiography is carried out in a confined area. Also, this method reduces beam scatter and increases radiograph quality.

3.1.2.5 Radiographic Film

Most often, the method employed to record radiographic test results is that of a radiographic film which is basically a sheet of transparent, blue tinted, cellulose material that is coated on either one or both sides with a photosensitive emulsion. The approximately 0.024 mm thick emulsion consists of gelatin in which is dispersed very fine grains of silver bromide that become sensitized when exposed to

37

radiation. After being exposed to radiation, the film is developed in the usual manner. Once dry, the film is viewed in front of a strong light and the areas of the film exposed to heavily attenuated X-rays are relatively transparent, while those areas exposed to high strength X-rays are very dark and opaque.

There are 3 basic grades of film for industrial radiography: course grain, fine grain, and extra-fine grain. The fine and extra-fine grains give the highest contrast, but require long exposure times. On the other hand, the coarse grain film gives lower quality or contrast, but requires short exposure times.

3.1.3 Radiation Protection

Naturally occurring radioactive materials, X-ray machines, and artificially produced radioactive materials have found wide application in nondestructive testing. The usefulness of the many available radiation sources used in exposing subsurface flaws has brought about a tremendous increase in the number of persons possessing such materials or machines and an increase in the risk of personnel being exposed. The exposure to personnel can be classed as either internal or external exposure. External exposure may come from a radiant source, from contamination outside a source container, or from contamination on the skin or clothing of a person. Internal exposure may come from radioactive material collected inside the body through inhalation, ingestion or absorption through the skin.

Radiation incident on living tissue has been shown to result in the damage or destruction of living cells. However, the human body can

tolerate a certain amount of radiation without impairing its overall function, just as it can tolerate a certain amount of sunlight without serious effects. In Table 3.1, extracted from the Nondestructive Testing Handbook [17], the exposure of man to common sources of radiation has been estimated. The units of radiation measurement are the rem and the roentgen (r). The roentgen is a quantity of X or gamma radiation such that the associated emission per 0.001293 gram of air in air produces ions carrying either a +1 or -1 charge. The rem is a measure of the dose of any ionizing radiation to body tissue, in terms of its estimated biological effect relative to a dose of 1 r of X-rays.

The National Committee on Radiation Protection has recommended the basic permissible weekly doses of ionizing radiation as shown in Table 3.2. As a result, safe working conditions must be ensured by accurate appraisal of radiation exposure and contamination through the proper use of suitable instruments.

3.1.4 X-ray Interpretation: Defect Appearance in a Radiograph

In this section, indications of various casting flaws will be explained in terms of their appearance on a radiograph.

3.1.4.1 Segregation

Segregation of metal appears as light and dark blotches on the radiograph and results when one or more of the constituents of a certain alloy have clustered together.

3.1.4.2 Gas Porosity

Gas holes, due to the entrapment of gas by either pouring metal

39

turbulence, trapped gas thrown out of solution by the metal itself, or gas evolved from green sand molds, appear on the radiograph as dark, smoothly outlined areas.

3.1.4.3 Inclusions

Inclusions appear on radiographs as dark or light spots or areas. When inclusions are heavier or denser than the metal in which they occur, the inclusions appear lighter than the surrounding metal in the radiograph.

3.1.4.4 Cold Shuts

As previously discussed, a cold shut occurs when a stream of metal has practically set and then meets an opposing stream in a mold. The metals have cooled to such an extent that they do not fuse into each other; instead, they form a cold shut. Cold shuts appear on the radiograph as well-defined, intermittent or continuous, dark lines.

3.1.4.5 Shrink Porosity

Shrink porosity, caused by the cooling and contracting of a metal in its mold, appears radiographically as raggedly outlined structures.

3.1.4.6 Cracks

Cracks appear on radiographs as dark, intermittent or continuous, lines. There are numerous causes for cracks such as improper casting design, rough handling and thermal stresses resulting from the cooling process.

3.1.5 Limitations and Advantages

3.1.5.1 Limitations

Radiography has a number of inherent disadvantages. In particular, the cost of X-ray films in film radiography is relatively high in comparison to other methods. Radiographic inspection of material that is small can be carried out quite economically; however, inspection of large components is exceedingly expensive. The cost of complete radiographic inspection of critical metal parts can sometimes exceed the cost of the material.

Furthermore, since radiation travelling in straight lines from a source must intercept the film at nearly right angles, the efficient examination of complex geometries is prevented.

Since penetrating radiation has serious biological effects, methods must be employed to protect radiographic personnel. Ultimately, this leads to higher operating costs and high risk for the operators.

Moreover, small discontinuities will often be undetected because they do not present a sufficient density differentiation to affect the attenuation of the X-rays.

3.1.5.2 Advantages

Radiography does have its limitations; however, these are far outweighed by its advantages. The extensive use of radiography by industry from basic production inspections to in-service tests is proof of its performance.

The radiographic method is superior to other non-destructive testing methods since it provides a permanent visual representation of the interior of test objects.

Most types of casting defects such as gas porosity, shrink porosity, inclusions, cold shuts, segregation and cracks can easily be identified in a radiograph. Furthermore, large, thick castings can be inspected with high voltage radiographic equipment.

3.2 ULTRASONIC INSPECTION

3.2.1 Physical Principles

The non-destructive testing method known as ultrasonic inspection is based on the generation, propagation, reflection, and detection of ultrasound (sound waves having a frequency greater than 20 kHz). The underlying physical principle on which this method is based is the ability of sound waves (whether compressional or transverse) to propagate through a solid, elastic material. In compressional waves, the displaced particles of the transmission media vibrate back and forth along the direction of wave propagation. On the other hand, in transverse waves the displaced particles of the wave-conducting material vibrate in a direction perpendicular to the propagation direction. The particle vibration in either a compressional (longitudinal) or transverse (shear) sound wave is, if the displacements are small, simple harmonic motion. Thus, the particle displacement, d, is described as $d = D \sin [2\pi(\frac{x}{\lambda} - \frac{t}{T}) + \phi]$ where D is the wave amplitude, x is distance measured along a line in the direction of wave propagation, λ is the wavelength, t is the time of interest, T is the period of particle vibration, and ϕ is a phase angle determined by initial conditions. The wave propagation velocity is denoted as V and is equal to $V = \lambda /T$.

The wave front of a wave is the imaginary surface connecting all particles having the same phase (i.e., same $2\pi(\frac{x}{\lambda} - \frac{t}{T}) + \phi$). A regular

42

succession of these wave fronts is a sound wave. An important property of small amplitude sound waves is their superposability; the displacement of a particle due to two sound waves is the vectorial sum of the displacements corresponding to each of the individual waves.

3.2.1.1 Ultrasonic Wave Packets

In nondestructive testing using ultrasonics, short bursts of ultrasound are employed which propagate through the material being inspected as a wave packet. A typical burst is shown in Fig. 3.7. Such a wave packet is formed by superposing an infinite number of infinitely extended harmonic components, each with the proper relative phase and amplitude.

It can be shown [18] that as the breadth of a wave packet (Δx) becomes smaller, the range of wavelengths making it up becomes greater. Thus, an infinitely short, equal amplitude wave packet contains harmonic components of all wavelengths from zero to infinity. This property is important in determining the resolving power of an ultrasonic test system.

A short ultrasonic wave burst will not generally retain its initial shape as it propagates. The harmonic components, propagating at different speeds, tend to get out of step. Thus, the wave packet broadens and loses its sharp trailing and leading edges as the precise phase relation is altered. This is known as dispersion.

3.2.1.2 Reflection, Refraction and Mode Conversion

When an ultrasonic wave or wave burst propagating in a medium encounters an interface with another medium, reflection, refraction, and

43

mode conversion may occur. The simple case of normal incidence is shown in Fig. 3.8. The phenomenon known as reflection occurs when a wave encounters an interface between two surfaces; part of the wave passes directly through the interface while part is reflected back. The wave amplitude ratios can be shown to be:

$$\frac{A_1}{A_0} = \frac{\rho_2 V_2 - \rho_1 V_1}{\rho_1 V_1 + \rho_2 V_2} \quad \text{and} \quad \frac{A_2}{A_0} = \frac{2 \rho_1 V_1}{\rho_1 V_1 + \rho_2 V_2} \quad , \quad (3.1)$$

where ρ is the respective material density and V is the ultrasound wave velocity of the material. The product, ρV, is called impedance. When the impedance ratio, $r = \frac{\rho_2 V_2}{\rho_1 V_1}$, is unity, no reflection occurs; however, when $r \gg 1$ reflection is nearly total.

As seen in Fig. 3.9, when a plane harmonic wave is incident on a plane interface at an angle of incidence other than zero, mode conversion occurs. Mode conversion is where part of a wave undergoes a conversion from a longitudinal type to a transverse wave or vice versa; the remainder of the wave passes through the interface in the same mode. This is true for both longitudinal and transverse waves with both reflection and transmission occurring. It can be shown that the reflection and refraction angles follow a generalized form of Snell's Law where:

$$\frac{\sin \theta_L^1}{V_L^1} = \frac{\sin \theta_L}{V_L^1} = \frac{\sin \theta_t}{V_t^1} = \frac{\sin \phi_L}{V_L^2} = \frac{\sin \phi_t}{V_t^2} \quad . \quad (3.2)$$

The velocity superscripts denote the relevant medium, the subscripts indicate either longitudinal (L) or transverse (t) waves. If the incident wave is transverse instead of longitudinal then θ_t^i and V_t^i must

44

be substituted for $\theta_L^!$ and $v_L^!$.

The phenomenon of mode conversion can be used to convert longitudinal waves into transverse waves for a specific ultrasonic inspection technique. The refracted longitudinal wave may be eliminated from the second medium by adjusting $\theta_L^!$ so that $\emptyset_L$ just exceeds 90^0. This value of $\theta_L^!$ is called the first critical angle of incidence and can be shown to be: $\theta_L^! \text{ FIRST} = \sin^{-1}\left[\dfrac{v_L^!}{v_L^2}\right]$. This is illustrated in Fig. 3.10.

If $\theta_L^!$ is further increased so that the angle of refraction of the transmitted shear wave ($\emptyset_t$) is 90^0, no energy enters medium 2. The resulting wave mode is partially longitudinal, partially transverse, and propagates along the interface of the two materials. These waves are called Rayleigh waves and are utilized in the ultrasonic inspection of surface defects.

Mode conversion generally occurs whenever an ultrasonic wave encounters a discontinuity in elastic properties. Mode conversion results in an energy loss from the mode of interest and is a source of false waves in the material being tested.

Furthermore, the loss of energy, or attenuation, of an ultrasonic wave travelling through a material is attributed to three other mechanisms: heat conduction, viscous friction, and elastic hysteresis [16]. The difficulty in matching experimental attentuation results with theoretical predictions suggests that there are other mechanisms which absorb energy from the sound wave.

3.2.1.3 Ultrasonic Beam Profile

As with all forms of wave motion, ultrasound waves are subject to

diffraction. Diffraction occurs when a wave encounters a discontinuity with an edge; and then it bends around that edge. Using the principles of diffraction, it can be shown [16] that for a circular transducer to produce a well-collimated beam, free from side lobes, its diameter must be large in comparison to the resulting wavelength it produces in the medium to which it, is attached.

Ultrasonic beam profiles can be altered by the use of acoustic lenses, usually attached to the transducer. The lens' material must have the same acoustic impedance as the transducer and the material to which it is coupled; however, the velocity of sound in the lens must be quite different from that of the metal medium. The focusing of an ultrasonic pulse increases its sensitivity at the focal point. However, the beam diverges after the focal point and thus becomes less sensitive to defects as seen in Fig. 3.11.

3.2.1.4 Reflection and Transmission

In brief, ultrasonic inspection utilizes the principles of ultrasonic wave generation, propagation, reflection, mode conversion, attenuation, diffraction, and detection. There are two basic methods by which it is performed. Either the energy transmitted through the inspection material or the energy reflected from areas within the material is monitored to indicate flaws. The ultrasonic beam travels with little loss through homogeneous material except when it is intercepted and reflected by discontinuities in the elastic medium. Either the decrease in transmitted energy or the reflected energy is detected at the receiver indicating the previously undetected flaw.

46

3.2.2 Ultrasonic Inspection Equipment

There are a number of variations of the basic ultrasonic test that are in use today for surface and subsurface flaw detection. Accordingly, there are numerous types of equipment set ups. However, the essential components of any ultrasonic test are described below.

a) Pulsed Oscillator - This electronic unit generates a burst of alternating voltage that can be varied in terms of its frequency, duration, envelope profile, and burst repetition rate. This voltage burst is applied to the sending transducer.

b) Sending Transducer - This serves to launch the ultrasonic waves into the elastic medium to which it is coupled by vibrating in compliance to the applied voltage from the pulsed oscillator.

c) Receiving Transducer - This unit converts ultrasonic waves that it encounters into a corresponding alternating voltage. Depending on the type of test, the sending and receiving transducers can be separate units or combined as one.

d) Receiver - The receiver amplifies the signal received from the receiving transducer.

e) Display Oscilloscope - This is used to observe the reflected or transmitted ultrasound passed through the test specimen.

f) Electronic Clock - The electronic clock or timer is a source of

logic pulses and reference voltage wave forms required by the pulsed oscillator and the sweep generators in the oscilloscope.

Specific test systems have additional features such as electronic compensators that compensate for signal loss caused by attenuation and electronic gates which monitor the return signal for pulses of selected amplitude occurring in a selected time delay range. The electronic gates are used when looking for a specific type of flaw at some prescribed depth.

3.2.3 Common Test Methods

Basically, there are two test methods commonly employed in casting inspection. They are the ultrasonic immersion test and the ultrasonic contact test. Furthermore, depending on the component shape, either the reflection or transmission method can be used.

3.2.3.1 Transmission Technique

This was the first technique used for ultrasonic inspection. In this method, ultrasound is generated from a sending transducer and sent through the test specimen. As the ultrasound passes through the flaws in the specimen, the amount of transmitted energy is reduced. A second transducer receives the ultrasound as it passes out of the specimen as shown in Fig. 3.12 (a). Pulsed ultrasonic beams are used to avoid setting up standing waves in a specimen since any standing waves severely influence the transmitted energy [16]. This method is generally used for inspecting thin specimens. Krautkramer [19] has used this technique to test specimens down to a thickness of 0.25 cm.

48

3.2.3.2 Reflection Technique

Also known as the pulse echo technique, the reflection technique is based on the phenomenon of reflection that occurs when ultrasound encounters an interface between two materials. In this method, ultrasound is generated from a sending transducer and passed through the specimen. As the ultrasound encounters flaws or defects, a part of it is reflected. The receiving transducer records these reflections as flaw indications. The reflection technique is generally preferred over the transmission technique and is more widely used. However, it cannot be used to inspect thin specimens. Fig. 3.12 (b) shows the reflection technique.

3.2.3.3 Contact Techniques

The process of moving the transducer over or along the test specimen is called scanning. The two common methods of scanning are the immersion and contact tests.

The ultrasonic immersion test utilizes high frequency mechanical vibrations to probe test objects. These vibrations or ultrasound are coupled to the test specimen by immersing the sending transducer in water or other suitable liquid. The liquid in which the transducer is immersed is called the couplant. According to the Nondestructive Testing Handbook [17], immersion testing can give castings of irregular shape a practically complete inspection, including fillet areas. Furthermore, since the transducer does not contact the surface of the specimen being inspected, pre-test surface machining is not required. Both reflection and transmission techniques can be used in ultrasonic

49

immersion tests.

In the ultrasonic contact method, the sending transducer vibrates in response to an input signal, sending out mechanical vibrations through a coupling medium and into the test specimen. The couplant may be almost any liquid providing that it wets the surface and stays between the transducer and the test material. Couplants must be used so that an intimate material-transducer coupling is achieved in the uneven spaces between them. Both the transmission and reflection techniques are used in this method. The through-transmission technique uses separate transducers for the transmitter and receiver while the reflection technique uses either one transducer as both transmitter and receiver or separate transducers for each function. According to the Nondestructive Testing Handbook [17], this technique can be used to penetrate medium-carbon steel castings up to 3 m with 1 to 5 MHz ultrasound. The contact method is shown in Fig. 3.12, where the transducers are applied directly to the test specimen's surface.

3.2.4 Presentation of Test Results

There are three basic methods of presenting transmission and reflection test oscilloscope results: the A-scan, the B-scan and the C-scan mode.

3.2.4.1 A-Scan Mode

The A-scan mode set up is shown in Fig. 3.13 and provides an oscilloscope display of the envelope of the initial voltage pulse applied to the transmitting transducer, the envelope of the voltage pulses generated by the receiving transducer as reflections are

received, and a timing trace. The vertical axis of the oscilloscope is the pulse amplitude scale while the horizontal axis is a measure of time. Usually, the oscilloscope is adjusted so that the reflected pulse from the surface appears at the left of the trace while the back surface reflection occurs at the right of the trace. The location of pulses resulting from flaw reflections with respect to the two surfaces enables the location or depth of the flaw to be gauged. The amplitude of a flaw-reflected pulse cannot be simply related to the size or severity of the defect; only when the nature of the flaw is known is this possible.

The result of a reflection type test using A-scan mode oscilloscope presentation is shown in Fig. 3.14. Illustrated are: the reflected ultrasound from the top surface (i.e. the surface the transmitter transducer is on), the reflection of a discontinuity within the material, and the reflection from the back surface. The small fourth pulse is a false reading due to interference. The fifth and final pulse is a repetition of the first signal.

3.2.4.2 B-Scan Mode

The basic B-scan schematic is shown in Fig. 3.15. The vertical axis of the oscilloscope is made proportional to time. The horizontal axis is set up so that it represents the linear scanning motion of the transducer. The intensity of the oscilloscope trace is modulated in proportion to the amplitude of the reflected signal. The resulting image represents a one-dimensional slice through the specimen with the specimen discontinuities appearing as corresponding discontinuities in the oscilloscope pattern. In practice, the B-scan has its deficiencies. The limit of the phosphor persistence time restricts the scan range;

and the more persistent phosphors tend to produce a smeared image, reducing resolution. Consequently, the B-scan method of test result presentation is seldom used.

A typical B-scan indication is schematically shown in Fig. 3.16 and represents a cross sectional view of the test specimen. The top line represents the top face of the test material. The discontinuous bottom line represents the back surface of the specimen. Between these two lines are signals from flaws in the test material. Note that these flaws prevent the ultrasound from reaching the back surface and so create a shadow on the bottom line.

3.2.4.3 C-Scan Mode

The essentials of the C-scan mode are shown in Fig. 3.17. In practice, an electromechanical recorder or microcomputer is used to produce a permanent record of the scan. For this mode of operation, an electronic gate is used to record only the output of the receiver a precise time after the pulse is transmitted. Since the pulse velocity is quite constant through the material, the electronic gate actually records the receiver output for a plane of the material at some specific depth. Thus, the C-scan presentation provides a two-dimensional plane view of the specimen at a selected depth below the surface. Unfortunately, this method must be repeated at various depths in order to determine the flaw detail.

3.2.5 Limitations and Advantages

3.2.5.1 Limitations

As with any non-destructive test method, ultrasonic inspection does

have its drawbacks. First, it is intrinsically a small area coverage method so that large area coverage requires complex mechanical scanning or the use of an array of transducers. Furthermore, a good, direct mechanical coupling between the transducer and the test article is required; unfortunately, this is often a requirement which is difficult to meet. Moreover, the test specimen geometry in terms of size, contour, complexity, and defect orientation greatly affects the test results. Also, the material's internal structure limits the application of ultrasonics.

The immersion method, in particular, requires submersion of the part being inspected. Sometimes if the couplant is water, this may not be possible, due to the material's composition or size. The contact test is limited to ultrasound with frequencies of 10 MHz because the required transducer crystals are very thin and fragile so that normal wear inherent in the contact method shortens the crystal's useful life.

3.2.5.2 Advantages

The principal advantages of ultrasonic inspection include its ability to penetrate substantial depth in most materials, its ability to test from one surface only, and its sensitivity in the detection of minute flaws. Moreover, this testing method uses electronic operation which enables the process to be easily automated.

Furthermore, the response time of a test is next to nothing; thus, it can be employed where rapid, automated inspection is required. The immersion test can be used to give a complete inspection of irregularly shaped components and does not require the machining of cast surfaces for an inspection. In addition, high test frequencies can be used with

the immersion test. On the other hand, ultrasonic contact testing can easily be moved from one location to another and requires a minimum of test instrumentation and accessories making it is the most suitable method for the inspection of large components.

CHAPTER 4

EXPERIMENTAL INVESTIGATIONS

The experimental process followed in this investigation is outlined in this chapter beginning with a description of the blank gear segment casting from which the sample blocks were obtained. A description of the sample blocks is provided along with the heat treatment and machining procedures followed to facilitate subsequent inspection. Moreover, the equipment and procedures utilized in the radiographic and ultrasonic nondestructive tests are explained. Finally, aspects of the destructive testing including the chemical analysis and the scanning electron microscopy are described.

4.1 PROCUREMENT AND PREPARATION OF THE STEEL SAMPLE BLOCKS

4.1.1 Cast 4340 Steel Blank Ring Gear Segment Description

The steel sample blocks of this investigation were obtained from a blank segment of a large ring gear used to drive the rotating cast-iron shell of an ore crushing ball mill. The blank, cast ring gear sample used in this investigation was from an eight segment, split ring gear with a nominal root diameter of 1146.0 cm and an 80.0 cm gear face width. The gear segment was cast in 1978 as a spare to be used only in the event of problems with the remaining 8 segments and weighed approximately 8300 kg after removal of the risers and gating system.

The gear segment after removal of its 6 risers is shown in Fig. 4.1. The thick sections seen at the gear ends are required to bolt the segment to its adjoining segments. The ribs protruding out of the gear

flange provide support to the outer edges of the 17.8 cm thick gear face. The through-thickness holes in the gear flange between the ribs and the end plates are to decrease the gear's weight.

The gear was cast from BB225 which is the manufacturer's (Dominion Engineering Works of Montreal) designation for a normalized and tempered steel similar in composition to wrought 4340 steel. Table 4.1 provides the chemical composition limits of 4340 steel. Furthermore, the monotonic properties are summarized in Table 4.2.

4.1.2 The Location and Cutting of the Steel Sample Blocks

An examination of the entire steel volume of the cast gear segment was not economically feasible. As a result, five important locations in the gear were selected as sites from which to cut the steel sample blocks. These locations are shown in Figs. 4.2 and 4.3. Locations 1 and 3 were on the gate side between the face-supporting ribs. The areas corresponding to 2 and 4 were on the riser side of the gear segment. In particular, location 2 was directly over a face-supporting rib while location 4 was between two adjacent ribs. Finally, location 6 corresponded to the end of the gear including the end plate and the gear face directly above the end plate.

Although the gate area of a casting is thought to have, in general, few defects, locations 1 and 3 were selected in an attempt to determine the character of any defects occurring in the area of the casting thought to be of the highest quality. Locations 2 and 4 were chosen from the riser side to investigate the defects in the regions very close to the risers. Furthermore, location 6 was selected to determine if the changes in the section at the end of the gear segment were conducive to

56

defect formation in this casting.

In brief, 4 blocks were cut from locations 1, 3, and 4 for a total of 12 blocks, while 7 blocks were cut from location 2 and 6 blocks were cut from location 6. An oxygen-acetylene torch was used in the cutting process. A swath of material approximately 1 cm wide was burned out with the torch per cut.

4.1.3 A Description of the Steel Sample Blocks

A total of 25 sample blocks were cut from the blank ring gear segment. The as-cut sample block weights ranged from 25 kg to 50 kg. A summary of the as-cut sample block weights is provided in Table 4.3. In total, 1061 kg of sample material was removed from the ring gear segment.

The as-cut sample blocks were of various sizes as a result of the inaccuracies in the manual cutting process. Furthermore, the as-cut surfaces of the blocks were rough and coated with slag from the oxygen-acetylene cutting process. However, the as-cast surfaces of the sample blocks corresponding to the inside, outside, and edges of the gear face were smooth and slag free. The dimensions of the as-cut sample blocks are also presented in Table 4.3.

4.1.4 Heat Treatment of the Steel Sample Blocks

To reduce the hardness of the heat affected zone resulting from the cutting procedure and to facilitate future machining, the blocks were tempered and annealed at Dominion Engineering Works to a Brinnel hardness number of 200. The details of this process are shown in Appendix A.

4.1.5 Identification of the Steel Sample Blocks

The steel sample blocks were removed from the foundry once the heat treatment was finished. The identification numbers stamped into the sample blocks prior to the cutting operation were replaced with a two-digit drilled identification number as shown in Fig. 4.4. The first number represented the general block location (from area 1, 2, 3, 4 or 6) while the second number identified the particular block in the specified location. The drilled numbers were placed in the upper left corner of each block on the surface corresponding to the outer face of the gear for locations 1 through 4 while the identification numbers were drilled on the surface corresponding to the gear end face for location 6. The specific orientation of the drilled identification numbers of the sample blocks with respect to the blank gear segment can be seen in Figs. 4.2 and 4.3.

4.2 MACHINING AND SECTIONING OF THE STEEL SAMPLE BLOCKS

4.2.1 Machining Details

The steel sample blocks, once cut from the ring gear segment, heat treated, and permanently identified, were machined to provide a suitable surface for the ultrasonic inspection , to provide a number of uniform block dimensions to facilitate the radiographic inspection and to expose internal surface in the search for defects. The machining was accomplished using a 10.16 cm diameter cup wheel with 8 straight tungsten carbide inserts rotating at 212 r.p.m. A 15.24 cm/min feed rate was selected with a 1.27 mm depth of cut. Initially, oil was used as a cutting lubricant; however, an excessive amount of smoke was

generated as seen in Fig. 4.5. Accordingly, the remaining machining was performed without the use of a cutting lubricant. The blue machine chips produced in the dry machining process shown in Fig. 4.6 indicate an efficient cutting procedure; the heat generated is being effectively removed through the chips and is not building up in the cutter tips.

Difficulty was encountered in machining the outer sections of the blocks because of the presence of the heat-affected zone and surface slag resulting from the oxygen-acetylene cutting process. The machining of this region resulted in many broken or chipped carbide inserts. Once the outer 3 mm of material was removed, the machining proceeded without problem. The setup used to clamp the blocks during machining is shown in Fig. 4.6.

4.2.2 A Description of the Machined Steel Sample Blocks

The machined steel sample blocks varied in weight from 15.9 kg to 34.0 kg, depending on the final block dimensions. Table 4.4 provides the weight of each machined sample block. In general, the sample blocks were machined into 3 size categories. In particular, 11 blocks were machined to 14.0 ± 0.1 x 14.0 ± 0.1 x 16.5 ± 0.1 cm, 5 blocks were machined to 15.9 ± 0.1 x 15.9 ± 0.1 x 16.5 ± 0.1 cm, and 4 were machined to 16.5 ± 0.1 x 16.5 ± 0.1 x 16.5 ± 0.1 cm. The remaining 5 blocks were were not machined to any particular size category. Fig. 4.7 shows the dimensions of the three size categories while Table 4.4 provides the actual dimensions of the machined sample blocks. Finally, Fig. 4.8 shows the dimensions of block 23L, the odd shape block which was removed from a section of the gear segment where a gear face support rib meets the inside of the gear face.

4.3 **RADIOGRAPHIC INSPECTION**

4.3.1 Radiographic Inspection Equipment

4.3.1.1 The Linatron 1500

A Linatron 1500 was used as the source of penetrating X-radiation to produce the radiographs of the steel sample blocks. This 7.5 Mega Electron Volt (MeV) linear accelerator with a 1500 RAD/min output at 1 m and a focal spot size of less than 2 mm was located in the Nondestructive Inspection Department of Canadian Steel Foundries Inc. of Montreal.

The Linatron 1500 consisted of the following four major components: the linear accelerator, the linear accelerator positioning apparatus, the control panel, and the electronic console. The theory of operation of the linear accelerator, the component in which the X-rays are produced, is detailed in Section 3.1.2.3. The actual Linatron 1500 and its positioning apparatus, suspended from an overhead crane using steel cables, can be seen in Fig. 4.9. The control panel through which the exposure time is controlled is shown in Fig. 4.10. The electronic console houses all the electronic circuits used to control the linear accelerator.

The linear accelerator was located in a subterranean pit surrounded with 2.13 m thick concrete walls on three sides while the fourth wall that shielded the control room and the operators was 2.74 m thick .

4.3.1.2 Penetrameters and Film Jackets

The source side penetrameters used to control the quality of the radiograph were in accordance with the ASTM Standard Method for

60

Controlling Quality of Radiographic Testing (E 142-77) [20]. Depending on the thickness being radiographed, a number 50, a number 60, or a number 80 lead penetrameter was employed. The details of the penetrameter type used are shown in Fig. 4.11, while Table 4.5 summarizes the metal thickness over which each penetrameter size is applicable. Furthermore, lead numbers were used to identify the resulting X-ray of the block being radiographed.

The X-ray film was placed in film jackets behind the blocks being inspected. These jackets provided protection against overexposure due to X-ray scattering from the sides of the blocks and from X-rays reflected from background sources. The film jacket also protected the film from scratches and exposure to light prior to development. The film jacket consisted of a 0.254 mm lead sheet in front and a 0.762 mm lead sheet in back of the film.

4.3.1.3 The Recording Film

The X-ray recording film used to record the radiographic indications was Kodak type AA. Large 35.5 cm x 43.2 cm sections of this high contrast film were employed to record the radiographic indications of four steel blocks in single exposures while smaller 20.2 cm x 25.3 cm film was used to record indications from exposures involving a single steel sample block. The exposure times as a function of the steel thickness radiographed for Kodak type AA film is provided in Fig. 4.12.

4.3.2 Orientation and Direction of X-Ray Exposures

The steel sample blocks, except numbers 64 and 23L, were radiographed in two mutually perpendicular directions. The details of

the two X-ray directions in addition to the faces of the blocks facing the radiation source can be seen in Fig. 4.13 and Fig. 4.14. With all of the blocks except block 64 and 23L, the face of the block with the drilled indentification number (face A - the face on which the gear teeth would be machined into) was towards the source for the direction 1 radiographs. Face D, the face corresponding to the gate side of the gear, was towards the radiation source for the direction 2 radiographs as seen in Fig. 4.13. This direction specification was carefully followed during the entire radiographic inspection procedure. Finally, the directions of the radiographs for blocks 64 and 23L are shown in Fig. 4.14. The multiple shots exposing the two different thicknesses of block 23L were performed separately.

4.3.3 Radiographic Inspection Procedure

The radiographic inspection procedure employed in this investigation was based on the ASTM Standard Recommended Practice for Radiographic Testing, designation E 94-77 [21] with penetrameters conforming to E 142-77 [20].

4.3.3.1 Initial Preparation

Once the film was loaded into the lead film jacket and placed on top of the stand, the blocks to be radiographed were moved into position on top of the film jacket as in Fig. 4.15. After installing the lead identification numbers and the appropriate ASTM penetrameter corresponding to the steel thickness being radiographed (see Table 4.5) the X-ray chamber was cleared of personnel and the blocks were exposed to the penetrating radiation.

4.3.3.2 The Radiographic Exposure

In every exposure, two films were exposed to guard against any film defects being interpreted as flaw indications. Using the exposure time vs. steel thickness graph of Fig. 4.12 for a target film distance of 1.83 m (6 ft) and an output of 1500 RAD/min at 1 m, the exposure time, in seconds, was determined and selected on the control panel. For example, a 19.8 cm (6.5 in) thick block with Kodak type AA film required a 12 second exposure time. With a 1.83 m (72 in) source to film distance, the resulting source to object distance was 1.67 m (65.5 in). This corresponded to a 500 RAD dose. A summary of the exposure dose, film type and size, source to object distance and penetrameter size for each block can be seen in Table 4.6.

4.3.3.3 Developing the Film and Evaluating the X-Ray Quality

After exposure to the penetrating radiation, the film was removed from the lead jacket in the darkroom and inserted into the X-Omat Model B automatic processing machine. This machine carried out the developing procedure including immersing and agitating the film in developer, rinsing and fixing, and then washing and drying the film. Once developed, the X-rays were inspected using an X-ray viewer to determine if a good quality radiograph had been obtained. If the 2T hole of the penetrameter was visible, a high quality X-ray had been achieved.

4.4 ULTRASONIC INSPECTION

4.4.1 Ultrasonic Reference Blocks

4.4.1.1 Description

The five ultrasonic reference blocks, cut from sample block 11,

were used in the calibration procedure of the ultrasonic inpsection of the steel sample blocks. In particular, the reference blocks were used to construct a Distance Amplitude Correction (DAC) curve required in the ultrasonic inspection procedure. This curve indicated the amount of ultrasound beam attenuation in the material being inspected and how the attenuation increased as the metal thickness increased.

The design of the reference blocks was based on the Standard Specification for Steel Castings, Carbon and Low Alloy, Ultrasonic Examination Thereof (ASTM designation A 609-83) [6]. The reference block shown in Fig. 4.16 represents those specified in the standard while Fig. 4.17 shows the actual blocks used in this investigation. As can be seen, there are a number of differences between the reference blocks specified in the standard and those actually used. These can be summarized as follows:

a) the actual blocks have a square cross section, while those specified in the standard have a round cross section;

b) the specified 32 r.m.s. surface finish was not reproduced on the top and bottom surfaces of the actual reference blocks used; and

c) the recommended counter bore in the flat bottom hole was omitted in the actual blocks.

To eliminate any possibility of corner effects interfering with the ultrasonic signal, the dimension of the square cross section was larger than the recommended diameter of the circular section. Furthermore, the reference blocks were not machined to the 32 rms surface finish in order to simplify the ultrasonic inspection procedure. The inspection face (the top surface opposite the surface with the flat bottom hole)

64

surface finish of the reference blocks was identical to the surface finish of the sample blocks. Thus, the procedure required to compensate for differences between the surface finish of the reference blocks and those to be inspected was not required. Finally, the counter bore in the 3.175 mm diameter flat bottom hole was omitted for two reasons. The first was to decrease the cost and time required for the machining. The second was to eliminate the possibility of secondary ultrasonic signals being generated by a counter bore which also was not encountered in any of the industrial applications that were investigated.

With respect to Fig. 4.17, the modified reference blocks had a 6.60 cm square cross section with a 3.175 mm diameter flat bottom hole drilled to a depth of 1.90 cm from the back surface. In brief, there were five reference blocks with various metal distances (the metal distance being the distance from the top surface on which the block is scanned to the beginning of the flat bottom hole) spanning the thickness of the cast steel sample blocks inspected. These distances are summarized in Fig. 4.17.

4.4.1.2 Radiographic Inspection

Once the machining had been completed, the ultrasonic reference blocks were radiographed to determine the presence of fine defects that would not have been indicated by the original radiographs of block 11. Since the thickness of the reference blocks being radiographed was much less than the thickness radiographed with block 11, the radiographs of the reference blocks would have a higher sensitivity than the original block 11 radiograph. The reference block radiographs were also used to

verify the quality of the flat bottom hole.

The radiographs were produced at Crawford McLeish NDE. Inc. using an Irridium 192 point source. Its strength was 52 curie at the time of the radiographic inspection. The five reference blocks were exposed simultaneously with a 69.8 cm source to film distance and a 42 min exposure time. Lead shielding was placed around the blocks to protect against scatter radiation effects. An ASTM number 35 penetrameter was employed and lead numbers were used to identify the blocks.

4.4.2 Ultrasonic Inspection Equipment and Materials

The equipment utilized in the inspection of the 24 cast steel sample blocks consisted of a Krautkramer USL-38 ultrasonic inspection unit. The USL-38 was a pulsed, reflection type instrument capable of generating, receiving, and amplifying ultrasound. Furthermore, a longitudinal wave 1.90 cm dia. Inotech Gamble SST 2.25 MHz probe was employed with a light oil couplant.

4.4.3 Ultrasonic Inspection Procedure

The ultrasonic inspection procedure employed to investigate the defects in the cast steel sample blocks was based on the ASTM Standard Specification for Steel Castings, Carbon and Low Alloy, Ultrasonic Examination Thereof, designation A 609-83 [6]. The test was performed in association with the firm Crawford McLeish NDE Inc. An ultrasound frequency of 2.25 MHz was used in this A-scan contact type test.

4.4.3.1 The DAC Curve

- The ultrasonic inspection of the cast steel sample blocks began

with the construction of the characteristic DAC curve. This was accomplished using the five reference blocks which spanned the thickness of the sample blocks being inspected. Each reference block was inspected individually; the amplitude of the reflected signal from the 3.175 mm dia. flat bottom hole was plotted against the metal distance for all of the five reference blocks. The actual DAC curve was plotted on the cathode ray tube shield of the inspection unit. A graphical reproduction of the DAC curve is presented in Fig. 4.18.

As can be seen from the graph, a higher gain (signal amplification) was employed for the last portion of the curve. This higher gain was necessary to counteract the increase in attenuation of the ultrasonic beam at the larger metal distances. The gain was selected to give near full screen pulse indications for the smallest metal distance of each section of the DAC curve. For instance, if a gain of more than 46 dB was used in the first section of the DAC curve, the indication from the flat bottom hole at a metal distance of 2.54 cm would have been off the amplitude scale and, consequently, unknown. Also, an excessively high gain was avoided close to the scanning surface since it produced characteristic grass like signal indications immediately after the couplant-test specimen interface. This tended to mask indications close to the scanning surface.

4.4.3.2 Ultrasonic Inspection Procedure for Cast Steel Sample Blocks

After construction of the DAC curve, the steel sample blocks were inspected from three mutually perpendicular surfaces. These inspection surfaces and their orientation with respect to the blank cast ring gear are shown in Fig. 4.19. During the inspection of each face, every pass

67

of the search unit over the face overlapped the previous pass by at least 10%. The scanning rate was limited to 15 cm/sec.

As any defect indications were discovered, their location on the block face, their depth as indicated by the inspection unit, and the corresponding pulse height in terms of the percent DAC curve were recorded on previously prepared charts. The recording charts corresponding to the block faces being scanned were carefully identified. All indications, except those from the drilled identification numbers, were recorded on the charts. Since the reference blocks were machined out of an actual sample block and had an identical scanning surface finish as the sample blocks, a procedure to compensate for surface roughness variation was not followed. Fig. 4.20 shows the inspection of a sample block.

4.5 MICROSCOPIC INSPECTION

A microscopic inspection procedure was utilized to investigate any microdefects (defects whose largest dimension is less than 0.5 mm) occurring in the cast steel sample blocks. This procedure involved cutting samples from the original sample blocks, pulling these samples until fracture in an MTS machine, and viewing the resulting fracture surfaces in a scanning electron microscope for the presence of microdefects. This segment of the overall defect characterization is summarized in this section.

4.5.1 Fracture Specimens

4.5.1.1 Description

In total, 30 fracture specimens were cut from the original cast

steel sample blocks. These as-cut fracture specimens were of various lengths ranging from 12.0 cm to 16.5 cm depending on which block and at what location in the block they were cut from. Furthermore, the specimens had a 1.3 x 1.3 cm cross section. The length of the specimens and the dimensions of the cross section were not required to follow close tolerances since a difference in length could easily be compensated for in the MTS tensile machine while the cross section dimensions would become irrelevant once the specimens were notched. The specimens were notched for two reasons; the smaller cross section area of the notch would be the weakest point in the specimen and thus the location of fracture and would require a fracture load within the range of the MTS machine.

The fracture specimens were cut from the corners of the original cast steel sample blocks by a 46 cm bandsaw using a 4 teeth/cm, 1.3 cm wide blade moving at 30 m/min. The fracture specimens were removed from the corners of the original sample blocks at various locations of the gear to minimize the associated machining costs. Since the heat-affected zone had already been machined off the original blocks, cutting fracture specimens from only the corners would not significantly influence the experimental results. A notched specimen ready for testing is shown in Fig. 4.21.

4.5.1.2 Location and Orientation

The location and orientation of the 30 fracture specimens with respect to the original sample blocks are documented in Appendix B. Every specimen was identified with a two digit, single letter code. The two digit number indicated the cast steel sample block from which the

fracture specimen was cut while the letter indicated the direction of the largest dimension of the specimen. For instance, the letter A indicated that the fracture specimen was perpendicular to the gear face, B indicated the particular fracture specimen was oriented across the gear perpendicular to its edges. Finally, C represented specimens which were oriented in a direction tangent to the gear's face. The orientation of the identification code in Appendix B is identical to the orientation of the actual code stamped into the fracture specimens. With blocks where the specimen face containing the identification is not in view in the drawing, the corners of the hidden face are labelled and shown in an auxiliary view along with the corresponding identification code.

4.5.1.3 Radiographic Inspection

Radiographic inspection was performed in an attempt to locate defects not shown on the previous, less sensitive radiographs. As usual, the fracture specimens were radiographed in two perpendicular directions. The two perpendicular directions for type A, B, and C specimens are shown in Fig. 4.22. Fig. 4.23 shows the specimen order in the associated radiographs.

The radiographs were produced at Crawford McLeish NDE. Inc using a 150 kV X-ray tube. A number 15 penetrameter was used with a 51 cm. source to film distance and a 7.2 min exposure time.

4.5.2 The Fracture Test

A Material Testing System (MTS) machine was used to pull the specimens until fracture.

4.5.2.1 The MTS Test Facility

The MTS test system consisting of an hydraulic power supply, a loading unit, a control console, a graphics display monitor, a decwriter, and a hard copy unit is shown in Figs. 4.24 through 4.27. The major components are described below.

a) Hydraulic Power Supply

The hydraulic power supply (HPS), illustrated in Fig. 4.24, uses a 37.3 kW motor to drive a 76.2 l/min fixed volume pump that provides the hydraulic power to the loading unit. The pressure output of the pump in the low pressure mode is 0.2 MPa while in·the high pressure mode a continuous output pressure of 20 MPa can be obtained.

An hydraulic fluid-to-water heat exchanger is incorporated into the HPS to maintain the working fluid below a maximum safe level. In the event that the working fluid exceeds a preset limit, a temperature sensitive switch deactivates the HPS.

b) Loading Unit

The loading unit, shown in Fig. 4.25, is composed of the load frame, the specimen grips, the hydraulic actuator, and the servovalves.

The load frame is a rigid structure consisting of two vertical columns joined by a moveable crosshead. To accomodate specimens of different lengths, the crosshead may be raised or lowered by means of hydraulic lifts. Once in position, the crosshead is hydraulically locked to the vertical columns to prevent backlash or slippage.

A pair of self-aligning grips, incorporating an hydraulically

locked spherical seat arrangement, are used to clamp the fracture specimens in the loading frame. The two grips are hydraulically actuated and capable of providing a constant specimen gripping force independent of the applied axial load.

The axial load is applied to the fracture specimens through an hydraulic linear actuator. The actuator piston, with a 15 cm stroke, a 45.3 cm^2 effective area, and a maximum available pressure of 20 MPa, provides a static load capacity of 100 kN.

The hydraulic actuator movement is controlled through two electro-mechanical servovalves. The servovalves convert the electrical control signal from the servocontroller into the mechanical movement of an internal spool. The movement of the spools regulate the flow of the high pressure hydraulic fluid into and out of either side of the piston, depending on the polarity of the command signal. Presently, two servovalves are used in parallel and, coupled with a dual manifold, double the flow rating to increase the system response.

The load applied to the specimens in the loading unit is monitored through a resistive bridge load cell having a 100 kN static rating and a 75 kN dynamic rating. This transducer's output voltage is directly proportional to the applied load.

The hydraulic actuator movement is monitored by means of a linear variable differential transformer (LVDT) mounted on the actuator. The AC output voltage generated by the LVDT is directly proportional to the actuator piston displacement.

c) The Control Console

The control console, seen in Fig. 4.26, incorporates various

control modules that precisely control and monitor the test parameters.
The function and important features of these modules are summarized
below.

The 436 control unit provides on-off control of the electronic
system components. The HPS is also controlled through this unit.
Furthermore, the control unit incorporates a built-in interlock circuit
that automatically deactivates the HPS if any abnormal conditions, such
as excessive fluid temperature or low reservoir fluid level, occur.
Finally, the control unit is linked with a function generator through
which waveforms of various frequencies can be selected.

The 442 controller performs the closed loop control functions and
performs the system programming, failsafe, and readout functions through
plug-in modules. These include the feedback selector, the servo-
controller, the valve driver, the limit detector, the AC stroke
conditioner, the DC strain conditioner, and the DC load conditioner.
The transducer conditioners supply the excitation voltage to their
respective transducer and condition the output voltages of the
transducers before being sent back to the feedback selector. The
feedback selector selects the output of a particular transducer as a
feedback signal that is processed by the servocontroller; this selected
transducer output is the controlled variable. Finally, the
servocontroller compares the command and feedback signals and generates
a control signal that operates the servovalves once amplified by the
valve driver. The limit detector module monitors the load, stroke, and
strain transducer outputs simultaneously and initiates a predetermined
task when any of these variables exceeds a preset limit. This can
include activating an indicator light on the controller front panel or

activating an interlock to shut the HPS off.

The 430 digital indicator is used in the MTS system to continuously monitor and display, in digital form, the voltage of any one of the various parameters in the test such as load, stroke, or strain.

The Digital Equipment Corporation PDP 11/04 control processor incorporates three important features: automatic start up, the ability to use a conventional keyboard as an operator's console, and a hardware diagnostics package. Moreover, the PDP 11/04 control processor is linked to an MTS digital processor interface unit which, in addition to data acquisition and function generation, provides real time control of a test. Data storage is achieved through a Digital RX dual disk drive.

d) Input/Output Devices

The remaining components of the MTS system, shown in Fig. 4.27, are the input/output devices including the Tektronix 4010-1 computer display terminal, the Digital decwriter II, and the Tektronix 4631 hard copy unit. The computer display terminal provides a communication link and display device to interface with the PDP 11/04. A permanent copy of the display screen can be produced via the hard copy unit. Finally, the decwriter, an interactive data communications terminal, incorporates a low-speed impact printer to provide hard copy printed output.

4.5.2.2 Fracture Test Procedure

The fracture tests were performed in the MTS testing machine using a tensile ramp loading function. A detailed step-by-step test procedure is provided in Appendix C. The tests were performed in stroke control with the relevant test parameters controlled through the computer

program PULT1M. This program was obtained from Dominion Engineering Works Ltd. and modified specifically for use in this investigation. A printout of PULT1M along with its interactive testing output are provided in Appendix D. Table 4.7 provides a summary of the blocks which were pulled until fracture along with their associated notch cross section area and summary of the relevant test parameters. Finally, a sample of the stress vs. stroke graphs for the fracture specimens is provided in Appendix E. Once fractured, the specimens were stored in a dessicator prior to the fractographic analysis. A fracture specimen is shown loaded in the MTS unit in Fig. 4.28.

4.5.3 Scanning Electron Microscopy

4.5.3.1 The Scanning Electron Microscope

The microscopic investigation of the specimen fracture surfaces and the microdefects exposed on these surfaces was performed by means of the scanning electron microscope (SEM) whose photograph is shown in Fig. 4.29. In brief, the SEM features a high resolution, a large depth of focus resulting in a three dimensional appearance of SEM images, and an ability to observe specimens at very low magnification. Consequently, the SEM is one of the most versatile instruments used to examine the microstructural characteristic of solid surfaces.

The major components of the SEM, schematically shown in Fig. 4.30, are the electron gun, the magnetic lens system, the vacuum system, the electron collector, the recording and visual cathode ray tubes, and the controlling electronics including the scan generator, the scan amplifier, and the video amplifier. The SEM theory of operation is described as follows referring to Fig. 4.30.

75

The electron gun provides a beam of electrons through a heated tungsten filament and an accelerating potential. The SEM used in this investigation was capable of providing electron beam energies between 1 and 30 kV. After generation by the electron gun, the electron beam passes through the magnetic lens system, consisting of the condenser lens, the scanning coils, and the objective lens. The electromagnetic condenser lens, attached beneath the electron gun, demagnifies the crossover image of the electron gun to yield a tiny spot at the specimen surface [22]. The condenser lens also determines the current of the electron beam incident on the specimen under observation. The electromagnetic objective lens brings the electron beam into focus at the specimen surface and governs the final spot size of the electron beam.

Located between the condenser and objective lenses are the scanning coils. The scanning coils deflect the electron beam to produce the scanning motion over the specimen. In operation, the scanning coils are powered by the scan generator which simultaneously operates the deflection coil of the cathode ray tubes. This synchronization produces a one-to-one correspondence between the position of the electron beam on the surface under investigation and that of the spot on the cathode ray tubes.

The electrons of the electron beam are accelerated towards the target specimen through the evacuated microscope column by means of the high negative potential of the electron-generating filament. The electron beam collides with the specimen maintained at earth potential. This beam-sample interaction produces primary backscattered electrons, secondary electrons, and X-rays. Primary backscattered electrons are

electrons from the incident primary beam that are scattered with little loss of energy and radiate out from the specimen surface. In contrast, secondary electrons are released from the outer orbitals of the specimen atoms as the primary beam electron collides with these atoms in its path. Finally, as with all electron-matter collisions, X-rays are emitted whose wavelengths are a characteristic feature of the elements of the target specimen.

The primary backscattered and the secondary electrons are monitored when information about the specimen topography is required while the X-rays are monitored when information about the composition of the specimen surface is needed.

The electron collector, maintained at a positive potential with respect to the target specimen, attracts the secondary electrons. The electrons, on impact with the scintillator in the collector, generate light which passes down the light guide and falls on the photocathode of the photomultiplier. The resulting electrical signals, amplified by the video amplifier, are used to modulate the intensity of brightness of the CRT displays. In brief, it is the intensity of either the backscattered or secondary electrons which produces the SEM topographic image. The electron gun accelerating potential, the lens current, the magnification, and the other SEM parameters are contolled from the control console.

4.5.3.2. <u>Scanning Electron Microscope Procedure</u>

As summarized in Table 4.7, the fracture surface of 8 of the fracture specimens were selected to be viewed using the SEM. The selection criteria was based mainly on the flatness of the fracture

77

surface, since focusing on extremely rugged surface topography in the SEM would be very difficult. The fracture surfaces selected for SEM examination were cut from the fracture specimens and glued onto standard 12.7 mm diameter aluminum stubs using a conductive graphite in isopropanol cement.

After the cement had dried, the fracture surface specimen was placed in the SEM vacuum chamber. A 1 x 10^{-5} torr vacuum was created in the chamber and a 30 KV accelerating potential was selected in the electron source module. The fracture surface was scanned at low magnification. The best image of the fracture surface was obtained by manipulating the focus and condenser controls, by adjusting the contrast and brightness of the viewing CRT, and by adjusting the vertical position of the specimen by means of a micrometric screw mounted on the vacuum chamber. Once a region of interest or a particular defect was located on the specimen surface that warranted recording, the contrast and brightness of the high resolution recording CRT were adjusted, and a picture was taken with the SEM camera.

This procedure was repeated for the remaining fracture surfaces selected for examination. General overviews of the surfaces at low magnification along with detailed high magnification shots of typical microdefects were produced.

4.6 CHEMICAL ANALYSIS

A chemical analysis was performed on the cast ring gear segment to determine if any variation in the constituent elements was present. This process involved drilling the steel sample blocks to provide a number of samples which were subsequently analyzed through an industrial

78

testing laboratory. The chemical composition of 10 elements were investigated including aluminum, carbon, chromium, copper, manganese, molybdenum, nickel, phosphorus, silicon, and sulphur.

4.6.1. Locations of Chemical Analysis

In total, 6 locations in the casting were investigated. One sample was removed from a sample block from the end face, 3 samples were removed from blocks on the riser side, and 2 samples were removed from blocks on the gate side of the casting. In all the cases, except for the end face, the samples for chemical analysis were removed from the gear face where the teeth would have been machined. Any irregular concentration of a constituent element would be most critical in this area; for example, a high concentration of silicon would seriously decrease the integrity of any weld-repaired defects in the area of the teeth.

The samples for analysis were obtained by drilling two adjacent 1.27 cm dia. holes to yield approximately 10 g of drill shavings per sample. The sample locations in the ring gear are shown in Fig. 4.31.

4.6.2. Method of Chemical Analysis

The procedures used to determine the composition of the 10 alloying elements, summarized in Table 4.8, are briefly described in this section.

4.6.2.1. Aluminum

The samples were analyzed for aluminum composition using the atomic absorption method. Every sample for aluminum analysis was dissolved in

79

hydrochloric acid, oxidized using nitric acid, and diluted as specified in the relevant standards. The resulting solution was burned in a nitrous oxide-acetylene flame of an atomic absorption spectrophotometer. Spectral energy of 309.3 nm was passed through the flame and the absorbance was compared with solutions of known aluminum concentrations.

4.6.2.2. Carbon

The samples for carbon analysis were burned in oxygen in an induction furnace. The resultant carbon dioxide was passed through an infrared absorption instrument calibrated to National Bureau of Standards samples. In this instrument the difference in infrared absorption between the sample and the reference caused an imbalance in pressure between the two detector tubes. This imbalance was measured by means of a diaphragm and electronically converted to a digital readout. With the amount of carbon known, the resultant concentration was easily calculated.

4.6.2.3. Chromium

The chromium concentration was determined as per ASTM E 350-84, section 269 [24]. In this method, the sample was dissolved in mineral acids. This sample solution was aspirated into a nitrous oxide-acetylene flame of an atomic absorption spectrophotometer. Then, spectral energy at approximately 357.9 nm (from a chromium hollow-cathode lamp) was passed through the flame and the absorbance was measured. Calibration of the spectrophotometer was achieved with solutions of known chromium concentrations.

4.6.2.4. Copper

The copper content was determined using the method of atomic absorption whereby the samples were dissolved in hydrochloric acid, oxidized through the additon of nitric acid, diluted, and then aspirated in an air-acetylene flame of an atomic absorption spectrophotometer. Spectral energy of 324.75 nm was passed through the flame with the absorbance being measured and compared with solutions of known copper concentrations.

4.6.2.5. Manganese

Again, atomic absorption was implemented to determine the manganese composition of the samples. The samples were dissolved in hydrochloric acid, oxidized using nitric acid, diluted, and burned in the air-acetylene flame of a spectrophotometer. Spectral energy of 279.5 nm was used for the absorbance measurements.

4.6.2.6. Molybdenum

The atomic absorption method was also used for determining the molybdenum content. After dissolving in hydrochloric acid, oxidizing using nictric acid, and diluting, the samples were burned in a nitrous oxide-acetylene flame. Spectral energy of 313.3 nm was used in the absorbance measurements.

4.6.2.7. Nickel

The nickel content was also determined with the method of atomic absorption with the dissolved nickel solution burned in an air-acetylene

flame. Spectral energy of 232.0 nm was used in the absorbance measurements.

4.6.2.8. Phosphorus

The composition of phosphorus was determined by the alkalimetric method as specified in section 221 of ASTM E 350-84. In this method, phosphorus was separated as ammonium phosphomolybdate. The precipitate was dissolved in standard NaOH solution, and the excess NaOH titrated with nitric acid [24].

4.6.2.9. Silicon

The analysis for Silicon was carried out according to the gravimetric method specified in ASTM E 350-84. The sample was dissolved in hydrochloric acid and oxidized using nitric acid. After dissolution of the sample was complete, silicic acid was dehydrated by fuming with sulphuric acid. The solution was filtered and then the silica was ignited, weighed and volatized with hydrofluoric acid. The residue was ignited and weighed. The concentration was determined based on the loss of weight of the sample.

4.6.2.10 Sulphur

The sulphur content was determined using the combustion-iodate titration method as specified in ASTM E 350-84. In this method, the sample was burned in oxygen in an induction furnace. During combustion, the resultant SO_2 was absorbed in an acidified starch-iodide solution and then titrated with potassium iodate solution to determine the amount of sulphur present.

82

CHAPTER 5

ANALYSIS OF RESULTS

5.1 DATA PRESENTATION

The defect characterization of the cast steel ring gear of this investigation involved four basic tests including a milling machine sectioning procedure, a radiographic inspection, an ultrasonic inspection, and a microscopic inspection. Moreover, a chemical analysis was performed at various locations in the gear.

The results of the radiographic inspection are presented in Appendix F and include drawings which detail the radiographs in which defects were indicated. The ultrasonic inspection results of the entire set of sample blocks are provided in Appendix G. The results of the microscopic inspection including the radiographs of the fracture specimens prior to fracture and the fractograph flaw data obtained with the SEM are presented in Appendix H and Table 5.10. Finally, the numerical results of the chemical analysis are provided in Table 5.12.

5.2 DISCUSSION OF RESULTS

5.2.1 The Mechanical Sectioning

The machining of the steel sample blocks was carried out to provide a suitable ultrasonic inspection surface, to provide a number of uniform block dimensions, and to expose internal surfaces of the cast ring gear. This multi-purpose sectioning operation exposed no internal casting defects visible to the unaided eye. In fact, no defects were discovered during this procedure when a 100 X portable light microscope was employed to view the machined surfaces.

83

Approximately 15000 cm2 of internal casting surface was exposed and investigated during this sectioning operation. The lack of discovery of any defects during this procedure can be mainly attributed to the action of the milling machine cutter tending to displace metal over any exposed flaws. This tendency of the cutter to cover defects was seen when the surfaces containing the 2.78 mm drilled identification holes were machined. In general, the 2.78 mm dia holes were half covered with metal while in 21 cases the entire hole was covered and had to be cleaned to read the identification number.

5.2.2 The Radiographic Inspection

Radiographic inspection was the first nondestructive testing technique employed to characterize the internal casting defects in the ring gear steel sample blocks. Since there was no previous defect analysis dealing with casting defects in the ring gear sections of this investigation, the typical internal defect size range was unknown. Therefore, a worst-case-scenario-experimental procedure was synthesized whereby it was assumed that the ring gear segment contained large classical casting defects. Consequently, the entire set of steel sample blocks was radiographed as outlined in Section 4.3.

The X-ray results are summarized in Table 5.1 where the presence of flaw indications is presented for the two X-ray directions of the steel sample blocks. The location and size of the radiographic flaw indications are recorded in the drawings of Appendix F.

Three photographic reproductions of actual sample block X-rays are shown in Figs. 5.1 and 5.2. The radiograph of block 64 is shown in Fig. 5.1. The number 50 penetrameter can be seen in the center of the shot

while the holes of the drilled identification number can be easily seen in the upper right corner. Furthermore, flaw indications can be seen in the lower left corner. The flaw indications in the photographs are not as sharp as in the original radiographs since some radiograph quality is lost in the photographic reproduction process. Fig. 5.2 shows the two X-rays of block 62 taken in two perpendicular directions as explained in Section 4.3.2. Again, the drilled identification numbers and the lead identification numbers are clearly visible. A penetrameter is not in view in these two X-rays since both were obtained from a multiple block exposure with the penetrameter placed on one of the other blocks. The dark areas (areas receiving a higher intensity of X-rays) on the bottom and left sides of the X-rays are due to X-rays being scattered from the sides of the adjacent blocks in the multiple block exposures. This did not create any problems when the radiographs were viewed since the intensity of the viewing light could be adjusted to compensate for this effect.

The results of the radiographic inspection, summarized in Table 5.1, show that of the 25 sample blocks radiographed 15 displayed no radiographic indications of internal defects. However, the flaw indications observed in the remaining 10 sample blocks could be classified into 5 categories as summarized in Table 5.2. These flaws are two dimensional since the radiographic inspection provides only two dimensional flaw indications. However, as will be seen in Section 5.3.6, the nondestructive tests exhibit evidence that the flaws are planar and can be adequately described in two dimensions.

The first category of radiographic flaw indications were circular in shape ranging from 0.2 to 0.3 cm in diameter. The second class of

indications were circular in shape with diameters between 0.3 and 0.4 cm. The third class were also circular with diameters greater than 0.4 cm. The fourth class of flaw indications discovered in the X-rays were rectangular with slightly rounded ends having a width between 0.1 and 0.5 cm and a length between 0.2 and 0.8 cm. Finally, the fifth class of indications encountered were also round ended rectangular with a width between 0.1 and 0.5 cm but with a length greater than 0.8 cm.

A summary of the flaw indications measured from the X-rays is provided in Table 5.3 where the flaw type and flaw parameters are recorded along with the radiograph in which the flaw indication was found.

5.2.3 Sectioning and Radiographic Inspection of Sample Block 11

In preparation for the ultrasonic inspection, five reference blocks were machined from sample block 11 as outlined in Section 4.4.1.1. No internal defects were discovered on the surfaces exposed during the bandsaw cutting operation of block 11. These newly exposed surfaces were viewed with a 100 X portable light microscope; however, no defects were discovered. Moreover, no flaws were seen on the surfaces exposed during the milling operation in which the blocks were machined to the required dimensions.

The five reference blocks were then radiographed as outlined in Section 4.4.1.2. A photographic reproduction of the radiograph of reference block 4 is presented in Fig. 5.3 As seen in the center of the X-ray, a number 45 ASTM penetrameter was employed with the 2T hole at the top of the penetrameter clearly visible. The drilled flat bottom hole is also easily seen at the top of the X-ray along with the lead

identification number in the upper right hand corner. No internal defects are visible in the radiograph; the white spots seen in this X-ray are only dust particles arising in the printing of the photographic reproduction.

The results of the radiographic inspection of the five ultrasonic reference blocks are summarized in Table 5.4. In brief, all five reference blocks were free of macroscopic internal defects. The X-rays also indicated a very good quality flat bottom hole in each of the reference blocks as required for the ultrasonic tests.

5.2.4 The Ultrasonic Inspection

The ultrasonic inspection was the second nondestructive testing technique used to characterize the internal defects of the cast ring gear sample blocks. This technique was employed for two reasons; the first was to attempt to correlate the results of the radiographic inspection and the second was to investigate internal flaws too small to appear in the radiographs. The entire set of steel sample blocks were ultrasonically inspected as outlined in Section 4.4.

The results of the ultrasonic inspection are summarized in Table 5.5 where the sample block number, the inspection face, and the absence or presence of flaw indications are presented. The actual locations and severity of the flaw indications are recorded in the drawings of Appendix G. The ultrasonic indication of the drilled identification number is not recorded for every sample block. Furthermore, the severity of the flaw indication is provided in terms of the percentage of the DAC curve as explained in Section 4.4.

The results of the ultrasonic inspection, summarized in Table 5.5,

show that of the 24 sample blocks inspected, 7 displayed no ultrasonic indication of internal flaws. The indications observed in the remaining 17 sample blocks were classified into 8 categories. The small nature of the flaw indications made it impossible to determine the exact flaw outline due to the limitations of the ultrasonic inspection unit. As a result, it was assumed the flaw indications were circular in shape for the spot indications. Furthermore, the shapes of the running ultrasonic indications were assumed to be rectangular with rounded corners. A summary of the flaw indication types is provided in Table 5.6. With reference to Table 5.6, the ultrasonic flaw indication categories consisted of 6 circular categories ranging from less than 0.1 cm in dia. to over 0.4 cm in dia. and 2 rectangular categories similar to those found in the radiographic inspection results. The evidence leading to the two dimensional character of the internal casting flaws is discussed further in Section 5.3.6.

A summary of the flaw indications obtained from the ultrasonic inspection is provided in Table 5.7 where the flaw type and flaw parameters are presented along with the block face from which the flaw indication was recorded.

5.2.5 The Radiographic Inspection of the Fracture Specimens

The results of the radiographic and ultrasonic inspections of the steel sample blocks indicated that the internal casting defects were relatively small. As a result of this and a desire to characterize the microdefects, a microscopic investigation was undertaken as described in Section 4.5. The results of the radiographic inspection of the fracture specimens, detailed in Section 4.5.1.3, are presented in photographic

88

reproductions of the actual X-rays in Appendix H. As usual, a considerable amount of X-ray quality is lost in the photographic reproduction process; however, this does not affect the experimental results.

A summary of the flaw indications obtained from the radiographic inspection is presented in Table 5.8 where the fracture specimen, the X-ray directions, as defined in Section 4.5.1.3, and the flaw indication description are detailed. Of the 30 fracture specimens radiographed, 18 displayed no flaw indications in either of the two X-ray directions. The remaining 12 specimens exhibited indications of shrinkage defects (characterized by their jagged, irregular appearance in the X-ray). The largest flaw exposed by the X-rays was a 0.5 x 0.5 cm shrink while the smallest observed on the X-rays was a 0.1 cm dia. gas porosity.

Moreover, the flaw indications of this section of the investigation were in the same size range as those observed during the ultrasonic inspection. For example, the largest flaw indication from the X-rays of the fracture specimens corresponded to a 160% DAC ultrasonic indication, while the smallest flaw indication from the fracture specimen X-rays corresponded to a 30% DAC ultrasonic indication. In fact, the flaw indications obtained from the ultrasonic inspection ranged from a 20% DAC to a 160% DAC indication. Accordingly, the results of this radiographic inspection and the ultrasonic inspection are in good agreement. In addition, two of the flaws indicated on the X-rays were also indicated by the ultrasonic test. With the use of Appendix B, Figs. 4.22 and 4.23, Appendix G, and the fracture specimen X-rays (Appendix H) it can be seen that the 0.3 x 0.5 cm shrink indication on the right side of X-ray 43A, direction 2, is

89

also indicated in the ultrasonic test result of block 43, face B. Similarly, the 0.5 x 0.5 cm shrink of X-ray 25B, direction 2, is also indicated in the ultrasonic inspection results of block 25, face B. Unfortunately, further agreement between the fracture specimen X-rays and the ultrasonic inspection results was not found. This can be attributed to the fact that all the fracture specimens were cut from edges of the original sample blocks. Any defects in this area, that is to say close to the side of the sample block, would not have been easily detected since a portion of the initial ultrasound beam would be reflected off the block's side before reaching the defect. Thus, a lower energy ultrasound packet would be reflected from the flaw and received by the transducer as compared to areas away from the sides of the block. As a result, the ultrasonic inspection would indicate a smaller flaw than there actually is. This was seen for fracture specimen 43A where the ultrasonic inspection indicated a 80% DAC flaw (approximately 0.25 cm dia.) while the flaw measured off the X-ray (i.e. actual size) was 0.3 x 0.5 cm. Similarly, the ultrasonic results indicated a 120% DAC flaw (approximately 0.38 cm dia.) in block 25 while the measured X-ray indication was 0.5 x 0.5 cm.

Indeed, the results of the radiographic inspection of the fracture specimens provide insight into the shape of the flaws which were indicated from the ultrasonic inspection. Furthermore, in 3 of the fracture specimens, flaw indications were present in one radiographic inspection direction but absent in the second, perpendicular direction. This was seen in the ultrasonic inspection results and implies a planar character of many of the internal flaws. Finally, a defect histogram was not constructed for the results of this section due to the fact that

the sample space investigated was very small.

5.2.6 The Microscopic Inspection

The microscopic inspection of the surfaces of the fracture specimens using the SEM, as detailed in Section 4.5.3, was carried out to characterize the internal casting defects too small to be discovered by the radiographic or ultrasonic inspection techniques. Although the microscopic inspection was destructive in nature and would rarely be employed in industry as a common inspection method, it did provide an extremely valuable insight into the types of internal casting defects since it provided pictures of the defects exposed on the fracture surfaces. In total, 8 fracture surfaces were viewed in the SEM as summarized in Table 4.7. The actual location and orientation of these specimens in the cast ring gear can be found using Fig. 4.2 and Appendix B.

A typical fractograph overview, obtained using the SEM, is presented in Fig. 5.4 where a section of the fracture surface of specimen 12B is shown at a relatively low magnification. The largest defects visible on the fractograph were circled and labelled with a flaw identification number to facilitate the flaw characterization process. A minimum flaw dimension was arbitrarily selected such that defects whose dimensions were smaller than this minimum dimension would not be recorded. Without this minimum flaw size, used in all the fractograph overviews, it would have been impossible to characterize the fractographs in a finite amount of time. The defect-selection process was carried out for the fracture surfaces of specimens 12B, 13A, 25B, 42B, 43C, and 62A. The fracture surface topography of specimens 24A and

25A was extremely steep and erratic, making it impossible to focus on a large section of the fracture surface at one time as required for an overview. Consequently, these two specimens were not used in the microscopic flaw characterization; however, they did provide excellent individual examples of typical casting defects.

The flaws observed in the six fractograph overviews were classified into 6 categories as summarized in Table 5.9 where the flaw type, flaw description, and relevant flaw parameters are detailed. The fractographs provided a 2-dimensional flaw image; consequently, the flaws exposed through the fracture surfaces were characterized using 2 dimensional shapes which closely approximated the actual flaws. The first type of flaw encountered on the fractographs were gas porosities, circular in shape with an actual diameter ranging from 0.01 mm to 0.17 mm. Flaw number 31 of Fig. 5.4, detailed in Fig. 5.5 at a higher magnification is typical of the type 1 defect. The smooth surface of the flaw and its symmetric shape are indicative of gas porosity. The second type of defects encountered were rectangular in shape with rounded ends. These were described by a maximum width, w, and a maximum length, 1. The type 2 flaws recorded from the fractographs ranged in size from the smallest with w = 0.01 mm and 1 = 0.04 mm to the longest with w = 1.2 mm and 1 = 0.37 mm. The peanut shaped flaw, number 8 in Fig. 5.4 and enlarged in Fig. 5.6, is typical of the second flaw category. Type 2 flaws were generally gas porosities as indicated by their smooth surface and symmetric shape. In addition, the flaw of Fig. 5.6 is an example of the approximation involved in categorizing the flaws. The third type of flaw exhibited by the fracture surface fractographs was slit shaped possessing very sharp tips of almost zero

92

radius. Two parameters were used to describe these flaws: the maximum flaw width, w, and the flaw length, l. The smallest type 3 flaw recorded had a width of 0.01 mm and a length of 0.04 mm while the largest recorded had a width of 0.09 mm and a length of 0.81 mm. Fig. 5.7 is a fine example of type 3 flaws which were generally shrinkage defects characterized by their rough surface, very sharp ends, and crack like appearance. This particular flaw type also contained micro hot tears resulting from a localized unidirectional contraction of the metal when it is in a brittle condition. The fourth type of flaws observed in the fractographs was similar to type 2 flaws but multi-branched. The type 4 defects were characterized by 4 parameters with n denoting the number of branches, θ_i denoting the angle, in degrees, between the ith and (i + 1)th branch, and w_i, l_i denoting the maximum width and length of the ith branch. These parameters are summarized in Table 5.9. The smallest type 4 flaw was a 3 branch gas porosity with all branches being 0.01 mm wide. One branch was 0.04 mm long with the remaining two 0.02 mm long. The largest type 4 flaw had two branches with one branch 0.06 mm wide by 0.26 mm long and one branch 0.06 mm wide by 0.24 mm long. Flaw number 32 of Fig. 5.4, enlarged in Fig. 5.8, is typical of the type 4 flaws. Its smooth surface and rounded ends, as seen in Fig. 5.8, are indicative of a gas porosity. The fifth type of flaws encountered were multi-branched slit shaped with very sharp tips as type 3 flaws. These flaws were described with the parameters n, θ_i, w_i, and l_i in the same manner as type 4 flaws. A summary of the flaw parameters and their meaning is provided in Table 5.9. The smallest type 5 flaw recorded had two branches with one of the branches 0.01 mm wide by 0.06 mm long and the second branch 0.01 mm wide by 0.04 mm long. The largest type 5 flaw

93

encountered was a two branch shrink with the first branch 0.03 mm wide by 0.12 mm long and the second 0.09 mm long. Fig. 5.9 is a typical example of the class 5 flaws. Again, the rough flaw surface and zero tip radius are indicative of a secondary shrinkage defect. The fact that the defect is multi-branched can be explained by the existence of localized multi-directional contraction where the casting is solidifying in more than one direction simultaneously.

Finally, the sixth type of flaw found in the fracture surfaces were inclusions occurring in a fan like pattern that could be approximated using a circle of diameter d. These inclusions ranged in diameter from 0.15 mm to 0.31 mm. A typical type 6 flaw is shown in Fig. 5.10 where the elongated inclusions are oriented in a fan like pattern. Also seen in Fig. 5.10 are spot inclusions that are probably sand particles.

A summary of the flaws observed in the six fractograph overviews is provided in Table 5.10 where the flaw identification number, the flaw type, the fractograph flaw parameters, and the actual flaw parameters are recorded along with the fracture specimen in which the flaw was found. The flaw identification number is simply an arbitrary number assigned to identify the flaw on each fractograph. The flaw type characterizes the flaw according to the previously defined six categories. The fractograph flaw parameters are the dimensions of the flaw as measured from the fractograph which are converted into the actual flaw dimensions of column 5 using the conversion factors of Table 5.11. These conversion factors simply account for the magnification of the particular fractograph.

5.2.7 The Chemical Analysis

The results of the chemical analysis, carried out to investigate the variation in concentration of the constituent elements throughout the casting, are presented in Table 5.12. The concentration in percent by weight for the 10 elements investigated is shown for the six samples analyzed. The procedure of the individual analyses as well as the sample locations are given in Section 4.6. The maximum and minimum compositions found for each of the 10 elements and the samples in which these extrema occurred are presented in Table 5.13. Furthermore, the percent variation between the maximum and minimum concentrations with the maximum used as the reference is also presented in Table 5.13.

The composition of the constituent elements at the six locations investigated generally fell within the limits specified for SAE 4340. However, there were a number of exceptions such as the carbon composition of sample 24 at 0.31% (Table 5.12) which was substantially lower than the lower carbon limit of 0.38% specified for SAE 4340 (Table 4.1). Moreover, the manganese composition of sample 11 at 0.81% was marginally higher than the upper limit of 0.80% specified for SAE 4340. The largest variation with respect to the composition limits specified for SAE 4340 was that of the silicon composition of the casting which was almost double the specified maximum composition. This was not detrimental to the casting since silicon functions as a desulphurizer and also increases the wear resistance of the alloy. Nevertheless, special care would have to be taken in welding this alloy since the localized welding heat could cause surface cavities and weld porosity if the silicon composition exceeded 0.35% [25]. In brief, the elemental compositions of chromium, molybdenum, nickel, phosphorus, and sulphur

were well within the compositionsl limits of SAE 4340.

The variation of the composition of chromium, copper, manganese, molybdenum, nickel, and silicon throughout the six sample locations was acceptable with all variations less than 10%. Considering the size and shape of the gear casting, this degree of variation was expected. However, there were four elements including aluminum, carbon, phosphorus, and sulphur that exhibited serious variations of 22.7%, 20.5%, 25.0%, and 44.8% respectively. Although the variations were quite large, the maximum compositions of phosphorus and sulphur were not high enough to be critical. For instance, the maximum sulphur composition of 0.029% was far below the 0.06% level above which welding problems would occur. Likewise, the maximum composition of phosphorus at 0.024% was also below the level 0.035% above which weldability quickly decreases. It is important to maintain the chemical composition such that the casting has excellent weldability since weld repair of the casting might be required sometime during the manufacturing process. On the other hand, the minimum carbon composition of 0.31% found in block 24 could be cause for concern since the sample was taken from the outside face of the gear where the teeth would normally be machined. Any low carbon compositions in this area would cause areas in which the hardenability of the steel would be decreased making the gear susceptible to wear and a possible premature failure.

5.3 THE DEFECT HISTOGRAM

The principles on which the defect histogram is based are be described in this section followed by the presentation of the defect histograms obtained from the radiographic, ultrasonic, and microscopic

inspections. A combined histogram based on the ultrasonic and radiographic results is also presented. Furthermore, the orientation of the defects discovered in this investigation is discussed.

5.3.1 The Formation of the Defect Histogram

At the outset of this discussion it must be realized that the primary goal of this investigation was to utilize destructive and nondestructive testing techniques to evaluate and characterize internal casting defects. A detailed statistical evaluation of the actual testing techniques was not a goal of this investigation. As a result, it is assumed that the results of the nondestructive inspections are absolute. For instance, it is assumed that a defect is present where indicated by either the radiographic or ultrasonic inspection. Furthermore, it is assumed that no defects are present if not indicated by the inspection methods. Although this is not totally correct since nondestructive tests sometimes indicate defects where none are present and vice-versa, certain simplifying assumptions must be made as in most other engineering problems. In fact, the performance of a particular inspection process is extremely difficult and time consuming to evaluate since nondestructive testing results are operator dependent and can vary day to day as the alertness of the operator changes.

With this assumption of absolute test results, the defect histogram is fabricated in the following manner. First, the nondestructive (or destructive) test results are evaluated and a finite number of defect categories are selected. The entire sample of defect indications are then classified with respect to the previously selected categories. Next, the size of the base element area is selected to accommodate the

largest flaw indication. Moreover, this unit area, once selected, must satisfy the requirement that the sum of the probabilities of occurrence of the entire group of defect classes is less than or equal to 1. The total area covered in the test is divided by the size of the base element to yield the number of base elements inspected. Each class of flaw indication is counted to provide the total number of occurrences of each defect class. This number is then divided by the number of unit areas inspected to provide the probability of the particular class of defect occurring in the base element or area unit. Finally, the results are presented in a conventional histogram with the exception that the probability of no defect occurring is not shown.

5.3.2 The Radiographic Inspection Defect Histogram

The results of the radiographic inspection, summarized in Section 5.2.2, yielded five categories of defects as shown in Table 5.2. Although the radiographic inspection provides a compressed two dimensional view of the internal volume of a particular block undergoing inspection, only the projected area (the actual area of the X-ray of the block) is used in the construction of the defect histogram. This X-ray area (or surface area of the block directly exposed to the incident radiation) is used since the radiographic inspection provides two dimensional defect images.

The surface area radiographed is calculated by summing the area of the faces of the blocks exposed to the incident radiation in the various X-ray directions. In brief, 11,632 cm^2 of steel sample block area was exposed as summarized in Tables 5.14 and 5.15. A 1.0 cm x 1.0 cm base element with an area of 1.0 cm^2 was selected since it would easily

accommodate the largest indicated defect with an area of 0.6 cm^2 within its boundary. Moreover, a 1.0 cm x 1.0 cm unit element was also quite convenient and satisfied the constraint that the sum of the resultant probabilities be less than or equal to 1. With the size of the base element as 1.0 cm^2, this meant that 11,632 base elements were inspected radiographically.

The number of occurrences of each of the five flaw types found during the radiographic inspection are recorded in column 2 of Table 5.16. The probability of occurrence is then found by dividing the number of occurrences by the number of base elements inspected. Finally, these probabilities are graphed in the defect histogram of Fig. 5.11. As seen from the histogram, type 3 flaws are the most common with a probability of occurrence of 2.15 x 10^{-3} in a 1.0 cm x 1.0 cm area. Type 1 flaws are the scarcest with a probability of occurrence of 1.72 x 10^{-4}.

5.3.3 The Ultrasonic Inspection Defect Histogram

The defects discovered with the ultrasonic inspection were classified into the eight categories of Table 5.6 as described in Section 5.2.4. In a similar manner as the radiographic inspection, the ultrasonic inspection provided two dimensional indications as the entire volume of a particular block was inspected from one face. Thus, the sample space inspected was based on the area of the face which was scanned. The total area scanned for the blocks conforming to the three size categories is provided in Table 5.17, while the area scanned for the odd-sized blocks is presented in Table 5.18. The total area scanned in the ultrasonic inspection was 17,570 cm^2.

The largest flaw found during the ultrasonic inspection was 0.476 cm by 1.0 cm and rectangular round ended. Thus, a 1.0 cm x 1.0 cm base element was used again to calculate the number of elements inspected. This base element could easily accommodate the largest flaw discovered via ultrasonic inspection, would satisfy the restriction on the resulting probabilities, and would facilitate the comparison between the radiographic results. With this 1.0 cm^2 base element, 17,570 elemental areas were ultrasonically inspected.

The number of occurrences of each of the eight flaw types arising from the ultrasonic inspection are summarized in column 2 of Table 5.19. The probability of occurrence of these flaw types, obtained by dividing the number of occurrences by the number of elemental areas inspected, is provided in column 3 of the same table. These probabilities are graphed to provide the defect histogram in Fig. 5.12. The last five ultrasonic inspection defect types correspond to the five radiographic inspection defect types. For example, the ultrasonic type 8 is the same as the radiographic type 5, the ultrasonic type 7 is the same as the radiographic type 4, and so on. The ultrasonic and radiographic probability results of these 5 defect types are summarized in Table 5.20 along with the % variation between the two methods.

The variation between the radiographic and ultrasonic probability of occurrence for the last 4 defect types range from 19% to 41%. On initial inspection these values seem large. However, when the subjectiveness involved in interpreting the output of the ultrasonic inspection instrument is taken into account, the probability of occurrence from the two tests are in very good agreement. Yet, this is not true for the first flaw type which exhibits a percent variation

between the ultrasonic and radiographic results of well over 1000. This variation can be attributed to the fact that the size of the defect type is very close to the radiographic inspection detection threshold while not yet near that of the ultrasonic inspection. The ultrasonic inspection is still very sensitive to defects of this size and records many more than the radiographic inspection. As a result, the probability of occurrence achieved through the ultrasonic inspection is much higher than that of the radiographic inspection.

5.3.4 The Microscopic Inspection Defect Histogram

The microscopic inspection provided six types of internal defects as described in Section 5.2.6. In total 91.7 mm^2 of fracture surface was investigated during the test as seen in Table 5.21. The largest defect discovered in this section of the investigation was a 0.073 mm^2 shrink defect. Thus, a 0.316 mm x 0.316 mm base element with a 0.1 mm^2 area was selected. This element was large enough to accommodate the largest flaw encountered and satisfied the requirement that the sum of the resulting probabilities be less than 1. This 0.1 mm^2 unit area selected led to 917 individual base elements viewed under the SEM.

The number of occurrences of the six flaw types is summarized in the second column of Table 5.22 and, using the number of base elements viewed, is converted into the probability of occurrence shown in column 3. The resulting defect histogram is shown in Fig. 5.13. The probability of occurrence of the flaws discovered through the microscopic inspection is in general 100 times larger than the probability of occurrence found in the ultrasonic inspection. Unfortunately, there was an insufficient number of flaws to compare the

ultrasonic and microscopic results. The largest flaws discovered from
the microscopic inspection were just below the lower threshold limit of
the ultrasonic inspection. However, the absence of any large flaws in
the microscopic inspection does not necessarily mean that the ultrasonic
inspection was providing false indications. This absence of large flaws
in the microscopic inspection can be explained by the small amount of
fracture surface actually investigated and the fact that the probability
of occurrence of such flaws (obtained from the ultrasonic inspection)
was also small. It is understandable no flaws large enough to overlap
with the ultrasonic indications were discovered.

5.3.5 The Combined Defect Histogram

The defect characterization provides a quantitative indication of
the quality of the ring gear casting and, more importantly, provides the
size and shape of the internal casting defects on which the FEM
calculation of the stress concentration factor, K_t, is based. To
facilitate the calculation of K_t and provide a unified set of results
for the defect characterization, the radiographic inspection defect
histogram and the ultrasonic inspection defect histogram are combined to
produce a single histogram. This histogram incorporates the entire set
of defect types found in the two tests. The microscopic inspection
results are intentionally omitted from the combined defect histogram
since they are already accounted for in the experimental evaluation of
the fatigue properties. The microdefects in the casting, also present
in the fatigue specimens machined from casting, provide locations from
which fatigue cracks can be initiated and propagate until failure. A
high occurrence of these microdefects in the casting and thus in the

102

fatigue specimen will provide many locations for fatigue crack initiation and, in general, lead to a lower fatigue life. Moreover, large microdefects will provide higher stress concentrations in the fatigue specimens leading to earlier fatigue crack initiation and a lower fatigue life as compared to specimens containing smaller microdefects. Consequently, the effect of these small defects must not be incorporated into the calculation of the stress concentration factor since they have already been taken into account in the fatigue properties.

The combined defect histogram is shown in Fig. 5.14. A summary of the eight defect classes, comprising the combined defect histogram and their equivalent radiographic and ultrasonic inspection defect classes, is provided in Table 5.23. The probability of occurrence in the combined defect histogram for the defect classes common to both the radiographic and ultrasonic inspections was taken as the highest value yielded by each of the test methods. For example, with respect to the combined defect histogram defect class 8 (radiographic inspection defect type 5 and ultrasonic inspection defect type 8), the probability of occurrence was 7.74×10^{-4} via the radiographic inspection while the ultrasonic yielded a probability of occurrence of 6.26×10^{-4}. Thus, in the combined defect histogram, the probability of occurrence of defect type 8 is taken as 7.74×10^{-4}. This process of selecting the largest probability of occurrence yields a somewhat conservative combined defect histogram while any attempt to average the probabilities of the two test methods would have been meaningless.

5.3.6 The Orientation of the Defects

The defect characterization will not be complete unless the defect orientation is discussed. First, in the radiographic and ultrasonic inspection of the cast steel blocks, many blocks exhibited defect indications in one direction; however, when the inspection of the same block was carried out in a perpendicular direction very few defects were found. Many internal flaws discovered by the two test methods in one direction remained undetected in the second perpendicular direction. This occurrence is highlighted in the radiographic inspection of sample blocks 22, 26, 43, 44, and 64 (Appendix F) which exhibited flaws only in one of the X-ray directions. This phenomenon is also seen in the ultrasonic inspection of blocks 14, 21, 23, 32, 33, 62, and 66 (Appendix G). Even in blocks that exhibited defects in the two radiographic inspection directions and in the three ultrasonic inspection directions it was extremely rare that a particular flaw was indicated in more than one inspection direction. This evidence leads one to conclude that the flaws discovered in the nondestructive tests are planar.

Since the flaws are planar in shape, their orientation can be determined from either the X-ray direction in the radiographic inspection or from the sample block face scanned in the ultrasonic inspection. For example, it is seen from Fig. 4.13 and Fig. 4.2 that X-ray direction 1 is along the radial direction of the ring gear. Thus, flaws discovered in this direction lie in planes that are tangent to the gear surface and perpendicular to the radial lines. Such flaws will be defined as direction 1 flaws. Flaws discovered in X-ray direction 2 will lie in planes that are perpendicular to the gear face and parallel to the gear edges. Such flaws will be defined as direction 2 flaws.

The ultrasonic inspection results can also be classified with respect to their orientation. The ultrasonic inspection face A was intentionally selected so that the ultrasound beam in inspection from face A would be parallel to the radiation beam of X-ray direction 1. Similarly, the ultrasonic inspection face B was selected so that the ultrasound beam would be parallel to the radiation beam of X-ray direction 2. Therefore, flaws discovered via ultrasonic inspection from face A will be direction 1 flaws while flaws discovered from face B will be direction 2 flaws. The flaws discovered via ultrasonic inspection from face C will lie in planes that are perpendicular to the gear face and parallel to the gear ends. These flaws will be defined as direction 3 flaws. For clarity, the three flaw directions are summarized in Fig. 5.15.

The orientation of the flaws discovered in the two nondestructive tests can be obtained directly from Tables 5.3 and 5.7. Table 5.3 provides the X-ray direction for the flaws discovered in the radiographic inspection, while Table 5.7 provides the face being scanned for the flaws discovered in the ultrasonic inspection. Using Table 5.3, the number of flaws recorded in the two X-ray directions are counted and are presented in Table 5.24 for the five radiographic flaw types. Similarly, the ultrasonic results in Table 5.7 are classified with respect to the scanned face for the 8 ultrasonic flaw types. These results are summarized in Table 5.25.

The results of Table 5.24 and 5.25 are converted into percentages and summarized in Table 5.26 where the percentage direction 1, percentage direction 2 and percentage direction 3 are provided for the 8 combined histogram flaw types for both the radiographic and ultrasonic

inspections. As seen from Table 5.26, the first three flaw types tend to occur in direction 1 more than directions 2 or 3. Upon initial comparison, the radiographic and ultrasonic results for the fourth flaw type are not in agreement at all. However, the radiographic results can be ignored since only two flaw indications appeared with this test. Thus type 4 flaws also occurred more frequently orientated in direction 1. The radiographic and ultrasonic results for type 5 and 8 flaws generally agree in that the majority of these two types were orientated in direction 2. However, the radiographic and ultrasonic results do not agree at all for the type 6 and 7 combined histogram flaws. This discrepancy can be explained by the fact that only two directions were radiographically inspected.

In any event, the small flaws tended to be oriented in direction 1, while the larger flaws tended to be orientated in direction 2, although there were discrepancies here. However, the casting process is very complicated with many variables that can be purposely or inadvertently changed and cause the defects to occur in a radically different orientation than the ones encountered in this investigation. Accordingly, it would be safer to use the orientation of the defect which would produce the largest stresses in the FEM analysis to the determine stress concentration factor.

5.3.7 Comparison of Radiographic and Ultrasonic Inspection Results

The radiographic inspection results (Appendix F) and the ultrasonic inspection results (Appendix G) are in good agreement. There are a number of flaws indicated by both the radiographic and ultrasonic inspections. In particular, of the 55 radiographic flaw indications

documented in Appendix F, 69.1% were also indicated in the ultrasonic inspection. The fact that all of the radiographic indications were not .detected in the ultrasonic inspection can be attributed to human error and the planar character of the flaws and their location with respect to the scanning surface. For example, a planar flaw parallel to and close to the scanning surface would be masked by the characteristic grass-like pattern on the ultrasonic inspection unit's screen due to the transducer-couplant-scanning surface interface. This interference pattern occurring just after the scanning surface pulse was explained in Section 4.4.3.1. Furthermore, it would be impossible to pick up the flaw during the inspection of the two remaining perpendicular directions because the edges of the two dimensional flaw would not affect the ultrasonic beam to any appreciable degree. Thus, the flaw would not be discovered in the ultrasonic inspection.

Conversely, of the 306 ultrasonic flaw indications only 38, or 12.4%, were indicated by the radiographic inspection. This discrepency can be attributed to the fact that the flaws recorded by the ultrasonic inspection and missed by the radiographic inspection were very small. These small defects would not provide enough of a density variation to significantly affect the intensity of the penetrating radiation as recorded on the photographic film. Infact, the three smallest flaw categories discovered from the ultrasonic inspection were missed completely by the radiographic inspection. However, if the flaws which were below the detection threshold of the radiographic inspection (ie. the first 3 ultrasonic inspection flaw types) were ignored, then 55.4% of the 65 remaining ultrasonic indications would be indicated in the radiographic inspection results. This variation can be explained

107

because only two perpendicular directions were radiographed while three

perpendicular directions were ultrasonically inspected.

CHAPTER 6

CONCLUSIONS

6.1 CONCLUDING REMARKS

The objective of this thesis was to characterize the internal casting defects of a cast steel ball mill ring gear. The conclusions resulting from the analysis of the data obtained in this investigation can be summarized as follows:

1. The milling machine sectioning procedure used in this investigation proved to be an unsatisfactory method in the search for defects since it tended to displace metal over any exposed flaws.

2. The radiographic inspection of the steel sample blocks revealed the presence of internal casting defects. Five types of flaws were discovered in the X-rays. Moreover, this radiographic inspection technique did not indicate flaws less than 0.2 cm in diameter.

3. The ultrasonic inspection of the sample blocks revealed 8 internal flaw types down to a diameter of 0.06 cm. This nondestructive inspection method was able to detect much smaller flaws than the radiographic inspection of the sample blocks but did not provide the flaw shape as did the radiographic inspection.

4. The radiographic inspection of the fracture specimens indicated flaws in the same size range as those of the ultrasonic inspection. Furthermore, these X-rays showed the presence of gas porosity and secondary shrinkage type defects.

5. The radiographic and ultrasonic inspection of the sample blocks and the radiographic inspection of the fracture specimens provided evidence that the internal flaws were planar, or two dimensional,

in character.

6. The radiographic and ultrasonic test results were combined to produce a defect histogram with 8 flaw categories. These flaw categories contained both circular and rectangular round ended planar flaws with the probability of occurrence in a 1 cm^2 area ranging between 7.74×10^{-4} and 4.78×10^{-3}.

7. The nondestructive tests performed on the steel sample blocks including the radiographic and ultrasonic inspection were in good, but not total agreement. Inbrief, 69.1% of the radiographic inspection flaw indications were indicated in the ultrasonic inspection results. Furthermore, 55.4% of the ultrasonic flaw indications capable of being detected in the radiographic inspection were indicated in the X-ray results.

8. The microscopic inspection using the SEM to view 8 fracture surfaces provided 6 categories of microscopic defects including porosities, shrinkages, and inclusions. The probability of occurrence in a 0.1 mm^2 area for these flaws ranged from 4.0×10^{-3} to 1.67×10^{-1}.

9. In general, the composition of the constituent elements at the six locations investigated fell within the limits specified for SAE 4340. The variation of the composition of chromium, copper, manganese, molybdenum, nickel, and silicon was less than 10%. However, aluminum, carbon, phosphorus, and sulphur exhibited compositional variations in the six sample locations from 25.0% to 44.8%.

6.2 PROPOSALS FOR FURTHER RESEARCH

The results of this investigation have shown that the ring gear investigated was a relatively high quality casting. However, it must be remembered that the casting process incoporates many variables that can be purposely or inadvertently changed to affect the casting quality. Therefore, a number of sample blocks, comparable in size to the sample blocks of this investigation, should be designed into each ring gear casting. Prior to the casting upgrading process, these blocks would be cut from the blank ring gear and analysed for defects. This would provide a more accurate defect characterization as a result of the larger sample space.

This investigation has focussed on and implemented the standard ultrasonic pulse-echo inspection method commonly employed in industry. There is a need to develop this test further and link it with a computer program so that a three dimensional image of a particular defect could be constructed using the results of an ultrasonic inspection in three orthogonal directions.

Moreover, there is a need to investigate other methods to calculate the probability of occurrence of the flaws discovered through the inspection methods.

Finally, a micro X-ray analysis and sectioning procedure incorporating a polishing operation might yield more information about the internal casting defects. However, these tests would be expensive since large amounts of machining would be required to provide dependable results based on a sample space of sufficient size.

REFERENCES

1. Rolfe, S.T. and Barsom, J.M., "Fracture and Fatigue Control in Structures", Prentice-Hall, Inc., Englewood Cliffs, New Jersey, (1977).

2. Irwin, G.R., "Fracture Dynamics", Trans. ASM, Vol. 40A, pp. 147-166, (1948).

3. Wei, R.P., "Contribution of Fracture Mechanics to Subcritical Crack Growth Studies", in "Historical Developments and Applications of Linear Fracture Mechanics Theory", eds. G.C. Sih, R.P. Wei, F. Erdogan, Envo Publishing Co. Inc., pp. 287-302, (1975).

4. Provan, J.W., Chawla, U.S., Carmel, Y. and Hamilton, P.H.B., "On a Predictive Fatigue Crack Initiation Reliability for Large Steel Castings", in "Defects, Fracture and Fatigue", eds. G.C. Sih, J.W. Provan, Martinus Nijhoff, pp. 399-408, (1983).

5. E 186-81, "Standard Reference Radiographs for Heavy-Walled Steel Castings", in Vol. 03.03, "Metallography, Nondestructive Testing", 1984 Annual Book of ASTM Standards, American Society for Testing and Materials, Philadelphia, (1984).

6. A 609-83, "Standard Specification for Steel Castings, Carbon and Low Alloy, Ultrasonic Examination Thereof", in Vol. 01.02, "Ferrous Castings; Ferroalloys; Shipbuilding", 1984 Annual Book of ASTM Standards, ASTM, Philadelphia, (1984).

7. Wessel, E.T., Wilson, W.K. and Clark, W.G., "Development and Application of LEFM in Westinghouse", in "Historical Developments and Applications of Linear Fracture Mechanics Theory", eds. G.C. Sih, R.P. Wei, F. Erdogan, Envo Publishing Co. Inc., pp. 205-251, (1975).

8. Bownes, F.F., "Sand Casting", in "Castings Production Engineering Series", The Macmillan Press Limited, pp. 63-74, (1971).

9. Degarmo, E.P., "Materials and Processes in Manufacturing", 2nd ed., The Macmillan Company, New York, pp. 201-266, (1957).

10. "Steel Castings Handbook", 4th ed., ed. Charles W. Briggs, Steel Founders Society of America, Rocky River, Ohio, pp. 811-840, (1970).

11. Kondic, V., "Metallurgical Principles of Founding", Edward Arnold (Publishers) Ltd., London, pp. 168-210, 211-230, (1968).

12. Beeley, P.R., "Foundry Technology", Halsted Press Division, John Wiley and Sons Inc., New York, pp. 40-78, 180-249, 344-417, (1972).

13. McGonnagle, W.J., "Nondestructive Testing", McGraw-Hill Book Co. Inc., New York, (1961).

14. "Analysis of Casting Defects", 3rd ed., 1st rev., American Foundrymen's Society, Des Plaines, Ill., pp. 3-8, 16-22, 42-51, 56-58, 74-79, 111-116, (1974).

15. Gardner, C.G., "Radiography", in "Nondestructive Testing - A Survey", Technology Utilization Office, NASA, Washington, pp. 63-99, (1973).

16. McGonnagle, W.J., "Nondestructive Testing", McGraw-Hill Book Company Inc., New York, pp. 92-208, 209-278, (1961).

17. McMaster, R.C., "Nondestructive Testing Handbook", Society of Nondestructive Testing, The Ronald Press Company, New York, pp. 14.1-14.48, 19.1-19.49, 20.1-20.51, 22.1-22.16, 23.1-23.16, 24.1-24.42, 26.1-26.17, 43.1-43.53, 46.1-46.27, 48.1-48.31, (1959).

18. Leonard, B.E. and Gardner, C.G., "Ultrasonics", in "Nondestructive Testing - A Survey", Technology Utilization Office, NASA, Washington, pp. 7-26, (1973).

19. Krautkramer, J. and Krautkramer, H., "Ultrasonic Testing of Materials", Springler-Verlog, Berlin, pp. 364-371, (1961).

20. E 142-77, "Standard Method for Controlling Quality of Radiographic Testing", in Vol. 03.03, "Metallography, Nondestructive Testing", 1984 Annual Book of ASTM Standards, American Society for Testing and Materials, Philadelphia, (1984).

21. E 94-77, "Standard Recommended Practice for Radiographic Testing", in Vol. 03-03, "Metallography, Nondestructive Testing", 1984 Annual Book of ASTM Standards, American Society for Testing and Materials, Philedelphia, (1984).

22. Swift, J.A., "Electron Microscopes", Barnes and Noble, New York, pp. 64-83, (1970).

23. Achard, L., "Fatigue Properties of BB225 Steel", D.E.W. Report No. 1296-12, Lachine, Quebec, (1983).

24. E 350-84, "Standard Methods for Chemical Analysis of Carbon Steel, Low-Alloy Steel, Silicon Electrical Steel, Ingot Iron, and Wrought Iron", in Vol. 03.05, "Standards Relating to Chemical Analysis of Metals; Sampling and Analysis of Metal Bearing Ores", 1984 Annual Book of ASTM Standards, ASTM, Philedelphia, (1984).

25. Brumbaugh, J.E., "Welders Guide", Howard W. Sams and Co., Inc., Indianapolis, Indiana, pp. 767-768, (1973).

MATERIAL
DEFECT

CRITICAL ZONE
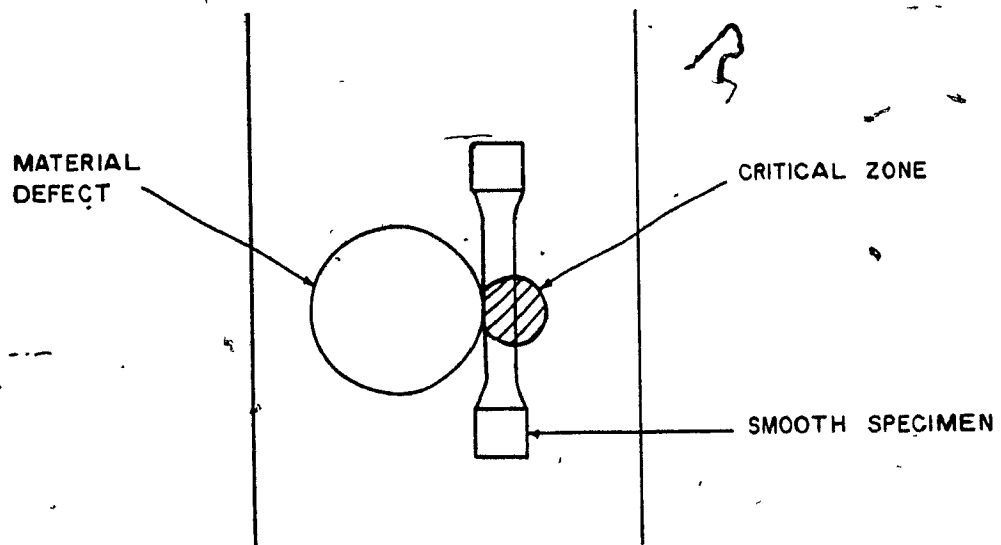
SMOOTH SPECIMEN

Fig.1.1 Smooth specimen representation of a
material filament at a defect.
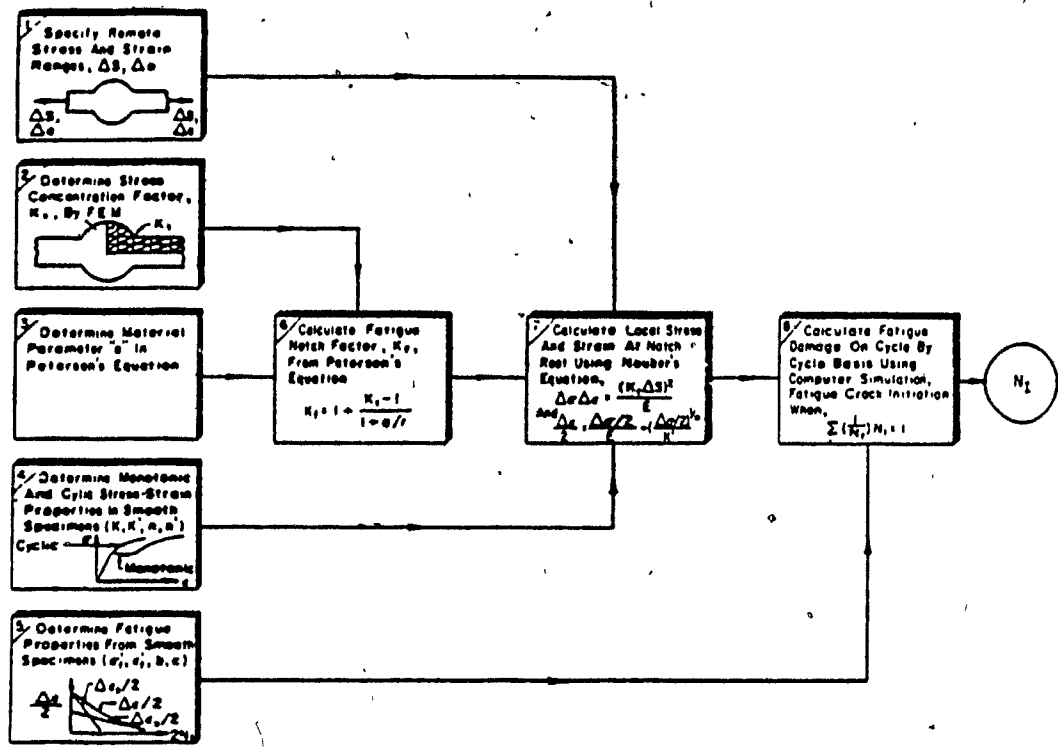
Fig. 1.2 Fatigue crack initiation life diagram.
(Mattos and Lawrence (1977))

SOLID   INTERFACE   LIQUID

MACROSCOPIC HEAT FLOW REQUIRED
FOR LIQUID TO CRYSTALLIZE

T_S q_L T_L

T_S - TEMPERATURE OF THE SOLID

T_L - TEMPERATURE OF THE LIQUID

q_L - LOCAL LATENT HEAT OF
CRYSTALLIZATION
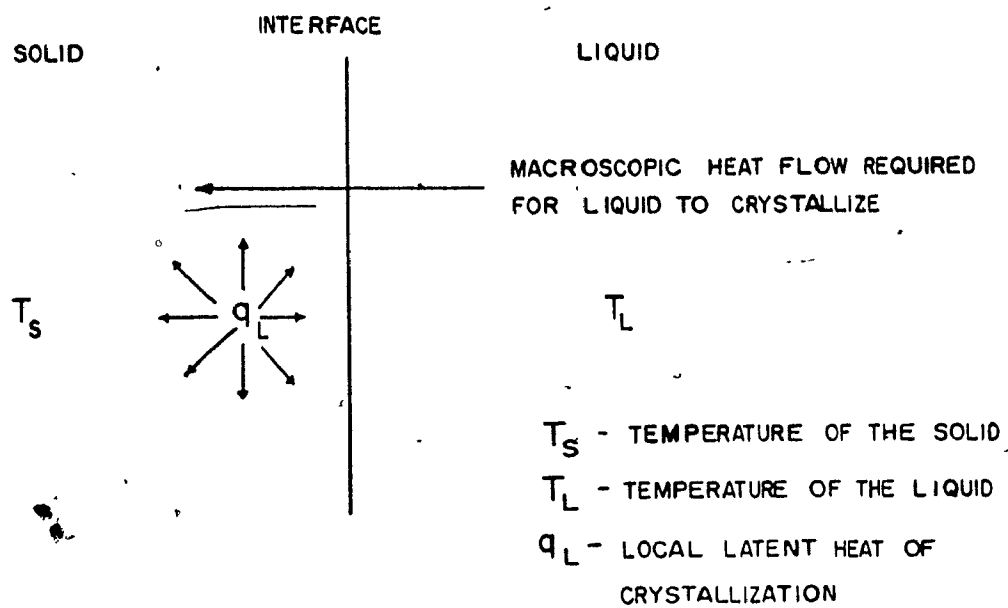
Fig. 2.1   Crystallization heat flow.

INTERFACE

SOLID   LIQUID

TEMPERATURE

GROWTH DIRECTION
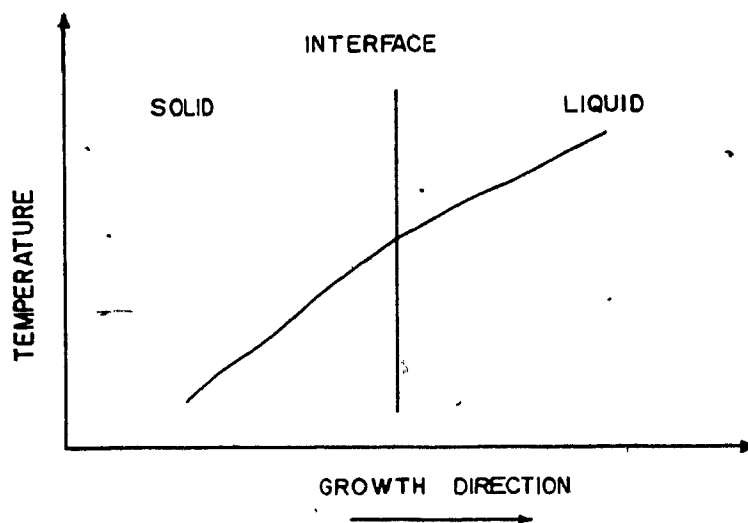
Fig. 2.2   Liquid-solid interface temperature gradient.

116
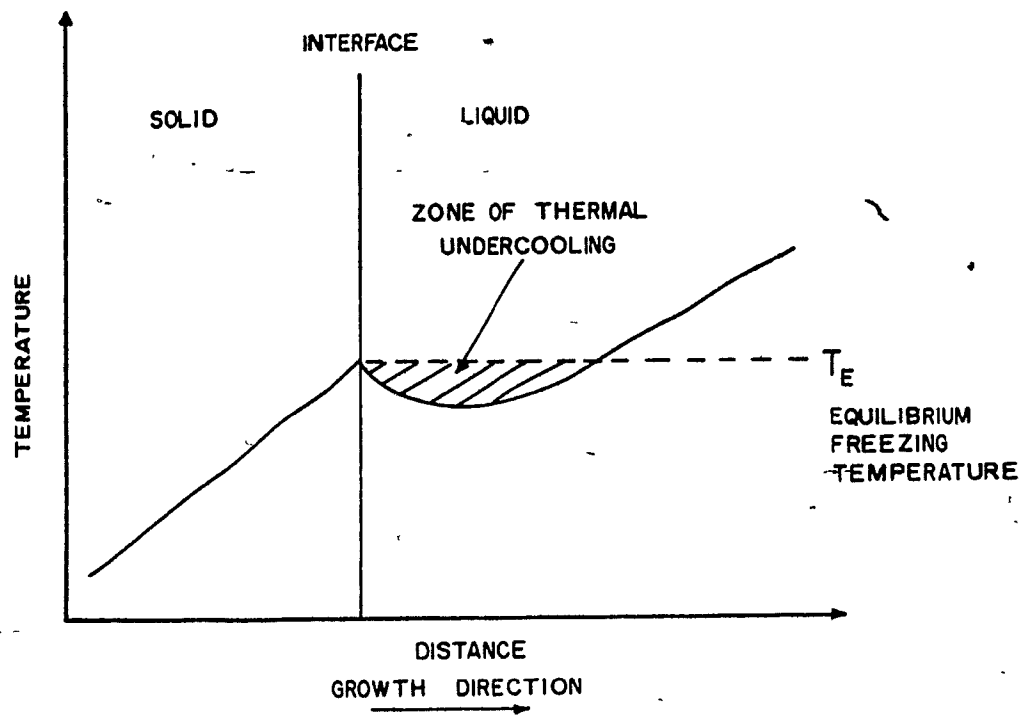
Fig. 2.3   Interface temperature gradient
           and undercooling.
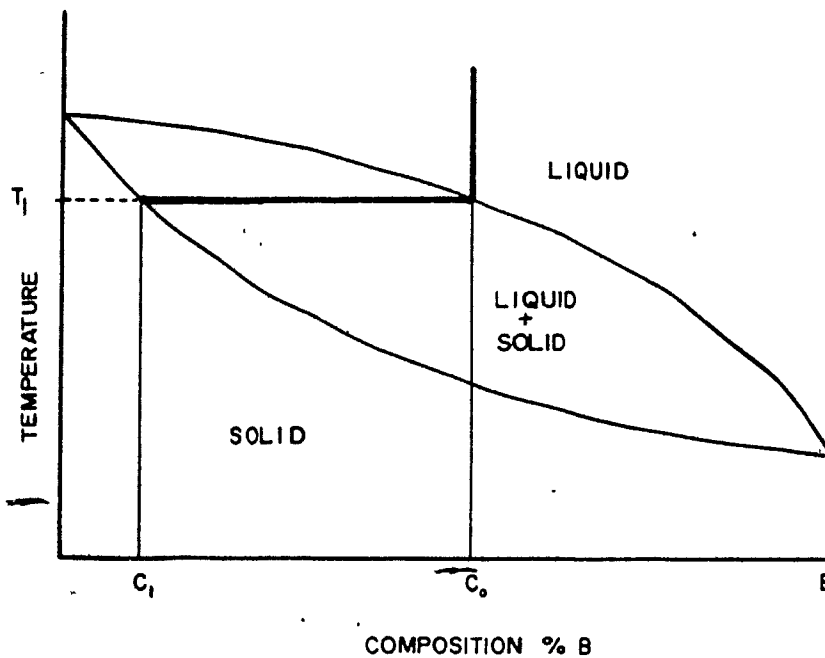
Fig. 2.4   Thermal equilibrium diagram for a
           two metal solid solution.

117
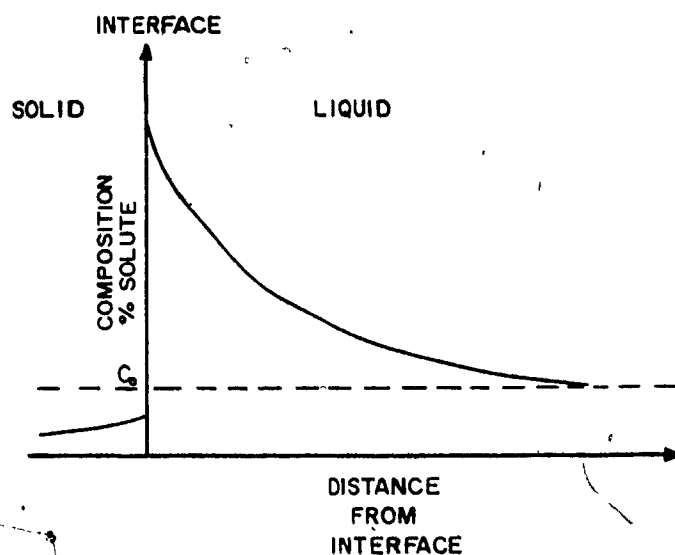
Fig. 2.5 Solute concentration in liquid
ahead of interface under
non-equilibrium conditions.
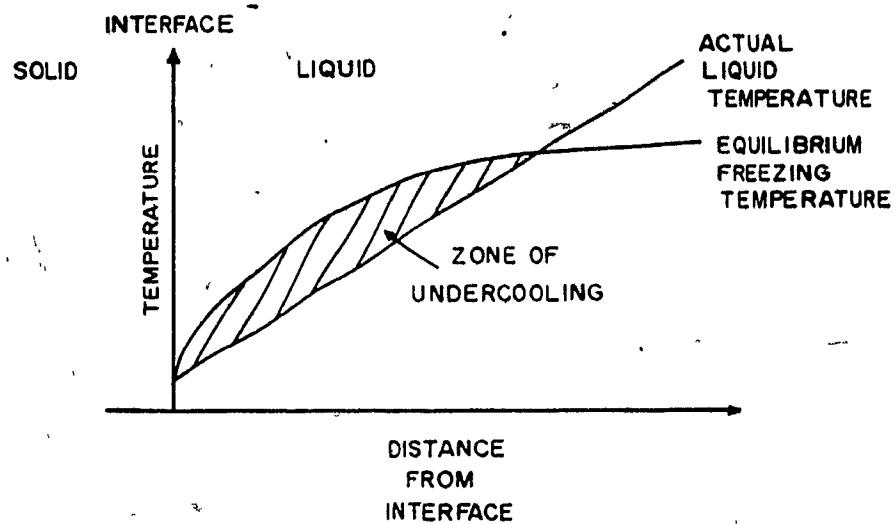
Fig. 2.6 Variation of the freezing temperature
and the zone of undercooling.

118

Mould wall | Liquid metal

Mould wall | Solid | Liquid metal

General growth direction

Direction of macroscopic heat flow
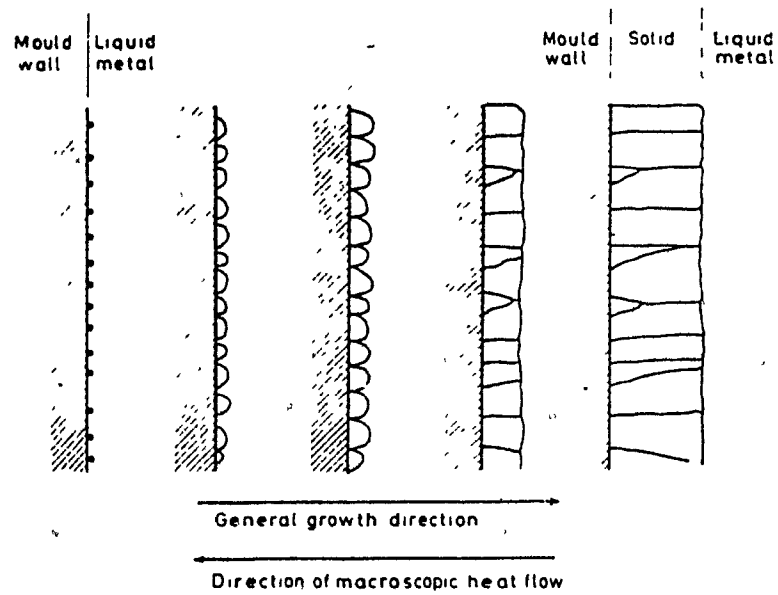
Fig. 2.7 Columnar growth. (Beeley (1972))
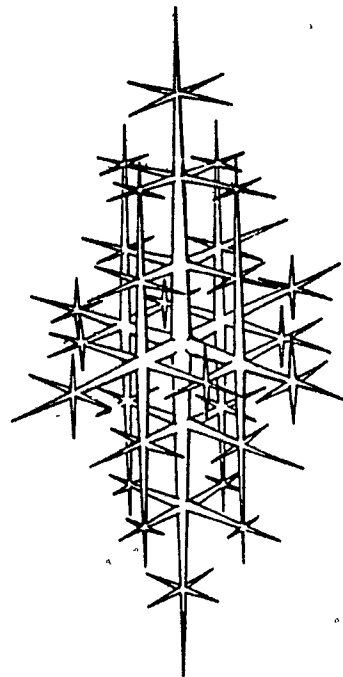
Fig. 2.8 Schematic of a dendrite formation.
(Sylvia (1972))

119
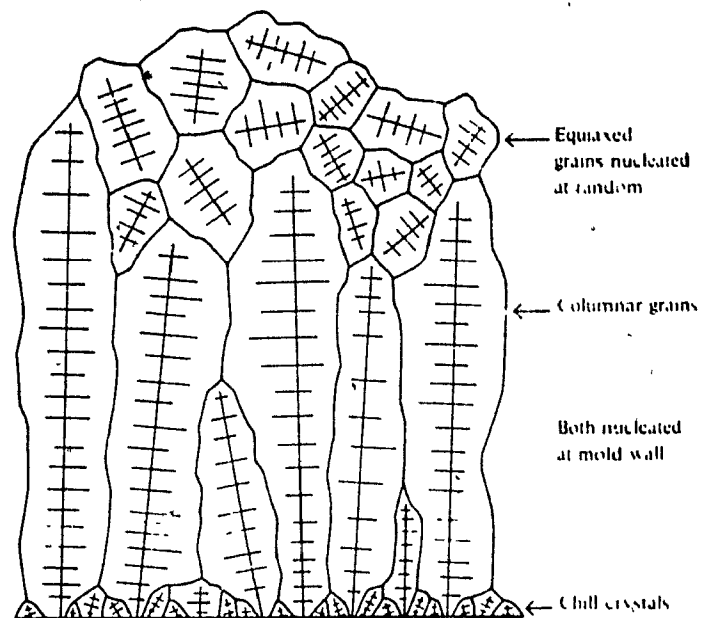
Fig. 2.9 Schematic of cast structure variation.
(Sylvia (1972))
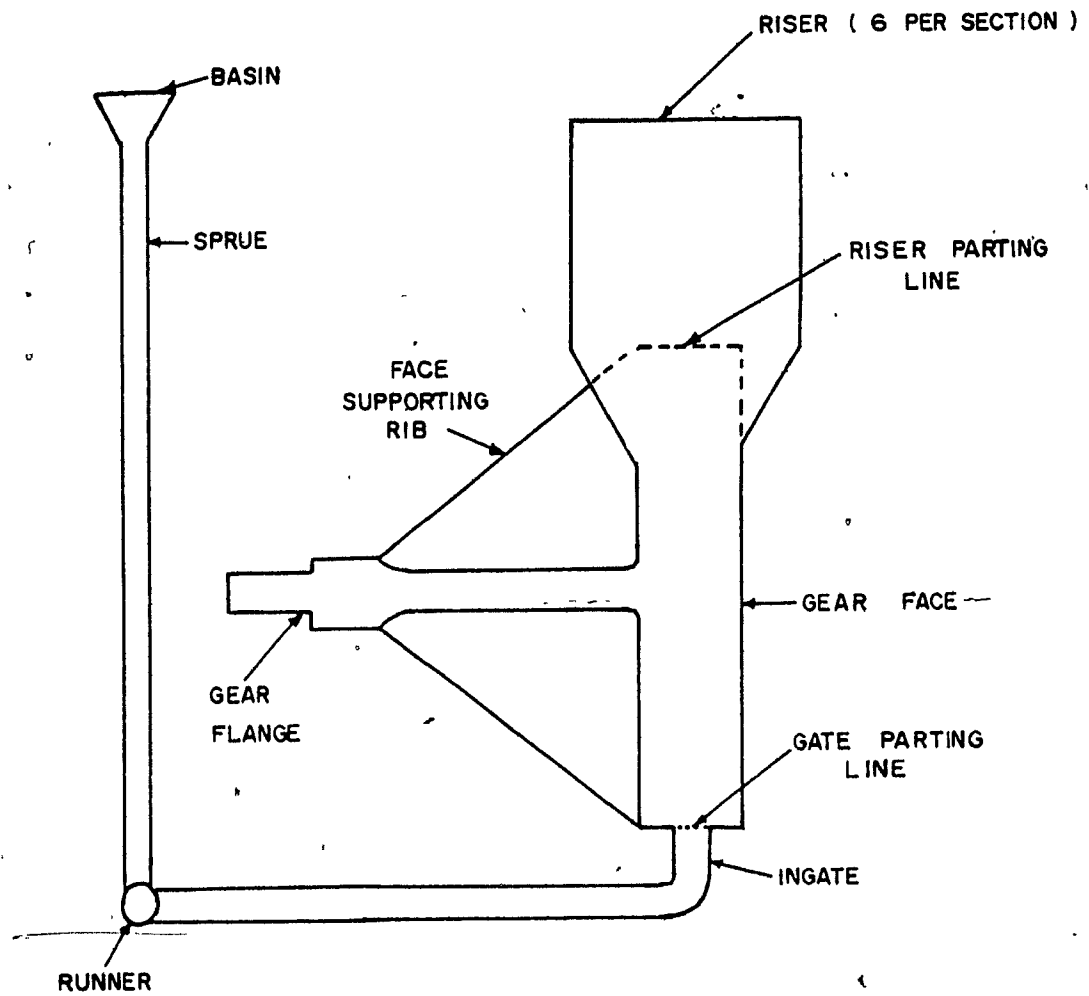
Fig. 2.10 Gating and riser systems
of a sand casting.
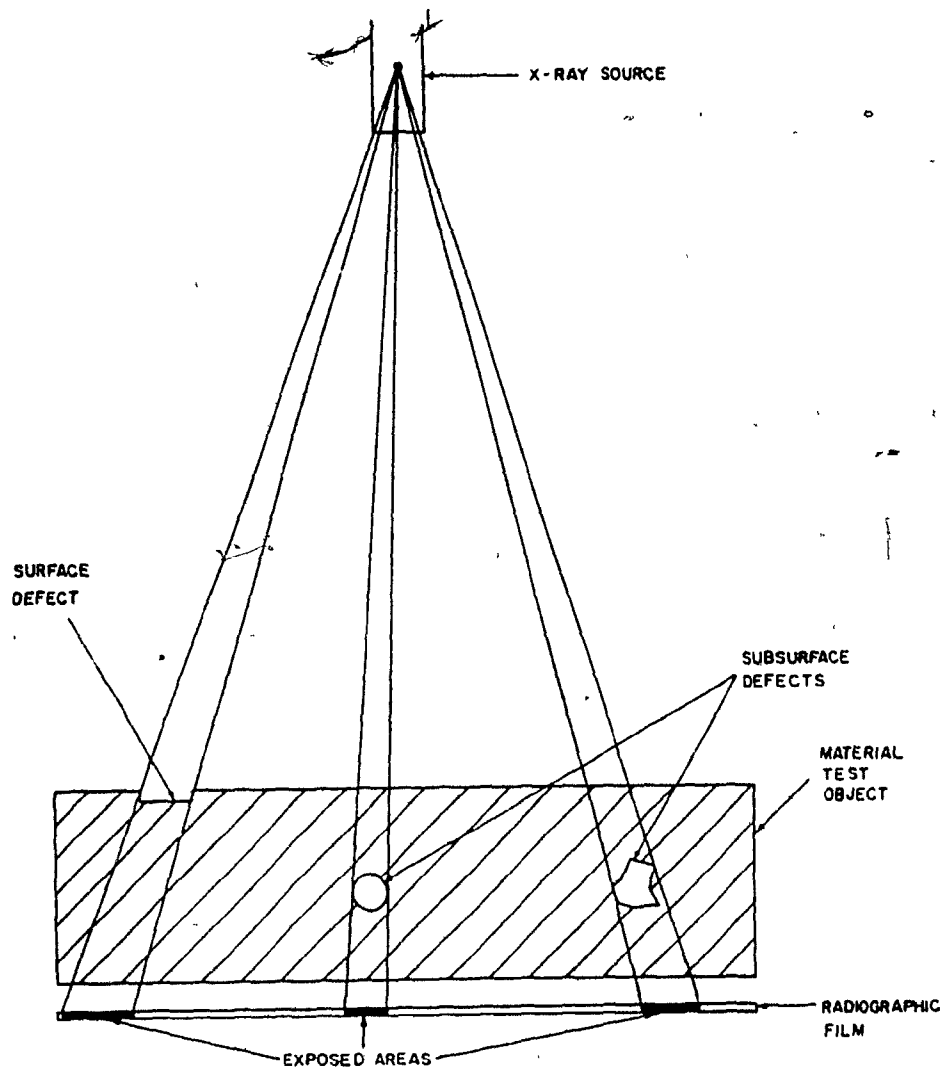
Fig. 3.1 General principle of X-radiography.

PHOTON ENERGY (eV)
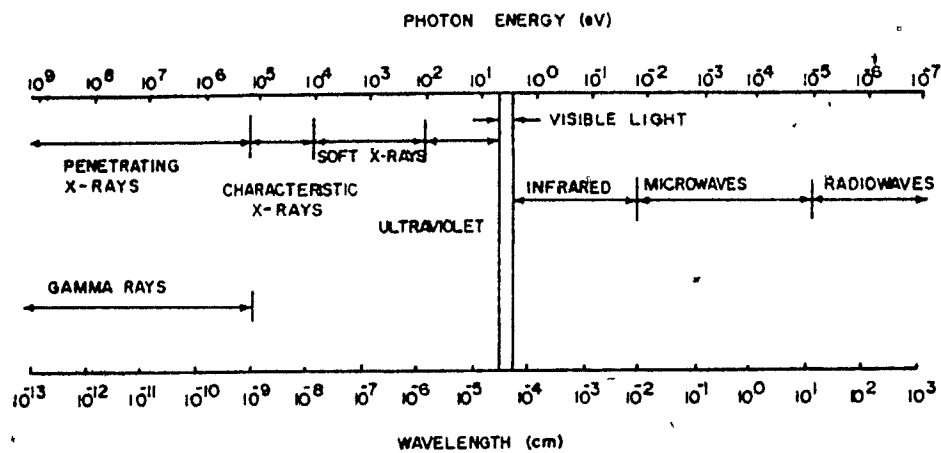
Fig. 3.2   The electromagnetic spectrum.
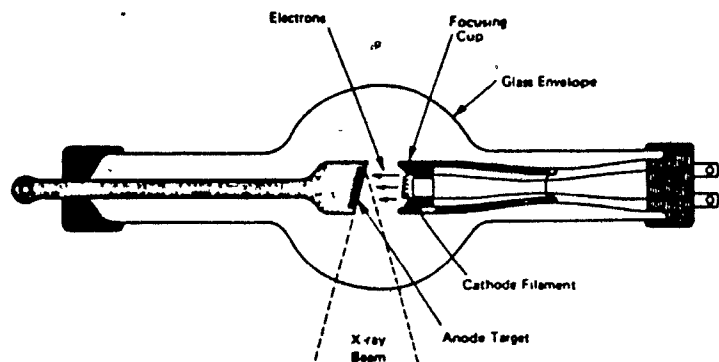
Fig. 3.3   The Coolidge X-ray tube.
(Gardner (1973))
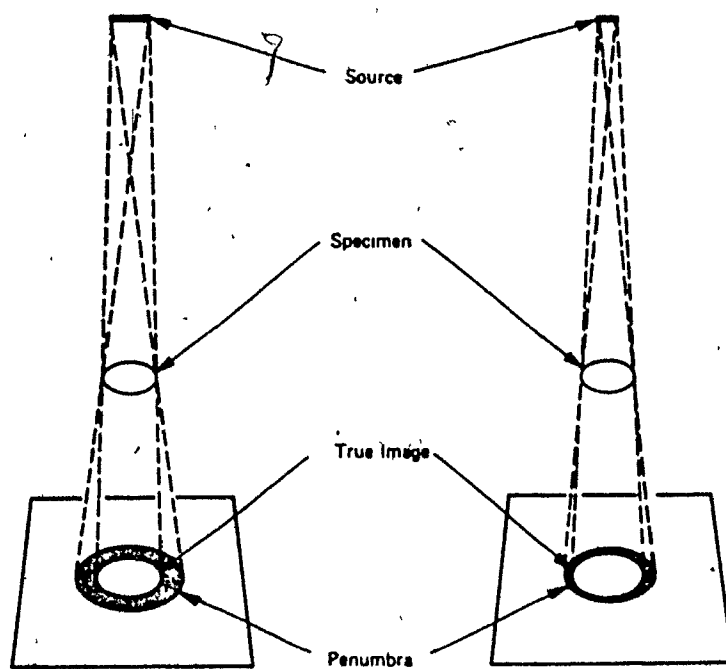
(a) The effect of source size on image sharpness.
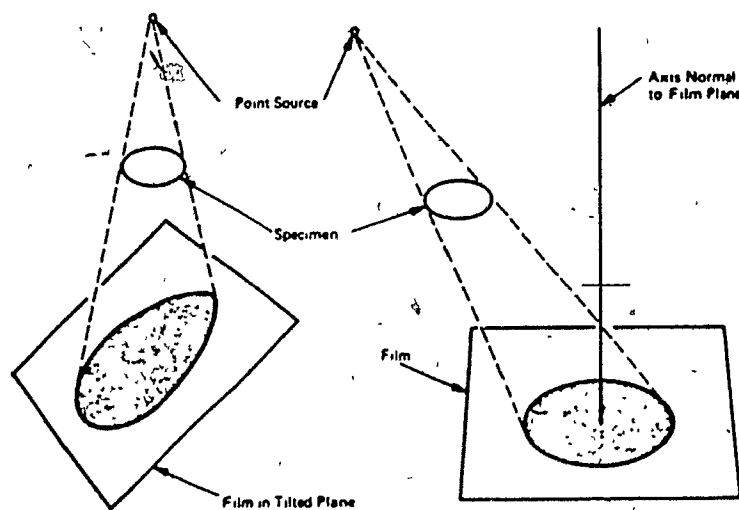
(b) Sources of image distortion.

Fig. 3.4   The effect of source size and
sources of image distortion.
(Gardner (1973))
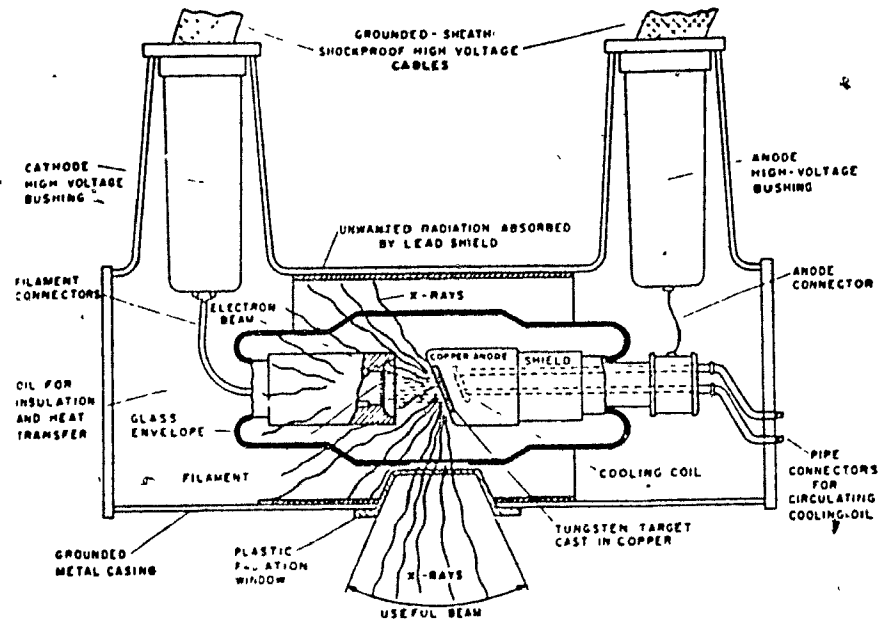
Fig. 3.5   The industrial X-ray tube.
(McMaster (1959))
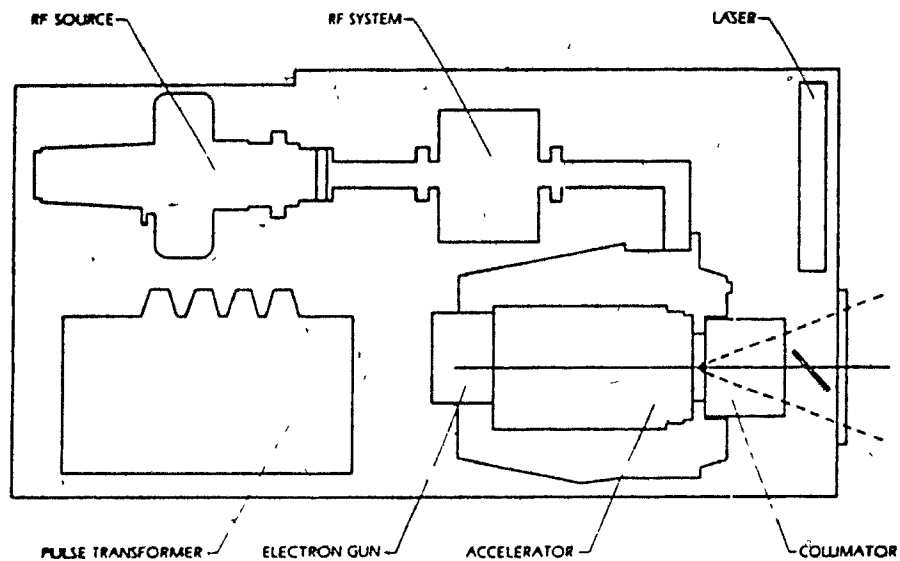
Fig. 3.6   The linear-accelerator X-ray unit.

125
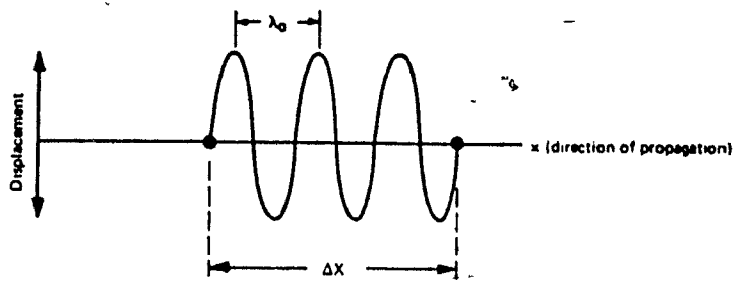
Fig. 3.7 Ultrasound wave packet.
(Leonard and Gardner (1973))
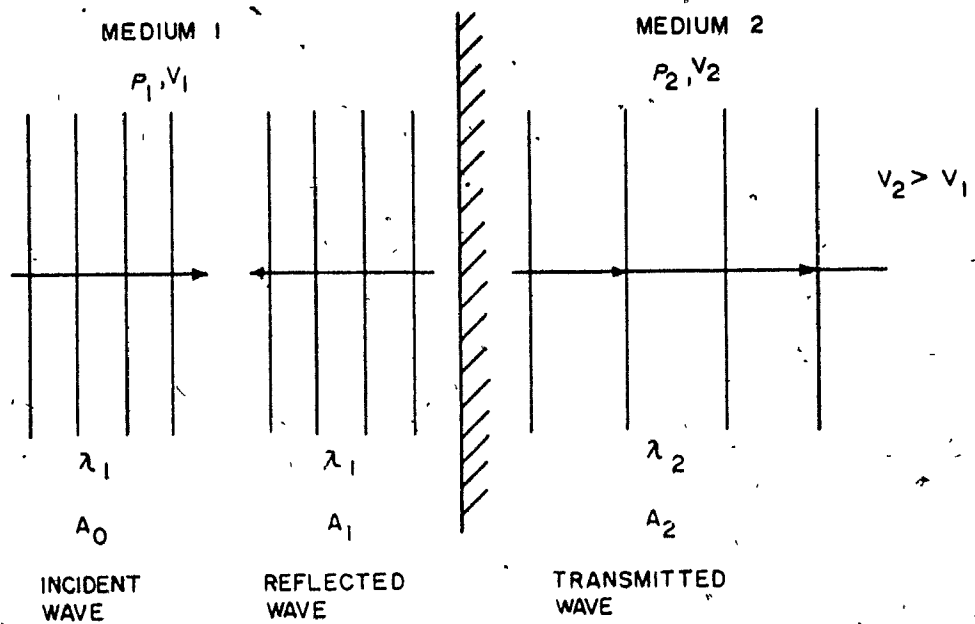
Fig. 3.8 Normal incidence - reflection,
refraction, and mode conversion.
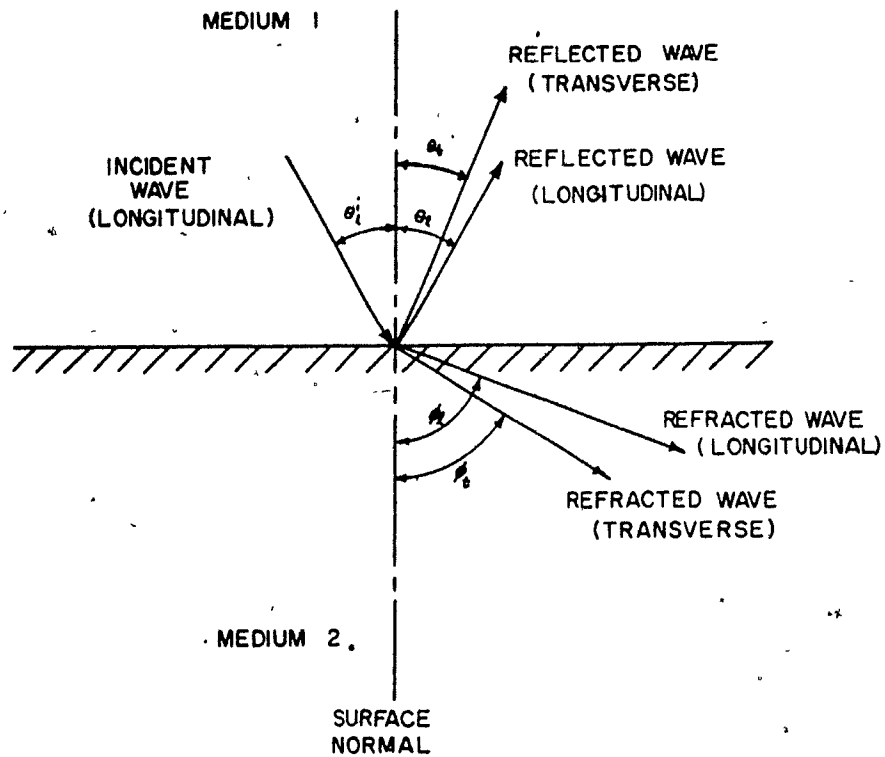
Fig. 3.9 General incidence of a plane harmonic
wave on a plane interface.
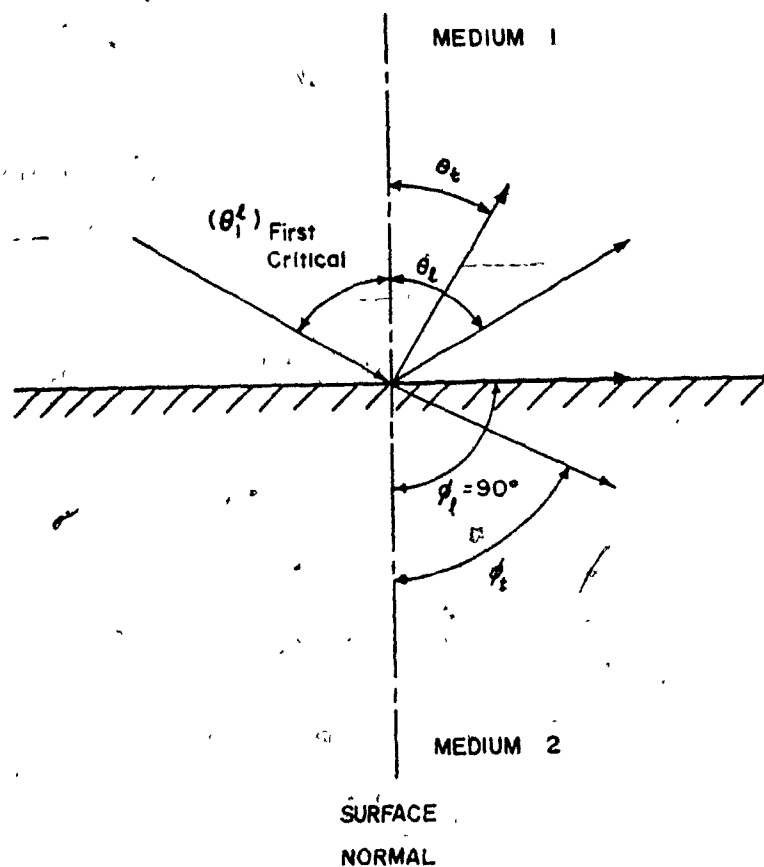
Fig. 3.10 The first critical angle.
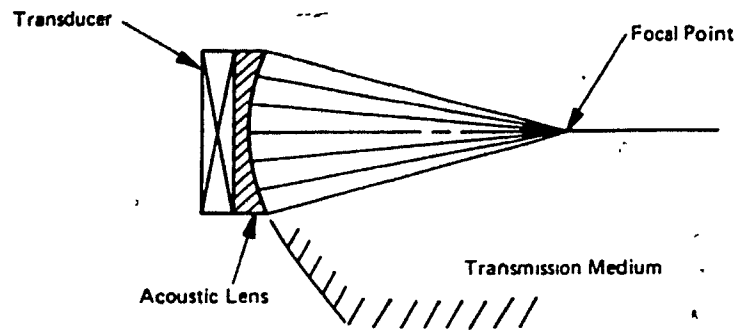
Fig. 3.11 Focussing transducer.
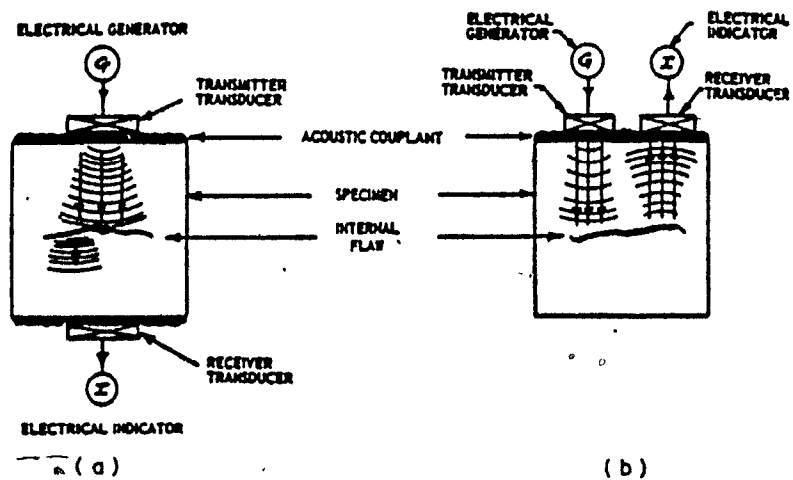
Fig. 3.12 Reflection and transmission ultrasonic inspection techniques.
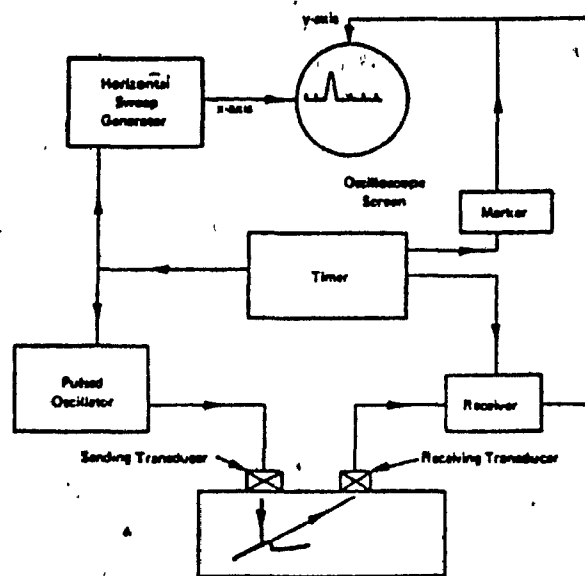
Fig. 3.13   General ultrasonic test unit
            in the A-scan mode.
            (Leonard and Gardner (1973))
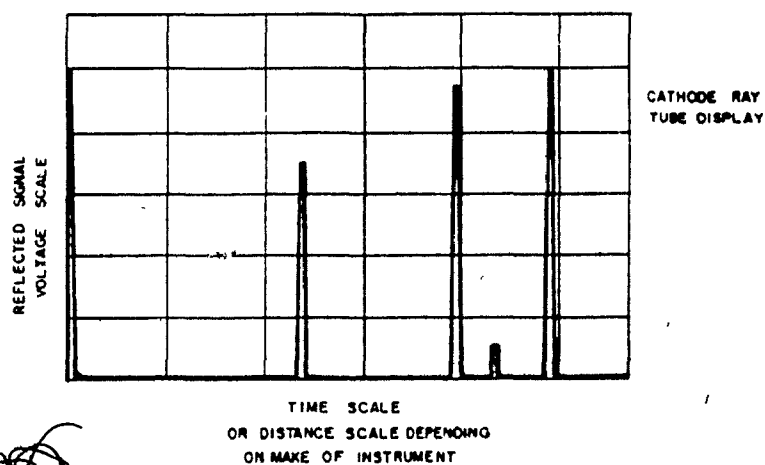
Fig. 3.14   A-scan mode test results.

130

Fig. 3.15 Basic B-scan system with persistent
phosphor CRT display.
(Leornard and Gardner (1973))

Fig. 3.16 B-scan mode test results.

131
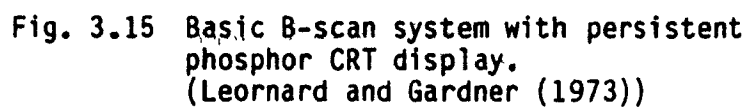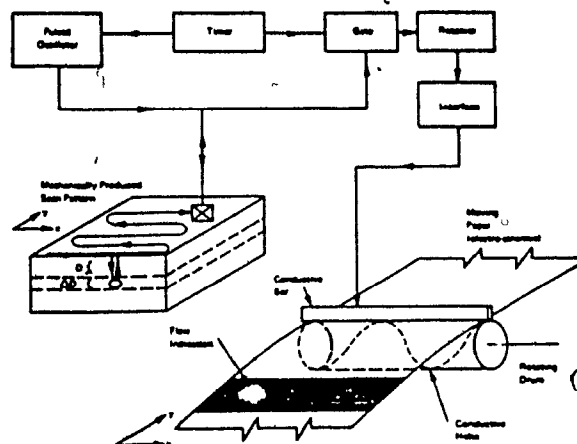
Fig. 3.17   Basic pulse echo C-scan system.
(Leonard and Gardner (1973))

Fig. 4.1   The cast ring gear segment.
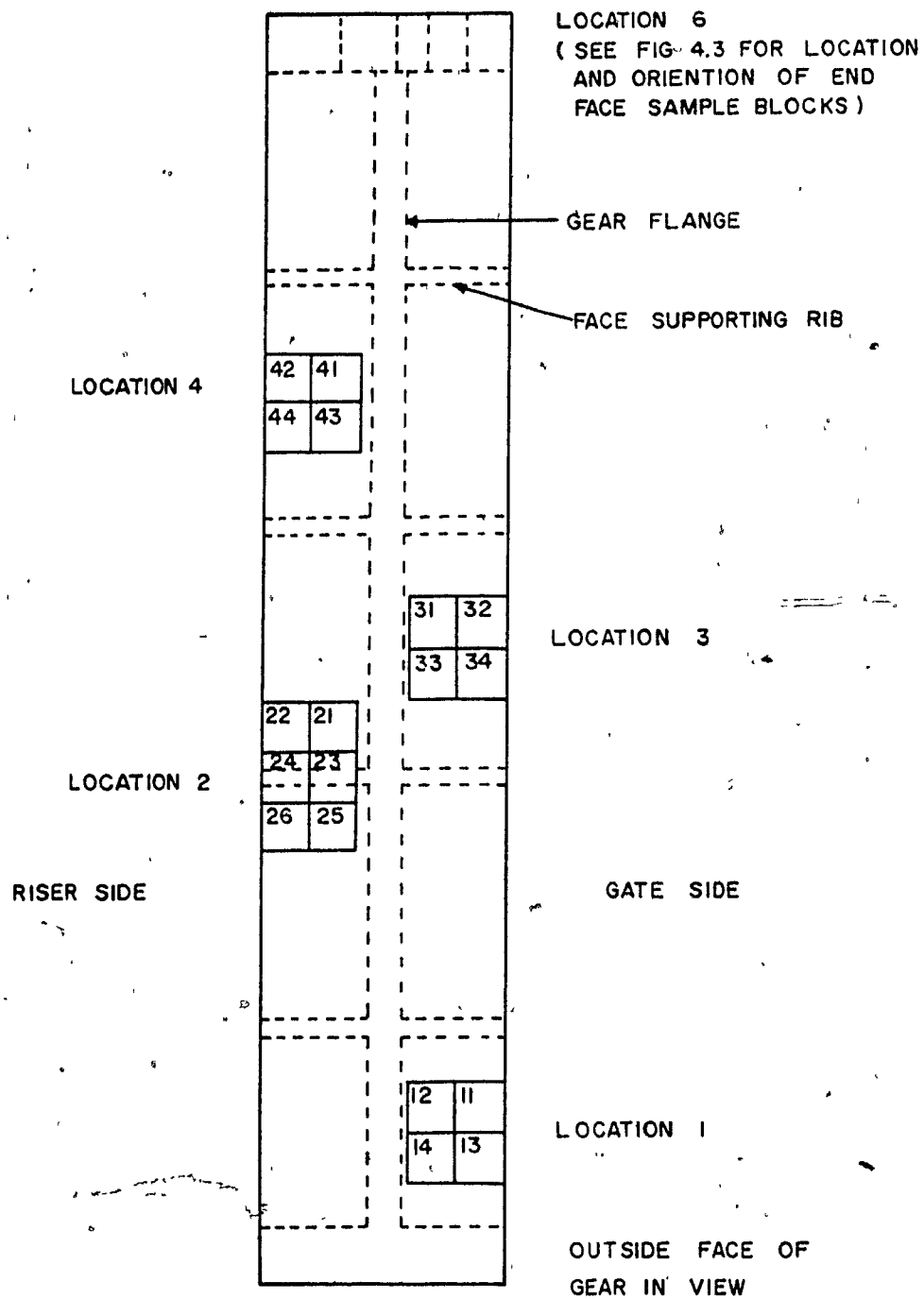
Fig. 4.2   Location of the steel sample blocks
removed from the gear face.

133
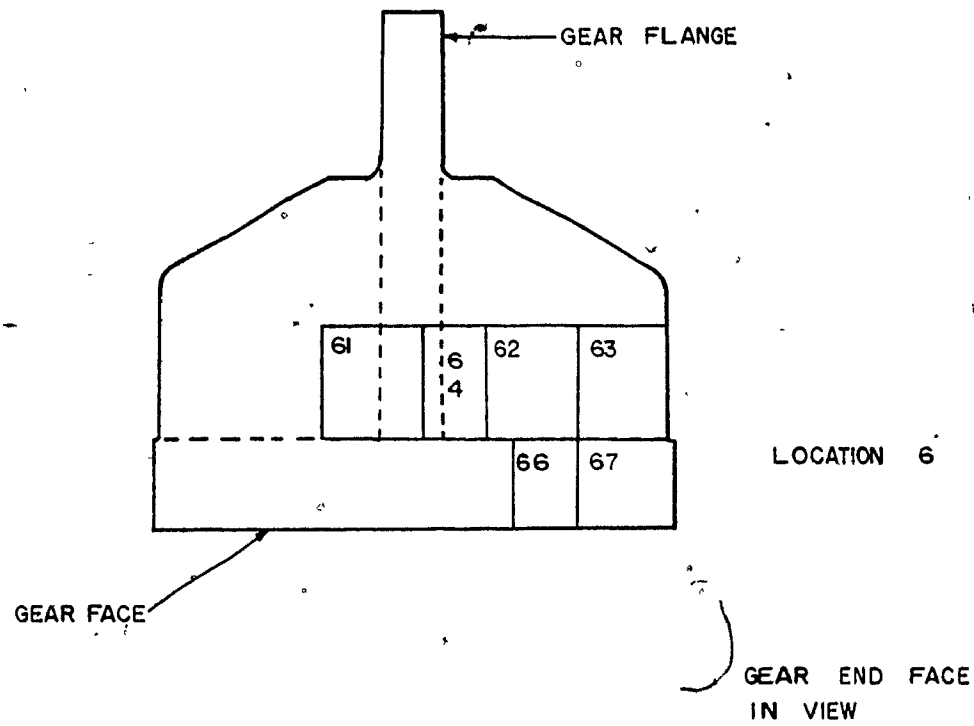
Fig. 4.3 Location of the steel sample blocks
removed from the gear end.

DRILLED
IDENTIFICATION
NUMBER

OUTER FACE OF
GEAR SEGMENT

23

RISER SIDE
OF GEAR
SEGMENT

GATE SIDE
OF GEAR
SEGMENT

SAMPLE BLOCK

(a) Blocks removed from gear face.

FLANGE SIDE OF
GEAR SEGMENT

DRILLED
IDENTIFICATION
NUMBER

END FACE OF
GEAR SEGMENT

61

RISER SIDE
OF GEAR
SEGMENT

GATE SIDE
OF GEAR
SEGMENT

SAMPLE BLOCK
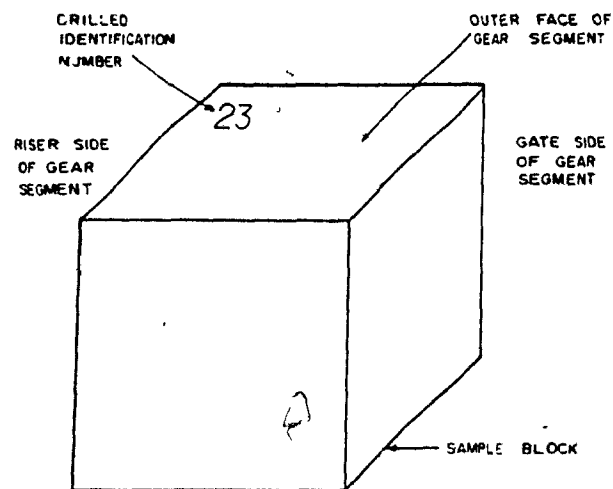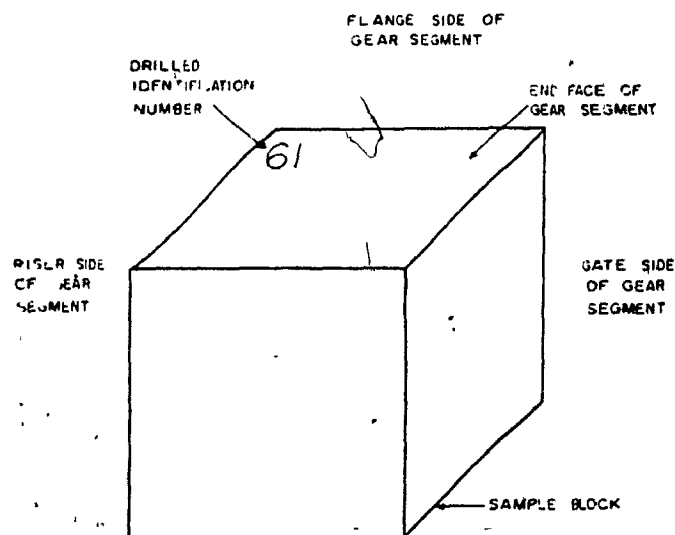
(b) Blocks removed from gear end.

Fig. 4.4 The orientation of the two digit
block identification number.
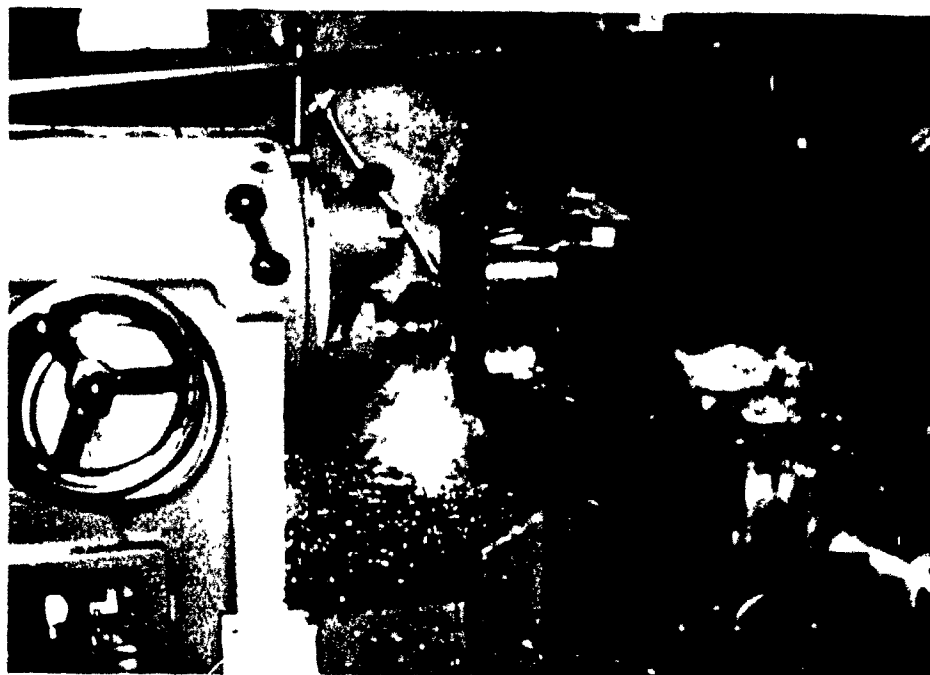
Fig. 4.5 Smoke generation in the lubricated machining process.

Fig. 4.6 The dry machining process.

136

DRILLED
IDENTIFICATION
NUMBER

RISER SIDE
OF GEAR
SEGMENT

GATE SIDE
OF GEAR
SEGMENT
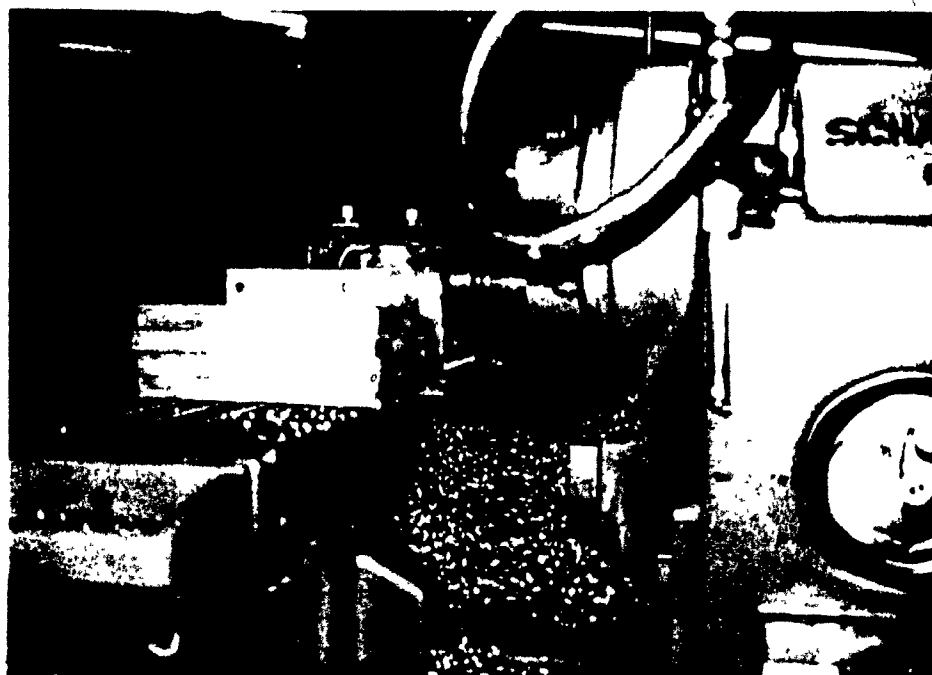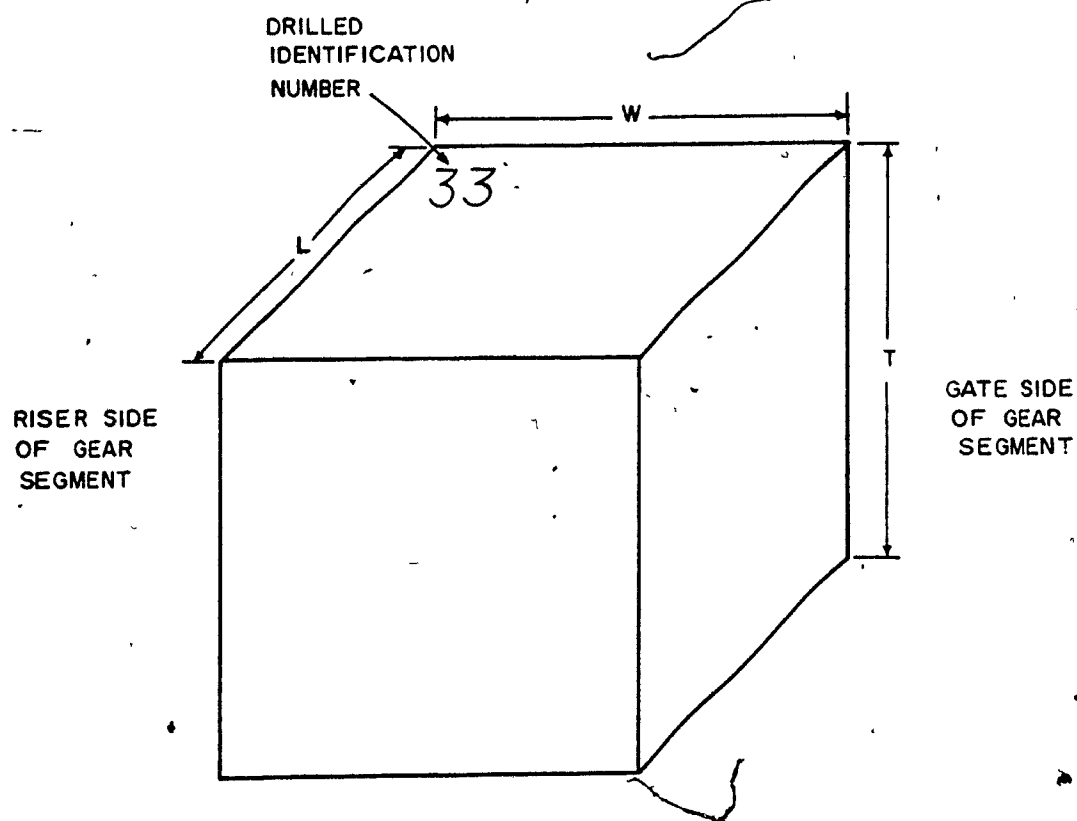
SIZE CATEGORY	L (cm)	W (cm)	T (cm)
1	14.0	14.0	16.5
2	15.9	15.9	16.5
3	16.5	16.5	16.5

ALL DIMENSIONS ± 0.1 cm

Fig. 4.7 The as-machined dimensions of
the three size categories.

137

DRILLED
IDENTIFICATION
HOLES

158

15.8

8.4

RISER SIDE
OF GEAR
SEGMENT

117

58

GATE SIDE
OF GEAR
SEGMENT

75°

219

90

125°

56

10.5

ALL DIMENSIONS IN cm
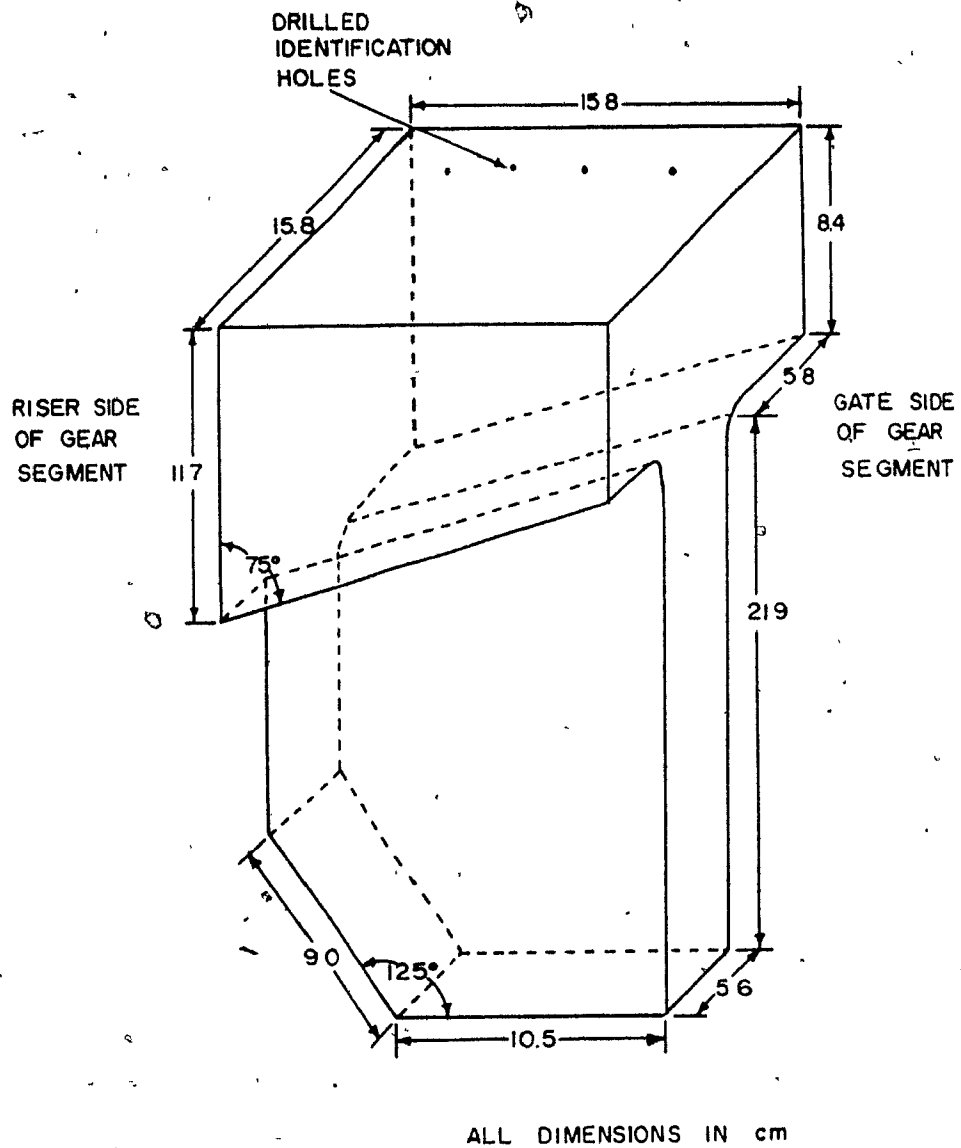
Fig. 4.8 The as-machined dimensions of block 23L.

138
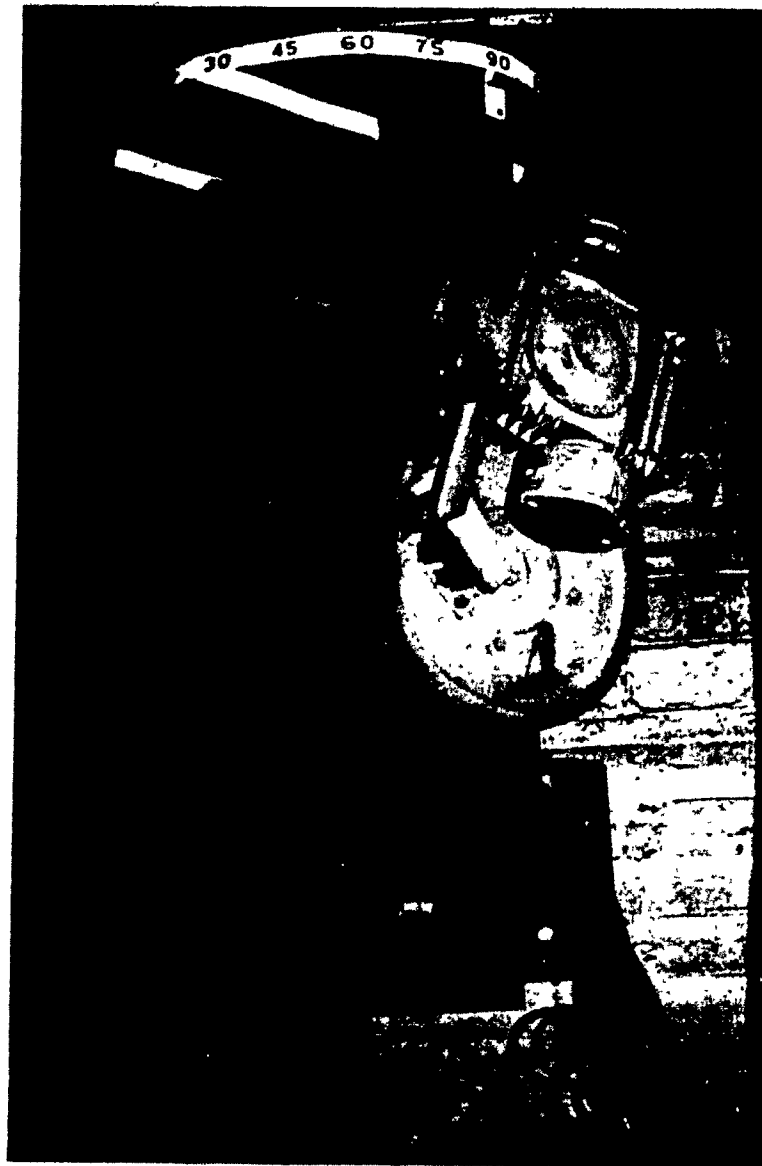
Fig. 4.9 The Linatron 1500.
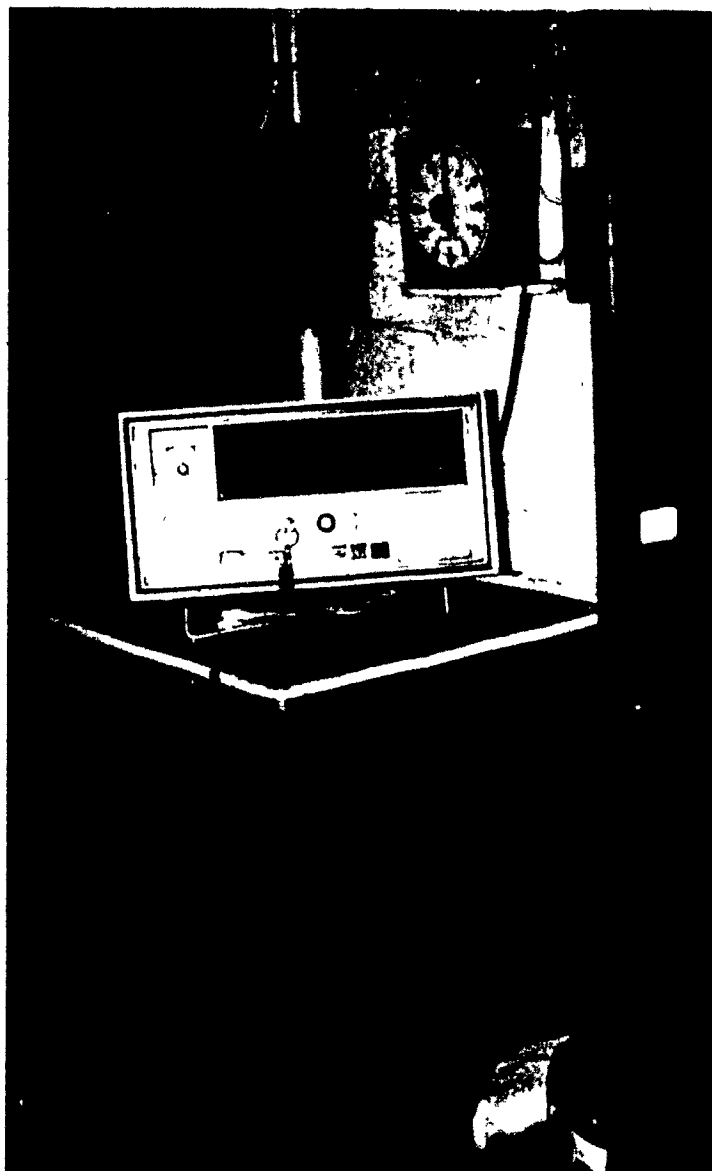
Fig. 4.10   The Linatron 1500 control panel.
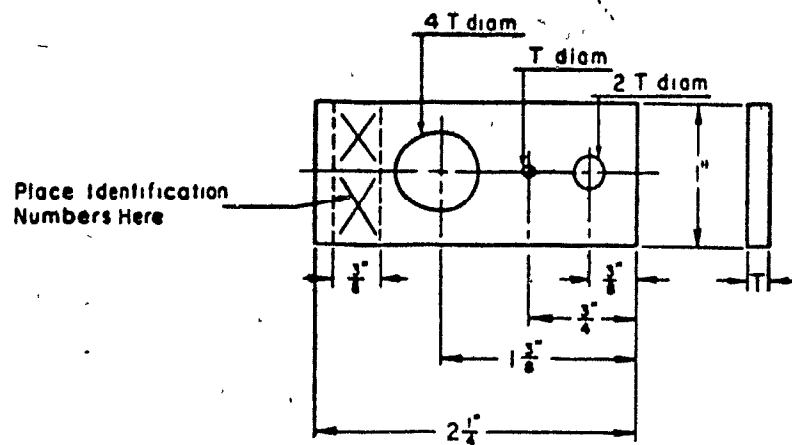
Design for penetrameter thickness from 0 060 in to 0 180 in. incl
Made in 0 010-in increments

Fig. 4.11 ASTM lead penetrameters.
           (E 142-77 (1983))

141

The chart shows EXPOSURE TIME (SECONDS) on the vertical axis versus THICKNESS (INCHES STEEL) on the horizontal axis, with curves labeled GAF-100, KODAK "O", GAF-200, KODAK "M", GAF-400, KODAK "T", GAF-1200, KODAK "AA", GAF-1600.

Handwritten notes on right side:
TARGET FILM - 6 FT
PB·F·010
B·030
DENSITY H·D·2.0
UNIT LINATRON 1500
ENERGY 15 m.eV
OUTPUT 1500/m/1m
PROCESSING: X-OMAT
MODEL "B"
MODIFIED TO
8 m.vurts D.E.V.
FOCAL-SPT LESS·2 MM

Fig. 4.12 Kodak type AA film exposure time
vs. metal thickness. (Courtesy of
Canadian Steel Foundaries Ltd.)

142

X-RAY DIRECTION I

DRILLED
IDENTIFICATION
NUMBER

22

X-RAY DIRECTION 2

RISER SIDE
OF · GEAR
SEGMENT

GATE SIDE
OF GEAR
SEGMENT
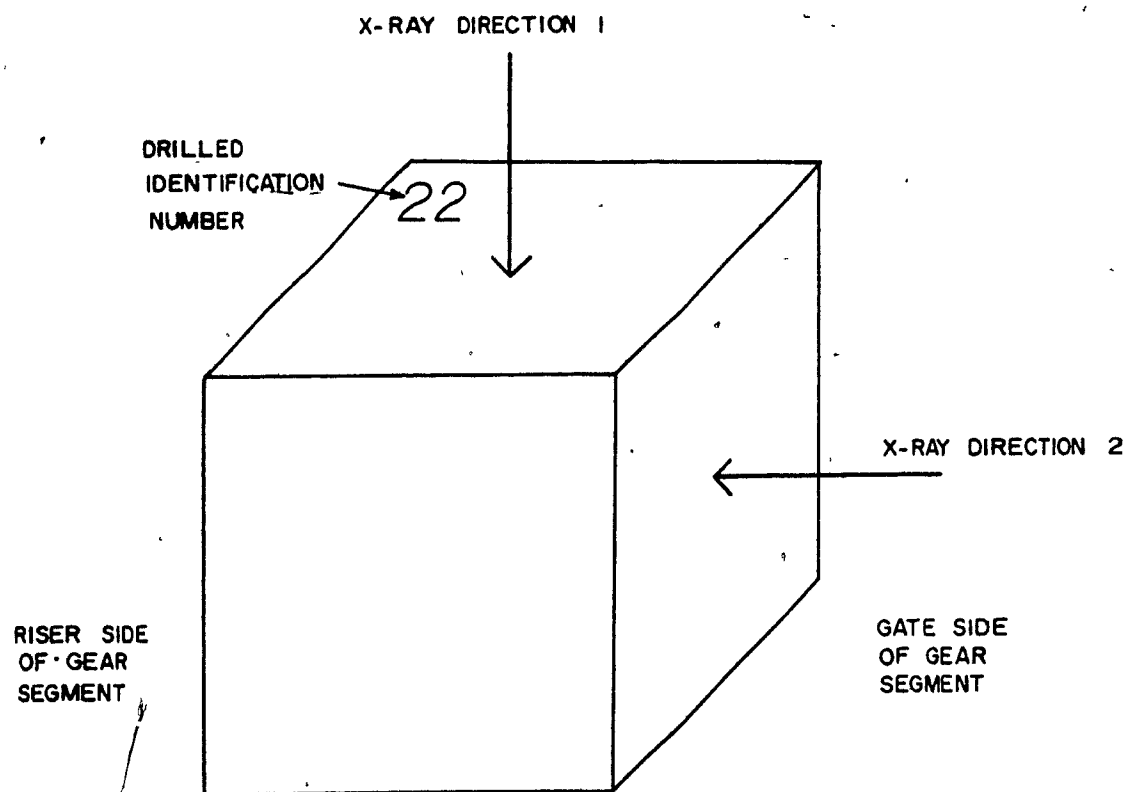
Fig. 4.13   X-ray directions for regular
shaped blocks.

DRILLED IDENTIFICATION
HOLES

RISER SIDE
OF GEAR
SEGMENT

GATE SIDE
OF GEAR
SEGMENT

DIRECTION OF
X-RAY EXPOSURE 1

DIRECTION
OF X-RAY
EXPOSURE 2

DIRECTION
OF X-RAY
EXPOSURE 3
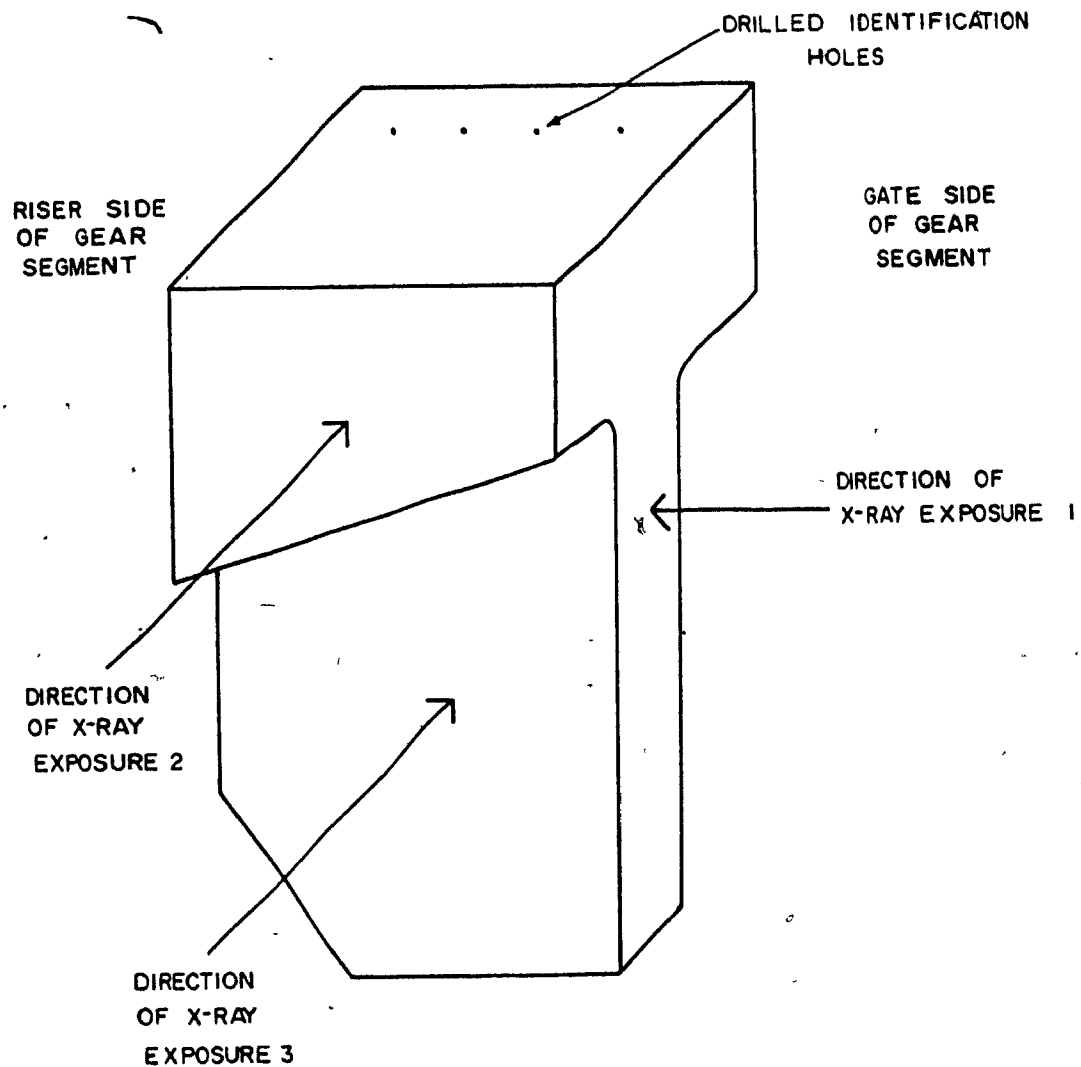
Fig. 4.14a   X-ray directions for block 23L.
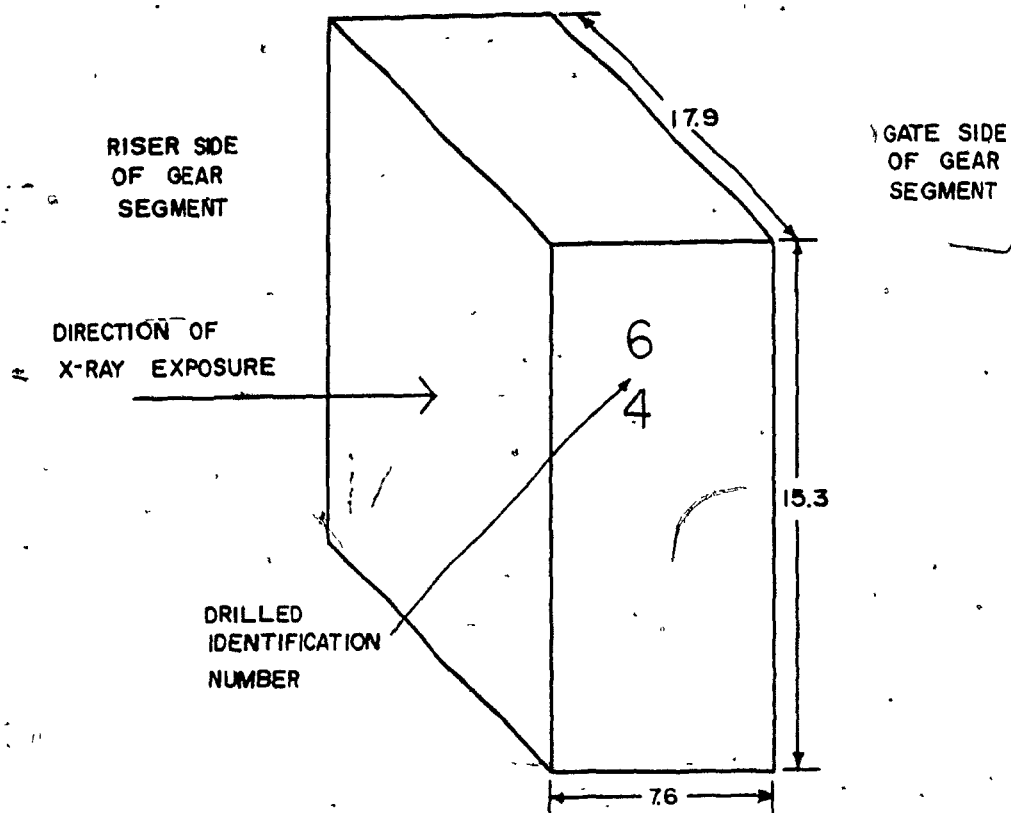
Fig. 4.14b X-ray direction for block 64.
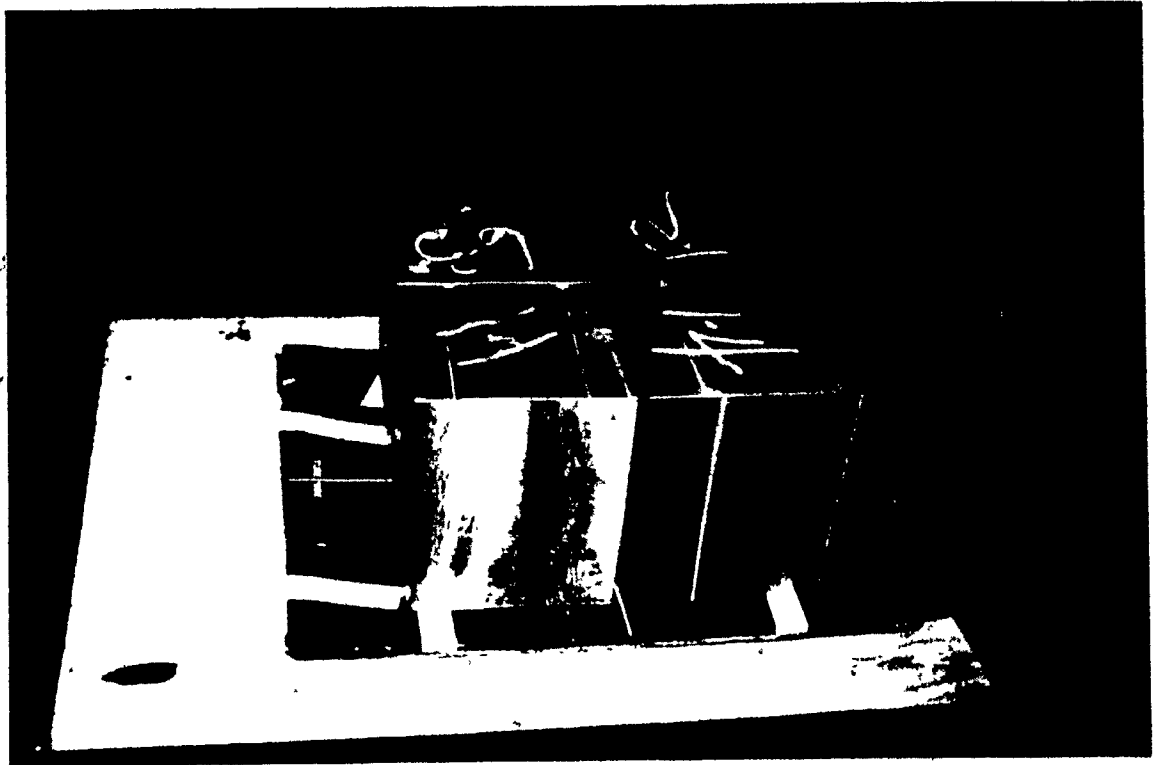
Fig. 4.15   The 4 block simultaneous
            exposure set up.
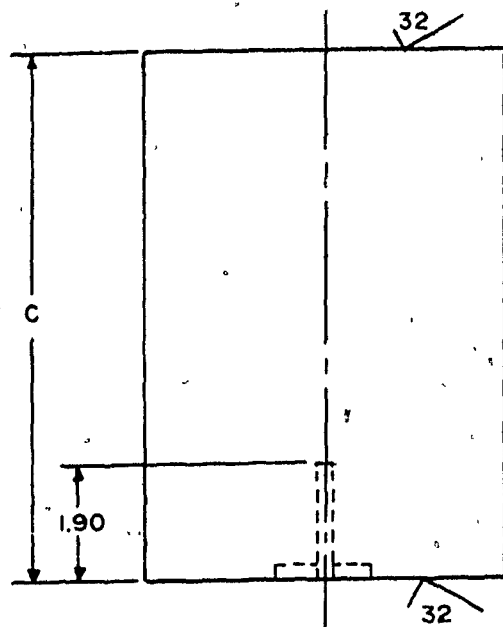
C= BLOCK LENGTH THAT VARIES
WITH DEPTH BEING INSPECTED

FRONT VIEW
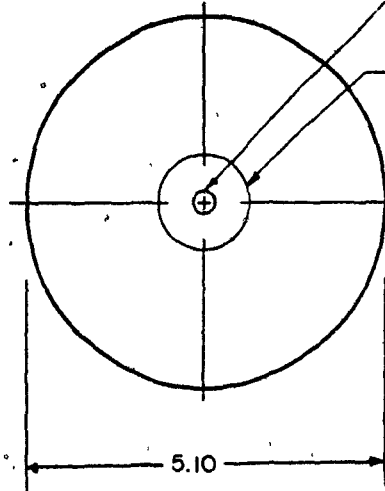
6 35 mm   DIA   FLAT
BOTTOM HOLE

12.7 mm DIA. BY 3 2 mm
DEEP COUNTER BORE

ALL TWO-PLACE   DECIMALS ± 0.02 cm

BOTTOM VIEW

Fig. 4.16 ASTM A 609-83 ultrasonic
reference blocks.
(A 609-83 (1983))

147
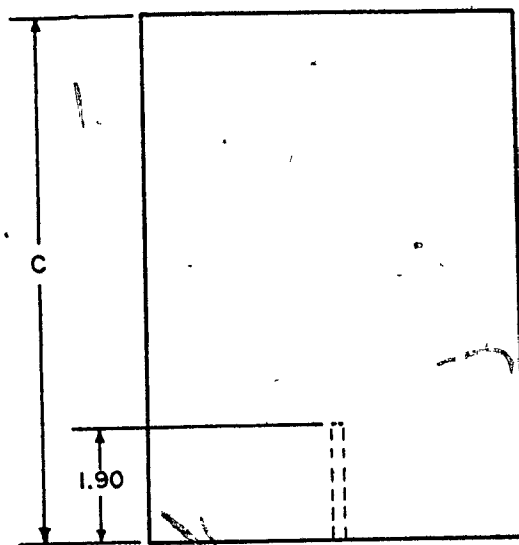
REFERENCE BLOCK	C cm ±0.02 cm
1	4.44
2	6.98-
3	9.52
4	12.06
5	14.60

FRONT VIEW

3.175 mm DIA. FLAT BOTTOM HOLE
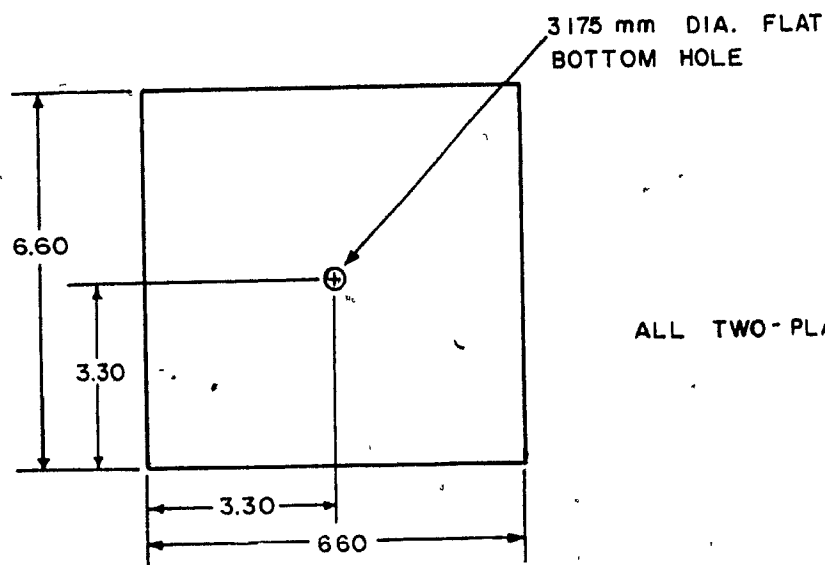
ALL TWO-PLACE DECIMALS ± 0.02 cm

BOTTOM VIEW

Fig. 4.17 Modified ASTM ultrasonic reference blocks.
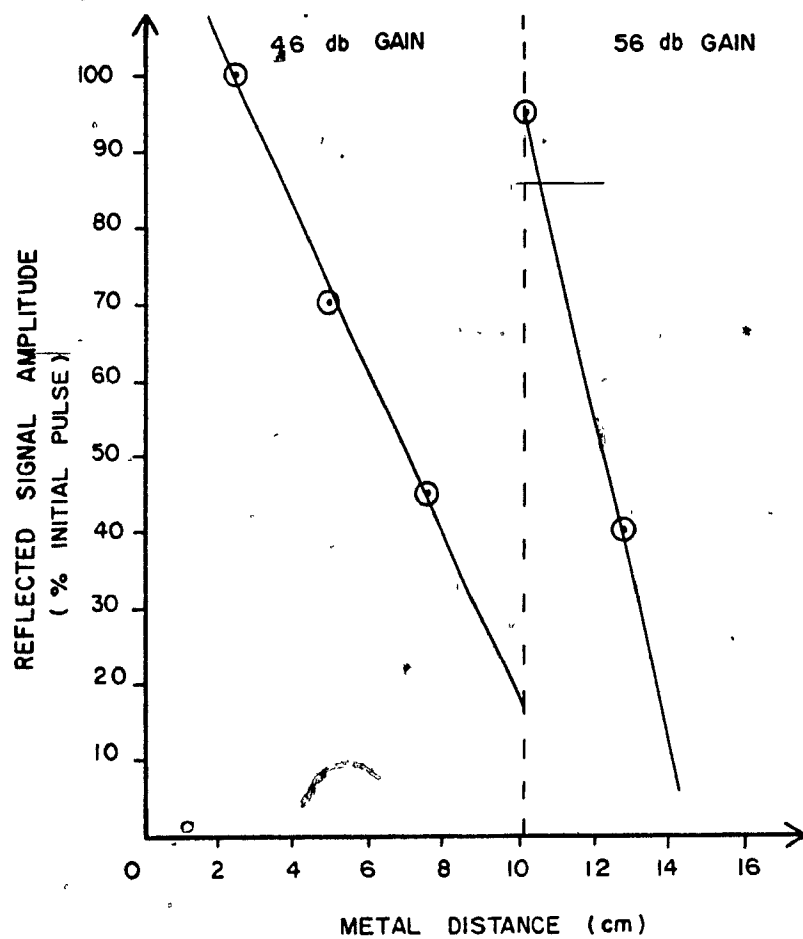
Fig. 4.18 Graphical presentation of the DAC curve.
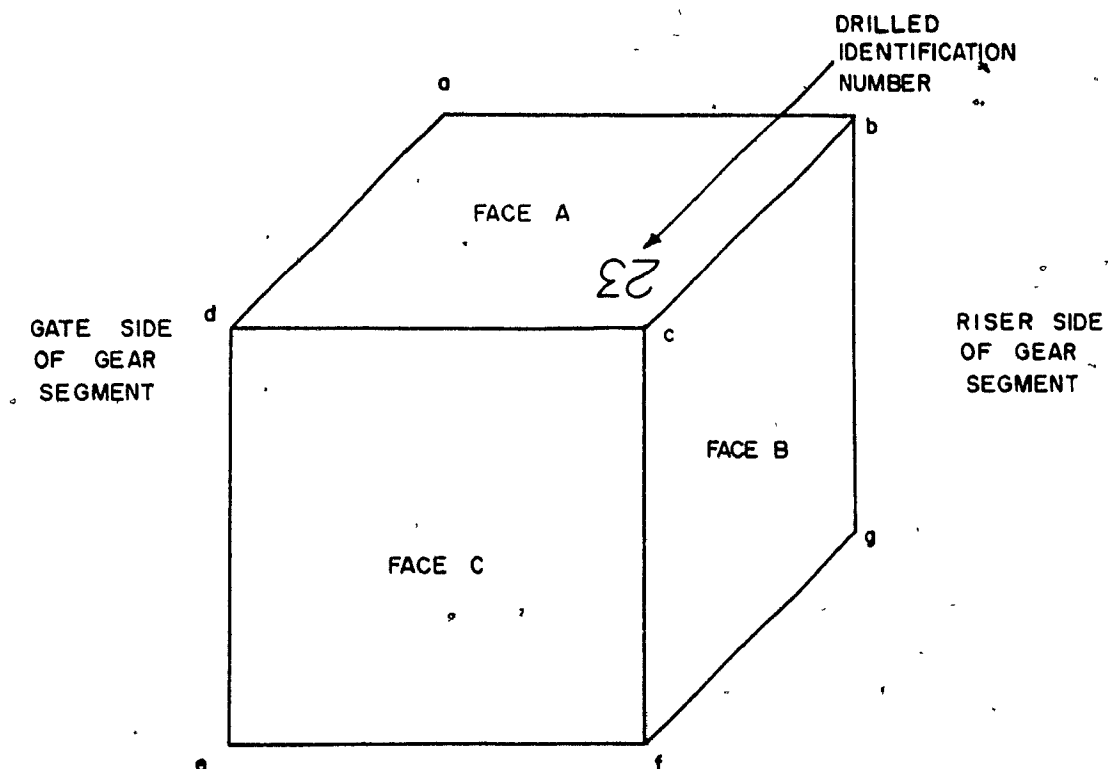
Fig. 4.19 Orientation of the ultrasonic
inspection surfaces.

Fig. 4.20 The ultrasonic inspection of
a sample block.
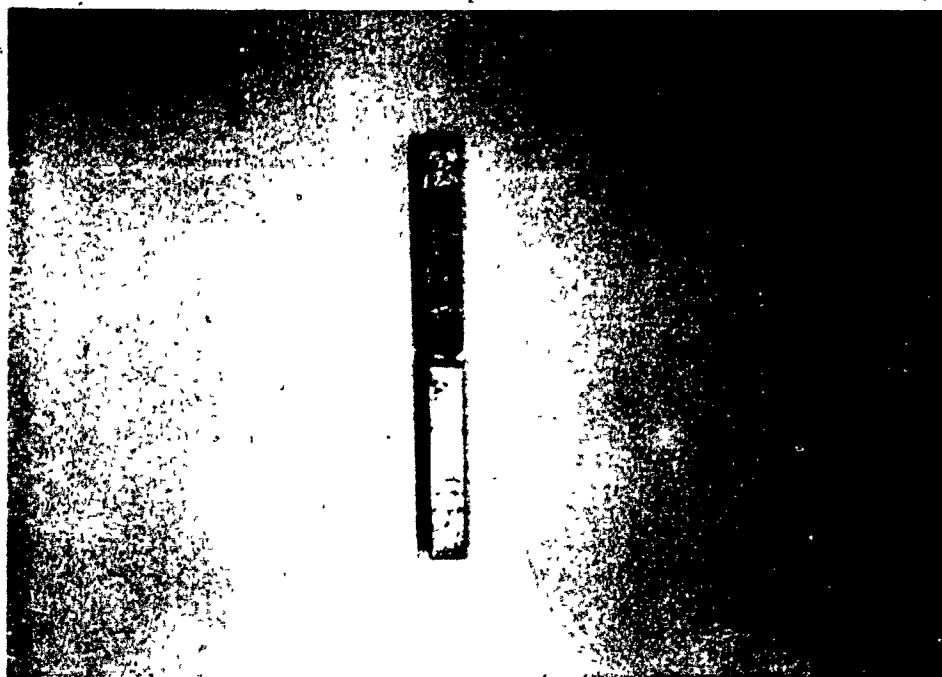
Fig. 4.21 A typical fracture specimen.
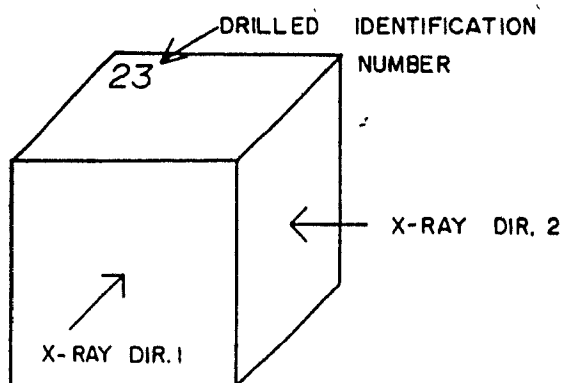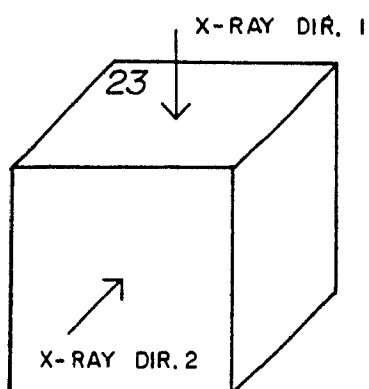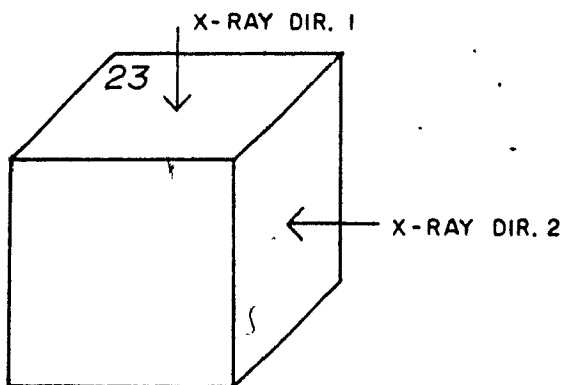
Fig. 4.22   Fracture specimen's X-ray directions.
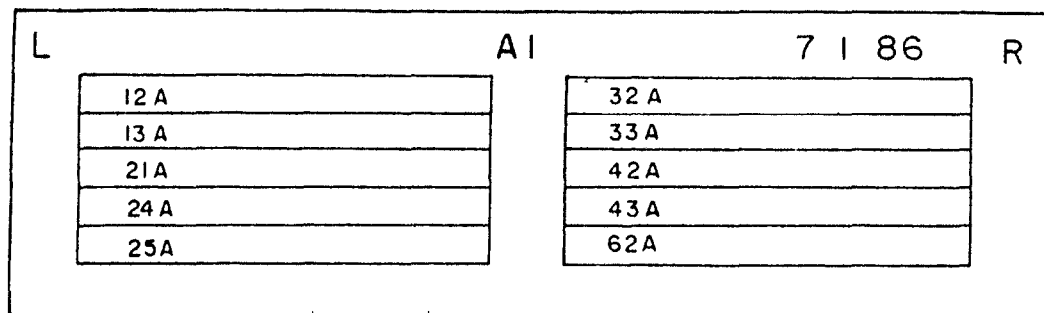
(a) Radiographs A1 and A2
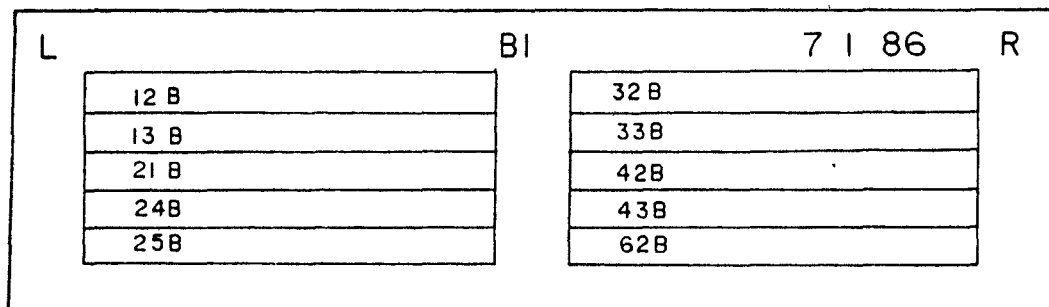
(b) Radiographs B1 and B2
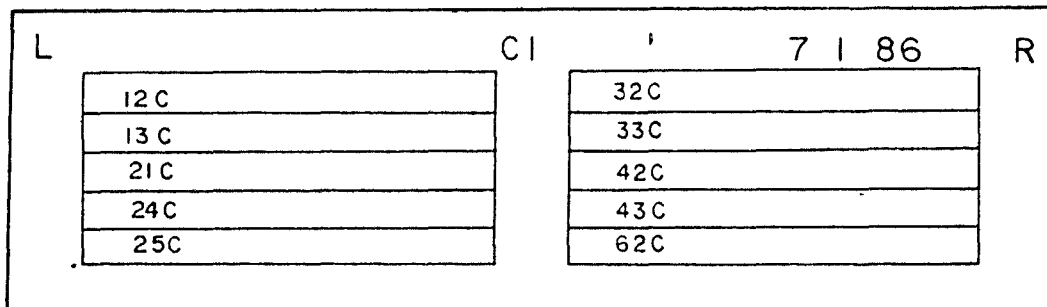
(c) Radiographs C1 and C2

Note: I.D. numbers on left end of fracture specimen in all cases.

Fig. 4.23 Direction and orientation of the
fracture specimens in the radiographs.
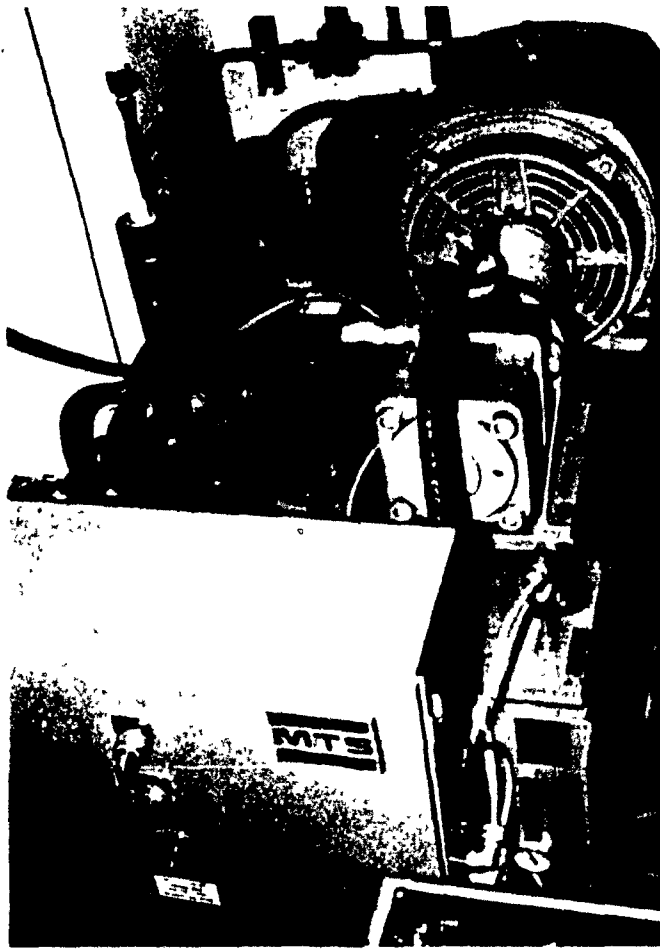
Fig. 4.24 The MTS hydraulic pressure supply.
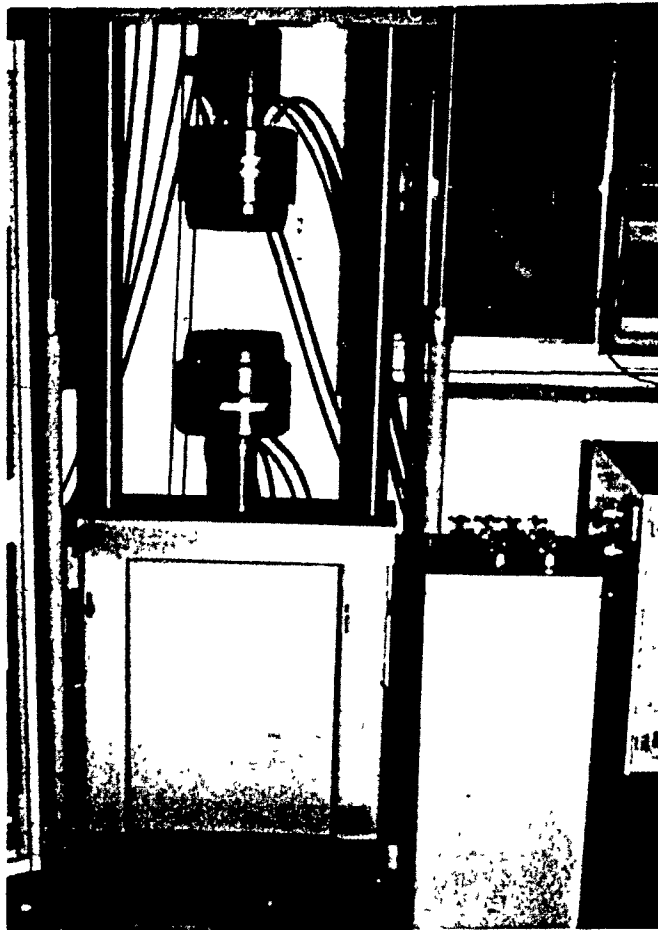
Fig. 4.25   The MTS loading unit.
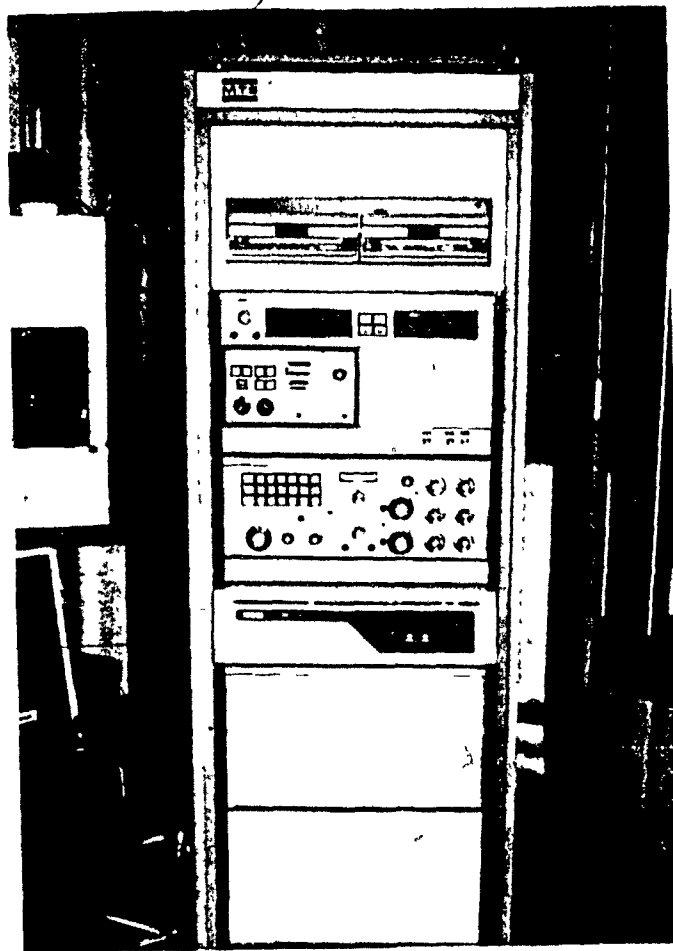
Fig. 4.26   The MTS control console.
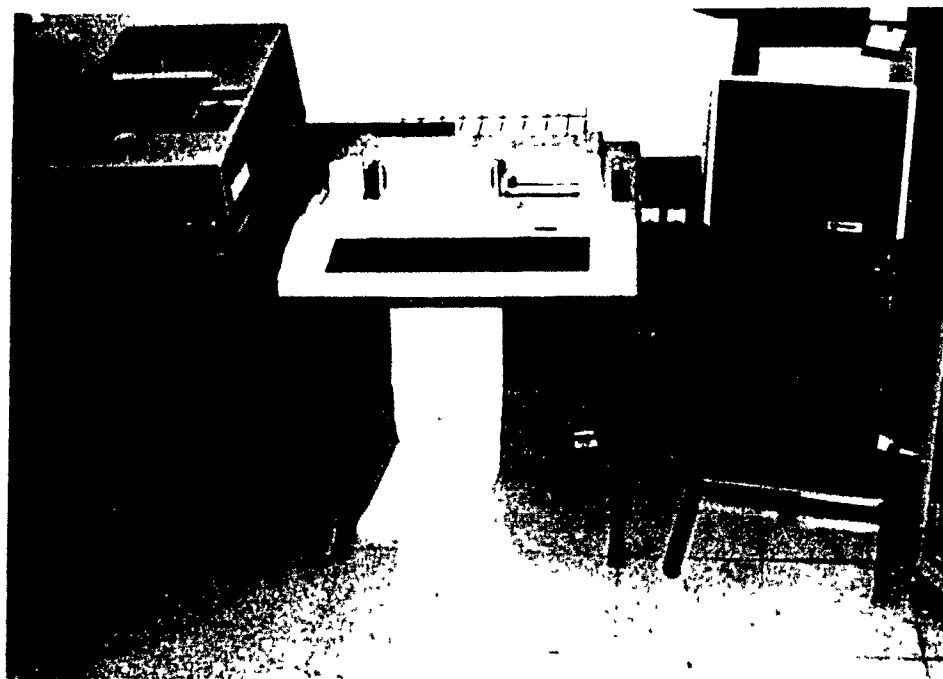
Fig. 4.27   The MTS input/output devices.
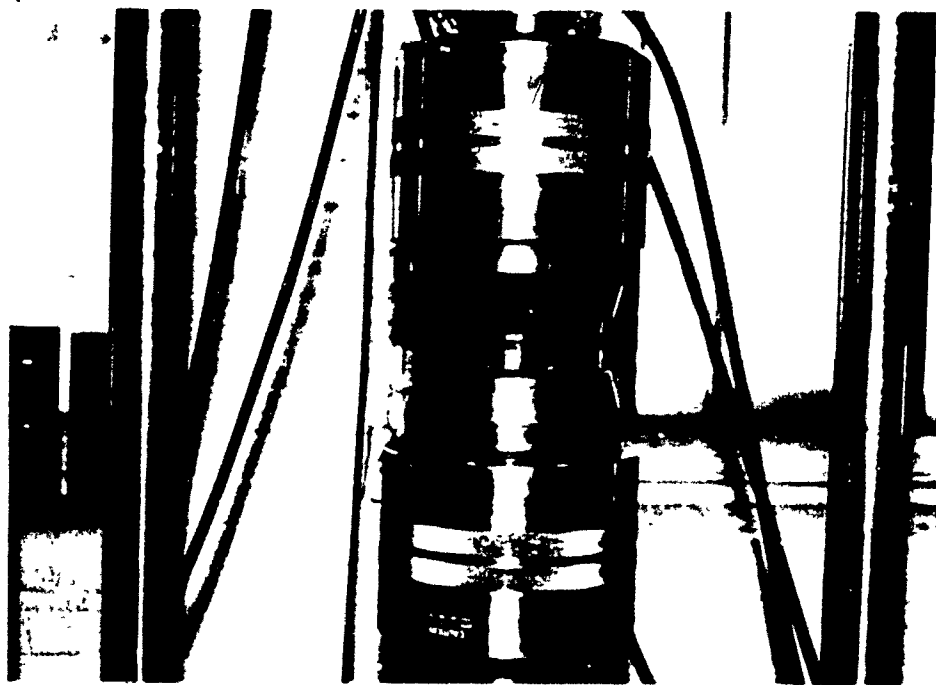
Fig. 4.28   Typical fracture specimen
loaded in MTS unit.
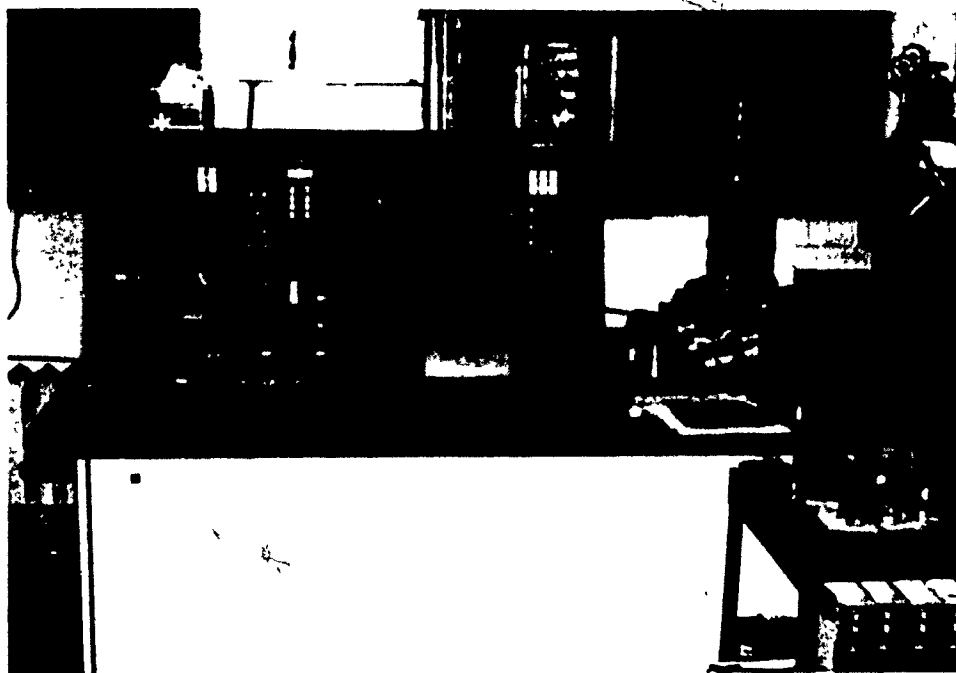
Fig. 4.29   The scanning electron microscope.
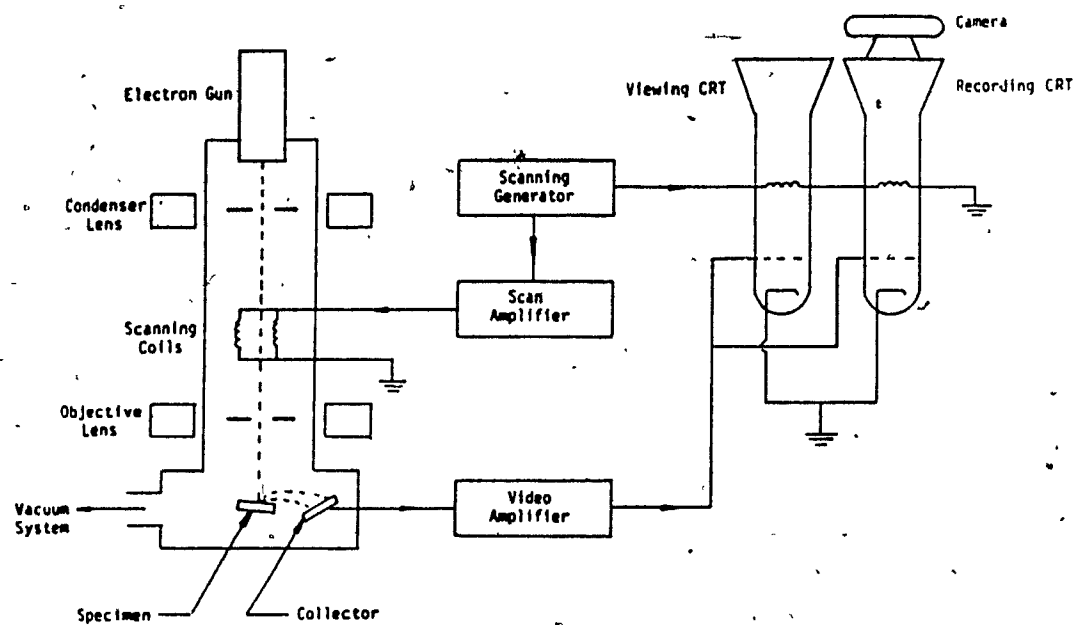
Fig. 4.30 The scanning electron microscope
schematic.
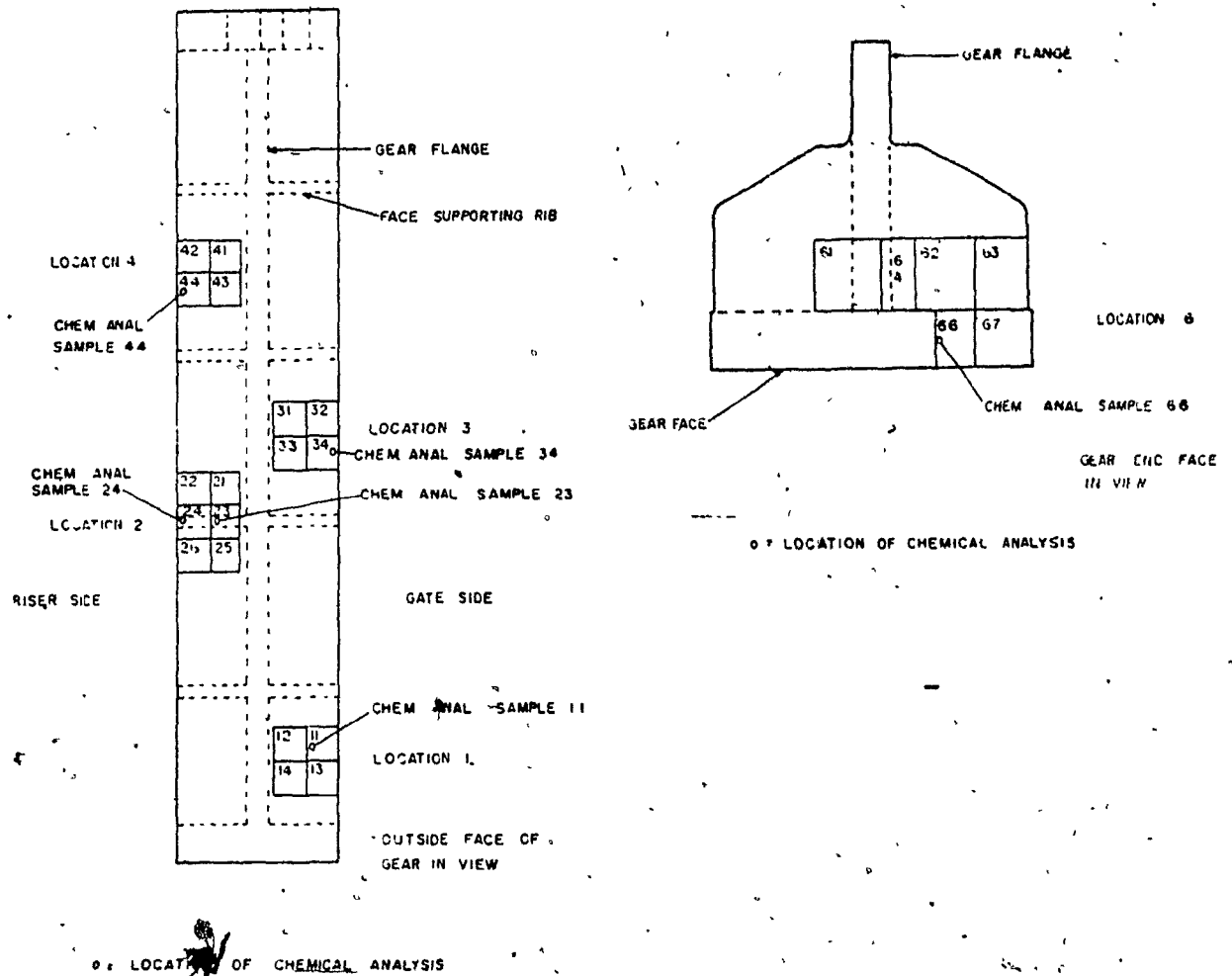
Fig. 4.31 The locations of chemical analysis.
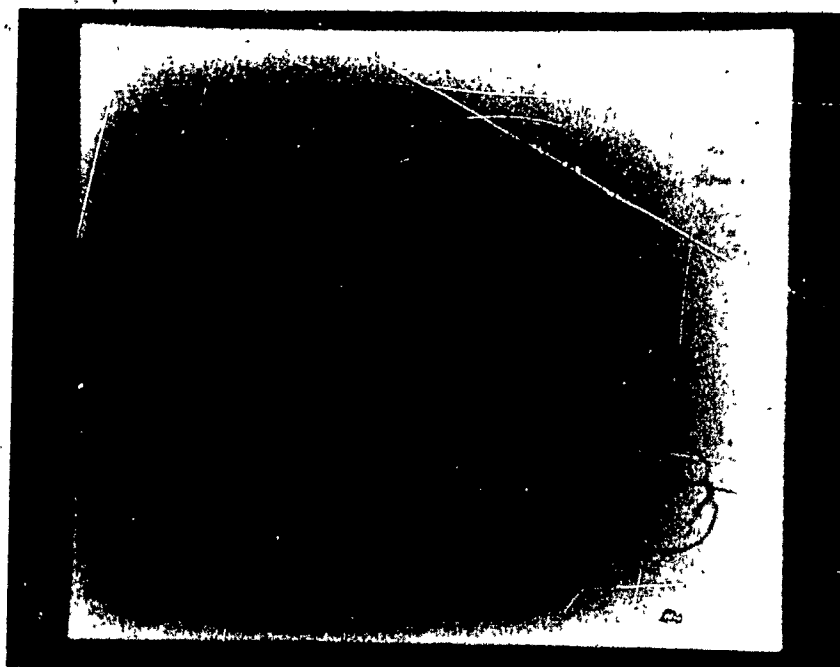
Fig. 5.1 Sample block 64 X-ray.
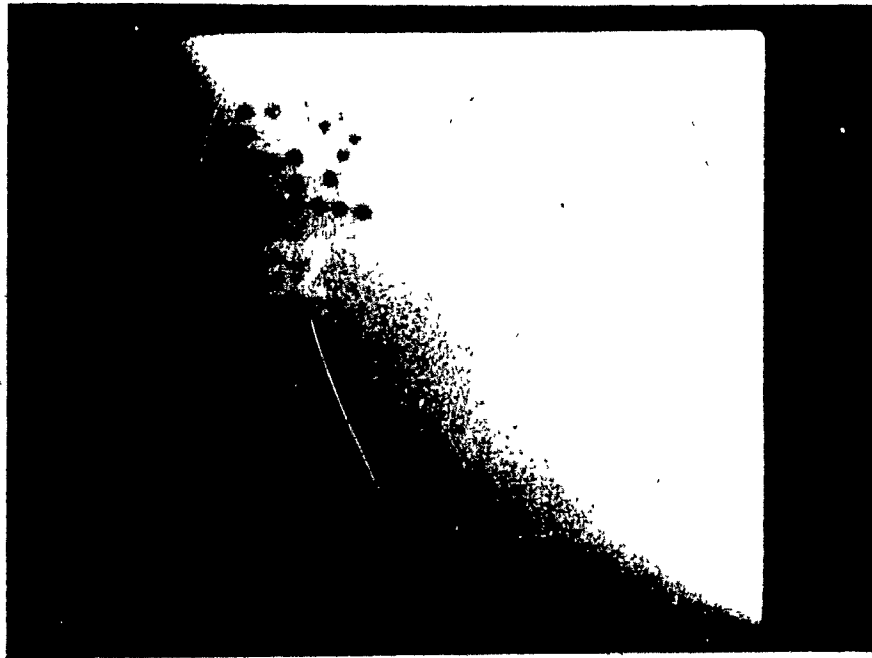
Fig. 5.2 Sample block 62 X-rays.

162

Fig. 5.3 Typical ultrasonic reference
block radiograph.
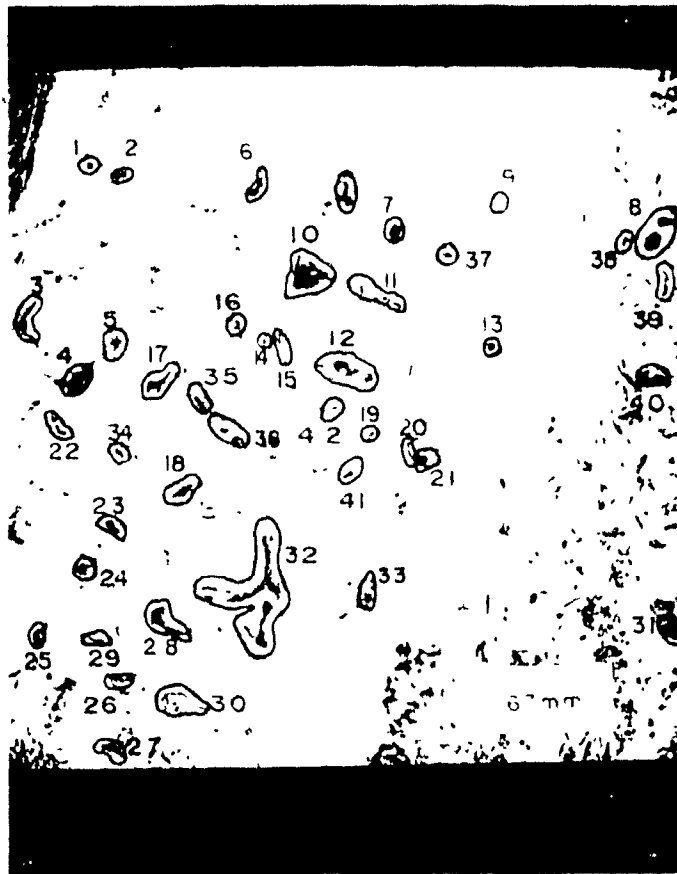
Fig. 5.4 SEM fractograph overview of specimen
12B fracture surface.

.042mm

Fig. 5.5 SEM fractograph of typical microscopic
inspection class 1 defect.

Fig. 5.6   SEM fractograph of typical microscopic
           inspection class 2 defect.

166
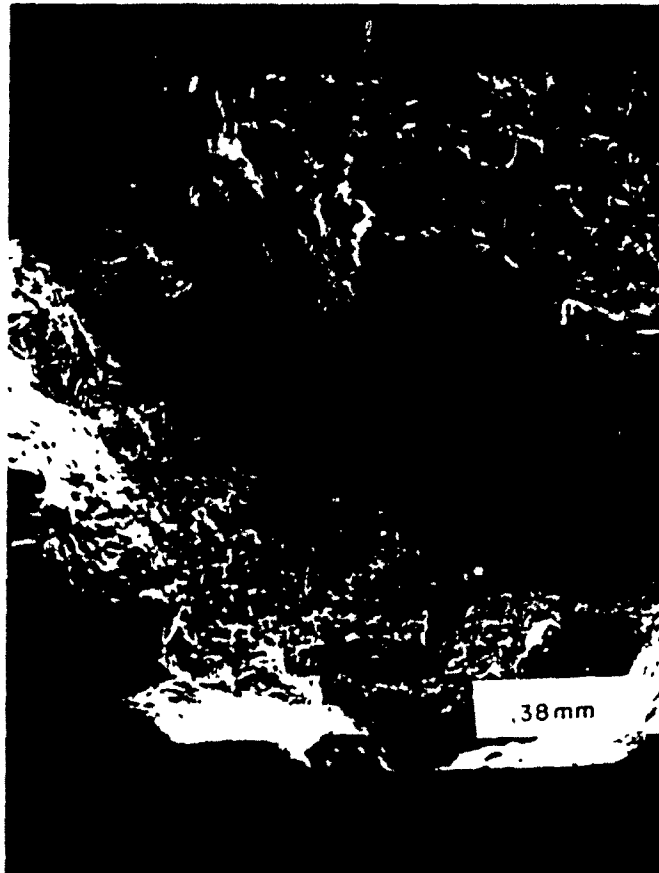
Fig. 5.7   SEM fractograph of typical microscopic
           inspection class 3 defect.

167
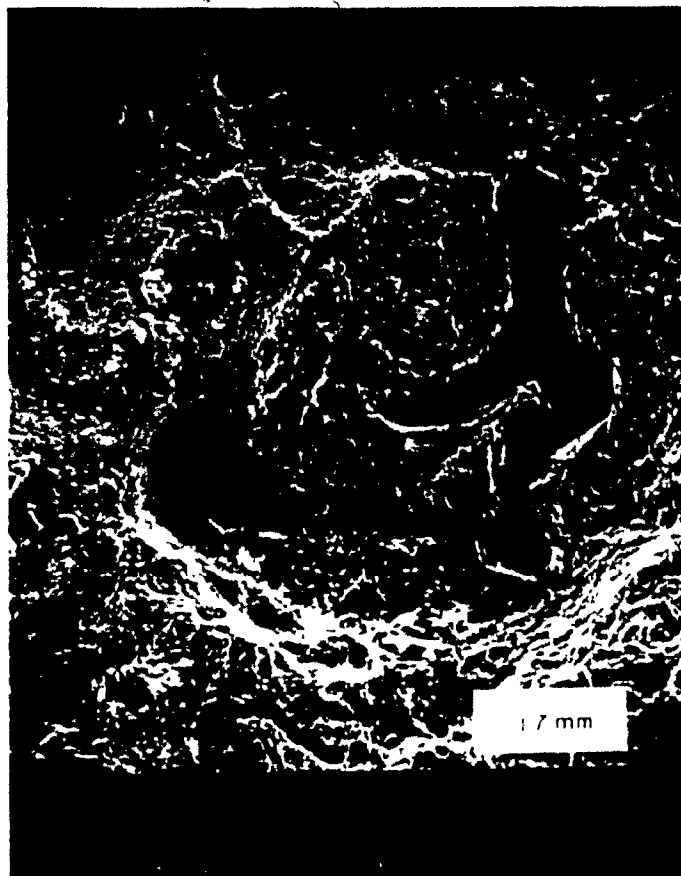
Fig. 5.8   SEM fractograph of typical microscopic
inspection class 4 defect.
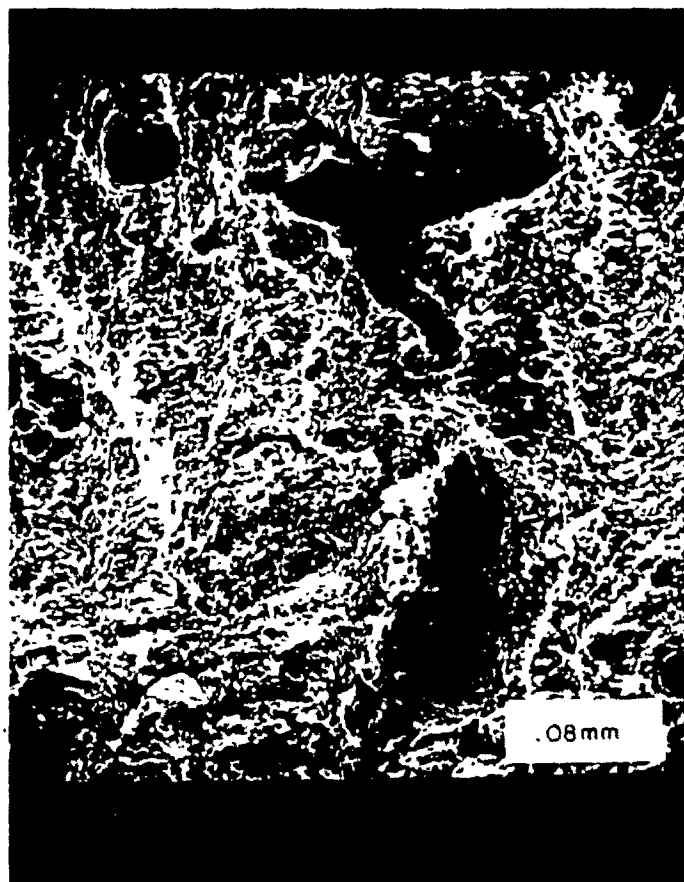
Fig. 5.9 SEM fractograph of typical microscopic inspection class 5 defect.
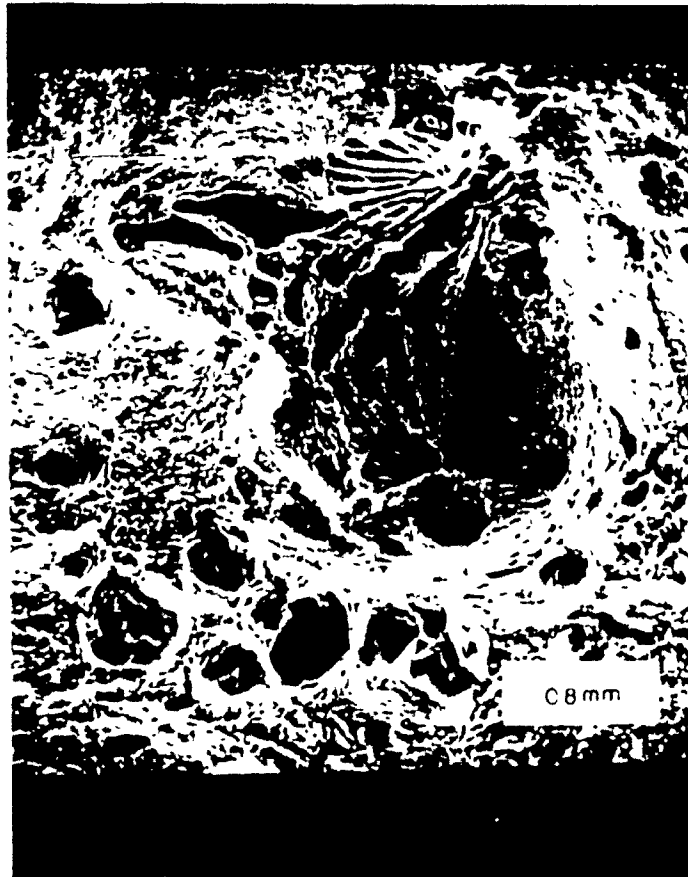
Fig. 5.10 SEM fractograph of typical microscopic
inspection class 6 defect.
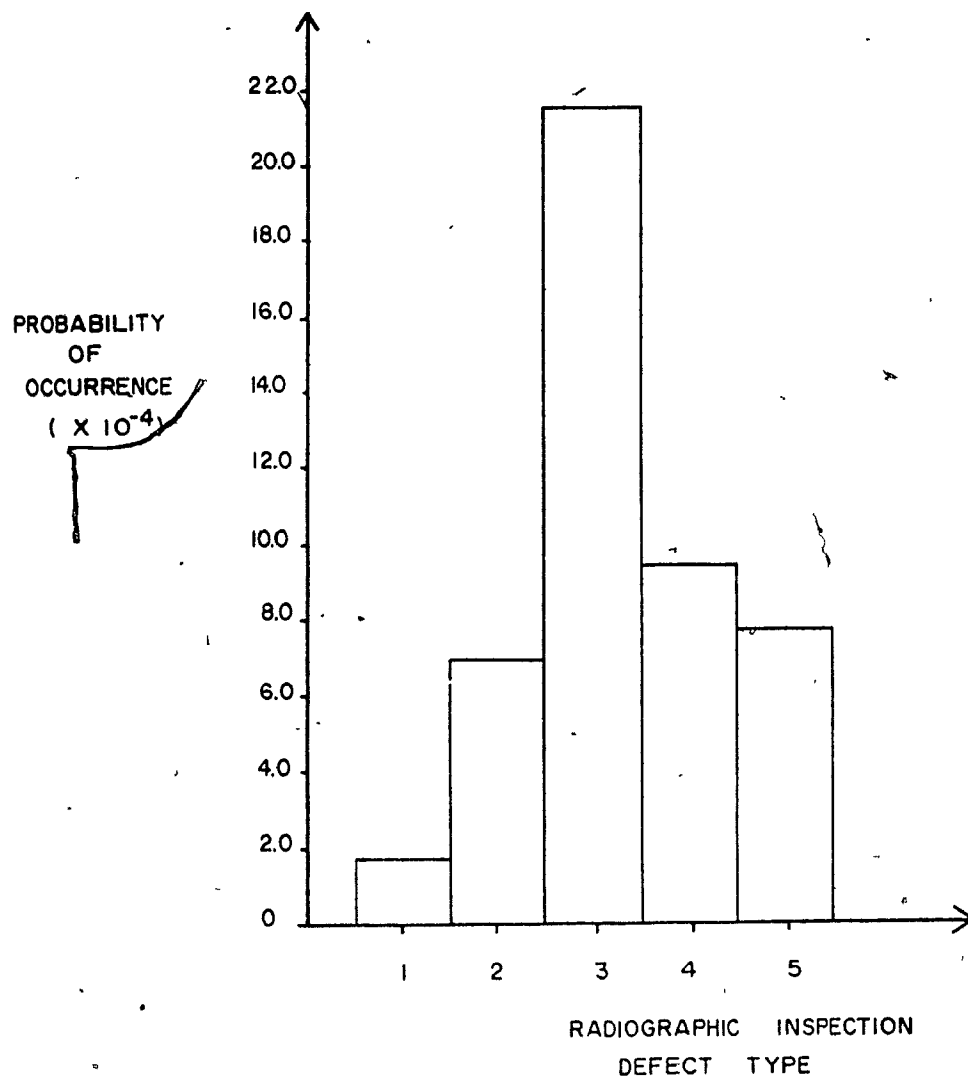
Fig. 5.11   Radiographic inspection defect histogram.
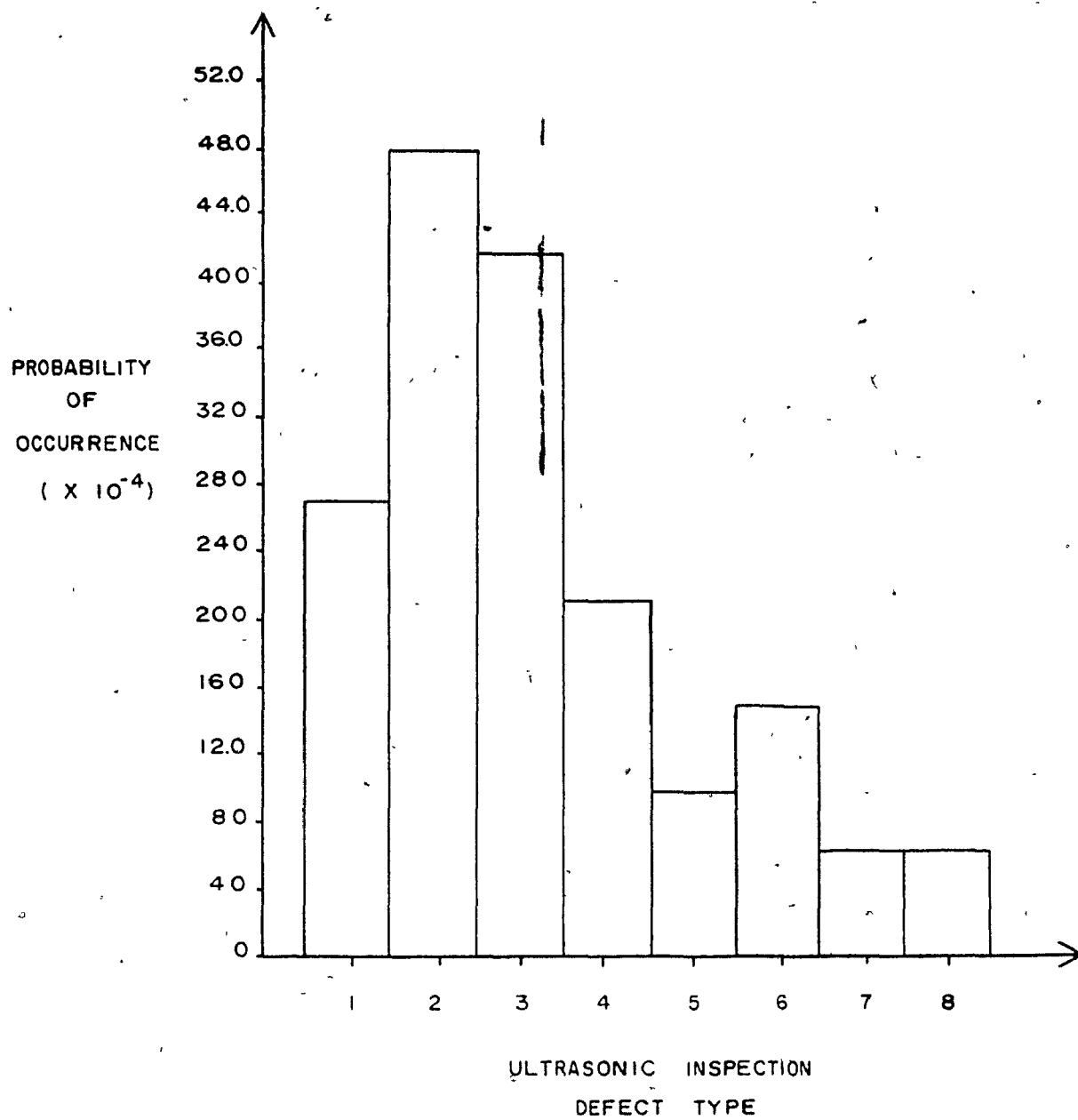
Fig. 5.12 Ultrasonic inspection defect histogram.
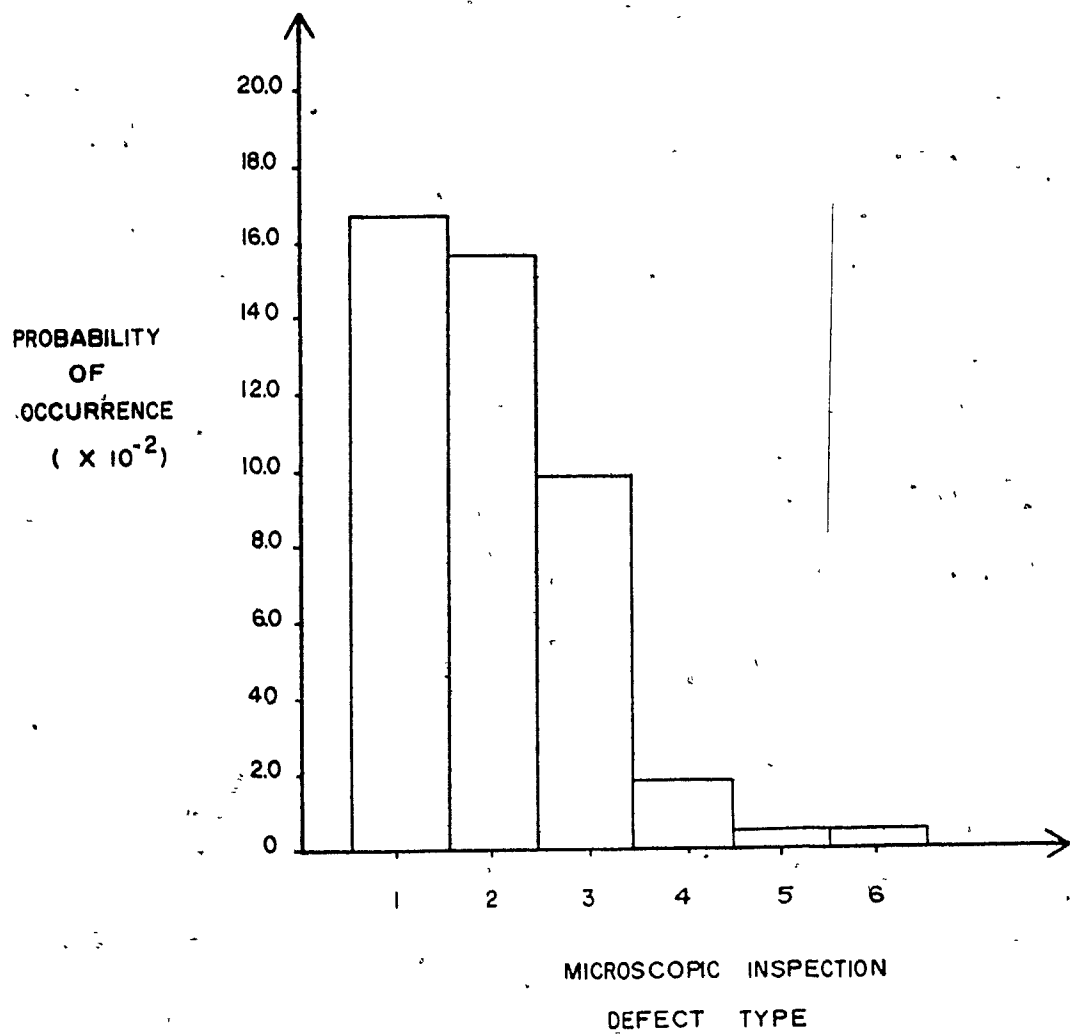
Fig. 5.13   Microscopic inspection defect histogram.
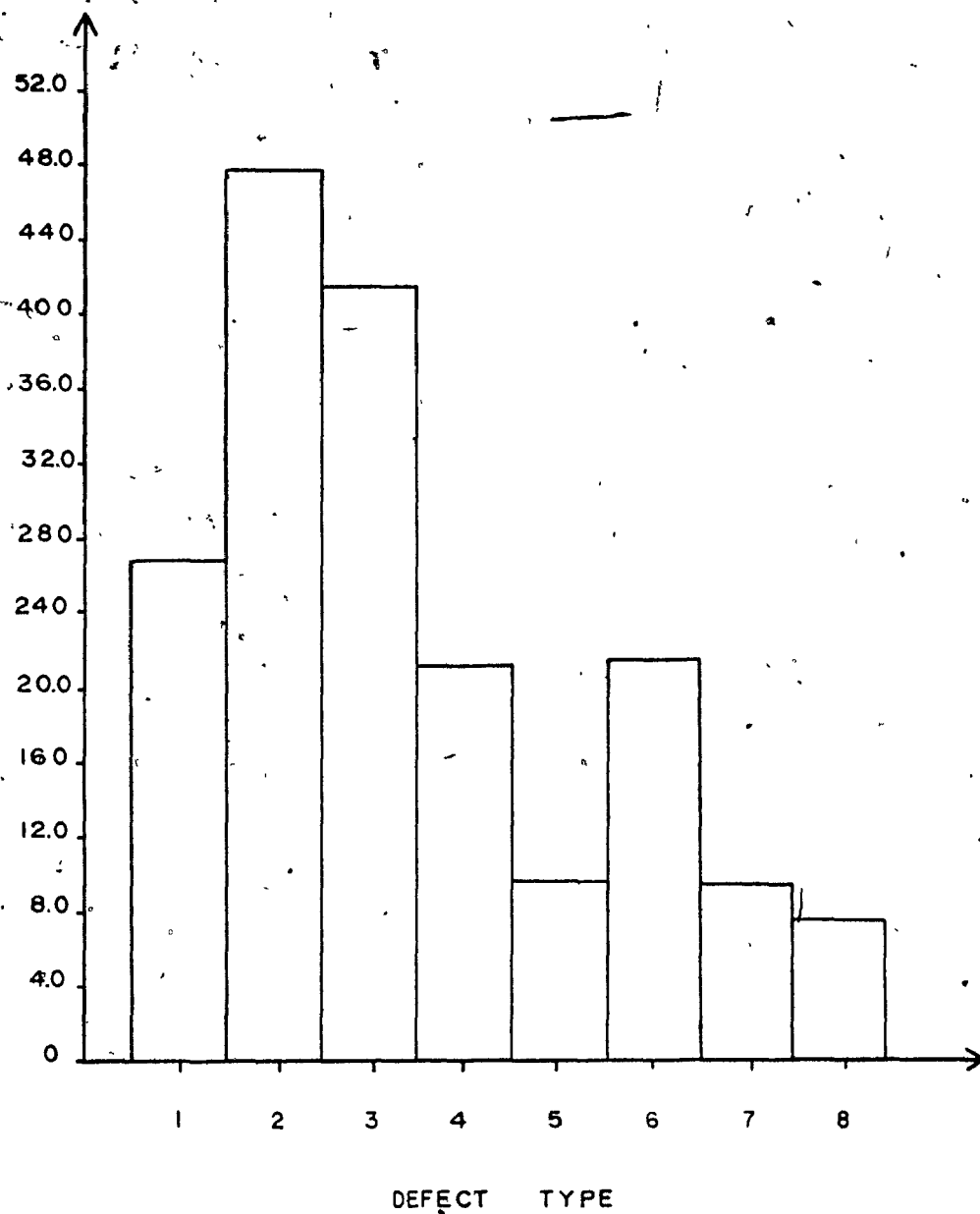
Fig. 5.14   The combined defect histogram.

GEAR SEGMENT
OUTER FACE

DIR. 2 FLAWS

DIR. I FLAWS

DIR 3 FLAWS

GEAR SEGMENT
EDGE

GEAR SEGMENT
END FACE
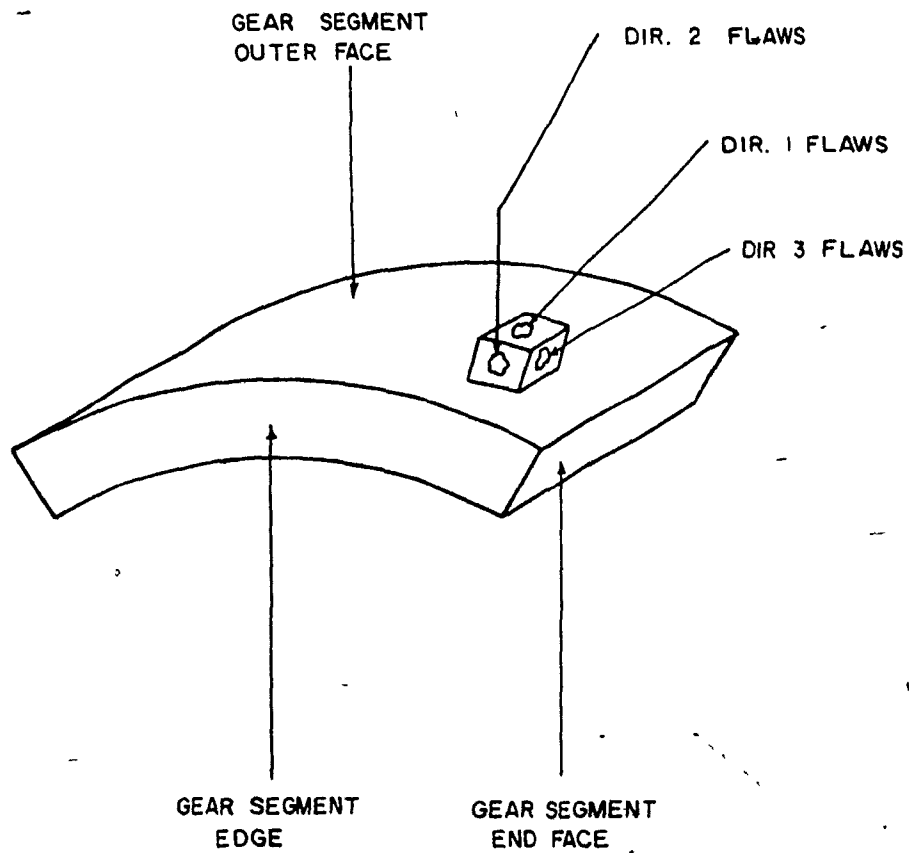
Fig. 5.15 - Orientation of the three
primary flaw directions.

175

TYPE OF EXPOSURE	DOSE
External exposure to naturally occurring radioactive materials and to cosmic rays	0.0002 rem/day
Average chest X-ray	0.1 to 2 r.
Dental X-ray	1.5 to 15 r.
Treatment of malignant tumors (local dose)	3000 to 7000 r.
Fatal dose applied to entire body in short period of time	200 to 800 r.
Permanent sterility dose for males and females	500 to 625 r.

Table 3.1   Estimated dose of common radiation exposure.

EXPOSURE	PERMISSIBLE DOSE	AVERAGE PERMISSIBLE DOSE
Radiation Workers:		
Total dose in any 13 consecutive weeks	3 rem	0.3 rem/week
Total dose in any 1 year	12 rem	
Total accumulated dose at N, where N is the person's age and greater than 18	5 x (N-18)	5 rem/yr.
Nonoccupational Personnel:		
Total dose in any 13 consecutive weeks	0.3 rem	0.03 rem/week
Total dose in any 1 year	1.2 rem	
Total accumulated dose at age N.	0.5 x (N-18)	0.5 rem/yr.

Table 3.2   Basic permissible radiation doses

CONSTITUENT ELEMENT	COMPOSITION LIMITS (% W/W)
Carbon	0.38 - 0.43
Chromium	0.70 - 0.90
Manganese	0.60 - 0.80
Molybdenum	0.20 - 0.30
Nickel	1.65 - 2.00
Phosphorus	0.035 max.
Sulphur	0.040 max.
Silicon	0.15 - 0.30

Table 4.1 Composition limits of the constituent elements of SAE 4340.

PROPERTY	AVERAGE VALUE
Modulus of elasticity	203.16 GPa
Yield strength (0.2% offset)	776.50 MPa
Ultimate strength	965.29 MPa
Reduction in Area	30%

Table 4.2   Average monotonic properties
            of BB225 [23].

SAMPLE BLOCK	L (cm)	W (cm)	T (cm)	MASS (kg)
11	17.1	17.1	18.4	38.5
12	17.8	17.1	19.7	39.0
13	17.8	17.1	18.4	36.2
14	16.5	15.9	19.0	34.9
21	17.1	17.8	20.3	47.6
22	17.1	17.8	19.7	43.0
23	17.8	17.8	14.0	31.7
23L	17.8	17.8	33.0	43.1
24	17.8	17.8	20.3	50.3
25	18.4	17.8	20.3	49.9
26	17.8	18.4	19.1	47.2
31	17.8	16.5	19.1	42.2
32	19.1	17.1	18.4	45.4
33	17.8	16.5	20.3	41.7
34	17.8	17.8	17.8	43.5
41	20.3	18.4	18.4	49.9
42	20.3	16.5	19.1	45.8
43	19.1	17.8	17.8	47.6
44	19.1	18.4	20.3	47.6
61	20.3	17.1	19.7	49.4
62	15.2	15.2	19.0	42.6
63	20.3	16.5	18.4	45.4
64	20.3	10.2	17.8	24.9
66	17.1	11.4	17.8	34.0
67	14.0	16.5	15.2	39.0

Note: see Fig. 4.7 for definition of L, W and T.

Table 4.3 Dimensions and weights of the as-cut steel sample blocks.

SAMPLE BLOCK	L (cm)	W (cm)	T (cm)	MASS (kg)
11	14.07	14.07	16.58	24.5
12	13.95	13.98	16.50	24.9
13	14.06	14.07	16.59	24.9
14	14.03	14.05	16.59	24.9
21	15.94	15.96	16.48	31.7
22	13.98	13.95	16.51	24.9
23	16.48	16.45	12.28	24.9
23L*	-	-	-	31.7
24	16.56	16.51	16.51	33.5
25	16.67	16.67	16.52	34.0
26	16.59	16.66	16.52	34.0
31	13.97	13.97	16.53	24.9
32	15.84	15.91	16.50	31.7
33	13.97	13.98	16.50	23.6
34	15.90	15.90	16.50	31.7
41	16.56	16.51	16.51	34.0
42	13.95	13.97	16.51	24.5
43	15.94	15.94	16.50	31.7
44	15.94	15.94	16.50	31.7
61	13.96	13.96	16.50	24.5
62	13.97	13.97	16.49	24.5
63	14.06	14.08	16.60	24.9
64	15.33	7.63	17.92	15.9
66	15.25	10.29	15.25	18.1
67	12.75	14.63	14.62	23.6

* See Fig. 4.8 for block 23L dimensions.
Note: see Fig. 4.7 for definition of L, W, and T.

Table 4.4   Dimensions and weights of the
machined steel sample blocks.

METAL THICKNESS RADIOGRAPHED	SOURCE SIDE ASTM PENETRAMETER
7.6 - 10.2 cm	50
10.2 - 15.2 cm	60
15.2 - 20.3 cm	80
20.3 - 25.4 cm	100

Table 4.5 ASTM penetrameters for various metal distances.

SAMPLE BLOCK	X-RAY DIRECTION	METAL THICKNESS (cm)	FILM TYPE	DOSE (rads)	SOURCE TO OBJECT DIST. (cm)	ASTM PENETRAMETER
11	1	16.5	AA	500	166.4	80
11	2	14.0	AA	300	168.9	60
12	1	16.5	AA	500	166.4	80
12	2	14.0	AA	300	168.9	60
13	1	16.5	AA	500	166.4	80
13	2	14.0	AA	300	168.9	60
14	1	16.5	AA	500	166.4	80
14	2	14.0	AA	300	168.9	60
21	1	16.5	AA	500	166.4	80
21	2	15.9	AA	440	167.0	80
22	1	16.5	AA	500	166.4	80
22	2	14.0	AA	300	168.9	60
23	1	12.3	AA	190	170.5	60
23	2	16.5	AA	500	166.4	80
23L	1	15.9	AA	440	167.0	80
23L	2	15.9	AA	440	167.0	80
23L	3	5.6	M	180	177.3	40
24	1	16.5	AA	500	166.4	80
24	2	16.5	AA	500	166.4	80
25	1	16.5	AA	500	166.4	80
25	2	16.5	AA	500	166.4	80
26	1	16.5	AA	500	166.4	80
26	2	16.5	AA	500	166.4	80
31	1	16.5	AA	500	166.4	80
31	2	14.0	AA	300	168.9	60
32	1	16.5	AA	500	166.4	80
32	2	15.9	AA	440	167.0	80
33	1	16.5	AA	500	166.4	80
33	2	14.0	AA	300	168.9	60
34	1	16.5	AA	500	166.4	80
34	2	15.9	AA	440	167.0	80
41	1	16.5	AA	500	166.4	80
41	2	16.5	AA	500	166.4	80
42	1	16.5	AA	500	166.4	80
42	2	14.0	AA	300	168.9	60
43	1	16.5	AA	500	166.4	80
43	2	15.9	AA	440	167.0	80
44	1	16.5	AA	500	166.4	80
44	2	15.9	AA	440	167.0	80
61	1	16.5	AA	500	166.4	80
61	2	14.0	AA	300	168.9	60
62	1	16.5	AA	500	166.4	80
62	2	14.0	AA	300	168.9	60
63	1	16.5	AA	500	166.4	80
63	2	14.0	AA	300	168.9	60
64	1	7.6	M	270	175.3	50
66	1	15.2	AA	380	167.6	60
66	2	10.3	AA	120	172.7	60
67	1	14.6	AA	330	168.3	60
67	2	14.6	AA	330	168.3	60

Table 4.6 Radiographic inspection parameters
of the steel sample blocks.

FRACTURE SPECIMEN	12B	13A	13C	24A	24C	25A	25B	32A	32C	33B	42B	43C	62A	62C
NOTCH AREA (mm^2)	63.6	58.5	56.2	58.8	59.3	48.9	47.5	44.8	55.1	52.0	61.6	58.1	60.4	57.7
VIEWED IN SEM	YES	YES	NO	YES	NO	YES	YES	NO	NO	NO	YES	YES	YES	NO

MTS LOAD RANGE ALL TESTS (KN)   100

MTS STROKE RANGE ALL TESTS (mm)   10

RAMP LOAD DURATION ALL TESTS (sec)   30

MTS CONTROLLER SPAN 1 ALL TESTS   300

PROGRAM SPAN ALL TESTS (% STROKE)   30

Table 4.7 Fracture test parameters.

184

ELEMENT	ASTM STANDARD	METHOD EMPLOYED	SPECTRAL ENERGY (nm)
Aluminum	-	Atomic Absorption	309.3
Carbon	-	Infrared Absorption	-
Chromium	E 350-84 Section 269	Atomic Absorption	357.9
Copper	-	Atomic Absorption	324.7
Manganese	-	Atomic Absorption	279.5
Molybdenum	-	Atomic Absorption	313.3
Nickel	E 350-84 Section 237	Atomic Absorption	232.0
Phosphorus	E 350-84 Section 221	Alkalimetric Method	-
Silicon	E 350-84 Section 46	Gravimetric Method	-
Sulphur	E 350-84 Section 37	Combustion-Iodate Titration Method	-

Table 4.8 Chemical analysis methods.

SAMPLE BLOCK	X-RAY DIRECTION	RESULT	COMMENTS
11	1	NDI	
11	2	NDI	
12	1	NDI	
12	2	NDI	
13	1	NDI	
13	2	NDI	
14	1	NDI	
14	2	NDI	
21	1	NDI	
21	2	NDI	
22	1	NDI	
22	2	D	1 rectangular, 2 circular
23	1	D	1 rectangular round ends, 2 circular
23	2	D	2 rectangular
23L	1	NDI	Drilled 1/8" dia. holes easily seen.
23L	2	NDI	The 4 1/8" dia. drilled holes easily seen.
23L	3	D	1 rectangular indication in the rib 7.6 cm below gear face bottom.
24	1	D	3 light rectangular indications
24	2	D	1 circular, 2 rectangular indications
25	1	NDI	
25	2	NDI	
26	1	NDI	
26	2	D	3 light spot indications
31	1	NDI	
31	2	NDI	
32	1	NDI	
32	2	NDI	
33	1	NDI	
33	2	NDI	
34	1	NDI	
34	2	NDI	
41	1	D	Rectangular round end indication, very faint shrinkage in center and right side but too light to measure and quantify.
41	2	D	Randomly distributed spot and rectangular indications.
42	1	D	2 spot indications
42	2	D	randomly distributed spot indications

NDI = No defects indicated
D = Defects indicated

Table 5.1   Summary of radiographic inspection results.

SAMPLE BLOCK	X-RAY DIRECTION	RESULT	COMMENTS
43	1	NDI	
43	2	D	2 circular, 1 rectangular. Also indications too light to quantify.
44	1	NDI	
44	2	D	Light indications uniform in block. Probably shrinkage.
61	1	NDI	
61	2	NDI	
62	1	NDI	
62	2	NDI	
63	1	NDI	
63	2	NDI	
64	-	D	4 circular indications
66	1	NDI	
66	2	NDI	
67	1	NDI	
67	2	NDI	

NDI = No defects indicated
D = Defects indicated

Table 5.1   cont.

FLAW INDICATION TYPE	FLAW INDICATION DESCRIPTION	FLAW INDICATION PARAMETERS*	PARAMETER RANGE (cm)
1	circular	d	$0.2 \leqslant d < 0.3$
2	circular	d	$0.3 \leqslant d < 0.4$
3	circular	d	$0.4 \leqslant d$
4	rectangular	w, l	$0.1 \leqslant w \leqslant 0.5$ $0.2 \leqslant l \leqslant 0.8$
5	rectangular	w, l	$0.1 \leqslant w \leqslant 0.5$ $0.8 < l$

* Circular flaw — d

Rectangular $\updownarrow w$ ← l →
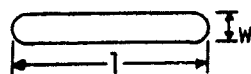
Table 5.2   Summary of flaw types obtained from radiographic inspection results.

RADIOGRAPH NUMBER	FLAW TYPE	FLAW PARAMETER(S) (cm)	FLAW AREA (cm^2)
22-2	5	w = 0.4 l = 1.0	0.400
22-2	3	d = 0.4	0.126
22-2	1	d = 0.2	0.031
23-1	3	d = 0.4	0.126
23-1	3	d = 0.5	0.196
23-1	4	w = 0.4 l = 0.7	0.280
23-2	4	w = 0.4 l = 0.8	0.320
23-2	4	w = 0.2 l = 0.7	0.140
23L-3	5	w = 0.5 l = 1.0	0.500
24-1	4	w = 0.3 l = 0.7	0.210
24-1	4	w = 0.3 l = 0.8	0.240
24-1	5	w = 0.5 l = 1.0	0.500
24-2	3	d = 0.7	0.385
24-2	5	w = 0.5 l = 1.0	0.500
24-2	4	w = 0.3 l = 0.8	0.240
26-2	3	d = 0.4	0.126
26-2	3	d = 0.6	0.283
26-2	3	d = 0.4	0.126
41-1	5	w = 0.4 l = 2.5	1.000
41-2	2	d = 0.3	0.071
41-2	4	w = 0.3 l = 0.8	0.240
41-2	2	d = 0.3	0.071
41-2	3	d = 0.4	0.126
41-2	3	d = 0.4	0.126
41-2	3	d = 0.4	0.126
41-2	3	d = 0.5	0.196
41-2	5	w = 0.5 l = 1.0	0.500
41-2	2	d = 0.3	0.071
41-2	5	w = 0.4 l = 1.5	0.600

Table 5.3   Summary of flaws indicated by radiographic inspection.

RADIOGRAPH NUMBER	FLAW TYPE	FLAW PARAMETER(S) (cm)	FLAW AREA (cm²)
41-2	4	w = 0.3 l = 0.8	0.240
42-1	3	d = 0.6	0.283
42-1	3	d = 0.5	0.196
42-2	2	d = 0.3	0.071
42-2	3	d = 0.4	0.126
42-2	2	d = 0.3	0.071
42-2	3	d = 0.4	0.126
42-2	3	d = 0.4	0.126
42-2	3	d = 0.5	0.196
42-2	5	w = 0.3 l = 1.0	0.300
42-2	3	d = 0.4	0.126
43-2	4	w = 0.2 l = 0.4	0.080
43-2	3	d = 0.4	0.126
43-2	3	d = 0.6	0.283
44-2	1	d = 0.2	0.031
44-2	3	d = 0.4	0.126
44-2	2	d = 0.3	0.071
44-2	3	d = 0.5	0.196
44-2	5	w = 0.4 l = 0.9	0.360
44-2	2	d = 0.3	0.071
44-2	4	w = 0.3 l = 0.8	0.240
44-2	4	w = 0.4 l = 0.8	0.320
64	3	d = 0.4	0.126
64	2	d = 0.3	0.071
64	3	d = 0.4	0.126
64	3	d = 0.6	0.196

Table 5.3 cont.

REFERENCE BLOCK	X-RAY RESULT	COMMENTS
1	NDI	The 3.175 mm dia. flat bottom hole clearly
2	NDI	seen in all ultrasonic reference
3	NDI	block radiographs.
4	NDI	
5	NDI	

NDI = No defects indicated

Table 5.4   Summary of ultrasonic reference block radiographic inspection results.

SAMPLE BLOCK	ULTRASONIC INSPECTION FACE	TEST RESULT	SAMPLE BLOCK	ULTRASONIC INSPECTION FACE	TEST RESULT
12	A	D	33	A	D
12	B	D	33	B	D
12	C	NDI	33	C	NDI
13	A	NDI	34	A	NDI
13	B	NDI	34	B	NDI
13	C	NDI	34	C	NDI
14	A	NDI	41	A	D
14	B	NDI	41	B	D
14	C	NDI	41	C	D
21	A	D	42	A	D
21	B	NDI	42	B	D
21	C	D	42	C	D
22	A	D	43	A	D
22	B	NDI	43	B	D
22	C	D	43	C	D
23	A	D	44	A	D
23	B	NDI	44	B	NDI
23	C	NDI	44	C	D
23L	A	D	61	A	D
23L	C	D	61	B	D
23L	D	D	61	C	D
23L	E	D	62	A	NDI
24	A	D	62	B	D
24	B	D	62	C	NDI
24	C	D	63	A	NDI
25	A	D	63	B	NDI
25	B	D	63	C	NDI
25	C	D	64	A	NDI
26	A	D	64	B	NDI
26	B	NDI	64	C	NDI
26	C	D	66	A	NDI
31	A	D	66	B	NDI
31	B	D	66	C	NDI
31	C	D	67	A	NDI
32	A	NDI	67	B	NDI
32	B	D	67	C	NDI
32	C	D			

NDI = No defects indicated
D = Defects indicated

Table 5.5 Summary of ultrasonic inspection results.

FLAW INDICATION TYPE	FLAW INDICATION DESCRIPTION	FLAW INDICATION PARAMETERS*	PARAMETER RANGE (cm)
1	circular	d	$d < 0.1$
2	circular	d	$0.1 \leqslant d < 0.5$
3	circular	d	$0.15 \leqslant d < 0.2$
4	circular	d	$0.2 \leqslant d < 0.3$
5	circular	d	$0.3 \leqslant d < 0.4$
6	circular	d	$0.4 \leqslant d$
7	rectangular	w,l	$0.1 \leqslant w \leqslant 0.5$ $0.2 \leqslant l \leqslant 0.8$
8	rectangular	w,l	$0.1 \leqslant w \leqslant 0.5$ $0.8 < l$

* Circular: ⟶◯⟵ d
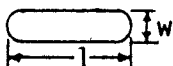
Rectangular: ⬭ ↕w |⟵ l ⟶|

Table 5.6 Summary of flaw indication types obtained from ultrasonic inspection results.

SAMPLE BLOCK	SAMPLE BLOCK FACE	% DAC CURVE	FLAW DIAMETER (cm)	FLAW WIDTH (cm)	FLAW LENGTH (cm)	FLAW AREA (cm²)	FLAW TYPE
12	A	30	0.095	-	-	0.007	1
12	A	50	0.159	-	-	0.020	3
12	B	50	0.159	-	-	0.020	3
12	B	35	0.111	-	-	0.010	2
12	B	90	0.286	-	-	0.064	4
12	B	30	0.095	-	-	0.007	1
12	B	30	0.095	-	-	0.007	1
12	B	55	0.175	-	-	0.024	3
12	C	125	0.400	-	-	0.126	6
12	C	160	0.507	-	-	0.202	6
14	C	130	0.412	-	-	0.133	6
21	A	55	0.175	-	-	0.024	3
21	A	70	0.222	-	-	0.039	4
21	A	55	0.175	-	-	0.024	3
21	A	50	0.159	-	-	0.020	3
21	A	65	0.206	-	-	0.033	4
21	A	65	0.206	-	-	0.033	4
21	A	45	0.143	-	-	0.016	2
21	A	80	0.254	-	-	0.051	4
21	A	50	0.159	-	-	0.020	3
21	A	40	0.127	-	-	0.013	2
21	A	50	0.159	-	-	0.020	3
21	A	40	0.127	-	-	0.013	2
21	A	80	0.254	-	-	0.051	4
21	C	40	0.127	-	-	0.013	2
21	C	60	0.190	-	-	0.028	3
21	C	35	0.111	-	-	0.010	2
21	C	45	0.143	-	-	0.016	2
21	C	45	0.143	-	-	0.016	2
21	C	50	0.159	-	-	0.020	3
21	C	40	0.127	-	-	0.013	2
21	C	40	0.127	-	-	0.013	2
21	C	150	0.476	-	-	0.178	6
21	C	125	0.400	-	-	0.126	6
22	A	30	0.095	-	-	0.007	1
22	A	30	0.095	-	-	0.007	1
22	A	35	0.111	-	-	0.010	2
22	A	30	0.095	-	-	0.007	1
22	A	30	0.095	-	-	0.007	1
22	B	100	-	0.317	1.0	0.317	8
22	B	100	0.317	-	-	0.079	5
22	C	35	0.111	-	-	0.010	2
22	C	30	0.095	-	-	0.007	1
22	C	40	0.127	-	-	0.013	2
22	C	40	0.127	-	-	0.013	2

Table 5.7 Ultrasonic inspection flaw indications.

SAMPLE BLOCK	SAMPLE BLOCK FACE	% DAC CURVE	FLAW DIAMETER (cm)	FLAW WIDTH (cm)	FLAW LENGTH (cm)	FLAW AREA (cm^2)	FLAW TYPE
22	C	50	0.159	-	-	0.020	3
22	C	55	-	0.175	0.6	0.105	7
22	C	20	0.063	-	-	0.003	1
22	C	50	0.159	-	-	0.020	3
22	C	135	0.428	-	-	0.143	6
22	C	65	0.206	-	-	0.033	4
23	A	35	0.111	-	-	0.010	2
23	A	35	0.111	-	-	0.010	2
23	A	150	-	0.476	1.0	0.476	8
23	A	120	0.380	-	-	0.133	5
23	A	150	0.476	-	-	0.178	6
23	B	65	-	0.206	1.0	0.206	8
23	B	130	-	0.412	1.0	0.412	8
23L	A	75	0.238	-	-	0.044	4
23L	A	60	0.190	-	-	0.028	3
23L	A	75	0.238	-	-	0.044	4
23L	A	40	0.127	-	-	0.013	2
23L	A	90	0.286	-	-	0.064	4
23L	D	90	-	0.286	0.7	0.200	7
23L	D	70	0.222	-	-	0.039	4
23L	D	35	0.111	-	-	0.010	2
23L	D	50	0.159	-	-	0.020	3
23L	D	50	0.159	-	-	0.020	3
23L	D	30	0.095	-	-	0.007	1
23L	D	45	0.143	-	-	0.016	2
23L	D	65	0.206	-	-	0.033	4
23L	C	55	0.175	-	-	0.024	3
23L	C	50	0.159	-	-	0.020	3
23L	C	60	0.190	-	-	0.028	3
23L	C	55	0.175	-	-	0.024	3
23L	E	45	0.143	-	-	0.016	2
23L	E	60	0.190	-	-	0.028	3
23L	E	60	0.190	-	-	0.028	3
24	A	40	0.127	-	-	0.013	2
24	A	35	0.111	-	-	0.010	2
24	A	160	0.507	-	-	0.202	6
24	A	130	0.412	-	-	0.133	6
24	A	40	0.127	-	-	0.013	2
24	A	65	0.206	-	-	0.033	4
24	A	40	0.127	-	-	0.013	2
24	A	40	0.127	-	-	0.013	2
24	A	30	0.095	-	-	0.007	1
24	B	60	0.190	-	-	0.028	3
24	B	150	0.476	-	-	0.178	6
24	B	50	0.159	-	-	0.020	3

Table 5.7 cont.

SAMPLE BLOCK	SAMPLE BLOCK FACE	% DAC CURVE	FLAW DIAMETER (cm)	FLAW WIDTH (cm)	FLAW LENGTH (cm)	FLAW AREA (cm^2)	FLAW TYPE
24	B	55	0.175	–	–	0.024	3
24	B	50	0.159	–	–	0.020	3
24	C	35	0.111	–	–	0.010	2
24	C	40	–	0.127	0.30	0.038	7
24	C	35	–	0.111	0.60	0.067	7
24	C	130	0.412	–	–	0.133	6
24	C	50	–	0.159	0.7	0.111	7
25	A	30	0.095	–	–	0.007	1
25	A	55	0.175	–	–	0.024	3
25	A	50	0.159	–	–	0.020	3
25	A	60	0.190	–	–	0.028	3
25	A	50	0.159	–	–	0.020	3
25	A	60	0.190	–	–	0.028	3
25	A	100	0.317	–	–	0.079	5
25	A	60	0.190	–	–	0.028	3
25	A	50	0.159	–	–	0.020	3
25	A	40	0.127	–	–	0.013	2
25	A	85	0.270	–	–	0.057	4
25	A	70	0.222	–	–	0.039	4
25	A	40	0.127	–	–	0.013	2
25	B	75	0.238	–	–	0.044	4
25	C	50	0.159	–	–	0.020	3
25	C	45	0.143	–	–	0.016	2
25	C	40	0.127	–	–	0.013	2
25	C	50	0.159	–	–	0.020	3
25	C	150	0.476	–	–	0.178	6
25	C	60	–	0.190	0.70	0.133	7
26	A	50	0.159	–	–	0.020	3
26	A	75	0.238	–	–	0.044	4
26	A	50	0.159	–	–	0.020	3
26	A	100	0.317	–	–	0.079	5
26	A	100	0.317	–	–	0.079	5
26	A	50	0.159	–	–	0.020	3
26	A	70	0.222	–	–	0.039	4
26	A	50	0.159	–	–	0.020	3
26	A	50	0.159	–	–	0.020	3
26	A	60	0.190	–	–	0.028	3
26	A	50	0.159	–	–	0.020	3
26	A	50	0.159	–	–	0.020	3
26	A	40	0.127	–	–	0.013	2
26	A	60	0.190	–	–	0.028	3
26	A	75	0.238	–	–	0.044	4
26	B	110	0.349	–	–	0.096	5
26	B	150	0.476	–	–	0.178	6
26	B	120	0.380	–	–	0.113	5

Table 5.7   cont.

SAMPLE BLOCK	SAMPLE BLOCK FACE	% DAC CURVE	FLAW DIAMETER (cm)	FLAW WIDTH (cm)	FLAW LENGTH (cm)	FLAW AREA (cm^2)	FLAW TYPE
26	C	40	0.127	-	-	0.013	2
26	C	30	0.095	-	-	0.007	1
26	C	30	0.095	-	-	0.007	1
26	C	70	0.222	-	-	0.039	4
26	C	40	0.127	-	-	0.013	2
26	C	45	0.143	-	-	0.016	2
31	A	45	0.143	-	-	0.016	2
31	A	35	0.111	-	-	0.010	2
31	A	30	0.095	-	-	0.007	1
31	A	65	0.206	-	-	0.033	4
31	A	40	0.127	-	-	0.013	2
31	A	35	0.111	-	-	0.010	2
31	B	25	0.079	-	-	0.005	1
31	B	60	-	0.190	2.2	0.418	8
31	B	40	0.127	-	-	0.013	2
31	B	40	0.127	-	-	0.013	2
31	B	60	0.190	-	-	0.028	3
31	B	50	0.159	-	-	0.020	3
31	B	50	0.159	-	-	0.020	3
31	B	30	0.095	-	-	0.007	1
31	B	60	0.190	-	-	0.028	3
31	C	30	0.095	-	-	0.007	1
31	C	85	-	0.270	0.30	0.081	7
31	C	40	0.127	-	-	0.013	2
32	B	30	0.095	-	-	0.007	1
32	B	30	0.095	-	-	0.007	1
32	C	50	-	0.159	0.30	0.048	7
32	C	25	0.079	-	-	0.005	1
33	A	25	0.079	-	-	0.005	1
33	A	30	0.095	-	-	0.007	1
33	A	40	0.127	-	-	0.013	2
33	A	40	0.127	-	-	0.013	2
33	A	30	0.095	-	-	0.007	1
33	A	40	0.127	-	-	0.013	2
33	A	30	0.095	-	-	0.007	1
33	A	50	0.159	-	-	0.020	3
33	B	45	0.143	-	-	0.016	2
33	B	40	0.127	-	-	0.013	2
33	B	35	0.111	-	-	0.010	2
33	B	25	0.079	-	-	0.005	1
33	B	40	0.127	-	-	0.013	2
33	B	50	-	0.159	2.7	0.429	8
33	B	35	0.111	-	-	0.010	2
41	A	35	0.111	-	-	0.010	2
41	A	35	0.111	-	-	0.010	2

Table 5.7   cont.

SAMPLE BLOCK	SAMPLE BLOCK FACE	% DAC CURVE	FLAW DIAMETER (cm)	FLAW WIDTH (cm)	FLAW LENGTH (cm)	FLAW AREA (cm²)	FLAW TYPE
41	A	40	0.127	-	-	0.013	2
41	A	30	0.095	-	-	0.007	1
41	A	100	-	0.317	1.00	0.317	8
41	A	45	0.143	-	-	0.016	2
41	A	70	0.222	-	-	0.039	4
41	A	55	0.175	-	-	0.024	3
41	A	40	0.127	-	-	0.013	2
41	A	30	0.095	-	-	0.007	1
41	A	60	0.190	-	-	0.028	3
41	A	35	0.111	-	-	0.010	2
41	A	40	0.127	-	-	0.013	2
41	A	30	0.095	-	-	0.007	1
41	B	45	0.143	-	-	0.016	2
41	B	100	0.317	-	-	0.079	5
41	B	75	-	0.238	1.00	0.238	8
41	B	50	0.159	-	-	0.020	3
41	B	35	0.111	-	-	0.010	2
41	B	100	0.317	-	-	0.079	5
41	B	40	0.127	-	-	0.013	2
41	B	100	0.317	-	-	0.079	5
41	B	35	0.111	-	-	0.010	2
41	B	110	-	0.349	1.00	0.349	8
41	C	30	0.095	-	-	0.007	1
41	C	50	0.159	-	-	0.020	3
41	C	55	0.175	-	-	0.024	3
41	C	45	0.143	-	-	0.016	2
41	C	45	0.143	-	-	0.016	2
41	C	140	0.444	-	-	0.155	6
41	C	155	0.491	-	-	0.189	6
41	C	50	0.159	-	-	0.020	3
42	A	25	0.079	-	-	0.005	1
42	A	40	0.127	-	-	0.013	2
42	A	25	0.079	-	-	0.005	1
42	A	150	0.476	-	-	0.178	6
42	A	40	0.127	-	-	0.013	2
42	A	75	0.238	-	-	0.044	4
42	A	55	0.175	-	-	0.024	3
42	B	30	0.095	-	-	0.007	1
42	B	50	0.159	-	-	0.020	3
42	B	120	0.380	-	-	0.113	5
42	B	150	0.476	-	-	0.178	6
42	B	30	0.095	-	-	0.007	1
42	B	25	0.079	-	-	0.005	1
42	B	40	0.127	-	-	0.013	2
42	B	50	0.159	-	-	0.020	3

Table 5.7 cont.

SAMPLE BLOCK	SAMPLE BLOCK FACE	% DAC CURVE	FLAW DIAMETER (cm)	FLAW WIDTH (cm)	FLAW LENGTH (cm)	FLAW AREA (cm^2)	FLAW TYPE
42	B	150	0.476	-	-	0.178	6
42	B	120	0.380	-	-	0.113	5
42	B	130	0.412	-	-	0.133	6
42	C	140	0.444	-	-	0.155	6
42	C	130	0.412	-	-	0.133	6
42	C	55	-	0.175	0.40	0.070	7
42	B	25	0.079	-	-	0.005	1
43	A	60	0.190	-	-	0.028	3
43	A	45	0.143	-	-	0.016	2
43	A	30	0.095	-	-	0.007	1
43	A	55	0.175	-	-	0.024	3
43	A	50	0.159	-	-	0.020	3
43	A	30	0.095	-	-	0.007	1
43	A	85	0.270	-	-	0.057	4
43	A	70	0.222	-	-	0.039	4
43	A	30	0.095	-	-	0.007	1
43	B	30	0.095	-	-	0.007	1
43	B	95	0.286	-	-	0.064	4
43	B	40	0.127	-	-	0.013	2
43	B	120	0.380	-	-	0.113	5
43	B	70	0.222	-	-	0.039	4
43	B	100	0.317	-	-	0.079	5
43	B	40	0.127	-	-	0.013	2
43	C	140	0.444	-	-	0.155	6
43	C	135	0.428	-	-	0.143	6
43	C	45	0.143	-	-	0.016	2
43	C	70	0.222	-	-	0.039	4
44	A	100	0.317	-	-	0.079	5
44	A	80	0.254	-	-	0.051	4
44	A	50	0.159	-	-	0.020	3
44	A	45	0.143	-	-	0.016	2
44	A	55	0.175	-	-	0.024	3
44	A	40	0.127	-	-	0.013	2
44	A	65	0.206	-	-	0.033	4
44	A	40	0.127	-	-	0.013	2
44	A	70	0.222	-	-	0.039	4
44	A	50	0.159	-	-	0.020	3
44	A	45	0.143	-	-	0.016	2
44	A	45	0.143	-	-	0.016	2
44	A	40	0.127	-	-	0.013	2
44	A	35	0.111	-	-	0.010	2
44	A	50	0.159	-	-	0.020	3
44	A	30	0.095	-	-	0.007	1
44	A	35	0.111	-	-	0.010	2
44	A	60	0.190	-	-	0.028	3

Table 5.7   cont.

SAMPLE BLOCK	SAMPLE BLOCK	% DAC	FLAW DIAMETER (cm)	FLAW WIDTH (cm)	FLAW LENGTH (cm)	FLAW AREA (cm^2)	FLAW TYPE
44	B	85	0.270	-	-	0.057	4
44	B	130	0.412	-	-	0.133	6
44	B	120	0.380	-	-	0.113	5
44	B	90	-	0.286	0.80	0.229	7
44	B	85	-	0.270	0.80	0.216	7
44	B	100	-	0.317	1.00	0.317	8
44	C	30	0.095	-	-	0.007	1
44	C	85	0.270	-	-	0.057	4
44	C	60	0.190	-	-	0.028	3
44	C	85	0.270	-	-	0.057	4
44	C	75	0.238	-	-	0.044	4
44	C	55	0.175	-	-	0.024	3
44	C	150	0.476	-	-	0.178	6
44	C	150	0.476	-	-	0.178	6
44	C	50	0.159	-	-	0.020	3
44	C	35	0.111	-	-	0.010	2
44	C	55	0.175	-	-	0.024	3
61	A	70	0.222	-	-	0.039	4
61	A	50	0.159	-	-	0.020	3
61	A	50	-	0.159	2.60	0.413	8
61	A	30	0.095	-	-	0.007	1
61	A	30	0.095	-	-	0.007	1
61	A	40	0.127	-	-	0.013	2
61	A	60	0.190	-	-	0.028	3
61	A	45	0.143	-	-	0.016	2
61	A	50	0.159	-	-	0.020	3
61	B	100	0.317	-	-	0.079	5
61	B	75	0.238	-	-	0.044	4
61	C	35	0.111	-	-	0.010	2
61	C	45	0.143	-	-	0.016	2
61	C	40	0.127	-	-	0.013	2
61	C	40	0.127	-	-	0.013	2
61	C	30	0.095	-	-	0.007	1
61	C	50	0.159	-	-	0.020	3
62	B	30	0.095	-	-	0.007	1
66	C	30	0.095	-	-	0.007	1

Table 5.7 cont.

200

FRACTURE SPECIMEN	X-RAY DIRECTION	RESULT	DESCRIPTION OF FLAW INDICATION
12A	1	NDI	
12A	2	NDI	
13A	1	NDI	
13A	2	NDI	
21A	1	NDI	
21A	2	NDI	
24A	1	NDI	
24A	2	D	0.2 x 0.3 cm S
25A	1	NDI	
25A	2	D	0.2 cm dia. S, 0.05 x 0.2 cm S
32A	1	D	0.25 cm dia. GP
32A	2	D	0.3 x 0.5 cm S
33A	1	NDI	
33A	2	NDI	
42A	1	NDI	
42A	2	NDI	
43A	1	D	0.2 cm dia. S
43A	2	D	0.3 x 0.3 cm S, 0.3 x 0.5 cm S, 0.2 x 0.2 cm S, 0.1 x 0.2 cm S
62A	1	NDI	
62A	2	NDI	
12B	1	NDI	
12B	2	NDI	
13B	1	NDI	
13B	2	NDI	
21B	1	D	0.2 x 0.4 cm S
21B	2	D	0.3 x 0.6 cm S
24B	1	NDI	
24B	2	D	0.3 x 0.6 cm S
25B	1	NDI	
25B	2	D	0.1 x 0.3 cm S, 0.5 x 0.5 cm S, 0.2 cm dia. S, 0.05 x 0.2 cm S
32B	1	NDI	
32B	2	NDI	
33B	1	NDI	
33B	2	NDI	
42B	1	D	0.1 x 0.4 GP
42B	2	D	0.1 x 0.6 GP
43B	1	NDI	
43B	2	NDI	
62B	1	NDI	

Note: S = shrinkage defect
           GP = gas porosity defect

Table 5.8   Summary of flaws indicated in radiographic inspection of fracture specimens.

FRACTURE SPECIMEN	X-RAY DIRECTION	RESULT	DESCRIPTION OF FLAW INDICATION
62B	2	NDI	
12C	1	NDI	
12C	2	NDI	
13C	1	NDI	
13C	2	NDI	
21C	1	NDI	
21C	2	NDI	
24C	1	D	0.3 cm dia. S, 0.1 cm dia. GP, 0.1 x 0.6 cm S, 0.1 cm dia. S
24C	2	D	0.35 dia. S, 0.2 cm dia. GP, 0.2 x 0.3 cm S, 0.1 x 0.2 cm S
25C	1	D	0.1 x 0.2 cm S, 0.05 x 0.15 cm S
25C	2	D	0.1 x 0.4 cm S
32C	1	NDI	
32C	2	NDI	
33C	1	D	0.1 x 0.4 cm S
33C	2	NDI	
42C	1	NDI	
42C	2	D	0.2 cm dia. GP, 0.4 cm dia. GP
43C	1	NDI	
43C	2	NDI	
62C	1	NDI	
62C	2	NDI	

Note: S = shrinkage defect
GP = gas porosity defect

Table 5.8 cont.

FLAW TYPE	FLAW DESCRIPTION	FLAW PARAMETERS
1	Circular	$\rightarrow\bigcirc\leftarrow d$
2	Rectangular, round ends	w, l
3	Slit, sharp ends	w, l
4	Multi-branched rectangular, round ends	branch $(i + 1)$ θ_i, W_i, l_i branch i $n =$ total number of branches
5	Multi-branched slit, sharp ends	branch $(i + 1)$ θ_i, W_i, l_i branch i $n =$ total number of branches
6	Circular inclusion	$\rightarrow\bigcirc\leftarrow d$
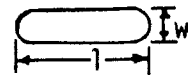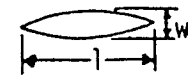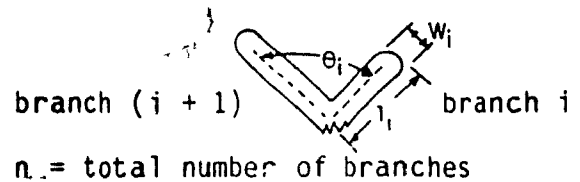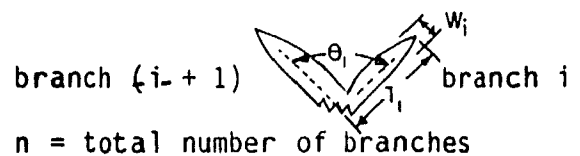
Table 5.9   Flaw types and their parameters observed in microscopic inspection.

FRACTURE SPECIMEN	FLAW I.D. NUMBER	FLAW TYPE	FRACTOGRAPH FLAW PARAMETERS (cm)		ACTUAL FLAW PARAMETERS (mm)	
12B	1	1	d = 0.07		d = 0.02	
12B	2	2	w = 0.05	l = 0.16	w = 0.02	l = 0.05
12B	3	3	w = 0.04	l = 0.54	w = 0.01	l = 0.18
12B	4	2	w = 0.17	l = 0.31	w = 0.06	l = 0.10
12B	5	1	d = 0.21		d = 0.07	
12B	6	3	w = 0.03	l = 0.215	w = 0.01	l = 0.07
12B	7	1	d = 0.13		d = 0.04	
12B	8	2	w = 0.22	l = 0.53	w = 0.07	l = 0.18
12B	9	1	d = 0.11		d = 0.04	
12B	10	1	d = 0.31		d = 0.10	
12B	11	2	w = 0.07	l = 0.65	w = 0.02	l = 0.22
12B	12	2	w = 0.23	l = 0.50	w = 0.08	l = 0.17
12B	13	1	d = 0.06		d = 0.02	
12B	14	3	w = 0.04	l = 0.28	w = 0.01	l = 0.09
12B	15	1	d = 0.09		d = 0.03	
12B	16	1	d = 0.11		d = 0.04	
12B	17	3	w = 0.11	l = 0.42	w = 0.04	l = 0.14
12B	18	2	w = 0.10	l = 0.30	w = 0.03	l = 0.10
12B	19	1	d = 0.10		d = 0.03	
12B	20	2	w = 0.06	l = 0.25	w = 0.02	l = 0.08
12B	21	1	d = 0.10		d = 0.03	
12B	22	3	w = 0.08	l = 0.30	w = 0.03	l = 0.10
12B	23	1	d = 0.10		d = 0.03	
12B	24	2	w = 0.08	l = 0.18	w = 0.03	l = 0.06
12B	25	1	d = 0.18		d = 0.06	
12B	26	3	w = 0.05	l = 0.32	w = 0.02	l = 0.11
12B	27	3	w = 0.09	l = 0.30	w = 0.03	l = 0.10
12B	28	2	w = 0.10	l = 0.50	w = 0.03	l = 0.17
12B	29	1	d = 0.10		d = 0.03	
12B	30	4	n = 2 $\quad$ $\theta_1 = 20^\circ$ $w_1 = 0.04$ $\quad$ $l_1 = 0.47$ $w_2 = 0.10$ $\quad$ $l_2 = 0.30$		n = 2 $\quad$ $\theta_1 = 20^\circ$ $w_1 = 0.01$ $\quad$ $l_1 = 0.16$ $w_2 = 0.03$ $\quad$ $l_2 = 0.10$	
12B	31	1	d = 0.25		d = 0.08	
12B	32	4	n = 3 $\theta_1 = 120^\circ$ $\quad$ $\theta_2 = 40^\circ$ $w_1 = 0.14$ $\quad$ $l_1 = 0.64$ $w_2 = 0.12$ $\quad$ $l_2 = 0.58$ $w_3 = 0.14$ $\quad$ $l_3 = 0.70$		n = 3 $\theta_1 = 120^\circ$ $\quad$ $\theta_2 = 40^\circ$ $w_1 = 0.05$ $\quad$ $l_1 = 0.21$ $w_2 = 0.04$ $\quad$ $l_2 = 0.19$ $w_3 = 0.05$ $\quad$ $l_3 = 0.23$	
12B	33	2	w = 0.10	l = 0.35	w = 0.03	l = 0.12
12B	34	3	w = 0.03	l = 0.15	w = 0.01	l = 0.05
12B	35	2	w = 0.10	l = 0.24	w = 0.03	l = 0.08
12B	36	2	w = 0.14	l = 0.46	w = 0.05	l = 0.15
12B	37	1	d = 0.12		d = 0.04	

Table 5.10 Details of flaws obtained from fractographs of fracture specimens.

FRACTURE SPECIMEN	FLAW I.D. NUMBER	FLAW TYPE	FRACTOGRAPH FLAW PARAMETERS (cm)		ACTUAL FLAW PARAMETERS (mm)	
12B	38	3	w = 0.10	l = 0.22	w = 0.03	l = 0.07
12B	39	3	w = 0.07	l = 0.41	w = 0.02	l = 0.14
12B	40	2	w = 0.12	l = 0.30	w = 0.04	l = 0.10
12B	41	2	w = 0.09	l = 0.28	w = 0.03	l = 0.09
12B	42	2	w = 0.06	l = 0.20	w = 0.02	l = 0.07
13A	1	3	w = 0.03	l = 0.41	w = 0.01	l = 0.17
13A	2	1	d = 0.20		d = 0.08	
13A	3	1	d = 0.19		d = 0.08	
13A	4	1	d = 0.14		d = 0.06	
13A	5	1	d = 0.10		d = 0.04	
13A	6	2	w = 0.06	l = 0.21	w = 0.04	l = 0.09
13A	7	2	w = 0.05	l = 0.18	w = 0.02	l = 0.07
13A	8	2	w = 0.09	l = 0.31	w = 0.04	l = 0.13
13A	9	2	w = 0.09	l = 0.24	w = 0.04	l = 0.10
13A	10	1	d = 0.14		d = 0.06	
13A	11	2	w = 0.03	l = 0.17	w = 0.01	l = 0.07
13A	12	2	w = 0.04	l = 0.25	w = 0.02	l = 0.10
13A	13	1	d = 0.07		d = 0.03	
13A	14	2	w = 0.14	l = 0.30	w = 0.06	l = 0.12
13A	15	3	w = 0.06	l = 0.27	w = 0.02	l = 0.11
13A	16	1	d = 0.10		d = 0.04	
13A	17	2	w = 0.11	l = 0.26	w = 0.04	l = 0.11
13A	18	2	w = 0.06	l = 0.23	w = 0.02	l = 0.10
13A	19	1	d = 0.10		d = 0.04	
13A	20	2	w = 0.15	l = 0.32	w = 0.06	l = 0.13
13A	21	3	w = 0.03	l = 0.18	w = 0.01	l = 0.07
13A	22	1	d = 0.11		d = 0.04	
13A	23	1	d = 0.12		d = 0.05	
13A	24	2	w = 0.04	l = 0.18	w = 0.02	l = 0.07
13A	25	1	d = 0.11		d = 0.04	
13A	26	3	w = 0.12	l = 0.53	w = 0.05	l = 0.22
13A	27	1	d = 0.08		d = 0.03	
13A	28	2	w = 0.07	l = 0.33	w = 0.03	l = 0.14
13A	29	3	w = 0.08	l = 0.14	w = 0.03	l = 0.06
13A	30	3	w = 0.04	l = 0.26	w = 0.02	l = 0.11
13A	31	1	d = 0.07		d = 0.03	
13A	32	3	w = 0.07	l = 0.50	w = 0.03	l = 0.21
13A	33	1	d = 0.16		d = 0.07	
13A	34	1	d = 0.16		d = 0.07	
13A	35	3	w = 0.14	l = 0.28	w = 0.06	l = 0.12
13A	36	2	w = 0.06	l = 0.14	w = 0.02	l = 0.06
13A	37	1	d = 0.23		d = 0.09	
13A	38	2	w = 0.10	l = 0.25	w = 0.04	l = 0.10

Table 5.10 cont.

FRACTURE SPECIMEN	FLAW I.D. NUMBER	FLAW TYPE	FRACTOGRAPH FLAW PARAMETERS (cm)		ACTUAL FLAW PARAMETERS (mm)	
13A	39	1	d = 0.11		d = 0.04	
13A	40	2	w = 0.16	l = 0.39	w = 0.07	l = 0.16
13A	41	3	w = 0.06	l = 0.35	w = 0.02	l = 0.14
13A	42	3	w = 0.07	l = 0.18	w = 0.03	l = 0.07
13A	43	2	w = 0.10	l = 0.24	w = 0.04	l = 0.10
13A	44	2	w = 0.06	l = 0.20	w = 0.02	l = 0.08
13A	45	2	w = 0.06	l = 0.20	w = 0.02	l = 0.08
13A	46	2	w = 0.11	l = 0.26	w = 0.04	l = 0.11
13A	47	3	w = 0.07	l = 0.18	w = 0.03	l = 0.07
13A	48	3	w = 0.05	l = 0.26	w = 0.02	l = 0.11
13A	49	2	w = 0.08	l = 0.22	w = 0.03	l = 0.09
13A	50	1	d = 0.10		d = 0.04	
13A	51	3	w = 0.05	l = 0.50	w = 0.02	l = 0.21
13A	52	1	d = 0.11		d = 0.04	
13A	53	1	d = 0.10		d = 0.04	
13A	54	2	w = 0.07	l = 0.26	w = 0.03	l = 0.11
13A	55	3	w = 0.07	l = 0.40	w = 0.03	l = 0.17
13A	56	4	n = 2	$\theta_1 = 120°$	n = 2	$\theta_1 = 120°$
			$w_1 = 0.06$	$l_1 = 0.14$	$w_1 = 0.02$	$l_1 = 0.06$
			$w_2 = 0.09$	$l_2 = 0.19$	$w_2 = 0.04$	$l_2 = 0.08$
13A	57	2	w = 0.13	$l_2 = 0.27$	w = 0.05	$l_2 = 0.11$
13A	58	1	d = 0.07		d = 0.03	
13A	59	1	d = 0.09		d = 0.04	
13A	60	2	w = 0.36	l = 0.63	w = 0.15	l = 0.26
13A	61	4	n = 2	$\theta_1 = 90°$	n = 2	$\theta_1 = 90°$
			$w_1 = 0.12$	$l_1 = 0.27$	$w_1 = 0.05$	$l_1 = 0.11$
			$w_2 = 0.15$	$l_2 = 0.20$	$w_2 = 0.06$	$l_2 = 0.08$
13A	62	3	w = 0.13	$l_2 = 0.32$	w = 0.05	$l_2 = 0.13$
13A	63	3	w = 0.07	l = 0.41	w = 0.03	l = 0.17
13A	64	1	d = 0.17		d = 0.07	
13A	65	1	d = 0.10		d = 0.04	
13A	66	3	w = 0.06	l = 0.23	w = 0.02	l = 0.10
13A	67	1	d = 0.13		d = 0.05	
13A	68	1	d = 0.10		d = 0.04	
13A	69	1	d = 0.12		d = 0.05	
13A	70	1	d = 0.34		d = 0.14	
13A	71	2	w = 0.13	l = 0.21	d = 0.05	l = 0.09
13A	72	2	w = 0.05	l = 0.19	w = 0.02	l = 0.08
13A	73	1	d = 0.20		d = 0.08	
13A	74	1	d = 0.29		d = 0.12	
13A	75	1	d = 0.15		d = 0.06	
13A	76	1	d = 0.11		d = 0.05	
13A	77	2	w = 0.06	l = 0.15	w = 0.02	l = 0.06
13A	78	1	d = 0.10		d = 0.04	

Table 5.10 cont.

FRACTURE SPECIMEN	FLAW I.D. NUMBER	FLAW TYPE	FRACTOGRAPH FLAW PARAMETERS (cm)		ACTUAL FLAW PARAMETERS (mm)	
13A	79	3	$w = 0.05$	$l = 0.22$	$w = 0.02$	$l = 0.09$
13A	80	1	$d = 0.12$		$d = 0.05$	
13A	81	1	$d = 0.10$		$d = 0.04$	
13A	82	1	$d = 0.07$		$d = 0.03$	
13A	83	3	$w = 0.10$	$l = 0.24$	$w = 0.04$	$l = 0.10$
13A	84	3	$w = 0.07$	$l = 0.34$	$w = 0.03$	$l = 0.14$
13A	85	3	$w = 0.07$	$l = 0.33$	$w = 0.03$	$l = 0.14$
13A	86	2	$w = 0.12$	$l = 0.25$	$w = 0.05$	$l = 0.10$
13A	87	3	$w = 0.05$	$l = 0.19$	$w = 0.02$	$l = 0.08$
13A	88	4	$n = 2$ $\quad \theta_1 = 100^0$ $w_1 = 0.12$ $\quad l_1 = 0.19$ $w_2 = 0.06$ $\quad l_2 = 0.26$		$n = 2$ $\quad \theta_1 = 100^0$ $w_1 = 0.05$ $\quad l_1 = 0.08$ $w_2 = 0.02$ $\quad l_2 = 0.11$	
13A	89	2	$w = 0.10$	$l = 0.20$	$w = 0.04$	$l = 0.08$
13A	90	1	$d = 0.09$		$d = 0.04$	
13A	91	2	$w = 0.05$	$l = 0.24$	$w = 0.02$	$l = 0.10$
13A	92	3	$w = 0.04$	$l = 0.12$	$w = 0.02$	$l = 0.05$
13A	93	1	$d = 0.09$		$d = 0.04$	
13A	94	1	$d = 0.17$		$d = 0.07$	
13A	95	4	$n = 2$ $\quad \theta_1 = 90^0$ $w_1 = 0.09$ $\quad l_1 = 0.19$ $w_2 = 0.13$ $\quad l_2 = 0.25$		$n = 2$ $\quad \theta_1 = 90^0$ $w_1 = 0.04$ $\quad l_1 = 0.08$ $w_2 = 0.05$ $\quad l_2 = 0.10$	
13A	96	3	$w = 0.04$	$l = 0.26$	$w = 0.02$	$l = 0.11$
13A	97	2	$w = 0.05$	$l = 0.12$	$w = 0.02$	$l = 0.05$
13A	98	4	$n = 2$ $\quad \theta_1 = 95^0$ $w_1 = 0.11$ $\quad l_1 = 0.23$ $w_2 = 0.08$ $\quad l_2 = 0.26$		$n = 2$ $\quad \theta_1 = 95^0$ $w_1 = 0.04$ $\quad l_1 = 0.09$ $w_2 = 0.03$ $\quad l_2 = 0.11$	
13A	99	1	$d = 0.25$		$d = 0.10$	
13A	100	1	$d = 0.15$		$d = 0.06$	
13A	101	1	$d = 0.15$		$d = 0.06$	
13A	102	3	$w = 0.10$	$l = 0.25$	$w = 0.04$	$l = 0.10$
13A	103	4	$n = 2$ $\quad \theta_1 = 100^0$ $w_1 = 0.05$ $\quad l_1 = 0.20$ $w_2 = 0.04$ $\quad l_2 = 0.16$		$n = 2$ $\quad \theta_1 = 100^0$ $w_1 = 0.02$ $\quad l_1 = 0.08$ $w_2 = 0.02$ $\quad l_2 = 0.07$	
13A	104	3	$w = 0.07$	$l = 0.24$	$w = 0.03$	$l = 0.10$
13A	105	2	$w = 0.09$	$l = 0.25$	$w = 0.04$	$l = 0.10$
25B	1	3	$w = 0.06$	$l = 0.65$	$w = 0.02$	$l = 0.27$
25B	2	2	$w = 0.14$	$l = 0.24$	$w = 0.06$	$l = 0.10$
25B	3	3	$w = 0.04$	$l = 0.18$	$w = 0.02$	$l = 0.07$
25B	4	1	$d = 0.18$		$d = 0.07$	
25B	5	2	$w = 0.04$	$l = 0.15$	$w = 0.02$	$l = 0.06$
25B	6	2	$w = 0.05$	$l = 0.11$	$w = 0.02$	$l = 0.04$
25B	7	1	$d = 0.05$		$d = 0.02$	
25B	8	1	$d = 0.06$		$d = 0.02$	

Table 5.10   cont.

207

FRACTURE SPECIMEN	FLAW I.D. NUMBER	FLAW TYPE	FRACTOGRAPH FLAW PARAMETERS (cm)		ACTUAL FLAW PARAMETERS (mm)	
25B	9	3	$w = 0.05$	$l = 0.20$	$w = 0.02$	$l = 0.08$
25B	10	1	$d = 0.10$		$d = 0.04$	
25B	11	1	$d = 0.16$	$\smile$	$d = 0.07$	
25B	12	2	$w = 0.05$	$l = 0.27$	$w = 0.02$	$l = 0.11$
25B	13	2	$w = 0.12$	$l = 0.63$	$w = 0.05$	$l = 0.26$
25B	14	3	$w = 0.07$	$l = 0.24$	$w = 0.03$	$l = 0.10$
25B	15	5	$n = 2$ $\theta_1 = 95^0$		$n = 2$ $\theta_1 = 95^0$	
			$w_1 = 0.08$	$l_1 = 0.30$	$w_1 = 0.03$	$l_1 = 0.12$
			$w_2 = 0.07$	$l_2 = 0.23$	$w_2 = 0.03$	$l_2 = 0.09$
25B	16	1	$d^2 = 0.11$		$d^2 = 0.04$	
25B	17	2	$w = 0.08$	$l = 0.33$	$w = 0.03$	$l = 0.14$
25B	18	1	$d = 0.07$		$d = 0.03$	
25B	19	1	$d = 0.07$		$d = 0.03$	
25B	20	1	$d = 0.10$		$d = 0.04$	
25B	21	4	$n = 3$		$n = 3$	
			$\theta_1 = 110^0$	$\theta_2 = 80^0$	$\theta_1 = 110^0$	$\theta_2 = 80^0$
			$w_1 = 0.09$	$l_1 = 0.27$	$w_1 = 0.04$	$l_1 = 0.11$
			$w_2 = 0.05$	$l_2 = 0.13$	$w_2 = 0.02$	$l_2 = 0.05$
			$w_3 = 0.07$	$l_3 = 0.11$	$w_3 = 0.03$	$l_3 = 0.05$
25B	22	2	$w = 0.07$	$l = 0.24$	$w = 0.03$	$l = 0.10$
25B	23	3	$w = 0.07$	$l = 0.90$	$w = 0.03$	$l = 0.37$
25B	24	2	$w = 0.07$	$l = 0.52$	$w = 0.03$	$l = 0.22$
25B	25	2	$w = 0.05$	$l = 0.36$	$w = 0.02$	$l = 0.15$
25B	26	2	$w = 0.04$	$l = 0.18$	$w = 0.02$	$l = 0.07$
25B	27	1	$d = 0.27$		$d = 0.11$	
25B	28	1	$d = 0.13$		$d = 0.05$	
25B	29	3	$w = 0.04$	$l = 0.38$	$w = 0.02$	$l = 0.16$
25B	30	1	$d = 0.10$		$d = 0.04$	
25B	31	2	$w = 0.10$	$l = 0.18$	$w = 0.04$	$l = 0.07$
25B	32	1	$d = 0.25$		$d = 0.10$	
25B	33	1	$d = 0.12$		$d = 0.05$	
25B	34	1	$d = 0.10$		$d = 0.04$	
25B	35	1	$d = 0.11$		$d = 0.04$	
25B	36	2	$w = 0.08$	$l = 0.21$	$w = 0.03$	$l = 0.09$
25B	37	1	$d = 0.10$		$d = 0.04$	
25B	38	2	$w = 0.10$	$l = 0.21$	$w = 0.04$	$l = 0.09$
25B	39	4	$n = 2$ $\theta_1 = 90^0$		$n = 2$ $\theta_1 = 90^0$	
			$w_1 = 0.05$	$l_1 = 0.19$	$w_1 = 0.02$	$l_1 = 0.08$
			$w_2 = 0.09$	$l_2 = 0.20$	$w_2 = 0.04$	$l_2 = 0.08$
25B	40	1	$d^2 = 0.07$		$d^2 = 0.03$	
25B	41	2	$w = 0.07$	$l = 0.22$	$w = 0.03$	$l = 0.09$
25B	42	1	$d = 0.11$		$d = 0.04$	
25B	43	1	$d = 0.08$		$d = 0.03$	
25B	44	2	$w = 0.08$	$l = 0.17$	$w = 0.03$	$l = 0.07$

Table 5.10   cont.

FRACTURE SPECIMEN	FLAW I.D. NUMBER	FLAW TYPE	FRACTOGRAPH FLAW PARAMETERS (cm)		ACTUAL FLAW PARAMETERS (mm)	
25B	45	2	$w = 0.10$	$l = 0.23$	$w = 0.04$	$l = 0.09$
25B	46	4	$n = 2$	$\theta_1 = 30^{\circ}$	$n = 2$	$\theta_1 = 30^{\circ}$
			$w_1 = 0.07$	$l_1 = 0.20$	$w_1 = 0.03$	$l_1 = 0.08$
			$w_2 = 0.06$	$l_2 = 0.16$	$w_2 = 0.02$	$l_2 = 0.07$
25B	47	2	$w = 0.11$	$l = 0.29$	$w = 0.04$	$l = 0.12$
25B	48	1	$d = 0.10$		$d = 0.04$	
25B	49	1	$d = 0.06$		$d = 0.02$	
25B	50	1	$d = 0.06$		$d = 0.02$	
25B	51	1	$d = 0.11$		$d = 0.04$	
25B	52	1	$d = 0.09$		$d = 0.04$	
25B	53	1	$d = 0.08$		$d = 0.03$	
25B	54	1	$d = 0.14$		$d = 0.06$	
25B	55	1	$d = 0.12$		$d = 0.05$	
25B	56	1	$d = 0.06$		$d = 0.02$	
25B	57	1	$d = 0.09$		$d = 0.04$	
25B	58	2	$w = 0.07$	$l = 0.21$	$w = 0.03$	$l = 0.09$
25B	59	1	$d = 0.09$		$d = 0.04$	
25B	60	3	$w = 0.05$	$l = 0.17$	$w = 0.02$	$l = 0.07$
25B	61	1	$d = 0.10$		$d = 0.04$	
25B	62	3	$w = 0.06$	$l = 0.20$	$w = 0.02$	$l = 0.08$
25B	63	2	$w = 0.08$	$l = 0.17$	$w = 0.03$	$l = 0.07$
25B	64	2	$w = 0.05$	$l = 0.18$	$w = 0.02$	$l = 0.07$
25B	65	1	$d = 0.07$		$d = 0.03$	
25B	66	1	$d = 0.11$		$d = 0.04$	
25B	67	2	$w = 0.13$	$l = 0.24$	$w = 0.05$	$l = 0.10$
25B	68	4	$n = 2$	$\theta_1 = 120^{\circ}$	$n = 2$	$\theta_1 = 120^{\circ}$
			$w_1 = 0.08$	$l_1 = 0.23$	$w_1 = 0.03$	$l_1 = 0.10$
			$w_2 = 0.08$	$l_2 = 0.15$	$w_2 = 0.03$	$l_2 = 0.06$
25B	69	1	$d = 0.13$		$d = 0.05$	
25B	70	2	$w = 0.04$	$l = 0.18$	$w = 0.02$	$l = 0.07$
25B	71	1	$d = 0.14$		$d = 0.06$	
25B	72	2	$w = 0.07$	$l = 0.16$	$w = 0.03$	$l = 0.07$
25B	73	3	$w = 0.04$	$l = 0.30$	$w = 0.02$	$l = 0.12$
25B	74	2	$w = 0.06$	$l = 0.48$	$w = 0.02$	$l = 0.20$
25B	75	2	$w = 0.15$	$l = 0.38$	$w = 0.06$	$l = 0.16$
25B	76	1	$d = 0.15$		$d = 0.06$	
25B	77	3	$w = 0.05$	$l = 0.34$	$w = 0.02$	$l = 0.14$
25B	78	2	$w = 0.17$	$l = 0.52$	$w = 0.07$	$l = 0.22$
25B	79	4	$n = 2$	$\theta_1 = 10^{\circ}$	$n = 2$	$\theta_1 = 10^{\circ}$
			$w_1 = 0.14$	$l_1 = 0.63$	$w_1 = 0.06$	$l_1 = 0.26$
			$w_2 = 0.15$	$l_2 = 0.59$	$w_2 = 0.06$	$l_2 = 0.24$
25B	80	2	$w = 0.09$	$l = 0.20$	$w = 0.04$	$l = 0.08$
25B	81	2	$w = 0.14$	$l = 0.45$	$w = 0.06$	$l = 0.19$
25B	82	1	$d = 0.16$		$d = 0.07$	

Table 5.10 cont.

FRACTURE SPECIMEN	FLAW I.D. NUMBER	FLAW TYPE	FRACTOGRAPH FLAW PARAMETERS (cm)		ACTUAL FLAW PARAMETERS (mm)	
25B	83	1	d = 0.11		d = 0.04	
25B	84	1	d = 0.12		d = 0.05	
25B	85	2	w = 0.10	l = 0.33	w = 0.04	l = 0.14
25B	86	3	w = 0.05	l = 0.25	w = 0.02	l = 0.10
25B	87	1	d = 0.41		d = 0.17	
25B	88	2	w = 0.15	l = 0.31	w = 0.06	l = 0.13
25B	89	2	w = 0.08	l = 0.22	w = 0.03	l = 0.09
25B	90	1	d = 0.22		d = 0.09	
25B	91	1	d = 0.15		d = 0.06	
25B	92	3	w = 0.10	l = 0.38	w = 0.04	l = 0.16
25B	93	1	d = 0.10		d = 0.04	
25B	94	1	d = 0.17		d = 0.07	
25B	95	1	d = 0.18		d = 0.07	
25B	96	2	w = 0.08	l = 0.30	w = 0.03	l = 0.12
25B	97	1	d = 0.22		d = 0.09	
25B	98	1	d = 0.10		d = 0.04	
25B	99	4	n = 2	$\theta_1 = 70^o$	n = 2	$\theta_1 = 70^o$
			$w_1 = 0.05$ $l_1 = 0.11$		$w_1 = 0.02$ $l_1 = 0.04$	
			$w_2 = 0.06$ $l_2 = 0.13$		$w_2 = 0.02$ $l_2 = 0.05$	
25B	100	1	d = 0.13		d = 0.05	
25B	101	2	w = 0.09	l = 0.23	w = 0.04	l = 0.09
25B	102	2	w = 0.04	l = 0.12	w = 0.02	l = 0.05
25B	103	2	w = 0.17	l = 0.47	w = 0.07	l = 0.19
25B	104	3	w = 0.07	l = 0.62	w = 0.03	l = 0.26
25B	105	2	w = 0.11	l = 0.18	w = 0.04	l = 0.07
25B	106	2	w = 0.13	l = 0.20	w = 0.05	l = 0.08
25B	107	1	d = 0.12		d = 0.05	
25B	108	1	d = 0.08		d = 0.03	
25B	109	2	w = 0.07	l = 0.15	w = 0.03	l = 0.06
25B	110	1	d = 0.14		d = 0.06	
25B	111	3	w = 0.06	l = 0.30	w = 0.02	l = 0.12
25B	112	1	d = 0.08		d = 0.03	
25B	113	3	w = 0.05	l = 0.18	w = 0.02	l = 0.07
25B	114	2	w = 0.10	l = 0.23	w = 0.04	l = 0.10
25B	115	1	d = 0.10		d = 0.04	
25B	116	1	d = 0.12		d = 0.05	
25B	117	3	w = 0.06	l = 0.18	w = 0.02	l = 0.07
25B	118	2	w = 0.13	l = 0.20	w = 0.05	l = 0.08
25B	119	1	d = 0.11		d = 0.04	
25B	120	1	d = 0.12		d = 0.05	
42B	1	2	w = 0.10	l = 0.26	w = 0.02	l = 0.04
42B	2	2	w = 0.17	l = 0.29	w = 0.03	l = 0.05
42B	3	2	w = 0.35	l = 0.54	w = 0.06	l = 0.09

Table 5.10 cont.

FRACTURE SPECIMEN	FLAW I.D. NUMBER	FLAW TYPE	FRACTOGRAPH FLAW PARAMETERS (cm)		ACTUAL FLAW PARAMETERS (mm)	
42B	4	2	$w = 0.07$	$l = 0.40$	$w = 0.01$	$l = 0.07$
42B	5	2	$w = 0.08$	$l = 0.22$	$w = 0.01$	$l = 0.04$
42B	6	2	$w = 0.12$	$l = 0.32$	$w = 0.02$	$l = 0.05$
42B	7	2	$w = 0.07$	$l = 0.24$	$w = 0.01$	$l = 0.04$
42B	8	1	$d = 0.17$		$d = 0.03$	
42B	9	4	$n = 2$ $\quad \theta_1 = 90^0$ $w_1 = 0.15$ $\quad l_1 = 0.30$ $w_2 = 0.09$ $\quad l_2 = 0.33$		$n = 2$ $\quad \theta_1 = 90^0$ $w_1 = 0.02$ $\quad l_1 = 0.05$ $w_2 = 0.01$ $\quad l_2 = 0.06$	
42B	10	2	$w = 0.10$	$l = 0.94$	$w = 0.02$	$l = 0.16$
42B	11	3	$w = 0.09$	$l = 0.35$	$w = 0.01$	$l = 0.06$
42B	12	3	$w = 0.13$	$l = 0.45$	$w = 0.02$	$l = 0.08$
42B	13	3	$w = 0.08$	$l = 0.27$	$w = 0.01$	$l = 0.05$
42B	14	2	$w = 0.07$	$l = 0.28$	$w = 0.01$	$l = 0.05$
42B	15	4	$n = 2$ $\quad \theta_1 = 70^0$ $w_1 = 0.14$ $\quad l_1 = 0.69$ $w_2 = 0.12$ $\quad l_2 = 0.28$		$n = 2$ $\quad \theta_1 = 70^0$ $w_1 = 0.02$ $\quad l_1 = 0.12$ $w_2 = 0.02$ $\quad l_2 = 0.05$	
42B	16	3	$w = 0.05$	$l = 0.25$	$w = 0.01$	$l = 0.04$
42B	17	2	$w = 0.08$	$l = 0.30$	$w = 0.01$	$l = 0.05$
42B	18	1	$d = 0.12$		$d = 0.02$	
42B	19	1	$d = 0.15$		$d = 0.02$	
42B	20	2	$w = 0.10$	$l = 0.30$	$w = 0.02$	$l = 0.05$
42B	21	1	$d = 0.16$		$d = 0.03$	
42B	22	2	$w = 0.17$	$l = 0.32$	$d = 0.03$	$l = 0.05$
42B	23	3	$w = 0.08$	$l = 0.42$	$w = 0.01$	$l = 0.07$
42B	24	1	$d = 0.17$		$d = 0.03$	
42B	25	1	$d = 0.30$		$d = 0.05$	
42B	26	3	$w = 0.07$	$l = 0.48$	$w = 0.01$	$l = 0.08$
42B	27	2	$w = 0.30$	$l = 0.58$	$w = 0.05$	$l = 0.10$
42B	28	2	$w = 0.11$	$l = 0.20$	$w = 0.02$	$l = 0.03$
42B	29	1	$d = 0.14$		$d = 0.02$	
42B	30	1	$d = 0.19$		$d = 0.03$	
42B	31	2	$w = 0.10$	$l = 1.83$	$w = 0.02$	$l = 0.31$
42B	32	1	$d = 0.14$		$d = 0.02$	
42B	33	2	$w = 0.09$	$l = 0.26$	$w = 0.01$	$l = 0.04$
42B	34	2	$w = 0.08$	$l = 0.30$	$w = 0.01$	$l = 0.05$
42B	35	2	$w = 0.10$	$l = 0.28$	$w = 0.02$	$l = 0.05$
42B	36	3	$w = 0.10$	$l = 0.48$	$w = 0.02$	$l = 0.08$
42B	37	2	$w = 0.08$	$l = 0.88$	$w = 0.01$	$l = 0.15$
42B	38	3	$w = 0.08$	$l = 0.38$	$w = 0.01$	$l = 0.06$
42B	39	3	$w = 0.04$	$l = 0.58$	$w = 0.01$	$l = 0.10$
42B	40	2	$w = 0.08$	$l = 0.89$	$w = 0.01$	$l = 0.15$
42B	41	5	$n = 2$ $\quad \theta_1 = 90^0$ $w_1 = 0.09$ $\quad l_1 = 0.40$ $w_2 = 0.07$ $\quad l_2 = 0.26$		$n = 2$ $\quad \theta_1 = 90^0$ $w_1 = 0.01$ $\quad l_1 = 0.07$ $w_2 = 0.01$ $\quad l_2 = 0.04$	

Table 5.10   cont.

FRACTURE SPECIMEN	FLAW I.D. NUMBER	FLAW TYPE	FRACTOGRAPH FLAW PARAMETERS (cm)		ACTUAL FLAW PARAMETERS (mm)	
42B	42	2	$w = 0.11$	$l = 0.31$	$w = 0.02$	$l = 0.05$
42B	43	2	$w = 0.11$	$l = 0.27$	$w = 0.02$	$l = 0.05$
42B	44	1	$d = 0.11$		$d = 0.02$	
42B	45	1	$d = 0.13$		$d = 0.02$	
42B	46	1	$d = 0.11$		$d = 0.02$	
42B	47	2	$w = 0.08$	$l = 0.31$	$w = 0.01$	$l = 0.05$
42B	48	3	$w = 0.04$	$l = 0.50$	$w = 0.01$	$l = 0.09$
42B	49	5	$n = 2$	$\theta_1 = 60^0$	$n = 2$	$\theta_1 = 60^0$
			$w_1 = 0.08$	$l_1 = 0.35$	$w_1 = 0.01$	$l_1 = 0.06$
			$w_2 = 0.05$	$l_2 = 0.24$	$w_2 = 0.01$	$l_2 = 0.04$
42B	50	4	$n = 3$		$n = 3$	
			$\theta_1 = 90^0$	$\theta_2 = 90^0$	$\theta_1 = 90^0$	$\theta_2 = 90^0$
			$w_1 = 0.07$	$l_1 = 0.23$	$w_1 = 0.01$	$l_1 = 0.04$
			$w_2 = 0.07$	$l_2 = 0.13$	$w_2 = 0.01$	$l_2 = 0.02$
			$w_3 = 0.07$	$l_3 = 0.10$	$w_3 = 0.01$	$l_3 = 0.02$
42B	51	2	$w = 0.10$	$l = 0.64$	$w = 0.02$	$l = 0.11$
42B	52	1	$d = 0.15$		$d = 0.03$	
42B	53	1	$d = 0.18$		$d = 0.03$	
42B	54	1	$d = 0.24$		$d = 0.04$	
42B	55	2	$w = 0.22$	$l = 0.48$	$w = 0.04$	$l = 0.08$
42B	56	1	$d = 0.32$		$d = 0.05$	
42B	57	1	$d = 0.64$		$d = 0.11$	
42B	58	2	$w = 0.14$	$l = 0.82$	$w = 0.02$	$l = 0.14$
42B	59	2	$w = 0.24$	$l = 0.84$	$w = 0.04$	$l = 0.14$
42B	60	1	$d = 0.25$		$d = 0.04$	
42B	61	2	$w = 0.05$	$l = 0.22$	$w = 0.01$	$l = 0.04$
42B	62	1	$d = 0.17$		$d = 0.03$	
42B	63	1	$d = 0.28$		$d = 0.05$	
42B	64	3	$w = 0.05$	$l = 0.69$	$w = 0.01$	$l = 0.12$
42B	65	3	$w = 0.06$	$l = 0.65$	$w = 0.01$	$l = 0.11$
42B	66	2	$w = 0.13$	$l = 0.53$	$w = 0.02$	$l = 0.09$
42B	67	2	$w = 0.13$	$l = 0.36$	$w = 0.02$	$l = 0.06$
42B	68	3	$w = 0.08$	$l = 0.63$	$w = 0.01$	$l = 0.11$
42B	69	1	$d = 0.28$		$d = 0.05$	
42B	70	2	$w = 0.69$	$l = 2.18$	$w = 0.12$	$l = 0.37$
42B	71	3	$w = 0.07$	$l = 0.36$	$w = 0.01$	$l = 0.06$
42B	72	1	$d = 0.30$		$d = 0.05$	
42B	73	2	$w = 0.13$	$l = 0.25$	$w = 0.02$	$l = 0.04$
42B	74	3	$w = 0.10$	$l = 0.56$	$w = 0.02$	$l = 0.09$
42B	75	2	$w = 0.17$	$l = 0.40$	$w = 0.03$	$l = 0.07$
42B	76	3	$w = 0.08$	$l = 0.27$	$w = 0.01$	$l = 0.05$
42B	77	3	$w = 0.04$	$l = 0.60$	$w = 0.01$	$l = 0.10$
42B	78	3	$w = 0.07$	$l = 0.64$	$w = 0.01$	$l = 0.11$
42B	79	3	$w = 0.06$	$l = 0.54$	$w = 0.01$	$l = 0.09$

Table 5.10   cont.

FRACTURE SPECIMEN	FLAW I.D. NUMBER	FLAW TYPE	FRACTOGRAPH FLAW PARAMETERS (cm)		ACTUAL FLAW PARAMETERS (mm)	
43C	1	1	d = 0.10		d = 0.02	
43C	2	1	d = 0.08		d = 0.01	
43C	3	1	d = 0.16		d = 0.03	
43C	4	2	w = 0.39	l = 0.48	w = 0.07	l = 0.08
43C	5	3	w = 0.18	l = 0.71	w = 0.03	l = 0.12
43C	6	2	w = 0.23	l = 0.52	w = 0.04	l = 0.09
43C	7	3	w = 0.04	l = 0.28	w = 0.01	l = 0.05
43C	8	3	w = 0.06	l = 0.27	w = 0.01	l = 0.05
43C	9	3	w = 0.06	l = 0.49	w = 0.01	l = 0.08
43C	10	3	w = 0.05	l = 0.27	w = 0.01	l = 0.05
43C	11	1	d = 0.12		d = 0.02	
62A	1	2	w = 0.12	l = 0.17	w = 0.05	l = 0.07
62A	2	3	w = 0.04	l = 0.26	w = 0.02	l = 0.11
62A	3	6	d = 0.44		d = 0.18	
62A	4	2	w = 0.13	l = 0.30	w = 0.05	l = 0.12
62A	5	2	w = 0.28	l = 0.61	w = 0.12	l = 0.25
62A	6	1	d = 0.14		d = 0.06	
62A	7	6	d = 0.76		d = 0.31	
62A	8	2	w = 0.10	l = 0.19	w = 0.04	l = 0.08
62A	9	2	w = 0.10	l = 0.14	w = 0.04	l = 0.06
62A	10	3	w = 0.08	l = 0.32	w = 0.03	l = 0.13
62A	11	1	d = 0.12		d = 0.05	
62A	12	3	w = 0.07	l = 0.25	w = 0.03	l = 0.10
62A	13	3	w = 0.07	l = 0.18	w = 0.03	l = 0.07
62A	14	2	w = 0.12	l = 0.26	w = 0.05	l = 0.11
62A	15	2	w = 0.10	l = 0.19	w = 0.04	l = 0.08
62A	16	1	d = 0.15		d = 0.06	
62A	17	2	w = 0.08	l = 0.19	w = 0.03	l = 0.08
62A	18	1	d = 0.13		d = 0.05	
62A	19	1	d = 0.12		d = 0.05	
62A	20	2	w = 0.07	l = 0.23	w = 0.03	l = 0.10
62A	21	2	w = 0.05	l = 0.24	w = 0.02	l = 0.10
62A	22	5	n = 2 $\quad$ $\theta_1 = 90^o$ $w_1 = 0.06$ $\quad$ $l_1 = 0.27$ $w_2 = 0.04$ $\quad$ $l_2 = 0.29$		n = 2 $\quad$ $\theta_1 = 90^o$ $w_1 = 0.02$ $\quad$ $l_1 = 0.11$ $w_2 = 0.02$ $\quad$ $l_2 = 0.12$	
62A	23	3	w = 0.10	$l = 0.33$	w = 0.04	$l = 0.14$
62A	24	6	d = 0.35		d = 0.15	
62A	25	1	d = 0.08		d = 0.03	
62A	26	3	w = 0.06	l = 0.39	w = 0.02	l = 0.16
62A	27	2	w = 0.08	l = 0.27	w = 0.03	l = 0.11
62A	28	2	w = 0.11	l = 0.24	w = 0.04	l = 0.10
62A	29	3	w = 0.06	l = 0.25	w = 0.02	l = 0.10
62A	30	3	w = 0.04	l = 0.48	w = 0.02	l = 0.20

Table 5.10 cont.

213

FRACTURE SPECIMEN	FLAW I.D. NUMBER	FLAW TYPE	FRACTOGRAPH FLAW PARAMETERS (cm)		ACTUAL FLAW PARAMETERS (mm)	
62A	31	2	w = 0.31	l = 0.50	w = 0.13	l = 0.21
62A	32	3	w = 0.06	l = 0.30	w = 0.02	l = 0.12
62A	33	1	d = 0.14		d = 0.06	
62A	34	3	w = 0.05	l ≠ 0.44	w = 0.02	l = 0.18
62A	35	2	w = 0.07	l = 0.22	w = 0.03	l = 0.09
62A	36	1	d = 0.12		d = 0.05	
62A	37	2	w = 0.10	l = 0.30	w = 0.04	l = 0.12
62A	38	3	w = 0.12	l = 0.34	w = 0.05	l = 0.14
62A	39	1	d = 0.15		d = 0.06	
62A	40	1	d = 0.16		d = 0.07	
62A	41	1	d = 0.08		d = 0.03	
62A	42	1	d = 0.09		d = 0.04	
62A	43	2	w = 0.08	l = 0.24	w = 0.03	l = 0.10
62A	44	1	d = 0.11		d = 0.05	
62A	45	2	w = 0.07	l = 0.18	w = 0.03	l = 0.07
62A	46	3	w = 0.50	l = 4.25	w = 0.09	l = 0.81
62A	47	3	w = 0.05	l = 0.51	w = 0.02	l = 0.21
62A	48	3	w = 0.07	l = 0.34	w = 0.03	l = 0.14
62A	49	6	d = 0.42		d = 0.17	
62A	50	2	w = 0.14	l = 0.70	w = 0.06	l = 0.29
62A	51	2	w = 0.15	l = 0.24	w = 0.06	l = 0.10
62A	52	2	w = 0.10	l = 0.34	w = 0.04	l = 0.14
62A	53	2	w = 0.09	l = 0.30	w = 0.04	l = 0.12
62A	54	2	w = 0.14	l = 0.61	w = 0.06	l = 0.25

Table 5.10 cont.

FRACTURE SPECIMEN	FRACTOGRAPH MAGNIFICATION	CONVERSION FACTOR (mm/cm)
12B	30 X	0.333
13A	24 X	0.417
25B	24 X	0.417
42B	58 X	0.172
43C	58 X	0.172
62A	24 X	0.417

Table 5.11 Conversion factors for fractographic overviews of fracture surfaces.

215

SAMPLE CONSTITUENT ELEMENT	11	23	24	34	44	66
ALUMINUM	0.034%	0.036%	0.036%	0.036%	0.034%	0.041%
CARBON	0.39%	0.38%	0.31%	0.39%	0.38%	0.36%
CHROMIUM	0.86%	0.85%	0.85%	0.86%	0.85%	0.85%
COPPER	0.14%	0.13%	0.13%	0.14%	0.14%	0.13%
MANGANESE	0.81%	0.79%	0.76%	0.80%	0.79%	0.77%
MOLYBDENUM	0.21%	0.21%	0.20%	0.21%	0.22%	0.21%
NICKEL	1.89%	1.81%	1.83%	1.86%	1.84%	1.83%
PHOSPHORUS	0.021%	0.024%	0.018%	0.022%	0.019%	0.021%
SILICON	0.52%	0.53%	0.50%	0.55%	0.53%	0.51%
SULPHUR	0.024%	0.029%	0.016%	0.026%	0.023%	0.022%

Table 5:12 Chemical composition at six locations in cast ring gear.

| CONSTITUENT | MINIMUM COMPOSITION | | MAXIMUM COMPOSITION | | % VARIATION |
ELEMENT	SAMPLE BLOCK(S)	% COMP. BY WEIGHT	SAMPLE BLOCK(S)	% COMP. BY WEIGHT	$\frac{\text{Max.-Min.}}{\text{Max.}} \times 100$
ALUMINUM	11,44	0.034	66	0.041	22.7
CARBON	24	0.31	11,34	0.39	20.5
CHROMIUM	23,24,44,66	0.85	11,34	0.86	1.1
COPPER	23,24,66	0.13	11,34,44	0.14	7.1
MANGANESE	24	0.76	11	0.81	6.2
MOLYBDENUM	24	0.20	44	0.22	9.1
NICKEL	23	1.81	11	1.89	4.2
PHOSPHORUS	24	0.018	23	0.024	25.0
SILICON	24	0.50	34	0.55	9.1
SULPHUR	24	0.016	23	0.029	44.8

Table 5.13 Maximum and minimum chemical composition
for elements investigated.

BLOCK SIZE CATEGORY	X-RAY DIRECTION 1 AREA (cm^2)	X-RAY DIRECTION 2 AREA (cm^2)	SINGLE BLOCK X-RAY AREA (cm^2)	NUMBER OF BLOCKS PER CATEGORY	CATEGORY AREA (cm^2)
1	196.0	231.0	427.0	11	4,697.0
2	252.8	262.3	515.1	5	2,575.5
3	272.3	272.3	544.6	4	2,178.4
				TOTAL CATEGORY AREA	9,450.9

Table 5.14   Radiographic inpsection area for
block size categories 1, 2 and 3.

BLOCK IDENTIFICATION NUMBER	X-RAY DIRECTION 1 AREA (cm^2)	X-RAY DIRECTION 2 AREA (cm^2)	X-RAY DIRECTION 3 AREA (cm^2)	TOTAL AREA PER BLOCK (cm^2)
23	267.3	198.9	-	466.2
23L	251.0	151.5	122.6	525.1
64	115.5	270.5	-	386.0
66	155.0	231.0	-	386.0
67	213.2	204.4	-	417.6
			TOTAL BLOCK AREA	2,180.9

Table 5.15 Radiographic inspection area of steel sample blocks not conforming to three size categories.

RADIOGRAPHIC INSPECTION FLAW TYPE	NUMBER OF FLAW INDICATIONS	PROBABILITY* OF OCCURRENCE
1	2	1.72×10^{-4}
2	8	6.88×10^{-4}
3	25	2.15×10^{-3}
4	11	9.46×10^{-4}
5	9	7.74×10^{-4}

* Probability calculated on the basis of 11,632 unit areas radiographically inspected.

Table 5.16 Probability of occurrence of radiographic inspection flaw types.

BLOCK SIZE CATEGORY	ULTRASONIC INSPECTION FACE AREA (cm^2)			SINGLE BLOCK ULT. INSP. AREA (cm^2)	NUMBER OF BLOCKS PER CATEGORY	AREA INSPECTED PER CATEGORY (cm^2)
	A	B	C			
1	196.0	231.0	231.0	658.0	11	7,238.0
2	252.8	262.3	262.3	777.4	5	3,887.0
3	272.3	272.3	272.3	816.9	4	3,267.6
					TOTAL CATEGORY AREA	14,392.6

Table 5.17 Ultrasonic inspection area for block
size categories 1, 2, and 3.

BLOCK IDENTIFICATION NUMBER	ULTRASONIC INSPECTION FACE AREA (cm^2)					TOTAL AREA PER BLOCK (mm^2)
	A	B	C	D	E	
23	267.3	198.9	200.1	-	-	666.3
64	115.5	270.6	135.3	-	-	521.4
66	155.0	231.0	155.0	-	-	541.0
67	213.2	204.4	213.2	-	-	630.8
23L	249.6	-	165.7	251.0	151.5	817.8
					TOTAL BLOCK AREA	3,177.3

Table 5.18 Ultrasonic Inspection area of steel sample blocks not conforming to three size categories.

ULTRASONIC INSPECTION FLAW TYPE	NUMBER OF FLAW INDICATIONS	PROBABILITY* OF OCCURRENCE
1	47	2.67×10^{-3}
2	84	4.78×10^{-3}
3	73	4.15×10^{-3}
4	37	2.10×10^{-3}
5	17	9.68×10^{-4}
6	26	1.48×10^{-3}
7	11	6.26×10^{-4}
8	11	6.26×10^{-4}

* Probability calculated on the basis of 17,570 unit areas ultrasonically inspected.

Table 5.19   Probability of occurrence of ultrasonic inspection flaw types.

FLAW* TYPE	PROBABILITY OF OCCURRENCE FROM RADIOGRAPHIC INSPECTION	PROBABILITY OF OCCURRENCE FROM ULTRASONIC INSPECTION	% VARIATION
RAD 1 ULT 4	1.72×10^{-4}	2.10×10^{-3}	1,120
RAD 2 ULT 5	6.88×10^{-4}	9.68×10^{-4}	41
RAD 3 ULT 6	2.15×10^{-3}	1.48×10^{-3}	31
RAD 4 ULT 7	9.46×10^{-4}	6.26×10^{-4}	34
RAD 5 ULT 8	7.74×10^{-4}	6.26×10^{-4}	19

* RAD = RADIOGRAPHIC INSPECTION DEFECT TYPE
  ULT = ULTRASONIC INSPECTION DEFECT TYPE

Note: % VARIATION is calculated with radiographic inspection
       probability assumed as true value.

Table 5.20 Comparison of probability of occurrence of
           the five common defect types.

FRACTURE SPECIMEN	FRACTOGRAPH MAGNIFICATION	FRACTOGRAPH SURFACE AREA (cm^2)	CONVERSION FACTOR (mm^2/cm^2)	ACTUAL AREA (mm^2)
12B	30X	81.6	0.1110	9.06
13A	24X	185.4	0.1740	32.30
25B	24X	167.0	0.1740	29.00
42B	58X	161.5	0.0296	4.78
43C	58X	81.3	0.0296	2.41
62A	24X	81.3	0.1740	14.10
			TOTAL ACTUAL AREA	91.70

Table 5.21 Surface area investigated to construct microscopic inspection defect histogram.

MICROSCOPIC INSPECTION FLAW TYPE	NUMBER OF FLAW INDICATIONS	PROBABILITY* OF OCCURRENCE
1	153	1.67×10^{-1}
2	143	1.56×10^{-1}
3	90	9.80×10^{-2}
4	17	1.80×10^{-2}
5	4	4.00×10^{-3}
6	4	4.00×10^{-3}

* Probability calculated on the basis of 917 unit areas viewed under the SEM.

Table 5.22 Probability of occurrence of microscopic inspection flaw types.

RADIOGRAPHIC INSPECTION FLAW TYPE	ULTRASONIC INSPECTION FLAW TYPE	COMBINED HISTOGRAM FLAW TYPE	FLAW DESCRIPTION AND PARAMETERS*	FLAW PARAMETER RANGE (cm)	COMBINED HISTOGRAM PROBABILITY OF OCCURRENCE
-	1	1	circular, d	$d < 0.10$	2.67×10^{-3}
-	2	2	circular, d	$0.1 \leqslant d < 0.15$	4.78×10^{-3}
-	3	3	ciruclar, d	$0.15 \leqslant d < 0.2$	4.15×10^{-3}
1	4	4	circular, d	$0.2 \leqslant d < 0.3$	2.10×10^{-3}
2	5	5	circular, d	$0.3 \leqslant d < 0.4$	9.68×10^{-4}
3	6	6	circular, d	$0.4 \leqslant d$	2.15×10^{-3}
4	7	7	rectangular round ends, w, l	$0.1 \leqslant w \leqslant 0.5$ $0.2 \leqslant l \leqslant 0.8$	9.46×10^{-4}
5	8	8	rectangular round ends, w, l	$0.1 \leqslant w \leqslant 0.5$ $0.8 < l$	7.74×10^{-4}

* Circular: →○← d
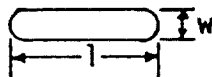
Rectangular round ends: ⊂⊃ ↕ w |←— l —→|

Table 5.23 Combined defect histogram flaw types and their probability of occurrence.

RADIOGRAPHIC INSPECTION FLAW TYPE	# FLAWS RECORDED X-RAY DIR. 1	# FLAWS RECORDED X-RAY DIR. 2
1	0	2
2	0	8
3	4	21
4	3	8
5	2	6

Table 5.24   Number of flaws recorded in the
two X-ray directions.

ULTRASONIC INSPECTION FLAW TYPE	# FLAWS RECORDED FROM FACE A	# FLAWS RECORDED FROM FACE B	# FLAWS RECORDED FROM FACE C
1	23	14	10
2	42	17	25
3	38	15	20
4	23	8	6
5	5	12	0
6	4	8	14
7	0	3	8
8	3	8	0

Table 5.25   Number of flaws recorded in the three ultrasonic inspection directions.

COMBINED HISTOGRAM FLAW TYPE	RADIOGRAPHIC INSPECTION RESULTS		ULTRASONIC INSPECTION RESULTS		
	% DIRECTION 1 FLAWS	% DIRECTION 2 FLAWS	% DIRECTION 1 FLAWS	% DIRECTION 2 FLAWS	% DIRECTION 3 FLAWS
1	-	-	48.9	29.8	21.3
2	-	-	50.0	20.2	29.8
3	-	-	52.0	20.6	27.4
4	0	100.0	62.2	21.6	16.2
5	0	100.0	29.4	70.6	0
6	16.0	84.0	15.4	30.8	53.8
7	27.3	72.7	0	27.3	72.7
8	25.0	75.0	27.3	72.7	0

Table 5.26 Directional distribution of flaw types.

APPENDIX A

CAST STEEL SAMPLE BLOCKS HEAT TREATMENT DETAILS

Heat Treatment Descriptions - Normalize and temper 25 cast steel BB225 sample blocks.

Heat Treatment:

1. Charge into cold furnace (one of the two pit furnaces at shop #1). Load in 2 or 3 batches.

2. Heat at a rate of 100^OF/hour maximum up to 1,650^{O}F

3. Soak for 7 hours at 1,650 25°F.

4. Air cool to room temperature.

5. Charge into cold furnace (shop #1).

6. Heat at a rate of 100^OF/hour up to 1,200^{O}F.

7. Soak for 10 hours at 1,200 25°F.

8. Air cool to room temperature.

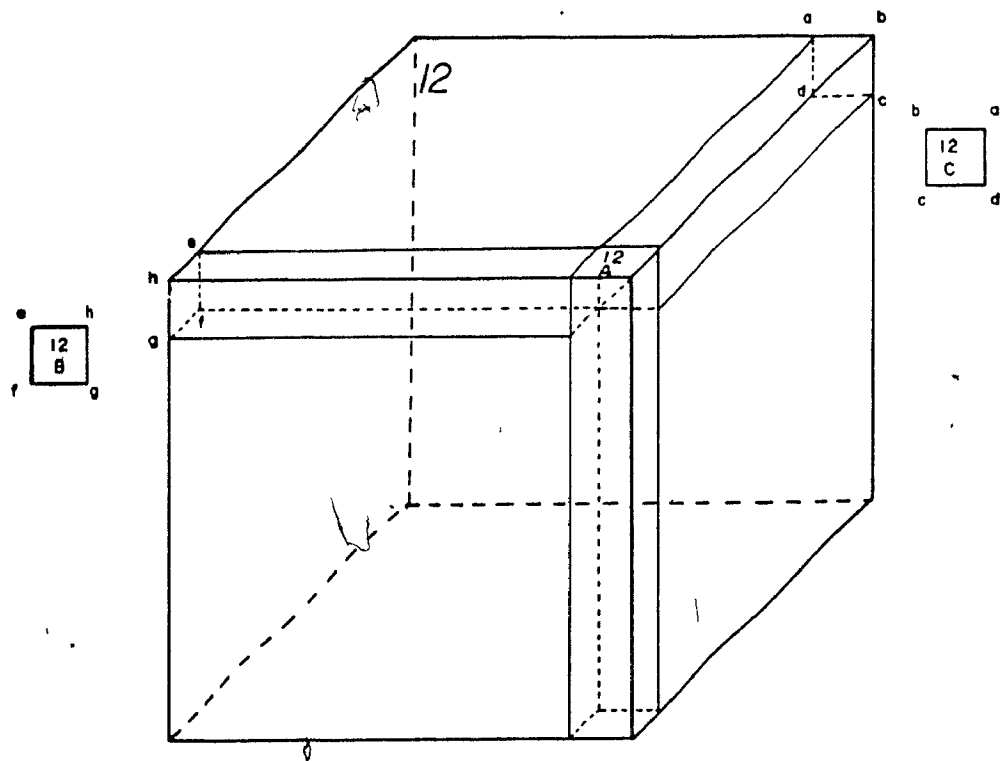## LOCATION AND ORIENTATION OF THE FRACTURE SPECIMENS
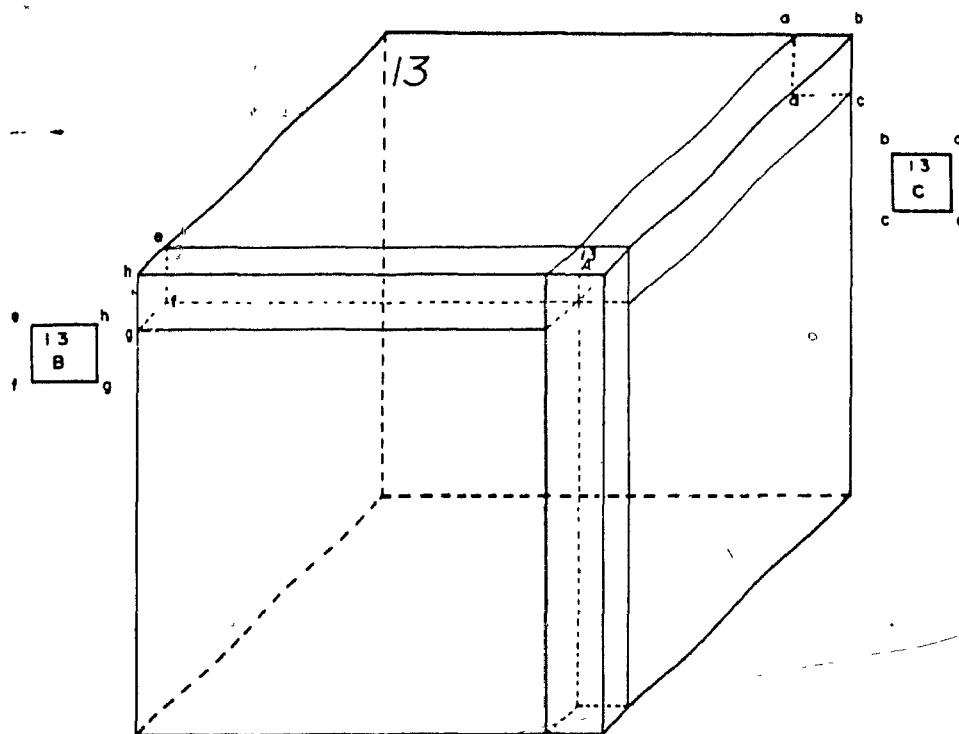

Fig. B.1 Sample block 12 fracture specimens.

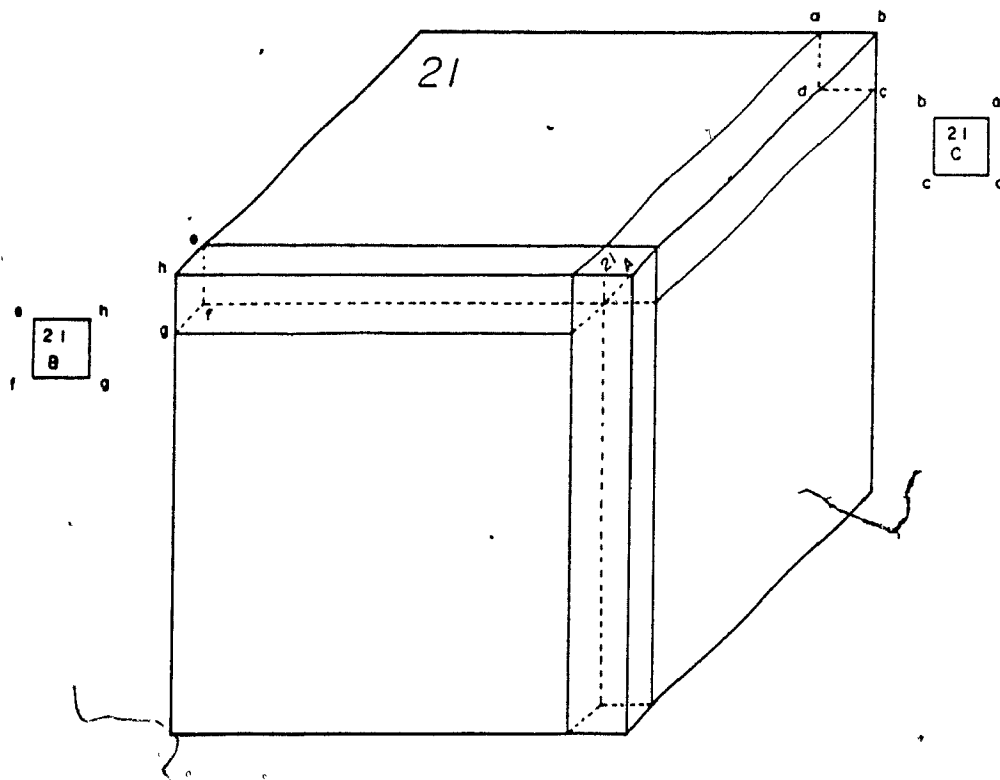Fig. B.2   Sample block 13 fracture specimens.
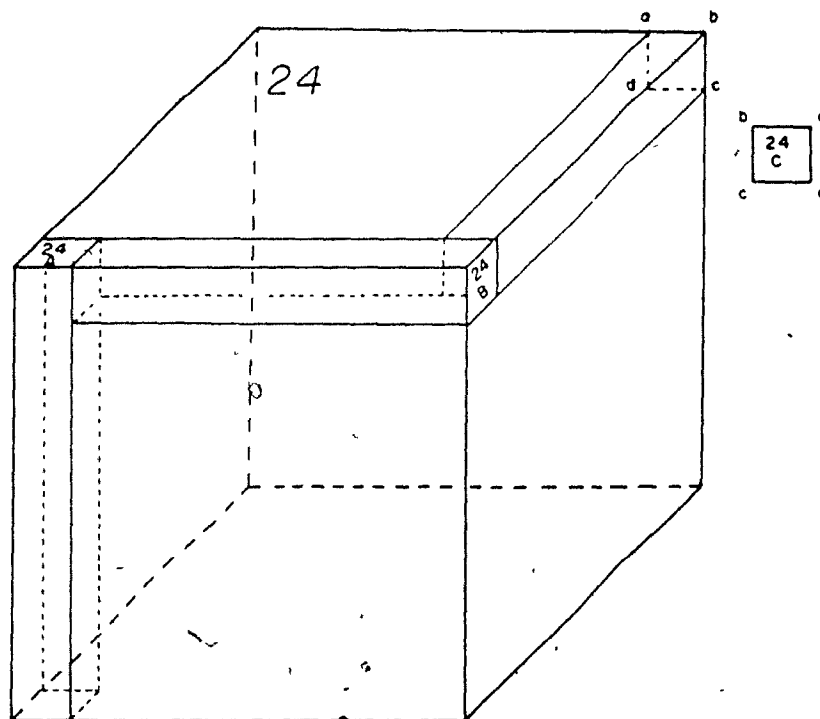
Fig. B.3 Sample block 21 fracture specimens.

Fig. B.4 Sample block 24 fracture specimens.
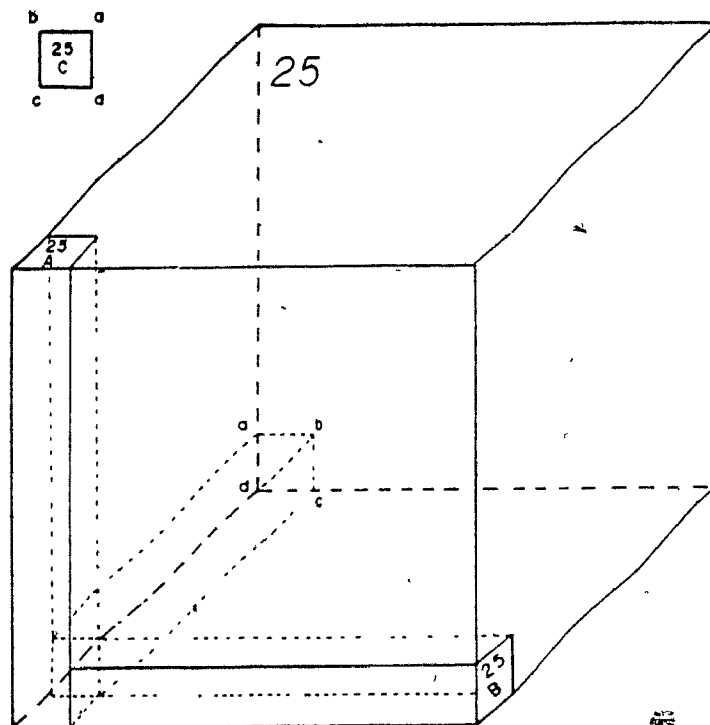
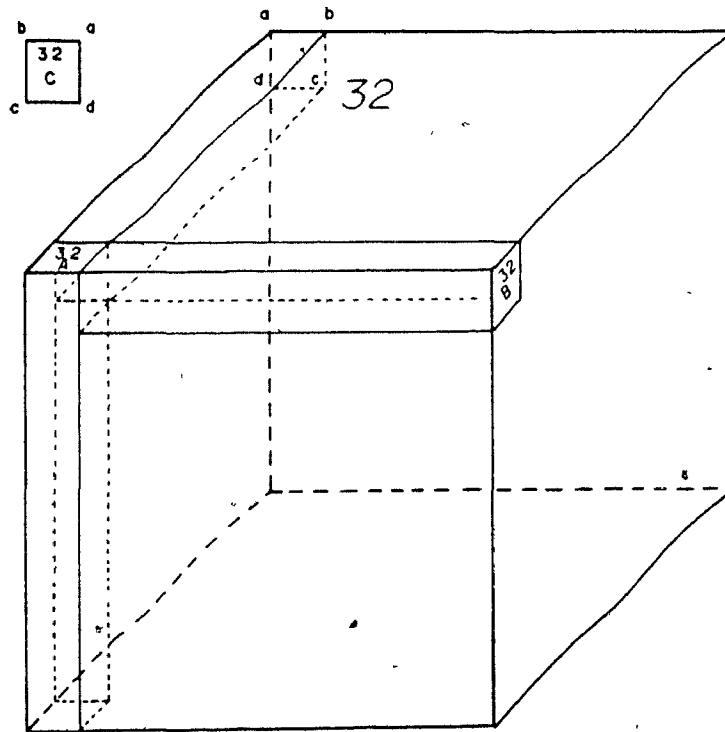Fig. B.5   Sample block 25 fracture specimens.

Fig. B.6   Sample block 32 fracture specimens.
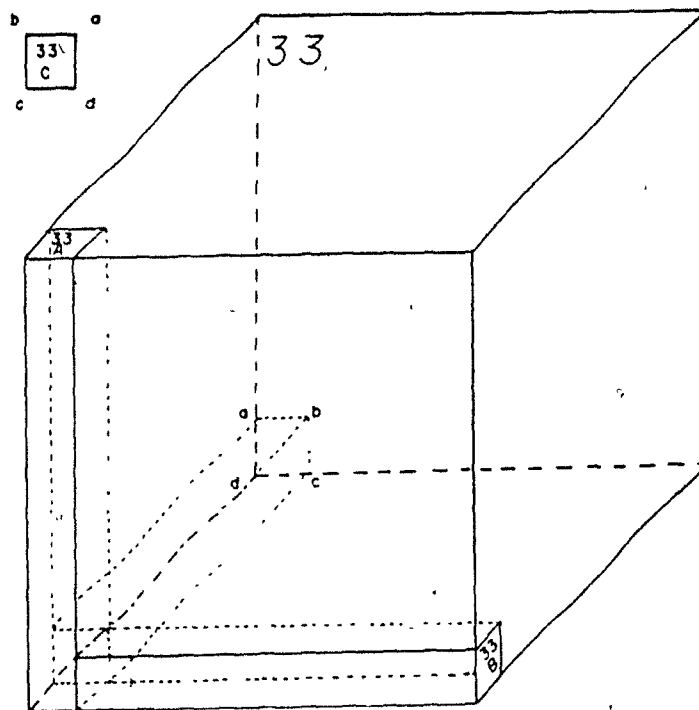
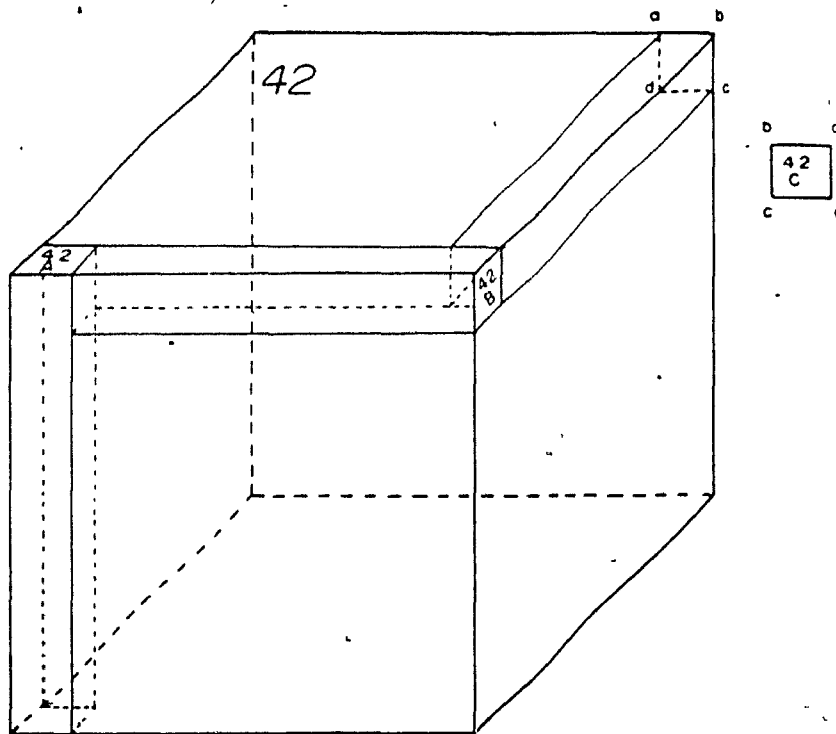Fig. B.7   Sample block 33 fracture specimens.
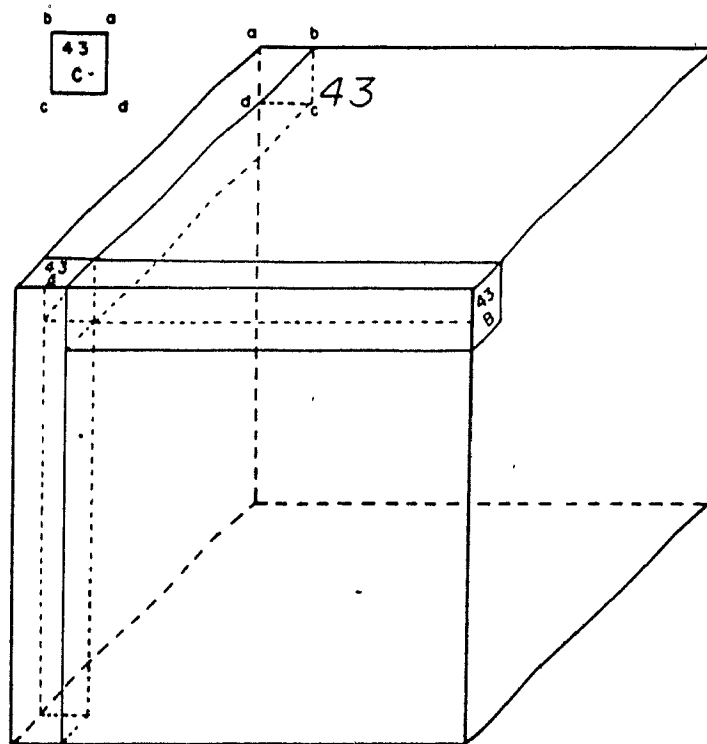
238

Fig. B.8 Sample block 42 fracture specimens.
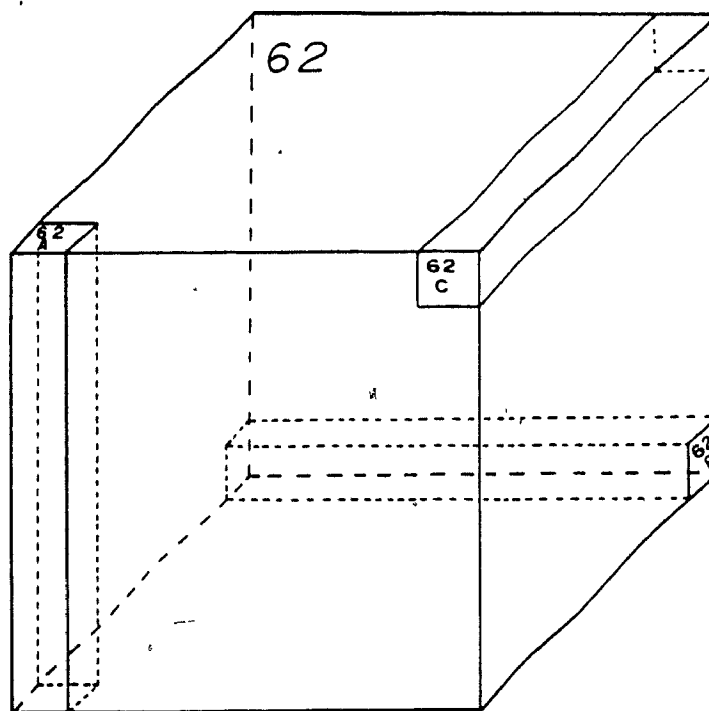
Fig. B.9   Sample block 43 fracture specimens.

Fig. B.10   Sample block 62 fracture specimens.

APPENDIX C

STEP-BY-STEP FRACTURE TEST PROCEDURE

In the following procedure, it is assumed that the static and dynamic calibrations have been performed for all the electronic modules in agreement with the relevant procedures as described in the MTS reference manual. With reference to Figs. 4.24 through 4.27, the fracture test procedure reads as follows:

Step 1: Turn the POWER switch of the 436 CONTROL UNIT to the on position.

Step 2: Turn on the PDP 11/04 COMPUTER CONSOLE, the TEKTRONIX 410 GRAPHICS DISPLAY MONITOR, the DIGITAL DECWRITER, and the TEKTRONIX HARD COPY UNIT.

Step 3: Place the HALT/CONT switch on the PDP 11/04 COMPUTER CONSOLE to the CONT position.

Step 4: Mount the floppy disk containing the program PULT1M in DRIVE O of the DISK DRIVE unit.

Step 5: Press the BOOT/INIT switch on the PDP 11/04 COMPUTER CONSOLE to the INIT position, then release it.

Step 6: Verify that the LINE/LOCAL switch of the TEKTRONIX 410 GRAPHICS DISPLAY MONITOR is in the LINE position.

Step 7: Type "DX" on the TEKTRONIX GRAPHICS DISPLAY MONITOR keyboard.

Step 8: Type in the current date. (The date must be input in the following form: "DATE 02-FEB-86".)

Step 9: Type "R BASIC".

Step 10: Type "A" in response to the star. This loads all of the optional functions into the PDP 11/04. Type "N" in response to "DIAGNOSTICS?" if the hardware diagnostics are not required.

Step 11: When "USER FNS LOADED" is displayed on the TEKTRONIX GRAPHICS DISPLAY MONITOR followed by "READY", load the controlling program PULT1M by typing "OLD PULT1M". The program is ready to run when the "READY" signal is displayed.

Step 12: Turn on the cooling water supply of the HYDRAULIC PRESSURE SUPPLY (HPS).

Step 13: Turn on the power of the HPS.

Step 14: Move the ERROR SWITCH of the 442 CONTROLLER into the D.C. ERROR POSITION.

Step 15: Adjust the ZERO dial on the DC LOAD CONDITIONER to 500.

Step 16:   Select RANGE 1 on the D.C. LOAD CONDITIONER.

Step 17:   Select 100% STROKE CONTROL by depressing the STROKE±% FS
button on the 442 CONTROLLER and selecting RANGE 1 on the A.C.
STROKE CONDITIONER.

Step 18:   Adjust the SET POINT dial on the 442 CONTROLLER to null the
O.C. ERROR METER. (THIS ENSURES NO DRIVE SIGNAL IS SENT TO
THE SERVOVALVES WHICH CONTROL THE HYDRAULIC FLUID FLOW OF THE
ACTUATOR. THIS STEP MUST BE FOLLOWED EVERY TIME THE HYDRAULIC
SYSTEM IS ACTIVATED.) Press the INTERLOCK RESET button on the
442 CONTROLLER.

Step 19:   Depress the LOW button on the 436 CONTROL UNIT to activate the
HPS LOW PRESSURE.

Step 20:   Depress the HIGH button on the 436 CONTROL UNIT to activate
the HPS HIGH PRESSURE.

Step 21:   Select a 1 Hz sine wave on the 436 CONTROL UNIT.

Step 22:   Adjust SPAN 1 on the 442 CONTROLLER to 0. Depress the RUN
button on the 436 CONTROL UNIT and slowly increase the SPAN 1
dial to 100. Let the hydraulic system warm up for 30 minutes.
If the SPAN 1 cannot be increased to 100 without the lower
grip contacting the upper grip, then the crosshead must be
raised. To raise the crosshead execute Steps 33 through 37

and proceed to step 23.

Step 23: Return the SPAN 1 dial to 0 and depress the STOP switch on the 436 CONTROL UNIT.

Step 24: Press the LOW button to move the HPS to low pressure.

Step 25: Turn the HPS off by depressing the HYD OFF button on the 436 CONTROL UNIT.

Step 26: Adjust the ZERO dial on the A.C. STROKE CONDITIONER to 500.

Step 27: Ensure RANGE 1 is selected on the A.C. STROKE CONDITIONER.

Step 28: Adjust the SET POINT to null the D.C. ERROR METER.

Step 29: Depress the INTERLOCK RESET button on the 442 CONTROLLER.

Step 30: Activate the HPS low pressure by depressing the LOW button on the 436 CONTROL UNIT.

Step 31: Activate the HPS high pressure by depressing the HIGH button on the 436 CONTROL UNIT.

Step 32: Adjust the SET POINT to 500. (The stroke, as indicated through input 3 of the DIGITAL DISPLAY, should read 0.00; otherwise, the servovalve electronic balance procedure must be

245

followed.)

Step 33: Close the UP and DOWN hand valves on the CROSSHEAD LIFT
CONTROL MANIFOLD.

Step 34: Switch the CROSSHEAD LOCK control to the UNLOCK POSITION.

Step 35: Wait at least 5 seconds to allow the hydraulic fluid in the
HYDRAULIC LOCKS to return to a condition of zero pressure.

Step 36: Open the UP hand valve to move the CROSSHEAD up so that the
UPPER GRIP is sufficiently far away from the LOWER GRIP to
facilitate specimen mounting. Once the CROSSHEAD is at the
appropriate height, close the UP hand valve.

Step 37: Switch the CROSSHEAD LOCK CONTROL to the LOCK POSITION.

Step 38: Open the UPPER GRIP RELEASE valve on the HYDRAULIC GRIP
PRESSURE SUPPLY CONSOLE, leave open for approximately 5
seconds then close. This ensures the grip is fully open.

Step 39: Insert the specimen into the UPPER GRIP with at least 3.0 cm
of the specimen in the grip.

Step 40: Open the UPPER GRIP PRESSURE VALVE, leave open for
approximately 10 seconds then close.

Step 41: Select INPUT 1 on the 430 DIGITAL DISPLAY to determine if the LOAD CELL is zeroed. If the readout is not 0.00, the load cell must be zeroed following the procedure in Step 42. If the LOAD CELL is already zeroed, select INPUT 3 on the 430 DIGITAL DISPLAY, turn the HPS off, and proceed to Step 43.

Step 42: Zero the LOAD CELL using the following procedure:

    a) Return the HPS to LOW pressure.

    b) Turn the HPS off.

    c) Select LOAD±% FS range on the 442 CONTROLLER.

    d) Note the setting of GAIN 1 on the FEEDBACK SELECTOR. Turn GAIN 1 to maximum.

    e) Reduce the commands of the SPAN controls to 0.

    f) Adjust the SET POINT to 500.

    g) Adjust the ZERO dial on the D.C. LOAD CONDITIONER to zero the digital readout while monitoring input 1.

    h) Return GAIN 1 on the FEEBACK SELECTOR to its initial setting.

    i) Select INPUT 3 on the 430 DIGITAL DISPLAY.

Step 43: With the HPS off, select 10% STROKE CONTROL by pressing the STROKE±% FS button on the 442 CONTROLLER and selecting RANGE 4 on the AC STROKE CONDITIONER.

Step 44: Adjust the SET POINT to null the D.C. ERROR METER.

Step 45: Depress the INTERLOCK RESET button.

Step 46: Activate the HPS LOW pressure.

Step 47: Activate the HPS HIGH pressure.

Step 48: Adjust the SET POINT so that the STROKE readout (INPUT 3 on the DIGITAL DISPLAY) is 0.00. The SET POINT should indicate 500.

Step 49: Open the LOWER GRIP RELEASE VALVE on the HYDRAULIC GRIP PRESSURE SUPPLY CONSOLE, leave open for approximately 5 seconds to fully open the grip, then close.

Step 50: Switch the CROSSHEAD LOCK CONTROL to the UNLOCK position.

Step 51: Open the DOWN hand valve to lower the crosshead so that at least 3.0 cm of the specimen will be in the lower grip.

Step 52: Switch the CROSSHEAD LOCK control to the LOCK POSITION.

Step 53: Close the LOWER GRIP by opening the LOWER GRIP PRESSURE VALVE on the HYDRAULIC PRESSURE CONTROL CONSOLE, leave open for approximately 5 seconds to ensure the grip is fully closed, then close the valve.

Step 54: Return the HPS to low pressure then off.

Step 55: Move the system into 100% LOAD CONTROL by pressing the LOAD
±%FS RANGE button on the 442 CONTROLLER.

Step 56: Be sure the D.C. ERROR METER is nulled and press the INTERLOCK
RESET button.

Step 57: Select INPUT 1 on the 430 DIGITAL DISPLAY.

Step 58: Activate low, then high pressure of the HPS.

Step 59: Open the ALIGNMENT RELEASE VALVE for 5 seconds then close.

Step 60: Slowly apply an alternating tension-compression 1 kN load to
the specimen by adjusting the SET POINT and monitoring INPUT 1
on the DIGITAL DISPLAY (1kN = 0.10 volts).

Step 61: Open the ALIGNMENT PRESSURE VALVE with the 1kN tensile load
applied. Leave open for 5 seconds then close.

Step 62: Adjust the load back to 0 by turning the SET POINT while
monitoring INPUT 1 of the DIGITAL DISPLAY.

Step 63: Return the HPS TO LOW pressure then off.

Step 64: Select 10% STROKE CONTROL by depressing the STROKE±% FS button
on the 442 CONTROLLER and selecting RANGE 4 on the A.C. STROKE
CONDITIONER. Select INPUT 3 on the DIGITAL DISPLAY. If the

readout is not 0.00, the STROKE TRANSDUCER must be zeroed following the procedure in Step 65. If the STROKE TRANSDUCER is zeroed then proceed to Step 66.

Step 65: Zero the STROKE TRANSDUCER in the following manner:

a) With the system in 10% STROKE CONTROL, note the setting of GAIN 3 on the FEEDBACK SELECTOR, then adjust to maximum gain.

b) Reduce the SPAN controls on the 442 CONTROLLER to 0.

c) Adjust the SET POINT to 500.

d) Adjust the ZERO control on the A.C. STROKE CONDITIONER to ZERO the STROKE readout. (INPUT 3 on the DIGITAL DISPLAY).

e) Return GAIN 3 back to its initial value.

Step 66: Adjust the UPPER and LOWER STROKE LIMITS on the LIMIT DETECTOR to 800 and select the INTERLOCK position of the STROKE INTERLOCK/INDICATE/PROGRAM toggle switch. Also, move the STROKE UPPER POLARITY toggle switch to the +VE position. Move the STROKE LOWER POLARITY toggle switch to the -VE position.

Step 67: Move the REMOTE/LOCAL switch on the FEEDBACK SELECTOR to the REMOTE position and verify that all the FEEDBACK SELECTOR GAINS are back to their initial values.

Step 68: Depress the INTERLOCK RESET button.

Step 69: Activate the HPS LOW pressure.

Step 70: Activate the HPS HIGH pressure.

Step 71: With the HPS in the high pressure mode, adjust the SET POINT to 500 to zero the STROKE readout indicated on the DIGITAL DISPLAY.

Step 72: Select INPUT 1 on the DIGITAL READOUT. With full hydraulic pressure applied, the SET POINT at 500, and the SPAN controls at 0, adjust the ZERO on the A.C. STROKE CONDITIONER to ZERO the LOAD on the specimen as indicated by the INPUT 1 readout. This will not affect the zero of the STROKE transducer as long as the HPS is activated.

Step 73: Select INPUT 3 on the DIGITAL DISPLAY.

Step 74: Record the initial stroke readings in terms of the STROKE TRANSDUCER output voltage (INPUT 1 of the DIGITAL DISPLAY) and the actual physical position.

Step 75: Type "RUN" on the TEKTRONIX GRAPHICS MONITOR KEYBOARD to initiate execution of PULTIM.

Step 76: When the test is completed record the final stroke position of the lower grip and the output of the STROKE TRANSDUCER.

Step 77: Return the HPS to LOW pressure.

Step 78: Depress the STOP button on the 436 CONTROL UNIT.

Step 79: Turn off the HPS.

Step 80: Return the REMOTE/LOCAL switch on the FEEDBACK SELECTOR to the LOCAL position.

Step 81: Select 100% STROKE CONTROL by depressing the STROKE±% FS button on the 442 controller and selecting RANGE 1 on the A.C. STROKE CONDITIONER.

Step 82: Adjust the SET POINT to null the D.C. ERROR METER and depress the INTERLOCK RESET button.

Step 83: Set SPAN 1 TO 0.

Step 84: Activate LOW pressure of the HPS. Activate HIGH pressure of the HPS.

Step 85: Increase the SET POINT to move the LOWER GRIP down.

Step 86: Open the HEAD ALIGNMENT RELEASE VALVE, leave open for approximately 5 seconds, then close.

Step 87: Open the LOWER GRIP RELEASE VALVE and remove the lower half of the fractured specimen then close the valve.

Step 88: Open the UPPER GRIP RELEASE VALVE and remove the upper half of the fractured specimen then close the valve.

Step 89: Turn off the HPS. If another test is to be performed then return back to Step 26. Otherwise turn off the HPS power and cooling water and proceed to Step 90.

Step 90: Remove the floppy disk from the disk drive. Turn off the components listed in Step 2.

MTS CONTROL PROGRAM PULT1M AND INTERACTIVE TEST OUTPUT

D.1 MTS CONTROL PROGRAM.

```
PULT1M   03-FEB-86   MTS BASIC V01B-02C

10 COMMON R1(400),R2(400),R3(400),L0$,E0$,S0$,A0$,D0$,G0,T$,L8,T1,S9$,R1
20 COMMON D0,R9
100 PRINT "THIS PROGRAM DEFORMS A TEST ITEM IN LOAD OR STROKE CONTROL"
110 PRINT "FROM AN INITIAL LOAD OR STROKE OF ZERO TO A MAXIMUM LOAD "
120 PRINT "OR STROKE SELECTED BY THE OPERATOR ( UP TO FULL SCALE LOAD"
130 PRINT "OR STROKE ) IN A TIME SPECIFIED BY THE OPERATOR."
140 PRINT "THROUGHOUT THE TEST , LOAD AND STROKE DATA POINTS"
150 PRINT "ARE STORED.  AT THE CONCLUSION OF THE TEST, THE STORED DATA"
160 PRINT "POINTS ARE PRINTED IN A TABLE; LOAD POINTS ARE DIVIDED BY"
170 PRINT "SPECIMEN AREA AND DISPLAYED IN UNITS OF STRESS.THE OPERATOR"
180 PRINT "MAY REQUEST THAT THE DATA BE STORED ON DISK AND HE HAS THE "
190 PRINT "OPTION TO CHAIN THIS PROGRAM TO THE GRAPHIC PROGRAM 'PULT2'"
200 PRINT "WHICH WILL PERFORM A DETAILED ANALYSIS OF THE DATA OBTAINED "
210 PRINT "IN THIS PROGRAM."\PRINT \PRINT
220 PRINT "******   SHOULD YOU PREFER NOT CHAINING WITH 'PULT2'    ******"
230 PRINT "******      BE SURE YOU REQUEST STORING OF THE DATA.    ******"
231 PRINT "******       IF FURTHER ANALYSIS IS REQUIRED            ******"
235 Q1$="STILL HAS AN OFFSET OF "\PRINT
241 PRINT "YOU MAY TURN ON THE HYDRAULICS, ZERO THE STROKE"
242 PRINT "TRANSDUCER, MOUNT SPECIMEN IN UPPER GRIP, ZERO THE"
243 PRINT "LOAD CELL, AND CLAMP SPECIMEN IN LOWER GRIP "
245 PRINT \PRINT "TURN ON HARD COPY UNIT."\PRINT \GOSUB 5200
260 DIM C(3)
270 PRINT "ENTER DATE OF TEST (DAY-MONTH-YEAR)";\INPUT D0$
280 PRINT "DATE IS ";D0$;".  IS THAT CORRECT (YES-NO)";\INPUT S$
290 IF S$ "YES" THEN IF S$ "NO" THEN 280
300 IF S$="NO" THEN 270
310 PRINT "DO YOU PREFER TO CONDUCT THE TEST IN STROKE CONTROL";\INPUT M$
320 IF M$ "NO" THEN IF M$ "YES" THEN 310\IF M$="YES" THEN  GOSUB 490
330 L0$="NN"
340 PRINT "ENTER LOAD RANGE (IN KN)";\INPUT L1
360 S0$="MM"\E0$="MM/MM"
370 PRINT "ENTER   STROKE RANGE (IN MM.)";\INPUT S1
420 PRINT "ENTER NOTCH AREA (SQUARE MM.)";\INPUT D0
430 A0$="SQ.M."\A1=D0/1.00000E+06
460 PRINT \PRINT "TIME MAY RANGE FROM 0.5 TO 2047 SEC. "
470 S$=" STROKE "\IF M$="NO" THEN MSW1(0)\S$=" LOAD "
500 PRINT "ENTER TIME FOR RAMP FROM 0 TO MAX";S$;"(SEC)";\INPUT T1
510 T=INT(T1/200*100)\IF M$="NO" THEN MSW1(0)
520 C(1)=INT(4095/(2*T1))\T1=4095/2/C(1)
530 IF C(1) =1 THEN 550
540 PRINT "RAMP TIME TOO LONG"\GO TO 460
550 IF C(1) 4096 THEN 570
560 PRINT "RAMP TIME TOO SHORT"\GO TO 460
570 PRINT "RAMP TIME WILL BE";T1;"SECONDS"
570 PRINT \PRINT "PLEASE ZERO ALL TRANSDUCERS AT THIS TIME"
580 PRINT "TO ASSIST YOU IN DOING THIS I WILL PRINT LOAD AND "
590 PRINT "STROKE ABOUT EVERY SECOND FOR 10 SECONDS"
700 PRINT \PRINT " LOAD"," STROKE"
710 PRINT " (VOLTS)"," (VOLTS)"
720 FOR I=1 TO 10
730 DACU(0,Z1,0,0)\DAEQ(0,Z3,2,0)
```

```
740 PRINT Z1*10/2047,Z3*10/2047
750 FOR J=1 TO 1000\NEXT J\NEXT I
770 PRINT 'WOULD YOU LIKE TO TRY THAT AGAIN (YES-NO) '\INPUT S$
780 IF S$='YES' THEN 700
790 IF ABS(Z1)>20 THEN  GOSUB 8000\Z1=.5
810 IF ABS(Z3)>20 THEN  GOSUB 8020\Z1=.5
820 IF Z1  .5 THEN 890
860 PRINT 'ARE YOU SURE YOU WANT TO START TESTING (YES-NO) '\INPUT S$
870 IF S$='NO' THEN 700\IF S$  'YES' THEN 860
890 F1=2047\IF M$='YES' THEN  GOSUB 7020\M1=2\GO TO 930
900 PRINT 'DO YOU WANT THE RAMP TO STOP BEFORE FS LOAD'\INPUT S$
910 IF S$  'NO' THEN PRINT 'INPUT MAX LOAD (KN)'\INPUT F1\F1 2047*F1/71
920 PRINT 'PUSH 'RUN' SWITCH ON CONTROL UNIT AND ADJUST 'SPAN' TO 10.00'
930 PRINT 'SET SAFETY INTERLOCKS AND RETURN TO CRT'\INPUT S$
940 C(2)=F1\C(3)=F1\C=3\QUIT\FG1(0)
950 DACQ(3,R1,0,T)\DACQ(6,R3,2,0)
970 CNTR(3)\FHYL(100,975,55,750)
980 CNTR(5)\PRINT ,'SPECIMEN : 'S9$,'DATE : 'D0$
990 SCAL(0,0,S1,0,L1)
1000 LABL('STROKE,MM','LOAD,KN',S1/5,L1/5,0)
1010 LABL(S1/10,L1/10,3)\SCAL(0,0,2047,0,2047)\IF M1=0 THEN BUTN(3000,1)
1030 EDMP\FG1(C,1,7,7)
1070 TIME(100)\BUTN(1)\STAR\I=0
1075 IF R3=I THEN 1075\PLOT(R3(R1),R1(R1))\I=I+1
1080 IF R1*T/100 1.05*F1 THEN T2=F1\GO TO 1110
1090 IF R1 400 THEN SDMP(1,Z9)\IF Z9=0 THEN 1075
1100 T2=R1*T/100
1110 QUIT\BUTN(-1)\GOSUB 6000\CNTR(3)\IF M1=2 THEN 1211
1120 PRINT 'I WILL MAINTAIN CONTROL AT THE CURRENT VALUE'
1130 PRINT 'DO YOU WANT TO RETURN TO THE STARTING LOAD VALUE '
1140 INPUT S$
1150 IF S$='NO' THEN 1230\IF S$  'YES' THEN 1150
1170 MSW1(0)\C(1)-(1/2*20)*40.95\C(2)-0\C(3)-0\C-3
1200 FG1(C,1,7,7)
1210 BUT1(X)\IF X =0 THEN 1210
1211 FOR I=1 TO R1\R1(I)=R1(I)*L1/2047
1212 R3(I)=R3(I)*S1/2047\NEXT I
1215 PRINT 'WOULD YOU LIKE TO DECREASE THE SPAN OF THE STROKE'
1216 PRINT 'SCALE ON THE LOAD VS. STROKE PLOT'\INPUT K$
1218 IF K$='NO' THEN 1230\IF K$  'YES' THEN 1215
1220 GOSUB 8050
1230 FOR I=1 TO R1\R1(I) R1(I)/A1\NEXT I
1280 PRINT 'SELECT 'LOCAL' ON THE 'LOCAL-LINE' SWITCH THEN PRESS 'CR' ON'
1290 PRINT 'TELETYPE TO OBTAIN THE TABLE OF DATA POINTS'\INPUT S$
1300 PRINT 'SPECIMEN : 'S9$\PRINT \PRINT ' TIME',
1310 PRINT ' STRESS','STROKE'
1320 PRINT ' (SEC.)','('&L0$&'/'&A0$&')','('&S0$&')'\PRINT
1330 FOR I=1 TO 9\PRINT ;I*T/100,R1(I),R3(I)\NEXT I
1340 FOR I=10 TO R1 STEP 5\PRINT ;I*T/100,R1(I),R3(I)\NEXT I
1350 IF I R1 THEN PRINT ;R1*T/100,R1(R1),R3(R1)\IF K9 0 THEN 1410
1370 PRINT 'CONTROL WAS SWITCHED TO STROKE AFTER';T/100*R9;'SECONDS.'
1380 PRINT 'AT THIS TIME, LOAD WAS';C0*L1/2047;L0$,
1385 PRINT ', STRESS WAS';R1(K9),L0$'/'&A0$;', '
1390 PRINT 'STROKE WAS';C2*S1/2047;S0$;
1410 PRINT 'TOTAL DURATION OF TEST WAS';T2;'SECONDS.'
1420 PRINT \PRINT 'NOW GO BACK TO 'LINE' THEN PRESS 'CR' ON THE TERMINAL '
1430 INPUT S$
1440 PRINT 'SHOULD I PLOT THE DATA '\INPUT F$
1450 FHYL(100,975,55,750)
1460 L9=0\S9=0
1470 FOR I=1 TO R1
1480 IF L9 =R1(I) THEN 1520\L9=R1(I)
1520 IF S9 =R3(I) THEN 1510\S9=R3(I)
1540 NEXT I\L8=L9*A1\IF F$='NO' THEN 1680
1570 N9=L9\GOSUB 5800\L9 N9
1590 N9=S9\GOSUB 5800\S9 N9
```

255

```
1600 SCAL(0,0,S9,0,L9)
1610 CNTR(3)\CNTR(5)\PRINT ,"SPECIMEN : ";S9$,"DATE:";DO$
1620 LABL("STROKE ,"&SO$,"STRESS ,"&LO$&"/"&AO$,S9/5,L9/5,0)
1630 LABL(S9/10,L9/10,3)
1640 FOR I=1 TO R1\PLOT(R3(I),R1(I))\NEXT I\GOSUB 6000
1675 PRINT "SHOULD I SAVE THE DATA ";\INPUT D$
1680 IF D$="NO" THEN 1700
1690 IF D$ "YES" THEN 1675\T$="YES"\GOSUB 5400
1700 PRINT "DO YOU WANT TO CHAIN THIS PROGRAM WITH"
1710 PRINT "THE GRAPHIC PROGRAM (PULT2'";\INPUT S$
1720 IF S$ "YES" THEN IF S$ "NO" THEN 1700
1730 IF S$="YES" THEN 1850
1760 STOP
1850 CHAIN "DX0:PULT2.BAS" LINE 20
3000 BUTN(-1)\MSW1(2,C2)\M1=2
3010 C(1)=INT(4095/(2*T1*(1-(C2/204/))))\FG1(C,1,7,7)
3020 R9=R1\CO=R1(R1)\T1=1/100*R9+4095/2/INT(C(1))\BUTN
5000 PRINT "WHEN YOU HAVE COMPLETED THIS, TYPE A CARRIAGE RETURN ";
5010 INPUT S$\RETURN
5300 PRINT "ENTER SPECIMEN NAME (FIRST CHARACTER IS A P,";
5310 PRINT "6 CHAR MAXIMUM)";\INPUT S9$\RETURN
5400 PRINT "INSTALL A DATA DISK IN DX1";\INPUT S$
5410 OPEN "DX1:"&S9$ FOR OUTPUT AS FILE #1 DOUBLE BUF
5420 PRINT #1;R1\FOR I=1 TO R1
5430 PRINT #1;R1(I)\PRINT #1;R2(I)\PRINT #1;R3(I)\NEXT I
5450 IF M1=0 THEN R9=R1
5470 PRINT #1;LO$\PRINT #1;EO$\PRINT #1;SO$\PRINT #1;AO$
5480 PRINT #1;DO$\PRINT #1;CO\PRINT #1;T$\PRINT #1;T1
5485 PRINT #  1;L8\PRINT #1;DO\PRINT #1;R9\CLOSE #1\RETURN
5800 N9=INT(N9*10^(INT(1-LOG10(N9)))+.5)/(10^(INT(1-LOG10(N9))))
5810 N9=N9+(10^(INT(LOG10(N9))))\RETURN
6000 CNTR(4)
6010 FOR I=1 TO 800\J=SIN(I)\NEXT I
6020 CNTR(3)\RETURN
7000 PRINT "SWITCH HYDRAULIC OFF TO PUT MACHINE IN STROKE CONTROL "
7005 PRINT "AND FEEDBACK SELECTOR TO REMOTE";\INPUT S$\PRINT
7010 PRINT "TURN HYDRAULIC ON";\INPUT S$\RETURN
7020 PRINT "PUSH "RUN" ON CONTROL UNIT, ADJUST SPAN FOR MAXIMUM STROKE"
7030 PRINT "DESIRED AND INPUT SPAN VALUE(% OF STROKE RANGE)";
7040 INPUT P2\RETURN
8000 PRINT "LOAD "&Q1$;Z1*10/2047;"VOLTS"\RETURN
8020 PRINT "STROKE "&Q1$;Z3*10/2047;"VOLTS"\RETURN
8050 PHYL(100,975,55,750)
8060 L9=0\S9=0
8070 FOR I=1 TO R1
8080 IF L9 =R1(I) THEN 8090\L9=R1(I)
8090 IF S9 =R3(I) THEN 9000\S9 R3(I)
9000 NEXT I\L8=L9
9010 N9=L9\GOSUB 5800\L9=N9
9020 N9=S9\GOSUB 5800\S9=N9
9030 SCAL(0,0,S9,0,L9)
9040 CNTR(3)\CNTR(5)\PRINT ,"SPECIMEN : ";S9$,"DATE :";DO$
9050 LABL("STROKE,MM","LOAD,KN",S9/5,L9/5,0)
9060 LABL(S9/10,L9/10,3)
9070 FOR I=1 TO R1\PLOT(R3(I),R1(I))\NEXT I\GOSUB 6000
9080 RETURN

READY
```

256

```
177777 000000 000000 000000
$
177732 000000 177772 173234
$D:
PT-11SJ     U020-02B

 DATE 03-FEB-86

.F BASIC

162600 NONEXISTENT
162610 NONEXISTENT
MTS BASIC U01B-02C
COPYRIGHT 1977, MTS SYSTEMS CORPORATION

$H
DIAGNOSTICS.TH

USER FNS LOADED


READY

OLD "PULTIM"

READY
```

RUN

PULT1M 10-FEB-86 MTS BASIC V01B-02C

THIS PROGRAM DEFORMS A TEST ITEM IN LOAD OR STROKE CONTROL
FROM AN INITIAL LOAD OR STROKE OF ZERO TO A MAXIMUM LOAD
OR STROKE SELECTED BY THE OPERATOR (UP TO FULL SCALE LOAD
OR STROKE) IN A TIME SPECIFIED BY THE OPERATOR
THROUGHOUT THE TEST , LOAD AND STROKE DATA POINTS
ARE STORED.   AT THE CONCLUSION OF THE TEST, THE STORED DATA
POINTS ARE PRINTED IN A TABLE; LOAD POINTS ARE DIVIDED BY
SPECIMEN AREA AND DISPLAYED IN UNITS OF STRESS THE OPERATOR
MAY REQUEST THAT THE DATA BE STORED ON DISK AND HE HAS THE
OPTION TO CHAIN THIS PROGRAM TO THE GRAPHIC PROGRAM 'PULT2'
WHICH WILL PERFORM A DETAILED ANALYSIS OF THE DATA OBTAINED
IN THIS PROGRAM.

****** SHOULD YOU PREFER NOT CHAINING WITH 'PULT2'   ******
******   BE SURE YOU REQUEST STORING OF THE DATA   ******
******   IF FURTHER ANALYSIS IS REQUIRED   ******

YOU MAY ACTIVATE THE HYDRAULICS.MOUNT SPECIMEN IN UPPER
GRIP,ZERO THE LOAD CELL,CLAMP SPECIMEN IN LOWER GRIP
TURN OFF THE HYDRAULICS,ZERO THE STROKE TRANSDUCER,REACTIVATE
THE HYDRAULICS,AND ZERO THE APPLIED LOAD USING THE STROKE ZERO

TURN ON HARD COPY UNIT.

ENTER SPECIMEN NAME (FIRST CHARACTER IS A P,6 CHAR MAXIMUM)?P24A
ENTER DATE OF TEST (DAY-MONTH-YEAR)?03-FEB-86
DATE IS 03-FEB-86, IS THAT CORRECT (YES-NO)?YES
DO YOU PREFER TO CONDUCT THE TEST IN STROKE CONTROL?YES
SWITCH HYDRAULIC OFF TO PUT MACHINE IN STROKE CONTROL
AND FEEDBACK SELECTOR TO REMOTE?

258

```
TURN HYDRAULIC ON?
ENTER LOAD RANGE (IN KN)?100
ENTER  STROKE RANGE (IN MM.)?10
ENTER NOTCH AREA (SQUARE MM.)?58.8

TIME MAY RANGE FROM 0 5 TO 2047 SEC
ENTER TIME FOR RAMP FROM 0 TO MAX STROKE (SEC )?30
RAMP TIME WILL BE 30.1103 SECONDS

PLEASE ZERO ALL TRANSDUCERS AT THIS TIME
TO ASSIST YOU IN DOING THIS I WILL PRINT LOAD AND
STROKE ABOUT EVERY SECOND FOR 10 SECONDS

LOAD              STROKE
(VOLTS)           (VOLTS)
0                 -4.88520E-03
0                 0
0                 0
4.88520E-03       4 88520E-03
0                 0
0                 0
4.88520E-03       0
4.88520E-03       0
4 88520E-03       0
4.88520E-03       0
WOULD YOU LIKE TO TRY THAT AGAIN (YES-NO) ?NO
PUSH "RUN" ON CONTROL UNIT, ADJUST SPAN FOR MAXIMUM STROKE
DESIRED AND INPUT SPAN VALUE(% OF STROKE RANGE)?30
SET SAFETY INTERLOCKS AND RETURN TO CRT?
```

WOULD YOU LIKE TO DECREASE THE SPAN OF THE STROKE
AND LOAD SCALES ON THE LOAD VS STROKE PLOT?YES

SELECT "LOCAL" ON THE "LOCAL-LINE" SWITCH THEN PRESS <CR> ON
TELETYPE TO OBTAIN THE TABLE OF DATA POINTS?
SHOULD I PLOT THE DATA ?YES

SHOULD I SAVE THE DATA ?NO
DO YOU WANT TO CHAIN THIS PROGRAM WITH
THE GRAPHIC PROGRAM 'PULT2'?NO

STOP AT LINE 1760

READY

SPECIMEN : P24A

TIME (SEC.)	STRESS (KN/SQ.M.)	STROKE (MM)
.15	3323.26	0
.3	27416.9	9.77040E-03
.45	56495.5	.0293112
.6	83081.6	.048852
.75	107175	.0683928
.9	132100	.0781632
1.05	159517	.0879336
1.2	182780	.107474
1.35	208535	.12213
1.5	231798	.1319
2.25	352266	.210064
3	461934	.293112
3.75	571601	.351734
4.5	674623	.429897
5.25	766843	.503175
6	849094	.576453
6.75	910584	.649731
7.5	959592	.718124
8.25	996148	.786517
9	1.02855E+06	.869565
9.75	1.05597E+06	.937958
10.5	1.08006E+06	1.01612
11.25	1.09668E+06	1.08451
12	1.11329E+06	1.16268
12.75	1.12492E+06	1.23596
13.5	1.13074E+06	1.30923
14.25	1.12576E+06	1.3874
15	2492.45	1.48022
15.75	3323.26	1.55349
16.5	830.816	1.62677
17.25	830.816	1.70982
18	0	1.77333
18.75	830.816	1.85149
19.5	0	1.92965
20.25	830.816	2.00293
21	830.816	2.07621
21.75	830.816	2.15437
22.5	830.816	2.22277
23.25	830.816	2.29604
24	830.816	2.37421
24.75	830.816	2.4426
25.5	830.816	2.52076
26.25	830.816	2.59404
27	1661.63	2.6722
27.75	0	2.7406
28.5	830.816	2.81387
29.25	830.816	2.89204
30	830.816	2.9702
30.75	0	3.04348
31.5	830.816	3.04348
31.65	0	3.04348

TOTAL DURATION OF TEST WAS 30.1103 SECONDS.

NOW GO BACK TO 'LINE' THEN PRESS CR ON THE TERMINAL?

261

SPECIMEN : F13H   DATE 01-FEB-86

SPECIMEN · F13C
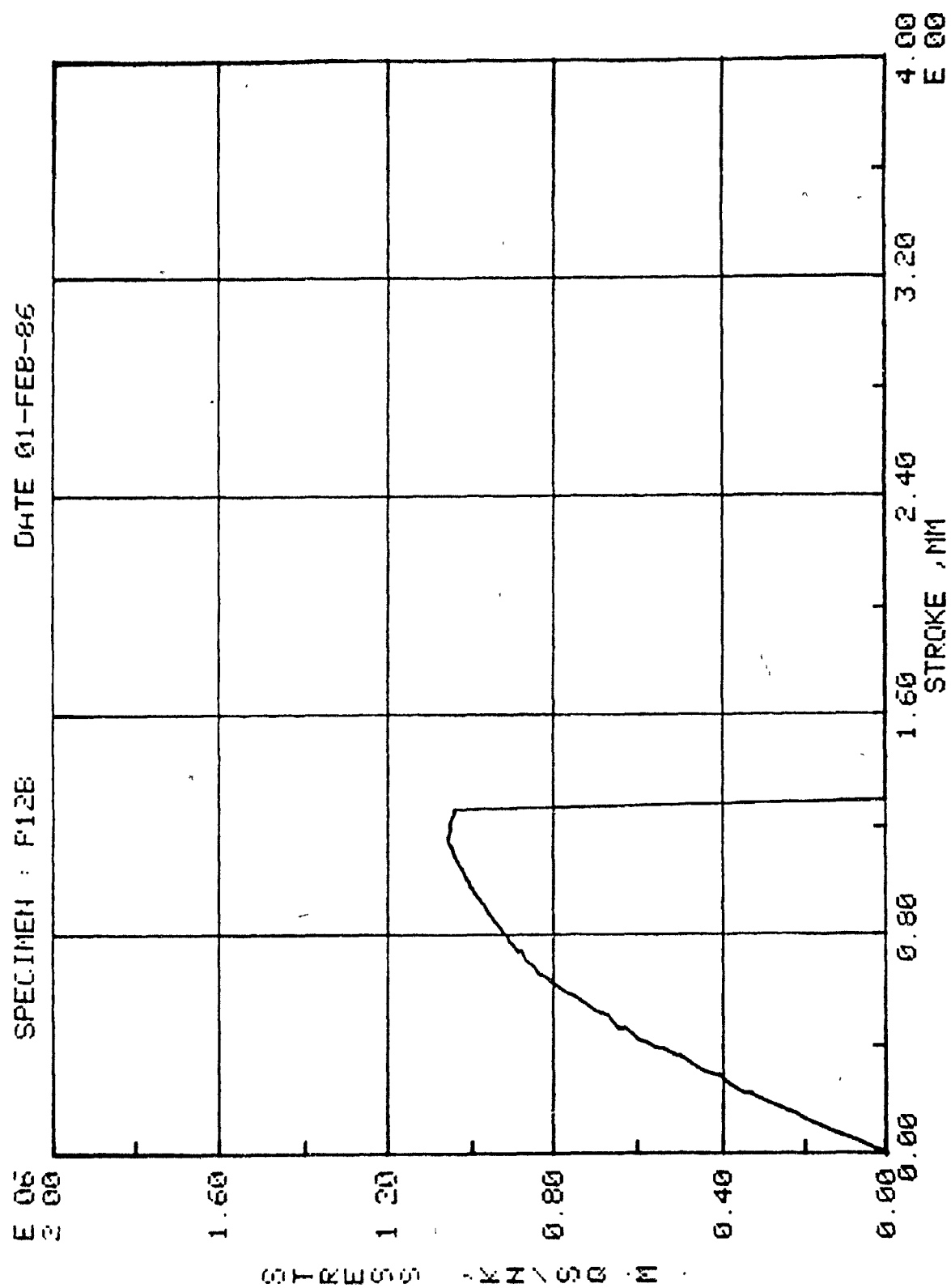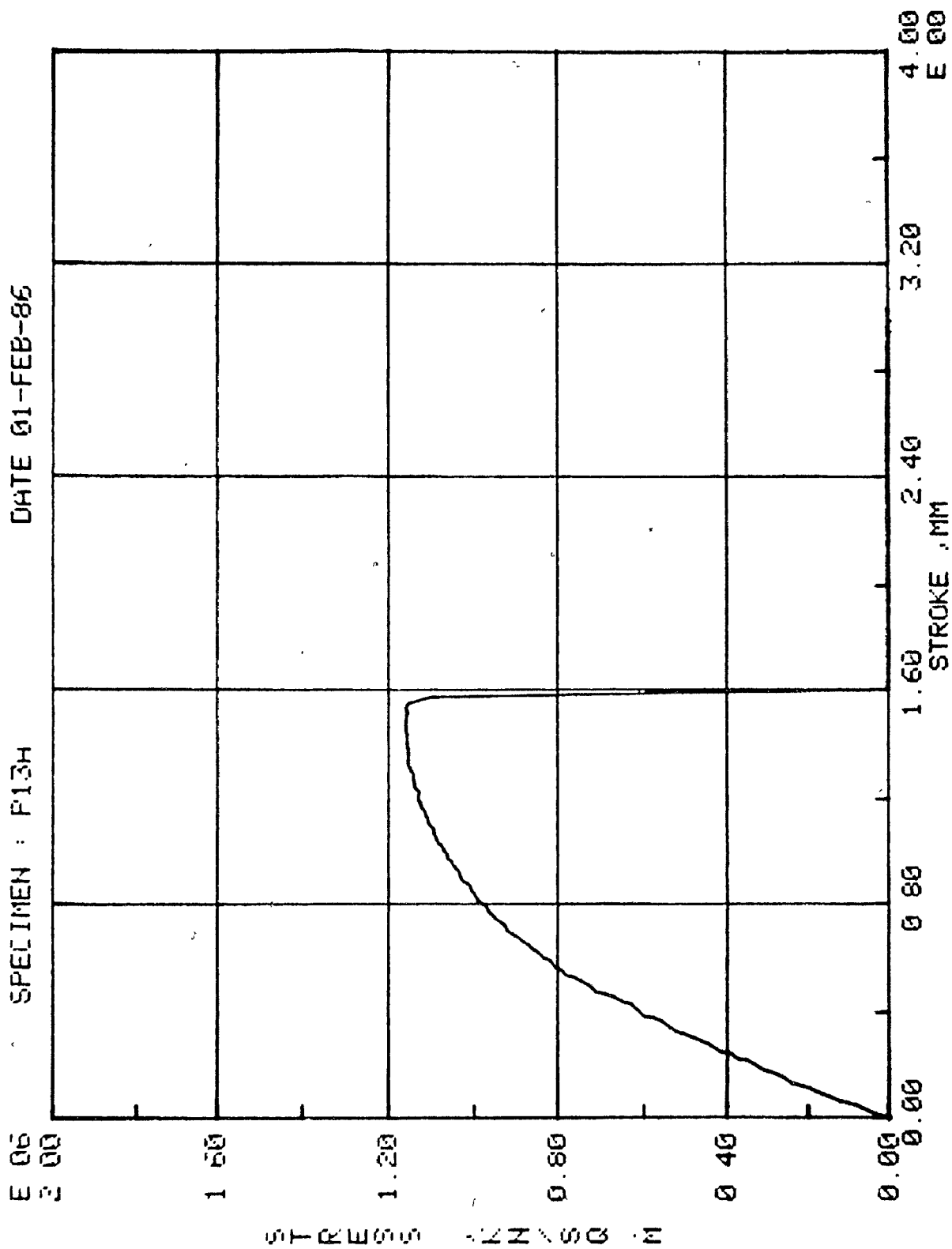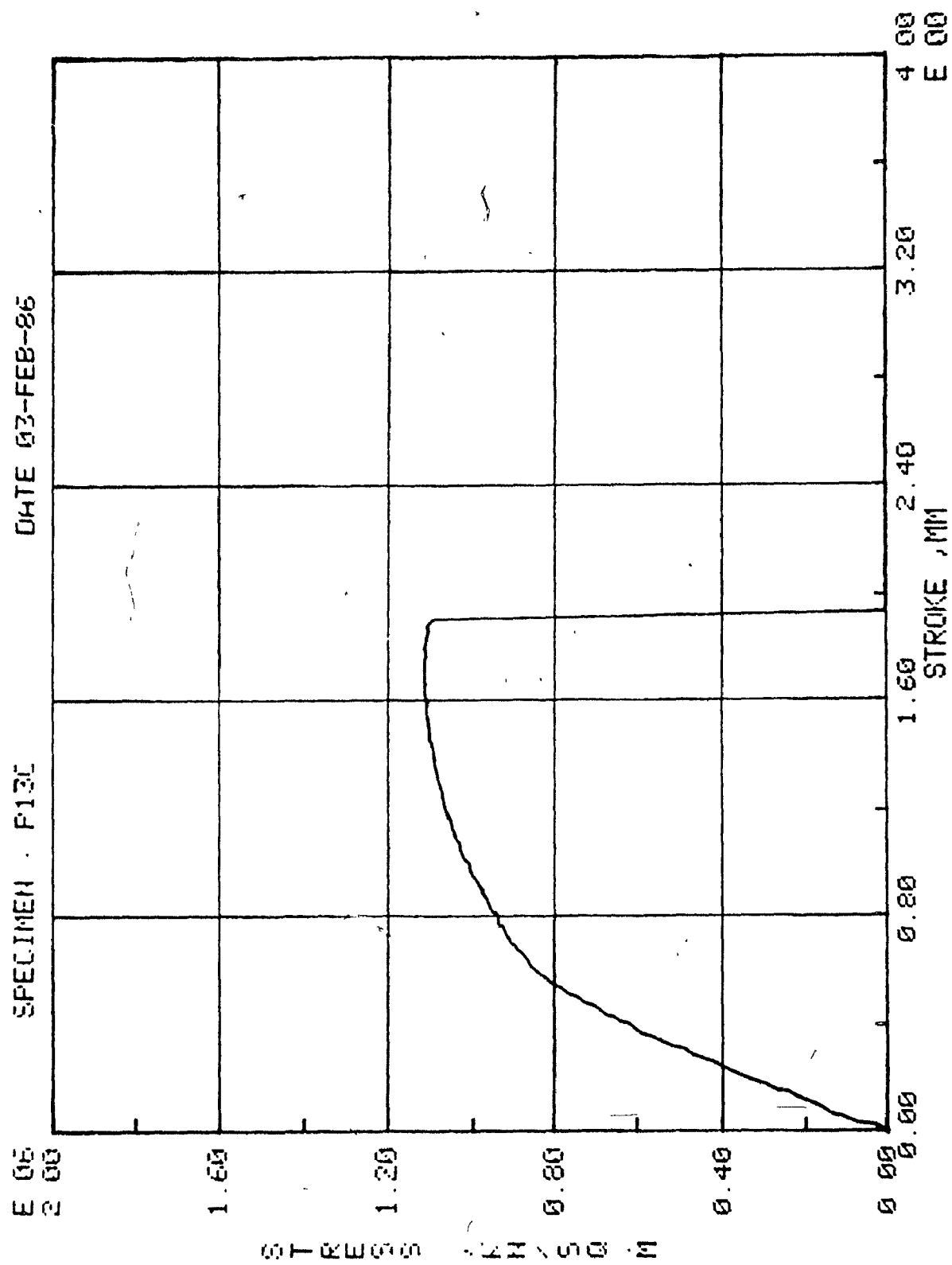
DATE 03-FEB-86

STROKE , MM

SPECIMEN   P24A   DATE:03-FEB-86

STRESS , KN/SQ MM

STROKE ,MM

265
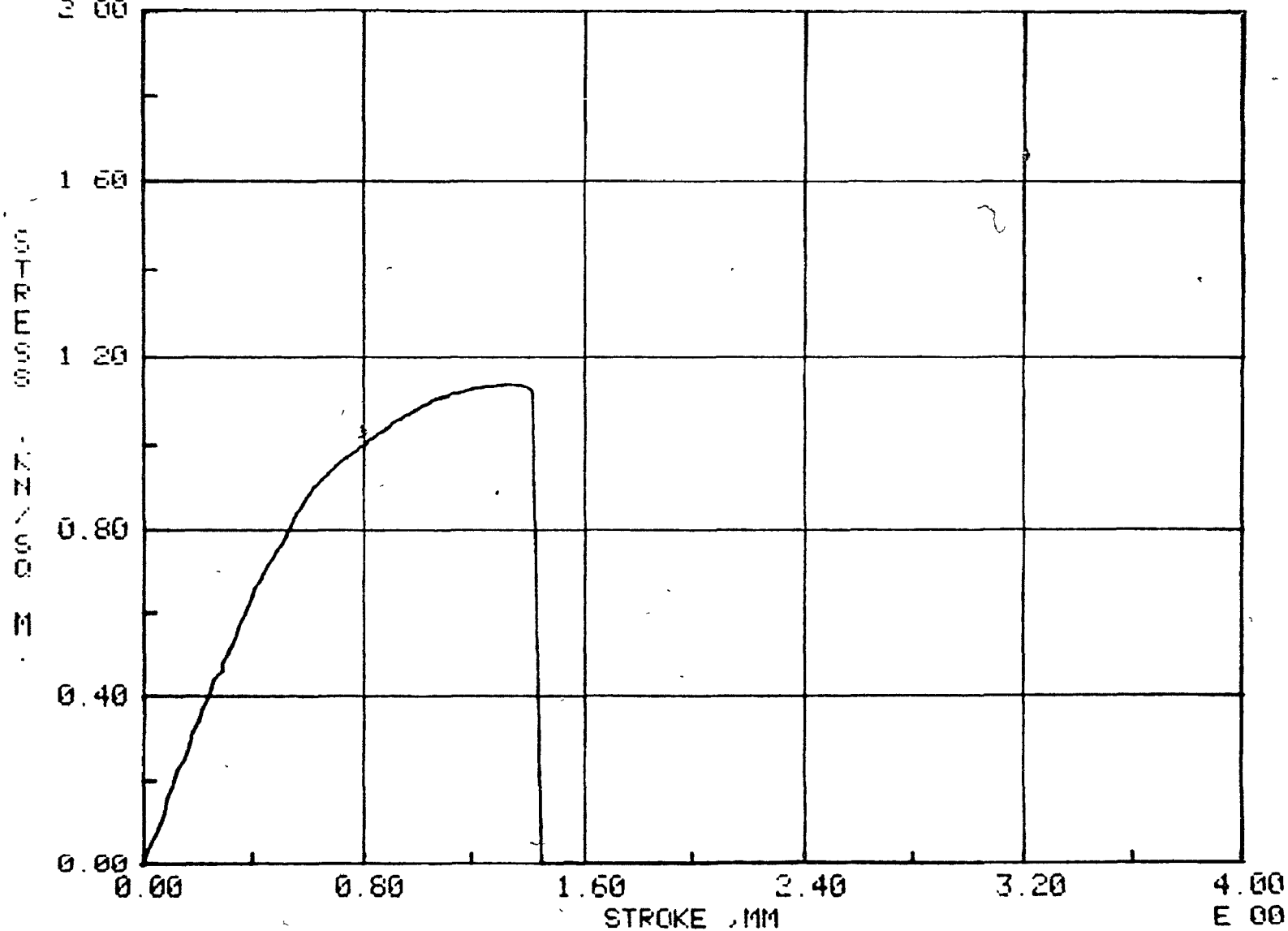
E 06
2 00

SPECIMEN · P25A   DATE:03-FEB-86
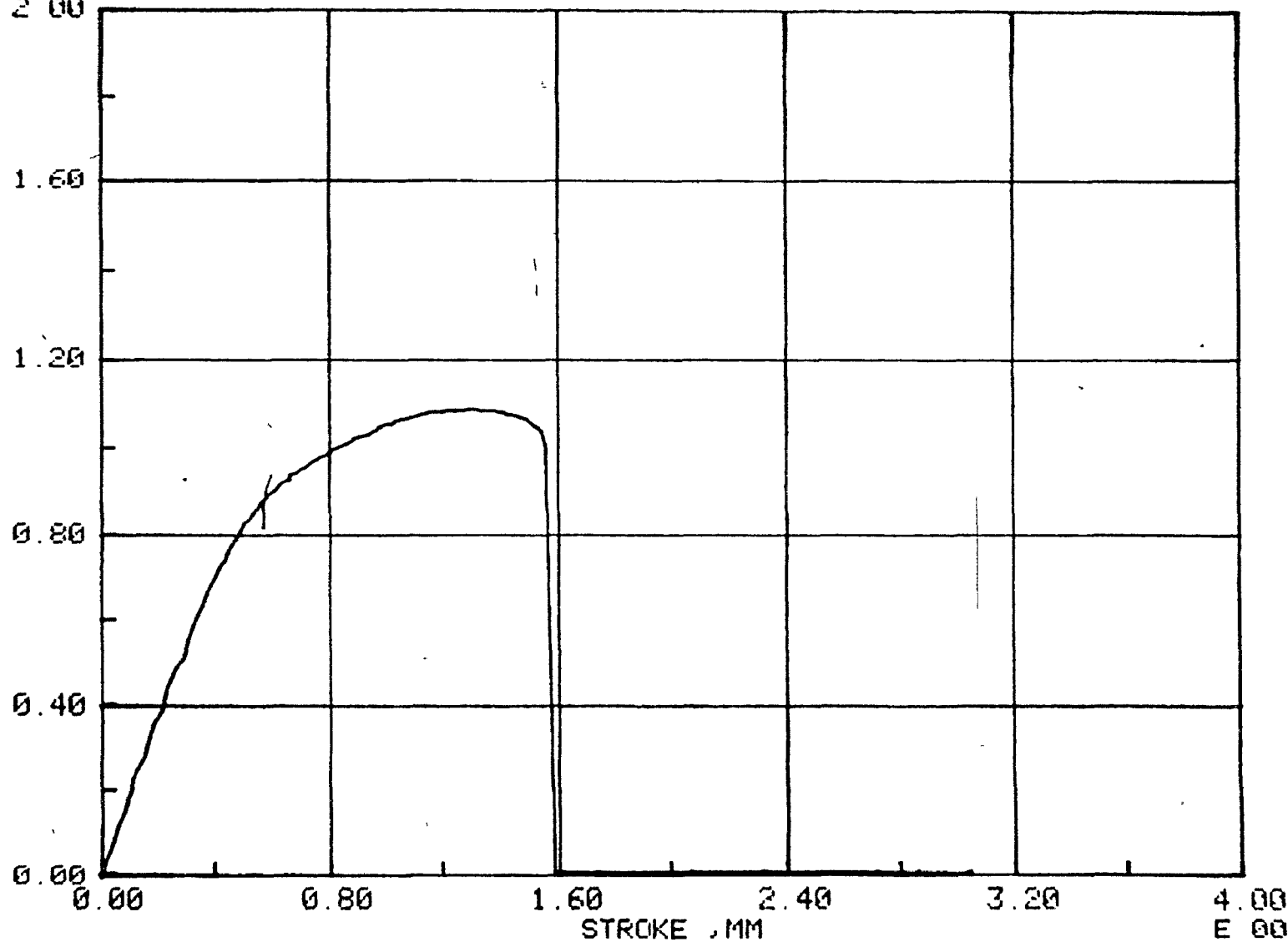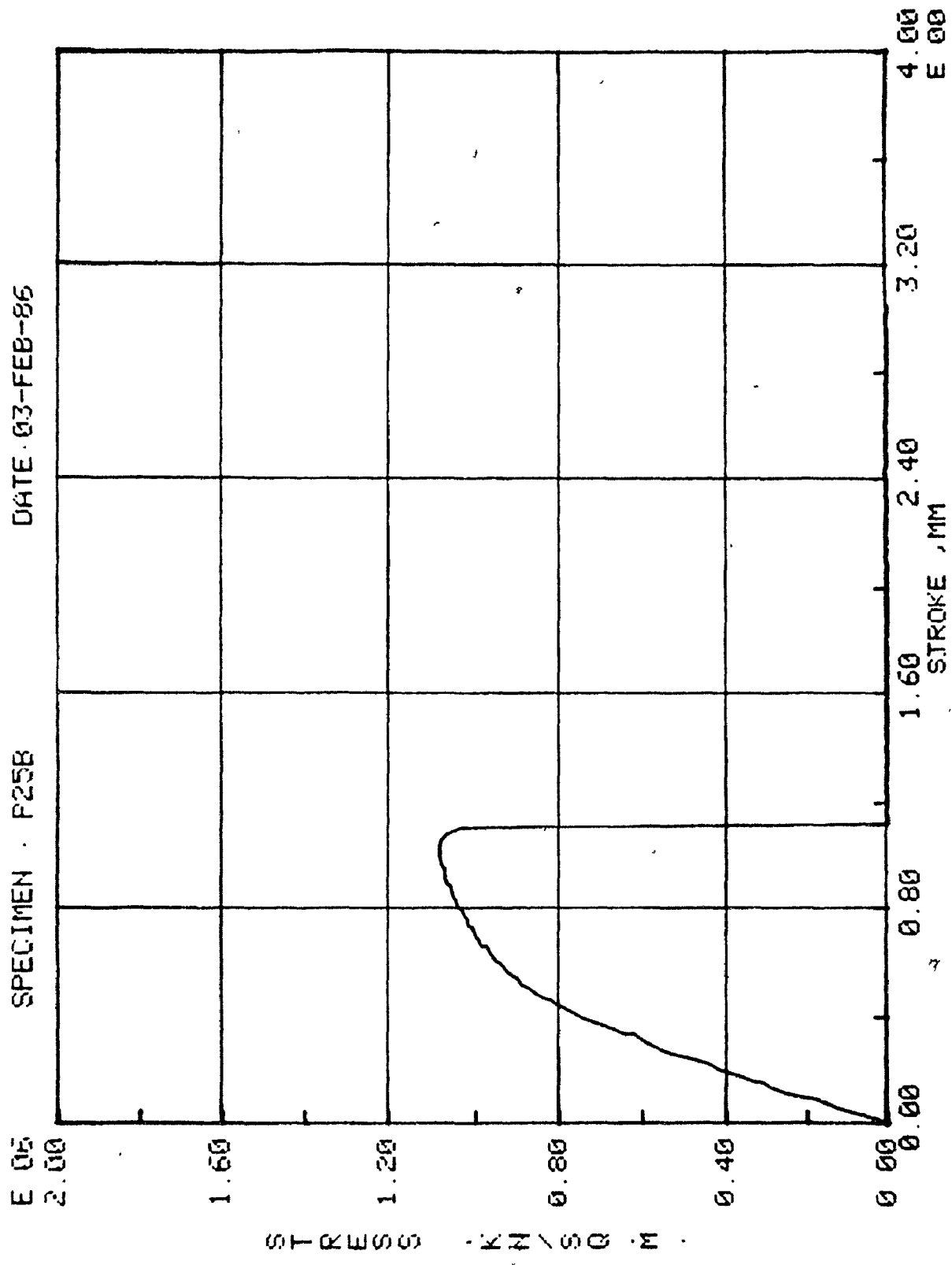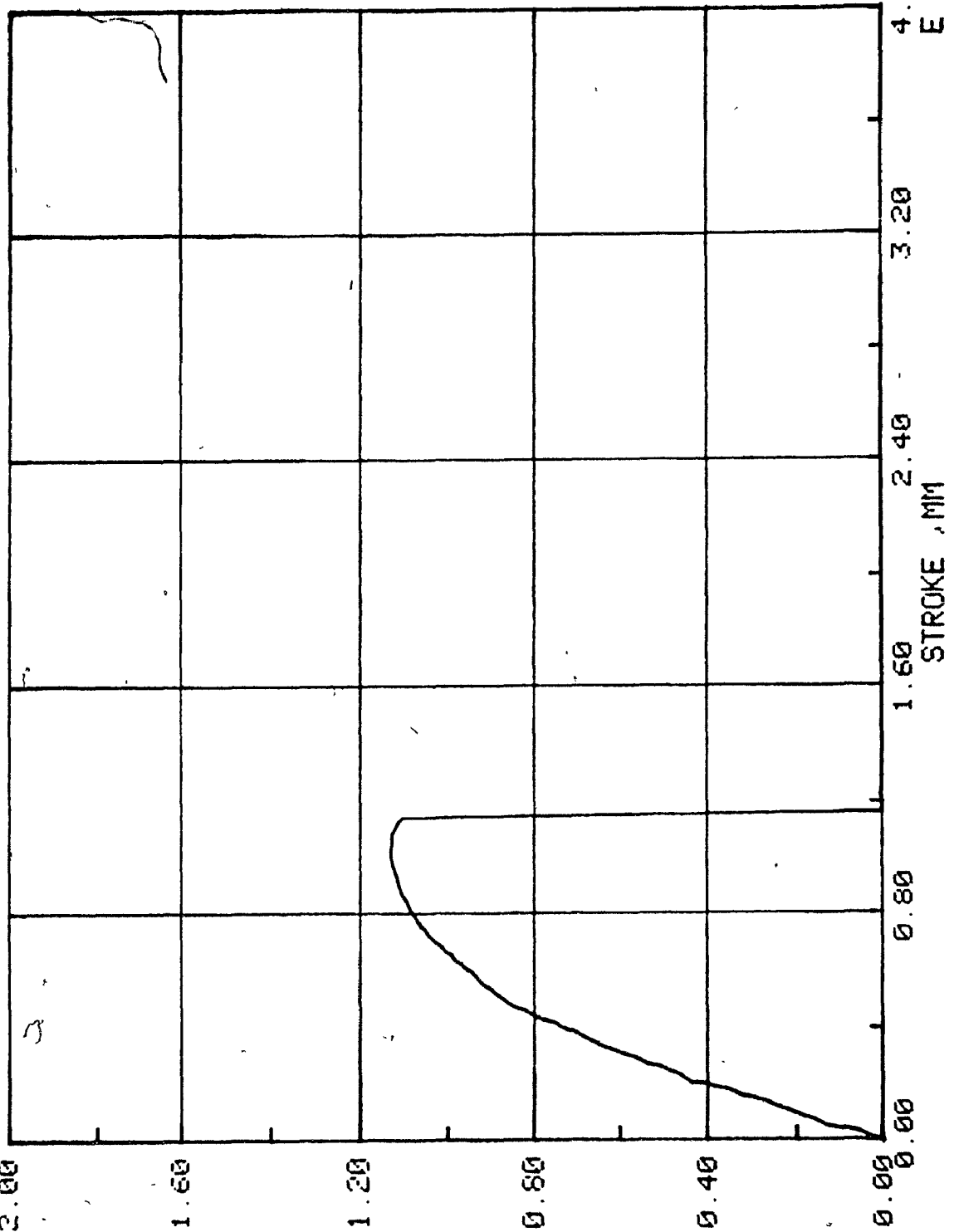
1.60

STRESS · KN/SQ·MM

1.20

0.80

0.40

0.00
0.00   0.80   1.60   2.40   3.20   4.00
                    STROKE ,MM   E 00

SPECIMEN · P25B   DATE · 03-FEB-86

STROKE , MM

STRESS · KN / SQ · M ·

SPECIMEN   F32C   DATE 01-FEB-86

SPECIMEN · F336   DATE:01-FEB-86

STROKE ,MM

STRESS · KN/SQ · M ·

SPECIMEN : P42B   DATE:03-FEB-86

STROKE ,MM

STRESS -KN\SQ M

SPECIMEN : P43C   DATE : 03-FEB-86

STRESS , KN/SQ.M.

STROKE , MM

SPECIMEN : P62A   DATE:03-FEB-86

STRESS , KN/SQ. M.

STROKE , MM

273
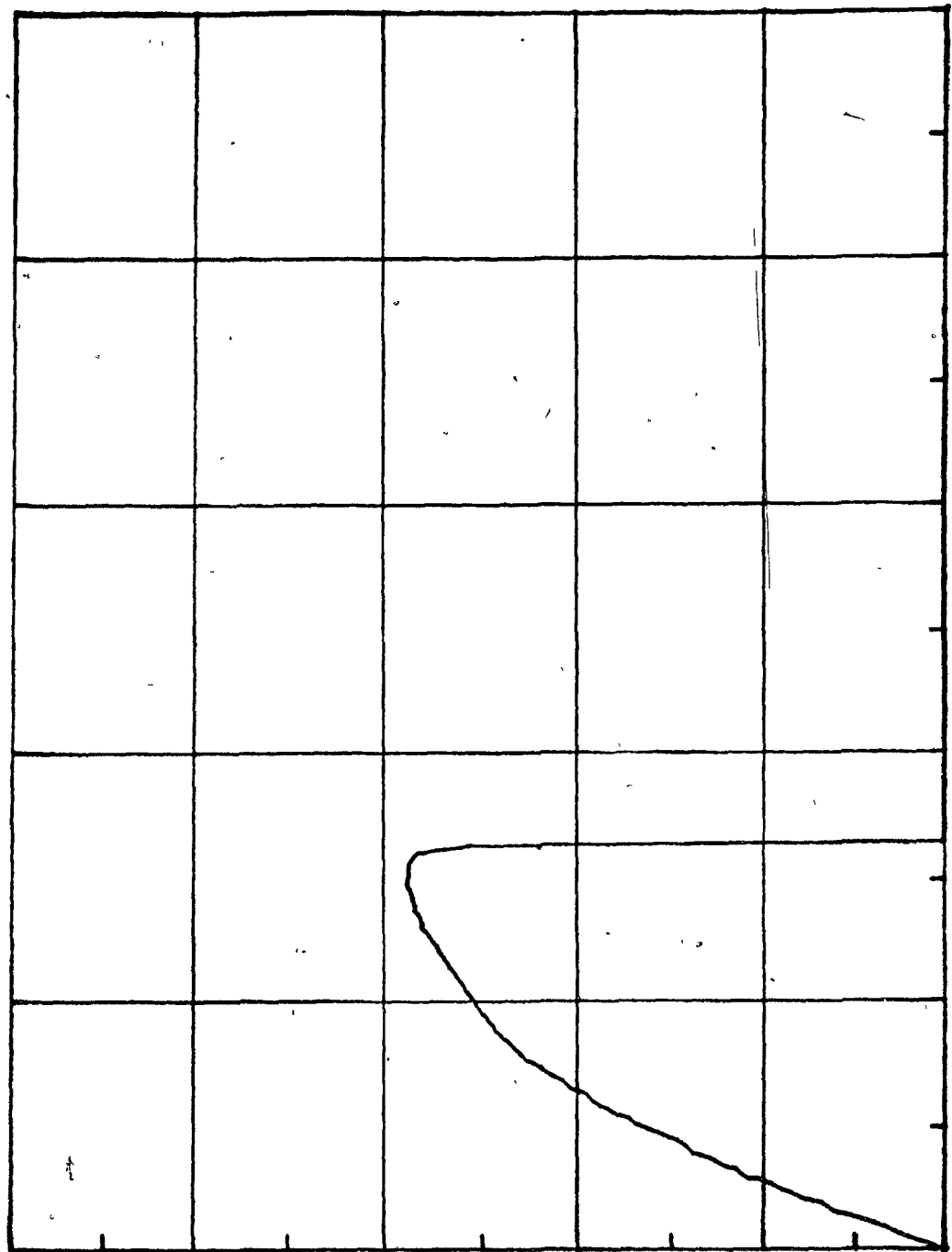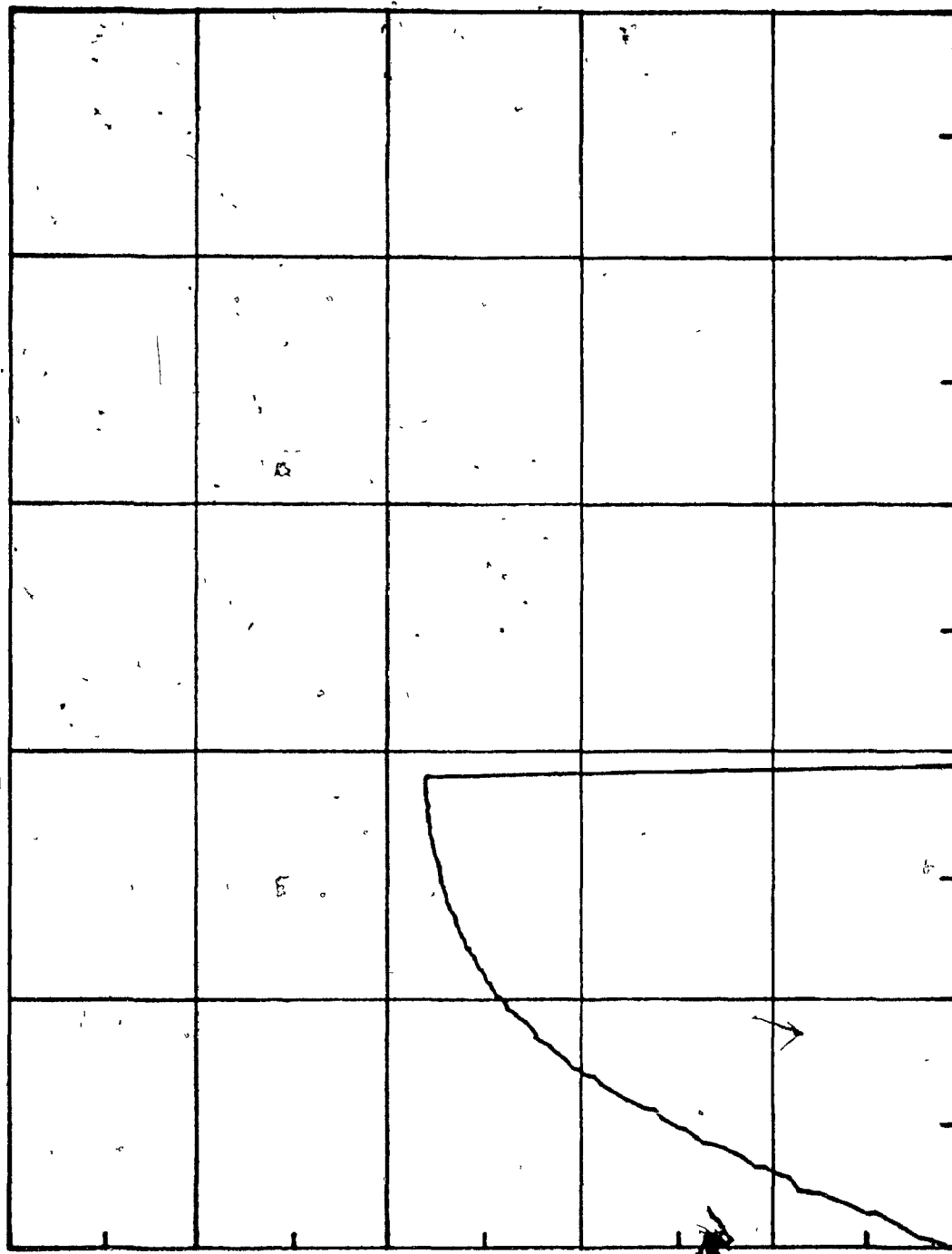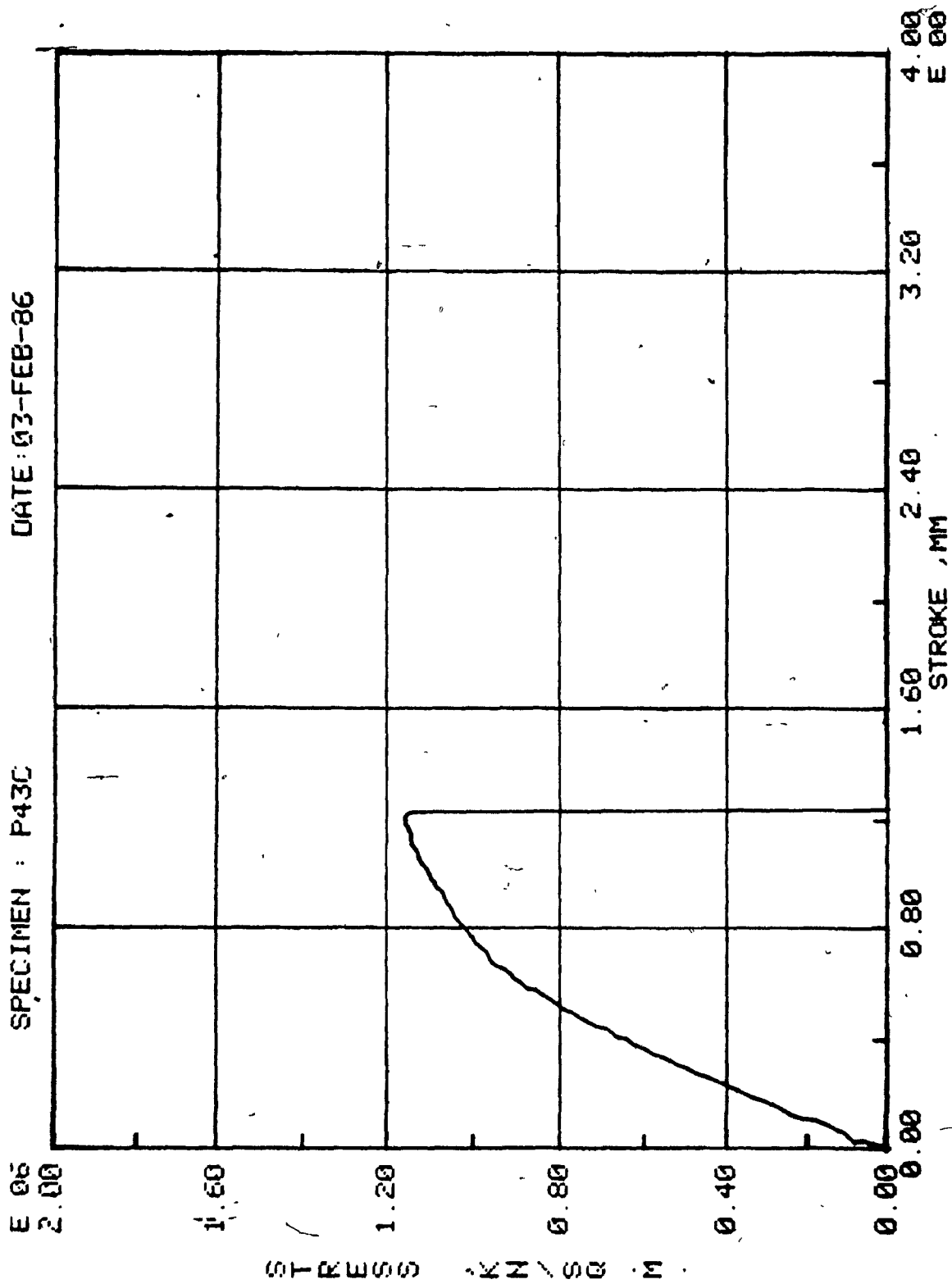
SPECIMEN : P62C   DATE : 03-FEB-86

STRESS , KN/SQ.M

STROKE , MM
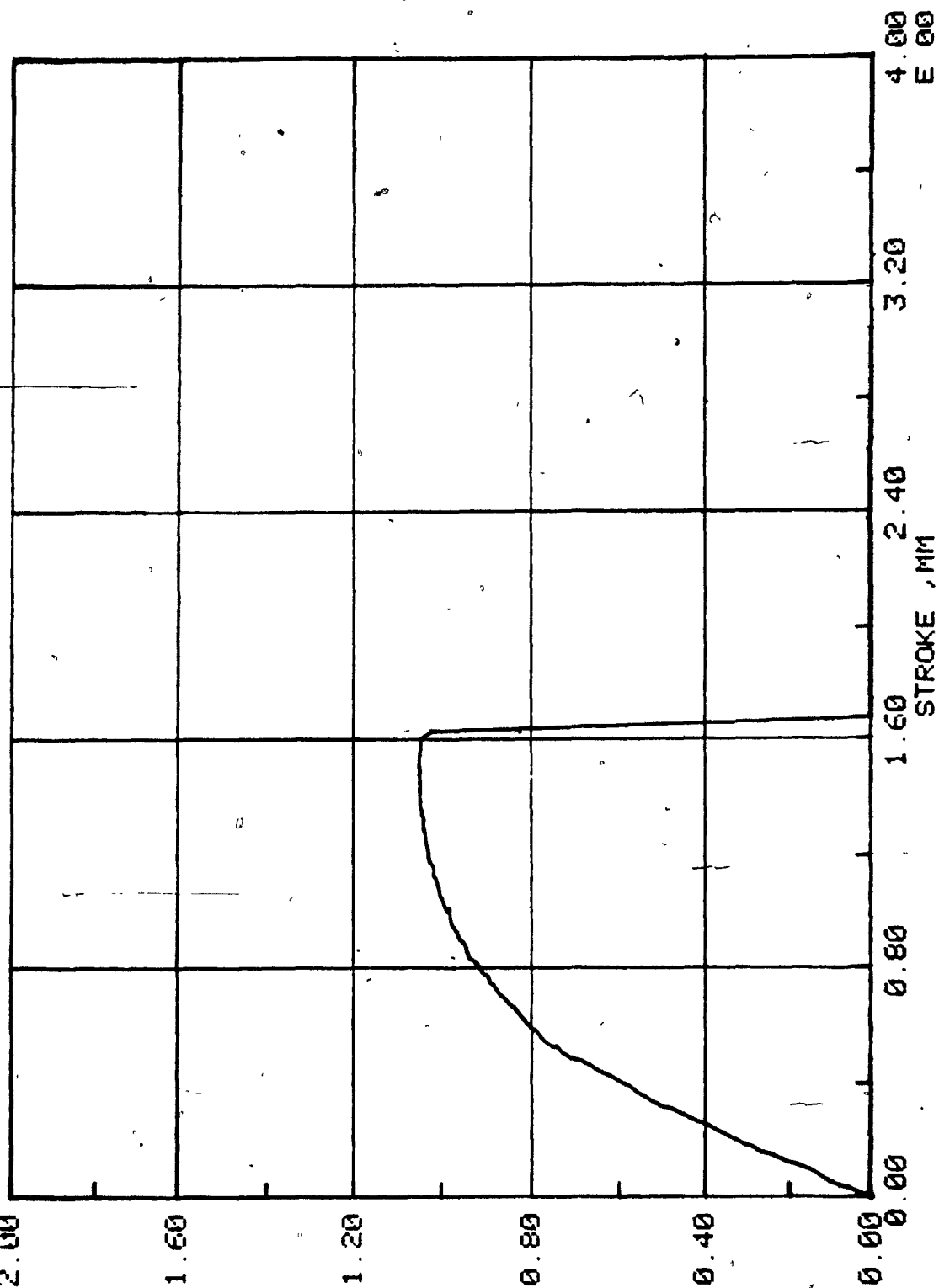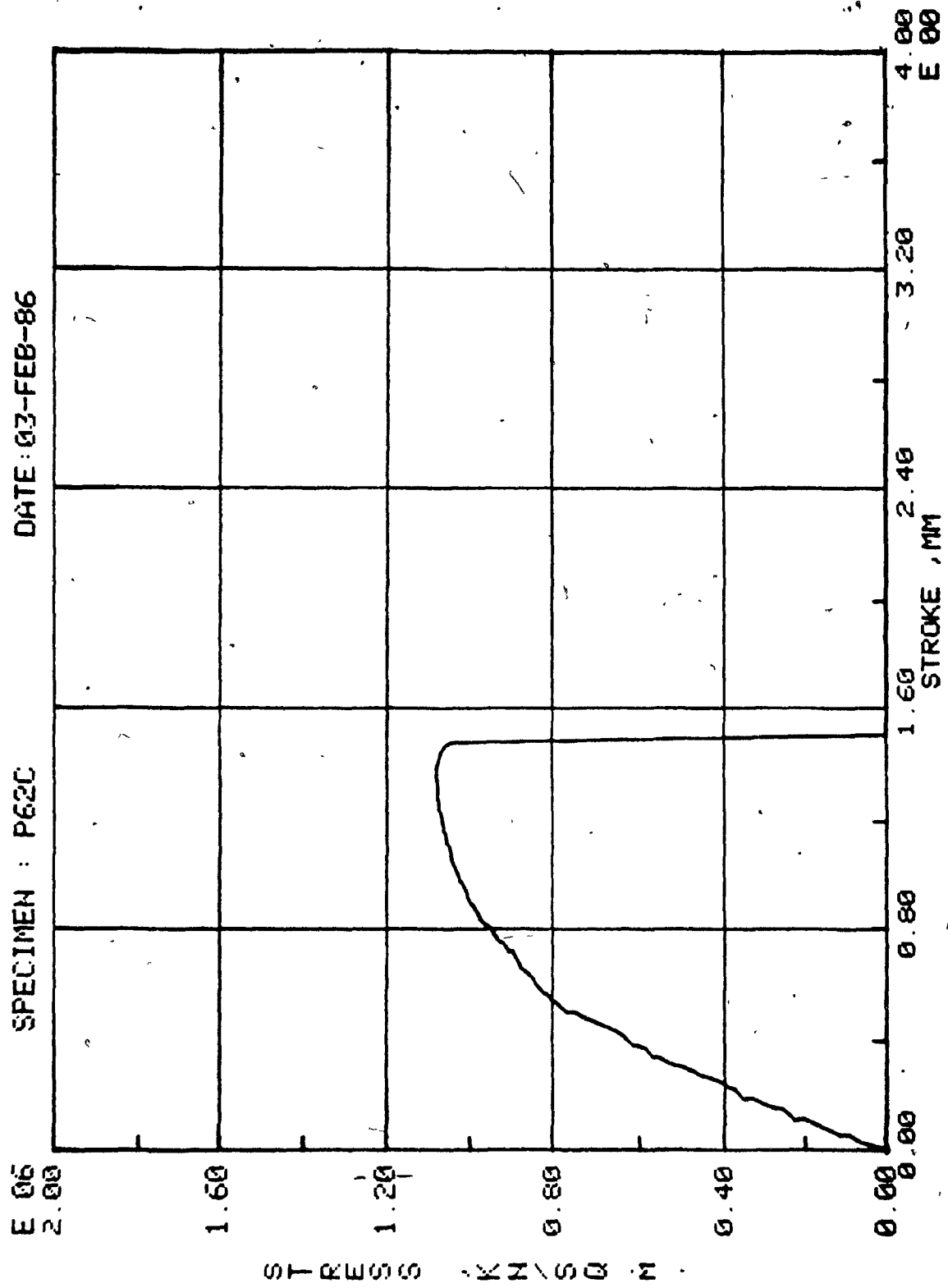
APPENDIX F

RADIOGRAPHIC INSPECTION RESULTS

BLOCK 22 X-RAY DIR 2

276

BLOCK 23   X-RAY DIR I

BLOCK 23 X-RAY DIR 2

278

78

Q5

1.0

8.4
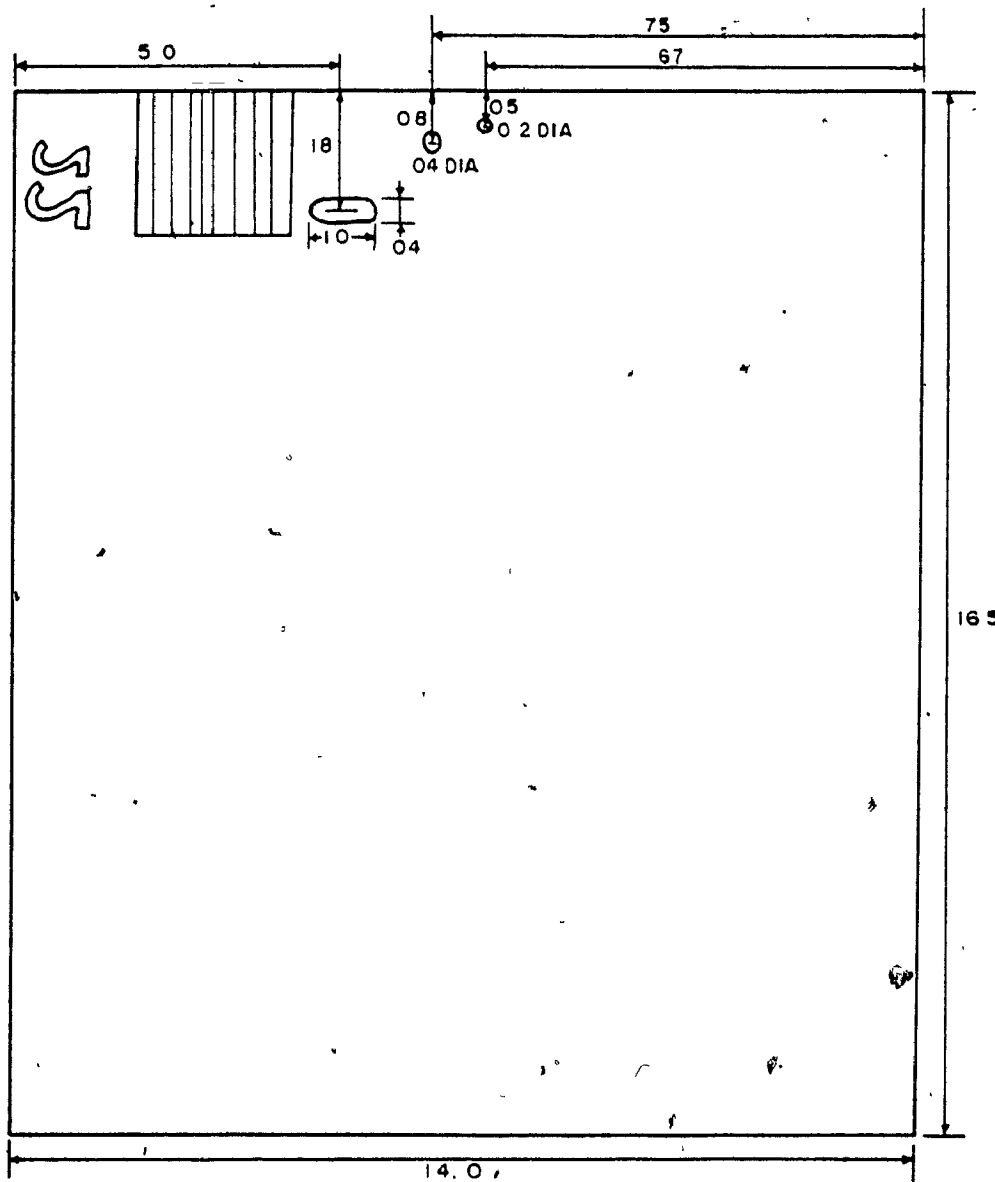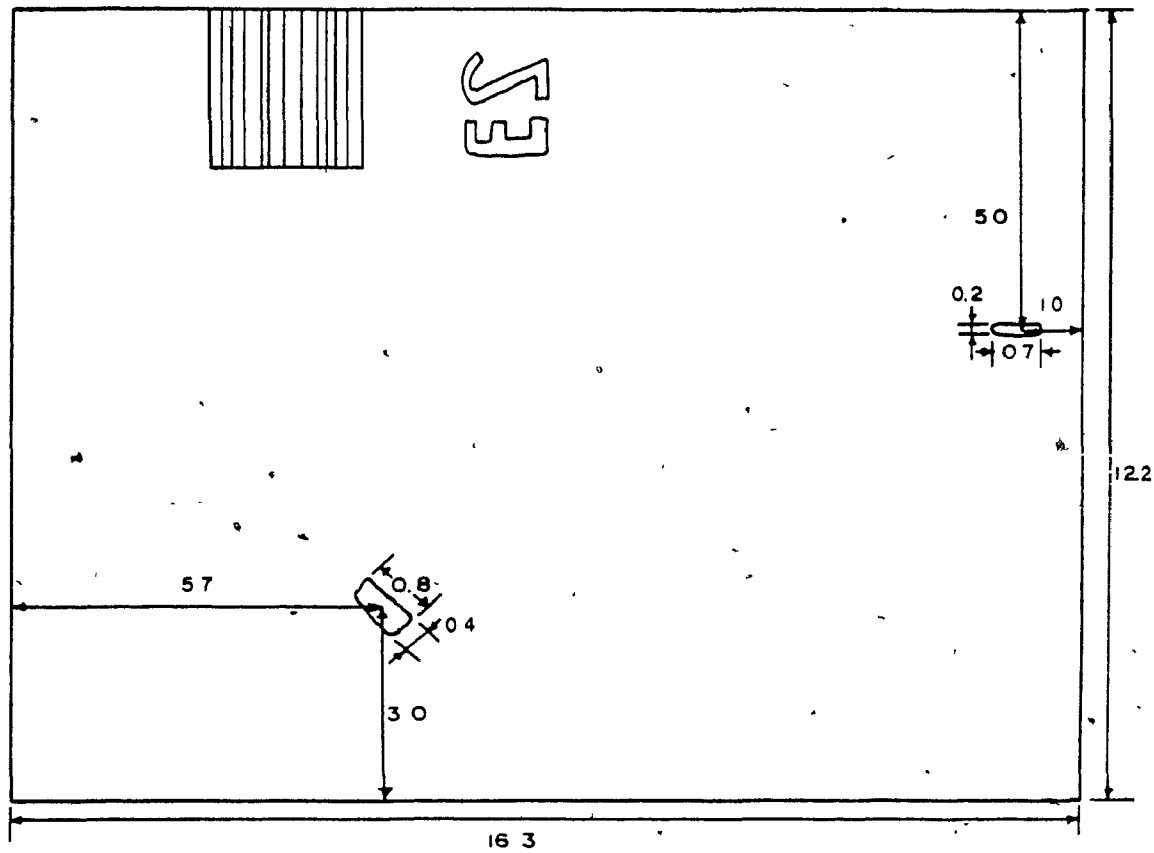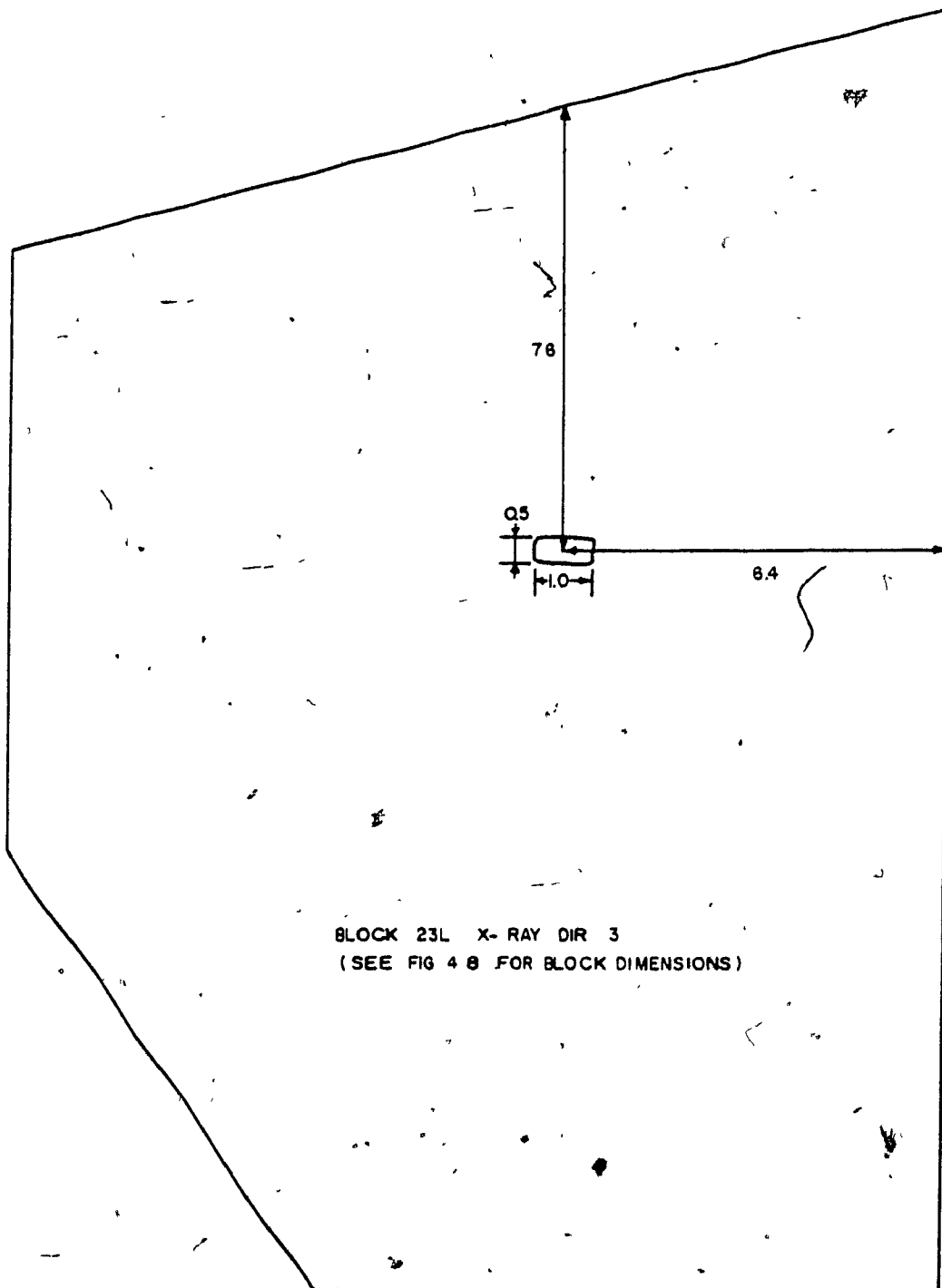
BLOCK 23L   X- RAY DIR 3
(SEE FIG 4 8 FOR BLOCK DIMENSIONS)

BLOCK 24 X-RAY DIR I

BLOCK 24   X-RAY   DIR 2

281

BLOCK 26 X-RAY DIR 2

282

16.5

16.5

41

60°

0.4

2.5

3.3

BLOCK 41   X-RAY   DIR I

283

BLOCK 41   X-RAY DIR 2

284
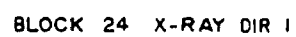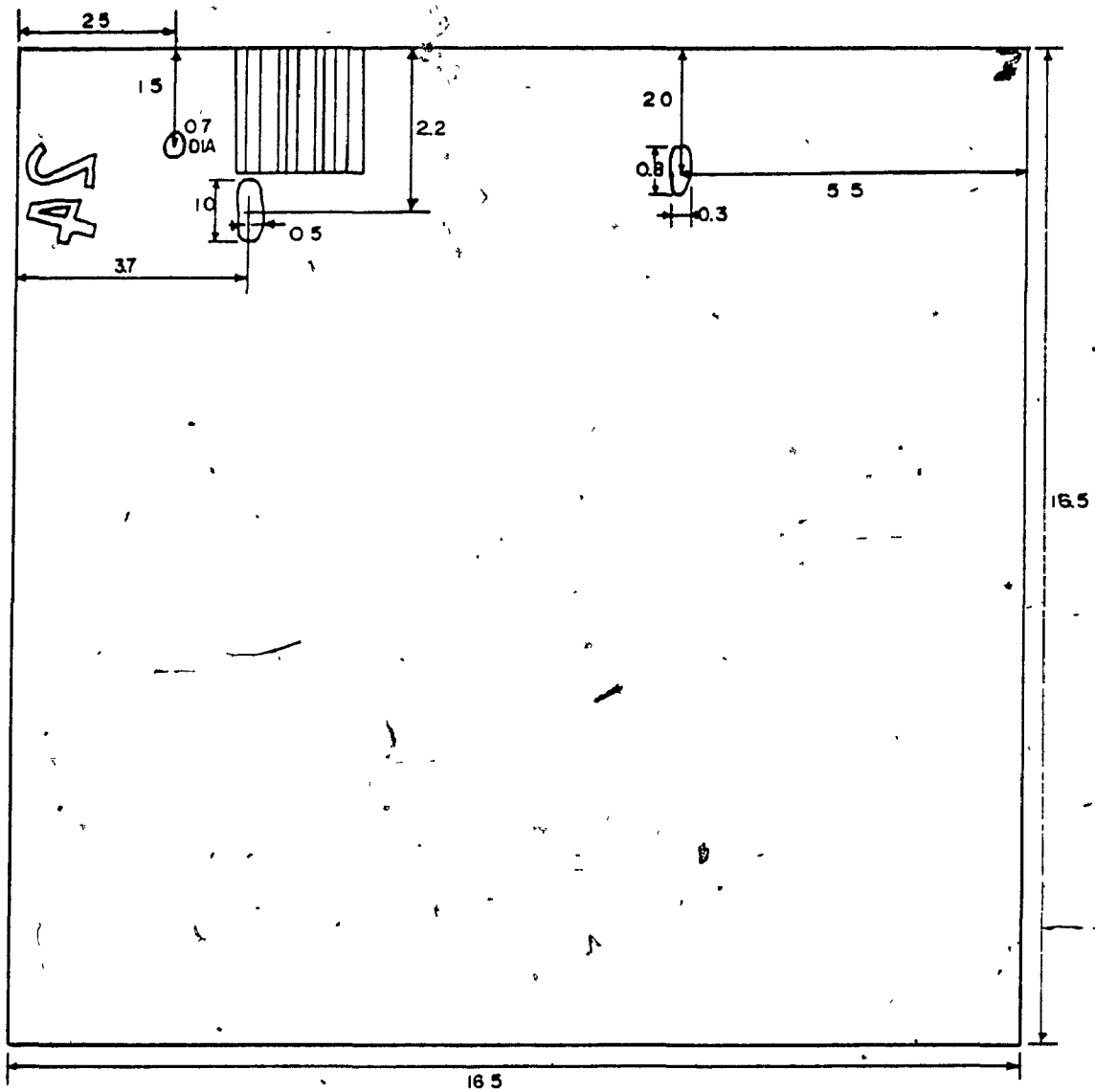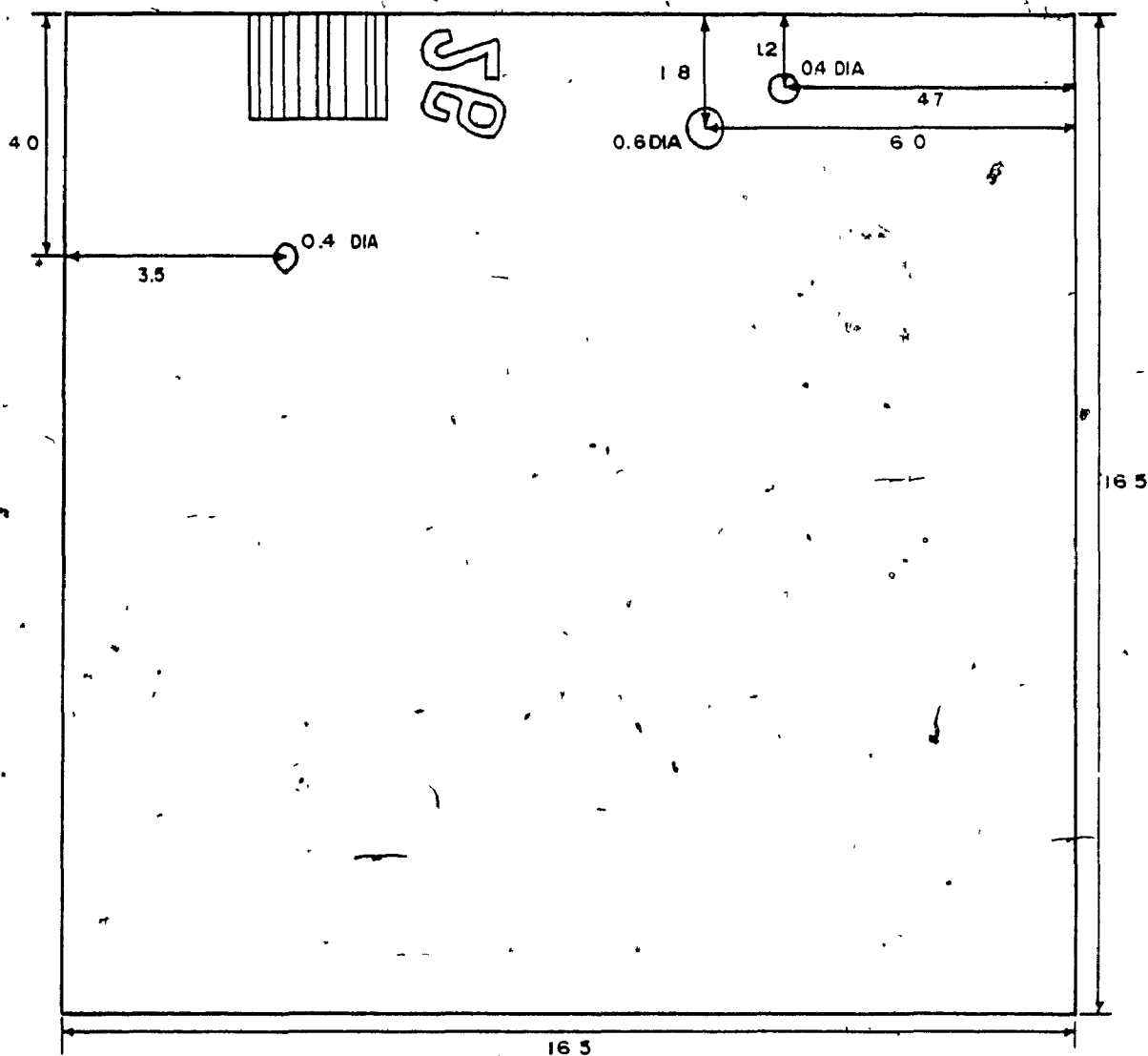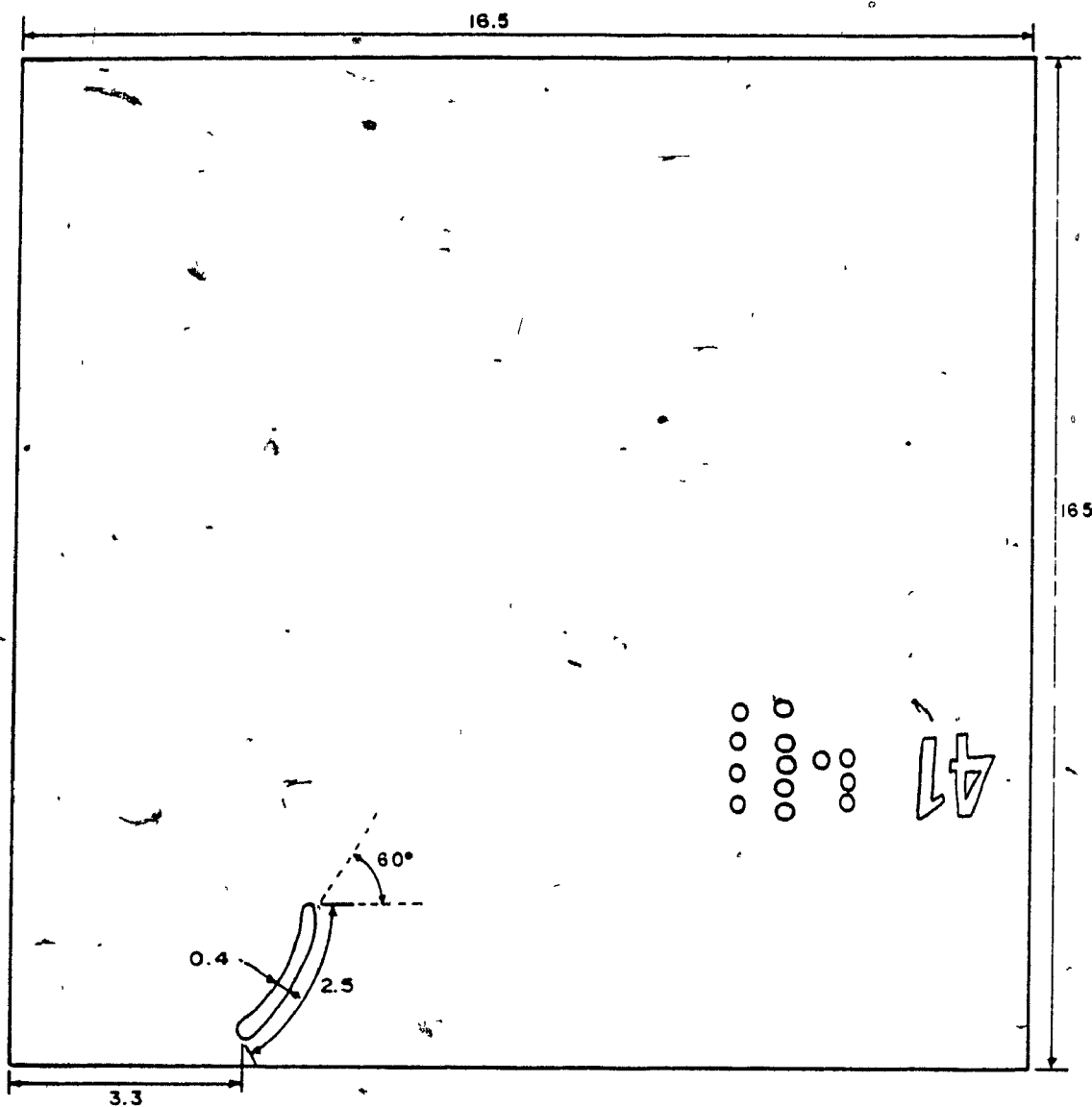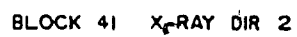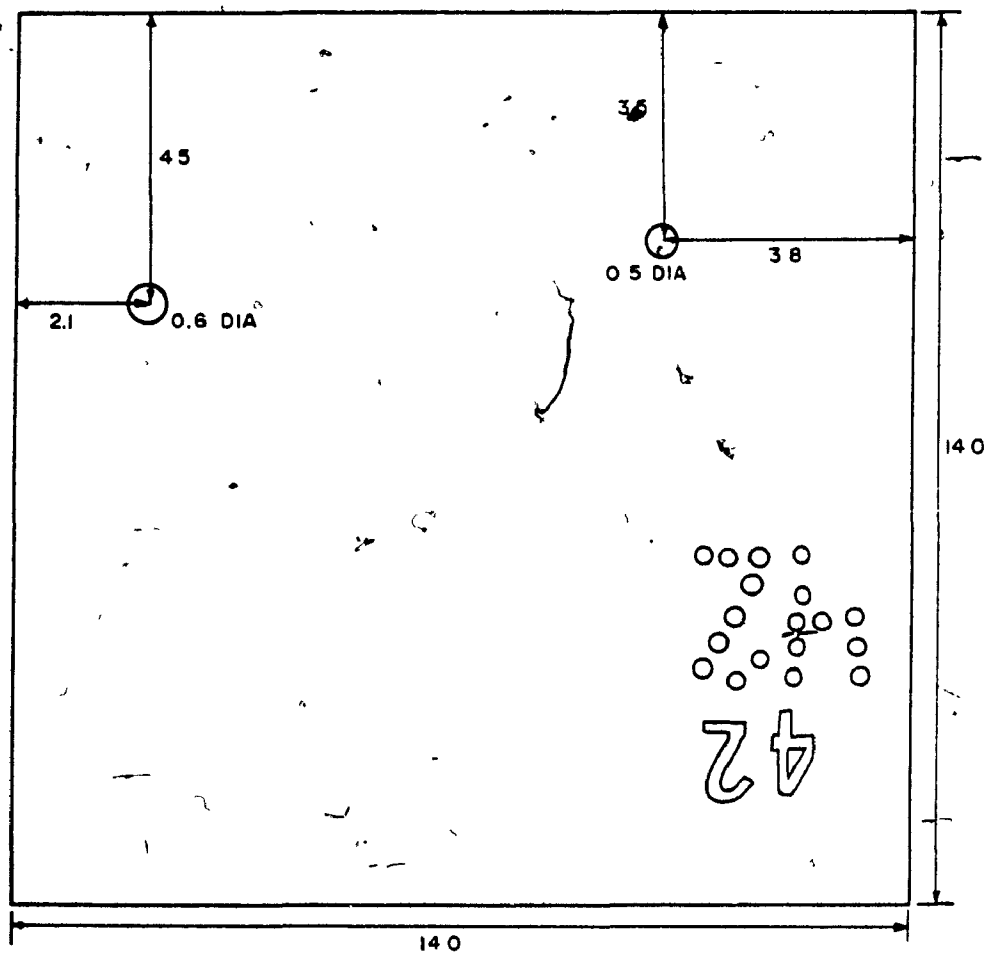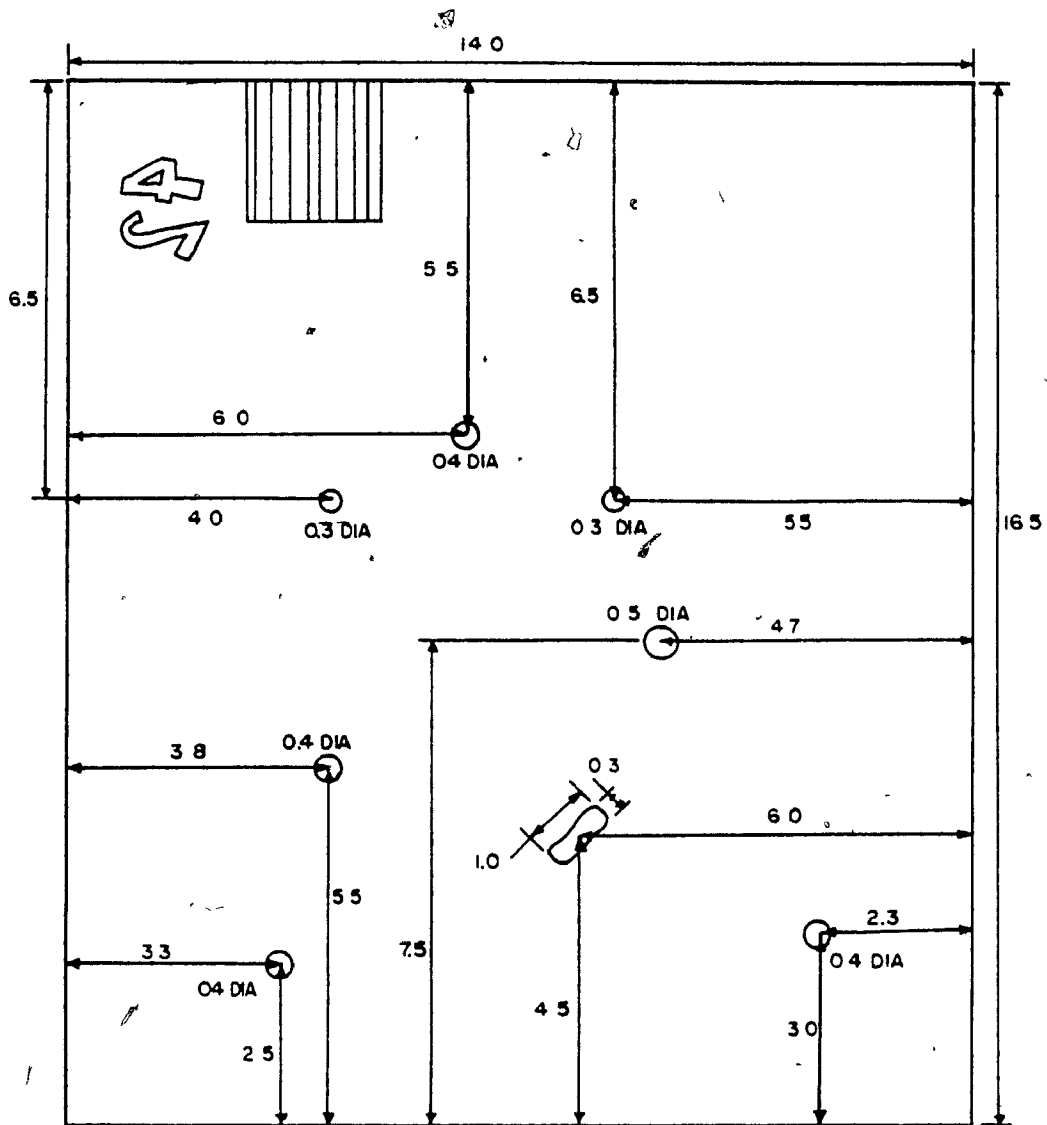
BLOCK 42 X-RAY DIR I

BLOCK 42 X-RAY DIR 2
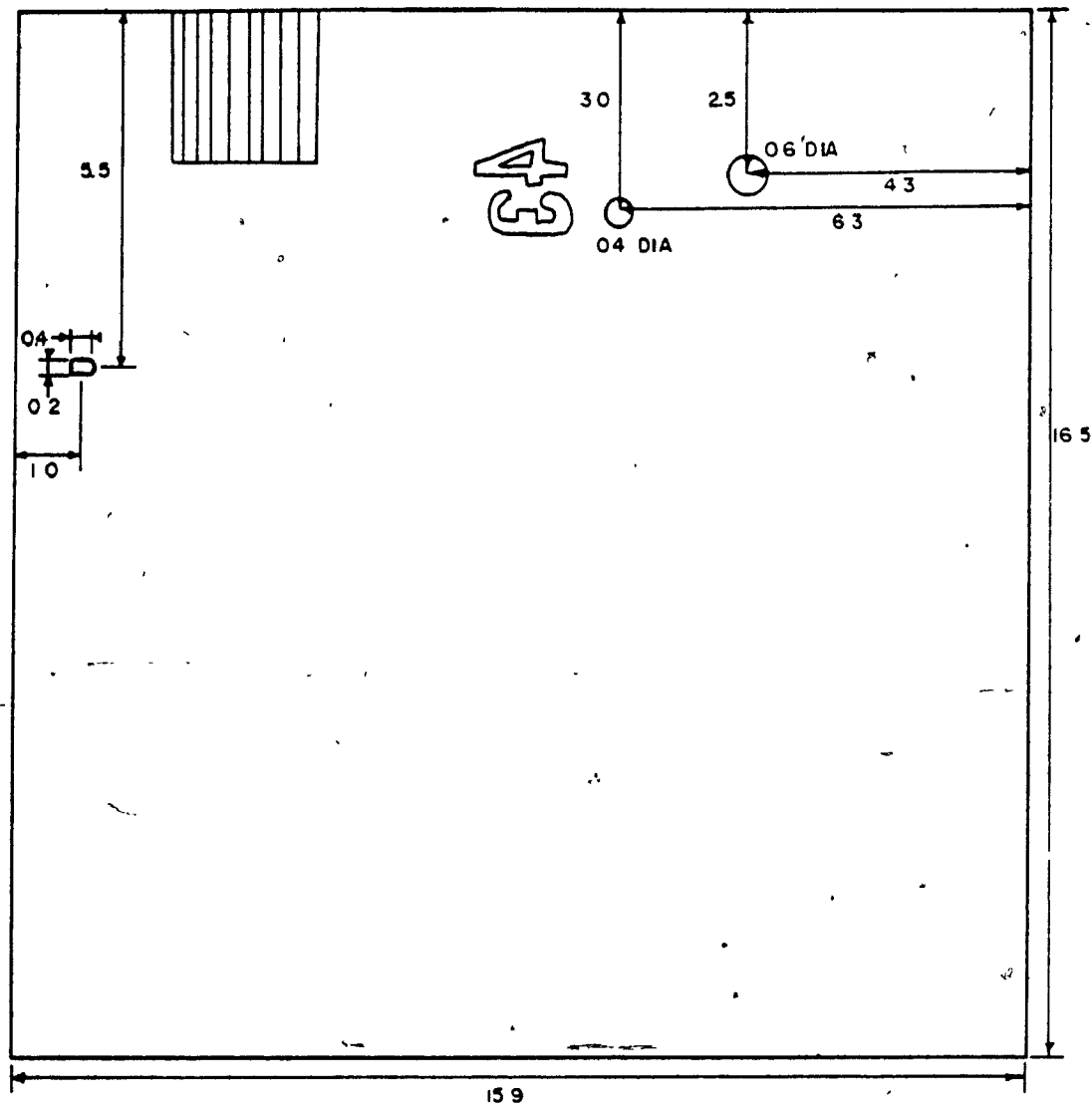
BLOCK 43 (X-RAY DIR 2

BLOCK 44 X-RAY DIR 2

288
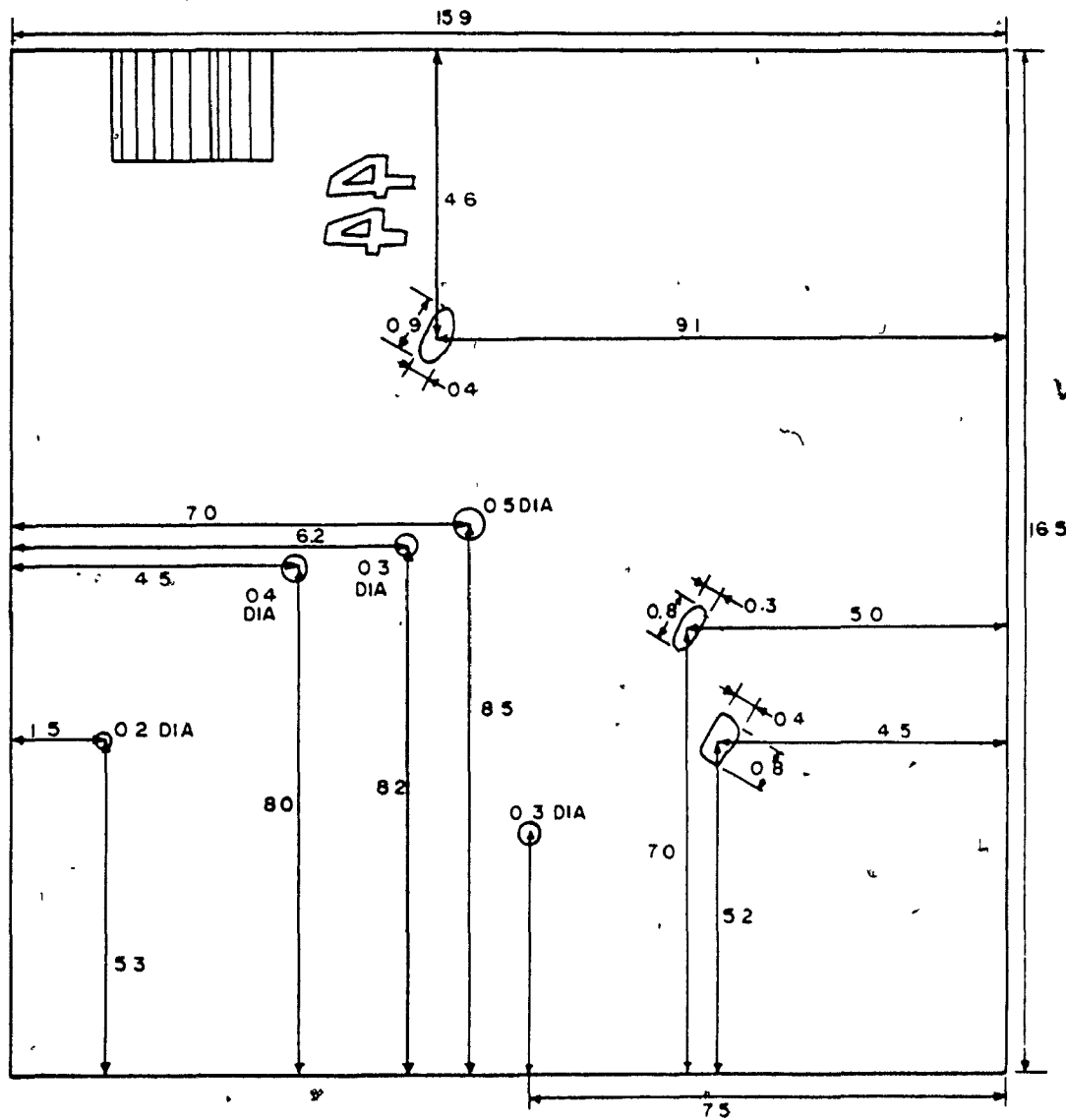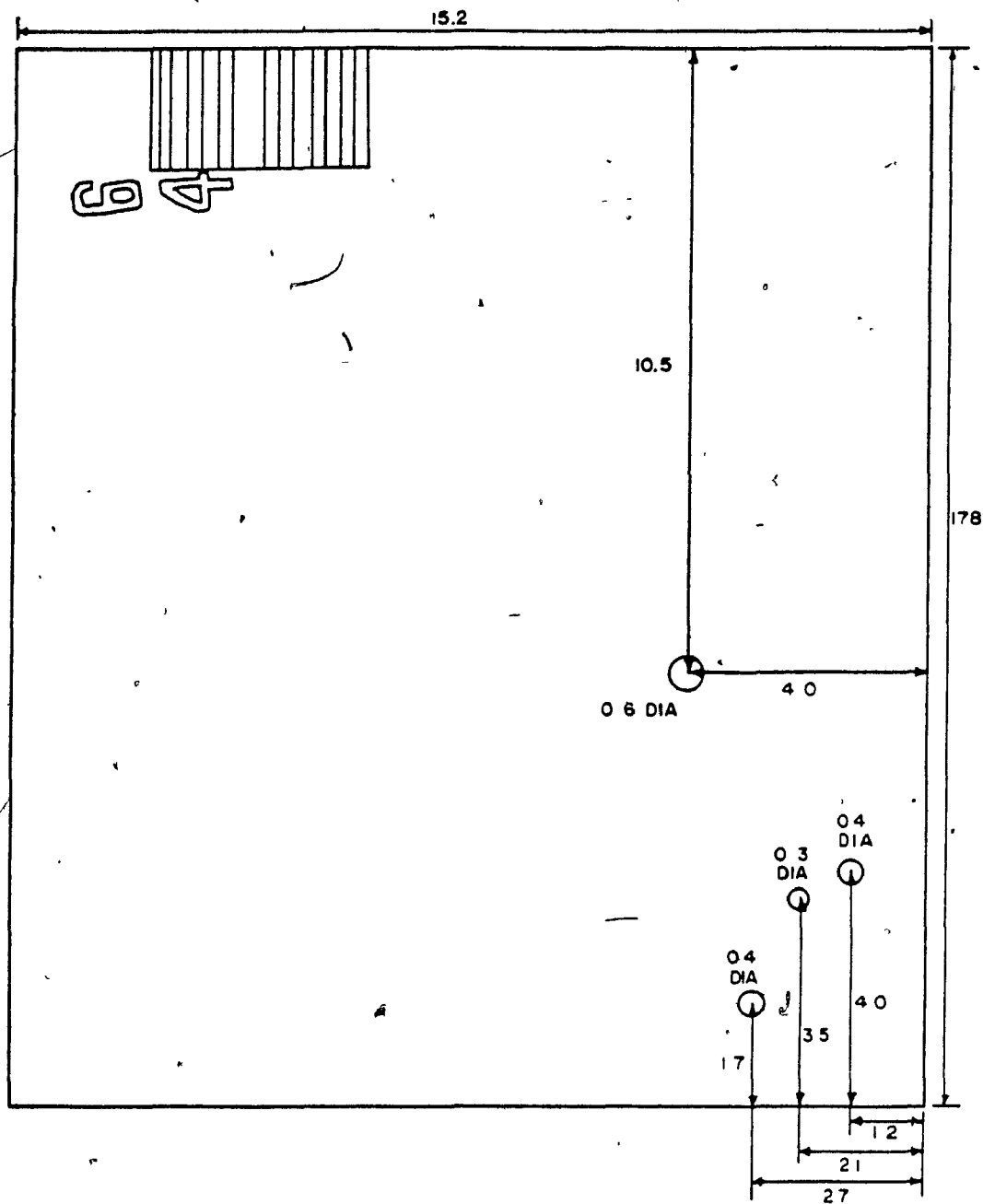
BLOCK 64

APPENDIX G

ULTRASONIC INSPECTION RESULTS

a   b

47

34 D
50% DAC

43

140

30% DAC
36 D

15
6

140

d   c

ALL DIMENSIONS IN CM
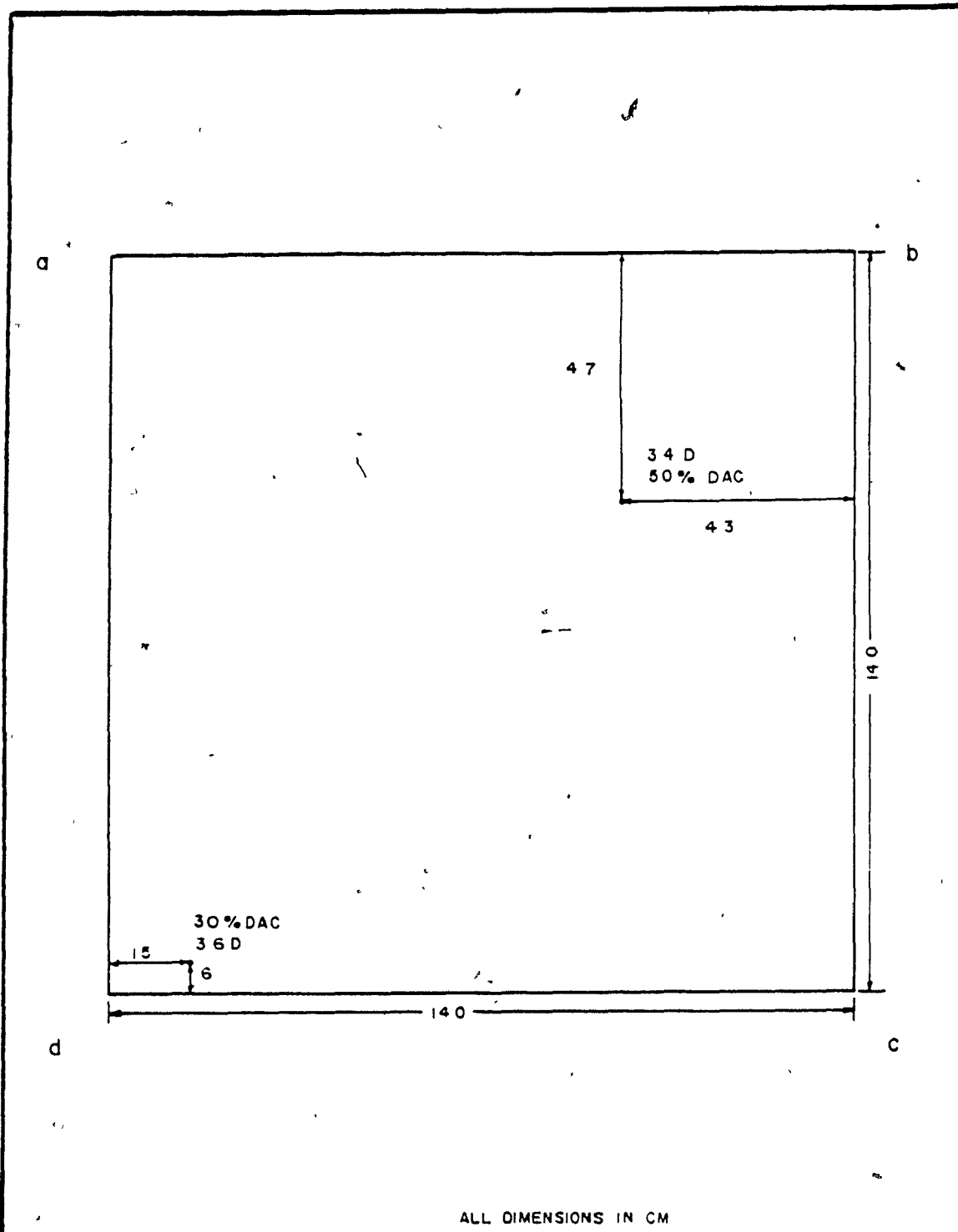
| BLOCK NO. 12 | FACE A | DATE SEPT 12, 1985 |

INSPECTION TECHNIQUE   ASTM A 609-83 (⅛"∅ FLAT BOTTOM HOLE)

INSPECTION FIRM   CRAWFORD McLEISH NDE INC

TECHNICIAN M ESKAMEL   DRAWN BY A KENDRICK

291

ALL DIMENSIONS IN CM
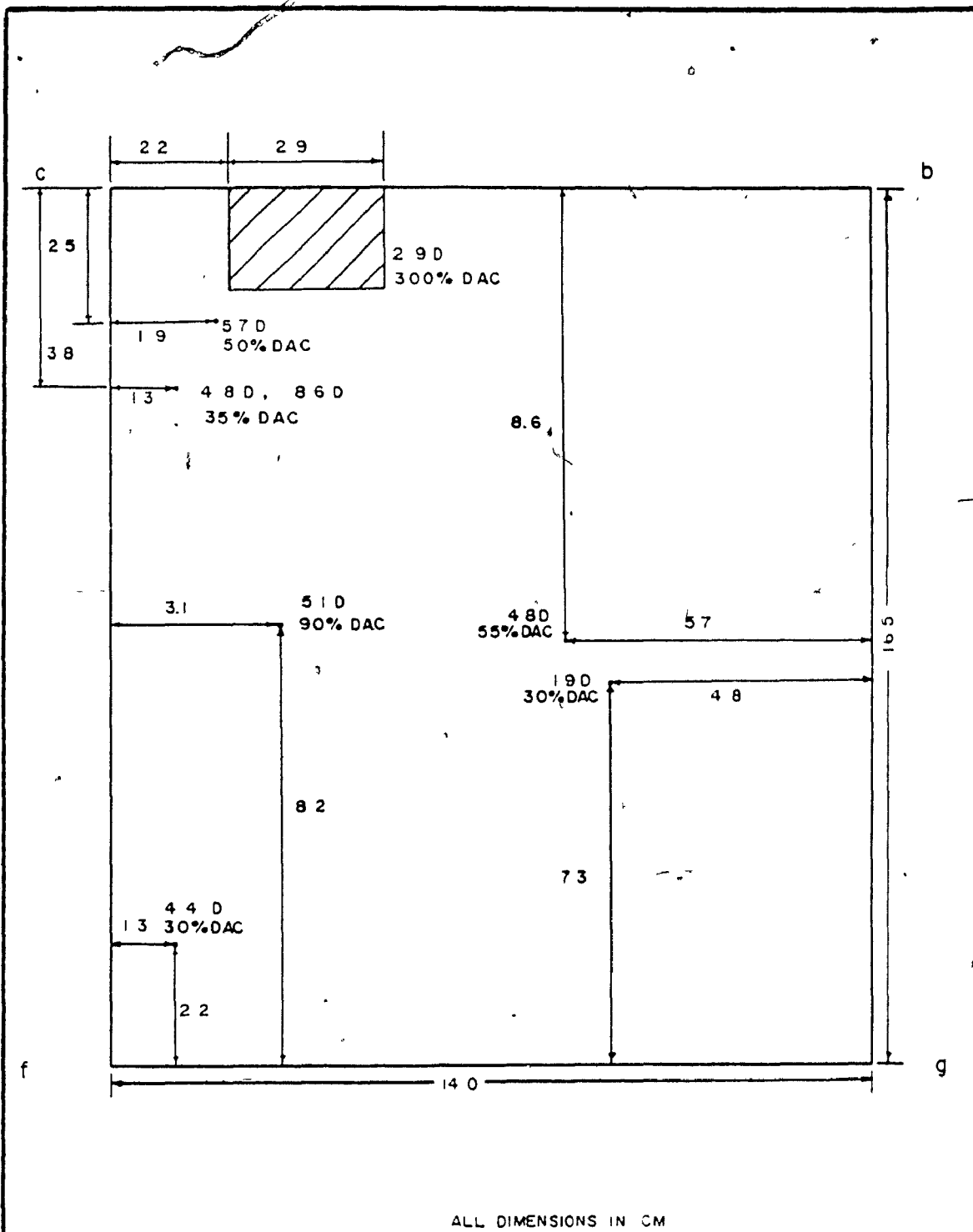
| BLOCK NO 12 | FACE B | DATE SEPT 12, 1985 |

INSPECTION TECHNIQUE ASTM A 609-83 (⅛"∅ FLAT BOTTOM HOLE)

INSPECTION FIRM CRAWFORD McLEISH NDE INC

TECHNICIAN M ESKAMEL DRAWN BY A KENDRICK

292

ALL DIMENSIONS IN CM

BLOCK NO. 12	FACE C	DATE SEPT. 12, 1985
INSPECTION TECHNIQUE ASTM A 609-83 (⅛"∅ FLAT BOTTOM HOLE)		
INSPECTION FIRM CRAWFORD McLEISH NDE INC		
TECHNICIAN M ESKAMEL DRAWN BY A KENDRICK		

a   b

51   48

14 6 D   14 6 D
150%DAC   100% DAC

3.8   3 5

                    RUNNING   INDICATION
                    BETWEEN HOLES
                    100-150 % DAC

                                                              14 0

              14.6 D
              220 % DAC

4 8

41

d   140   c

ALL DIMENSIONS IN CM

BLOCK NO. 13	FACE A	DATE SEPT -12, 1985

INSPECTION   TECHNIQUE   ASTM A 609-83 (⅛"ø FLAT BOTTOM HOLE)

INSPECTION   FIRM   CRAWFORD McLEISH NDE   INC

TECHNICIAN M ESKAMEL   DRAWN BY   A KENDRICK

294

29   22

c   b

16

2 5 D
100% DAC

165

4 4D 100 % DAC,
8 9 D 50 % DAC
4 4

8 9 D
160 % DAC

41

1 3   1 3

f   14 0   g

RUNNING INDICATIONS

ALL DIMENSIONS IN CM

BLOCK NO. 13	FACE B	DATE SEPT 12, 1985
INSPECTION TECHNIQUE ASTM A 609-83 (⅛"⌀ FLAT BOTTOM HOLE)		
INSPECTION FIRM CRAWFORD McLEISH NDE INC		
TECHNICIAN M ESKAMEL DRAWN BY A KENDRICK		

19   25

13

2.90
220% DAC

165

4 I D
65% DAC

9 5 D
200% DAC

51   51

I 3   I 3

d   c

e   14 0   f

RUNNING INDICATIONS

ALL DIMENSIONS IN CM

BLOCK NO. 13	FACE C	DATE SEPT 12, 1985

INSPECTION TECHNIQUE   ASTM A 609-83 (⅛"ø FLAT BOTTOM HOLE)

INSPECTION FIRM   CRAWFORD McLEISH NDE INC

TECHNICIAN M ESKAMEL   DRAWN BY A KENDRICK

a   b

140

d   140   c

NO   DEFECTS   INDICATED

ALL DIMENSIONS IN CM

BLOCK NO. 14	FACE A	DATE SEPT. 12, 1985
INSPECTION TECHNIQUE ASTM A 609-83 (⅛"ø FLAT BOTTOM HOLE)		
INSPECTION FIRM CRAWFORD McLEISH NDE INC		
TECHNICIAN M ESKAMEL DRAWN BY A KENDRICK		

297

c   b

2.5 D
200% DAC.

19

16

31

165

140

f   g

ALL DIMENSIONS IN CM

BLOCK NO. 14   FACE B   DATE SEPT. 12, 1985

INSPECTION TECHNIQUE   ASTM A 609-83 (⅛"ø FLAT BOTTOM HOLE)

INSPECTION FIRM CRAWFORD McLEISH NDE INC

TECHNICIAN M ESKAMEL   DRAWN BY A KENDRICK

298

d   c

| 19 | 19 |

13

3 5 D
100% DAG

165

31 D
130% DAC

44

60

e   f

140

ALL DIMENSIONS IN CM

| BLOCK NO. 14 | FACE C | DATE SEPT 12, 1985 |

INSPECTION TECHNIQUE ASTM A 609-83 ($\frac{1}{8}$"ø FLAT BOTTOM HOLE)

INSPECTION FIRM CRAWFORD McLEISH NDE INC

TECHNICIAN M. ESKAMEL   DRAWN BY A KENDRICK
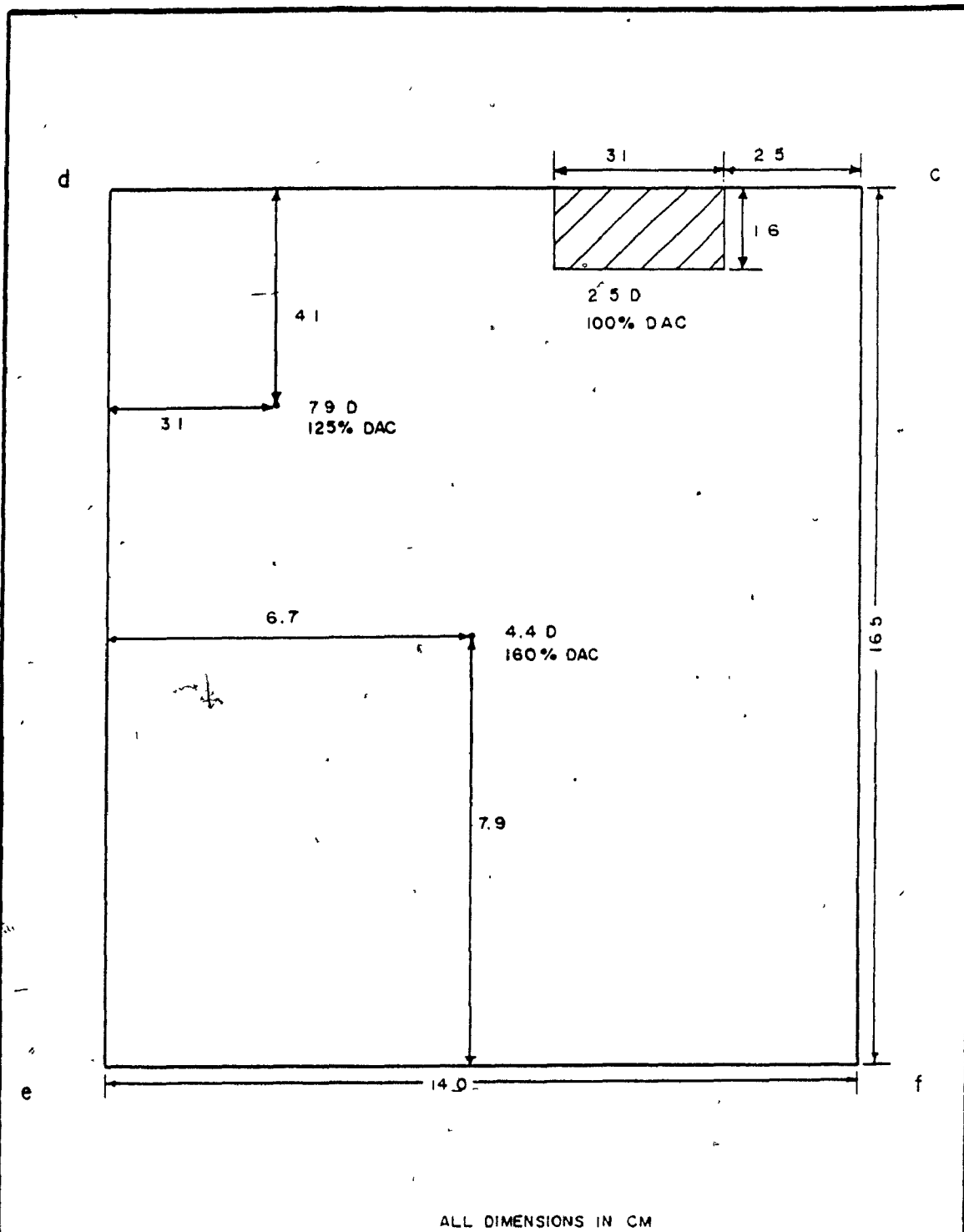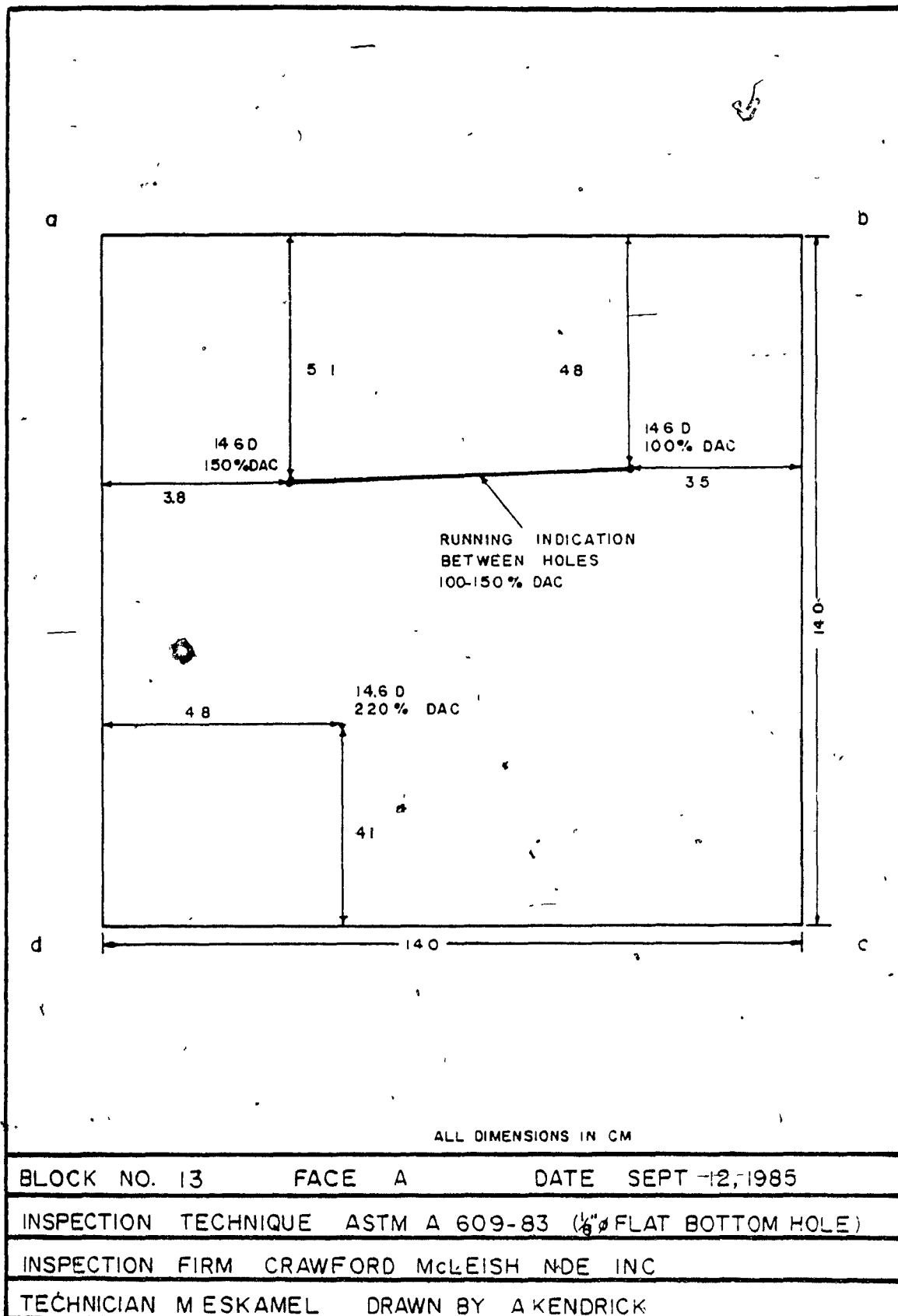
299

ALL DIMENSIONS IN CM

| BLOCK NO. 21 | FACE A | DATE SEPT 12, 1985 |

INSPECTION TECHNIQUE ASTM A 609-83 (⅛"⌀ FLAT BOTTOM HOLE)

INSPECTION FIRM CRAWFORD McLEISH NDE. INC

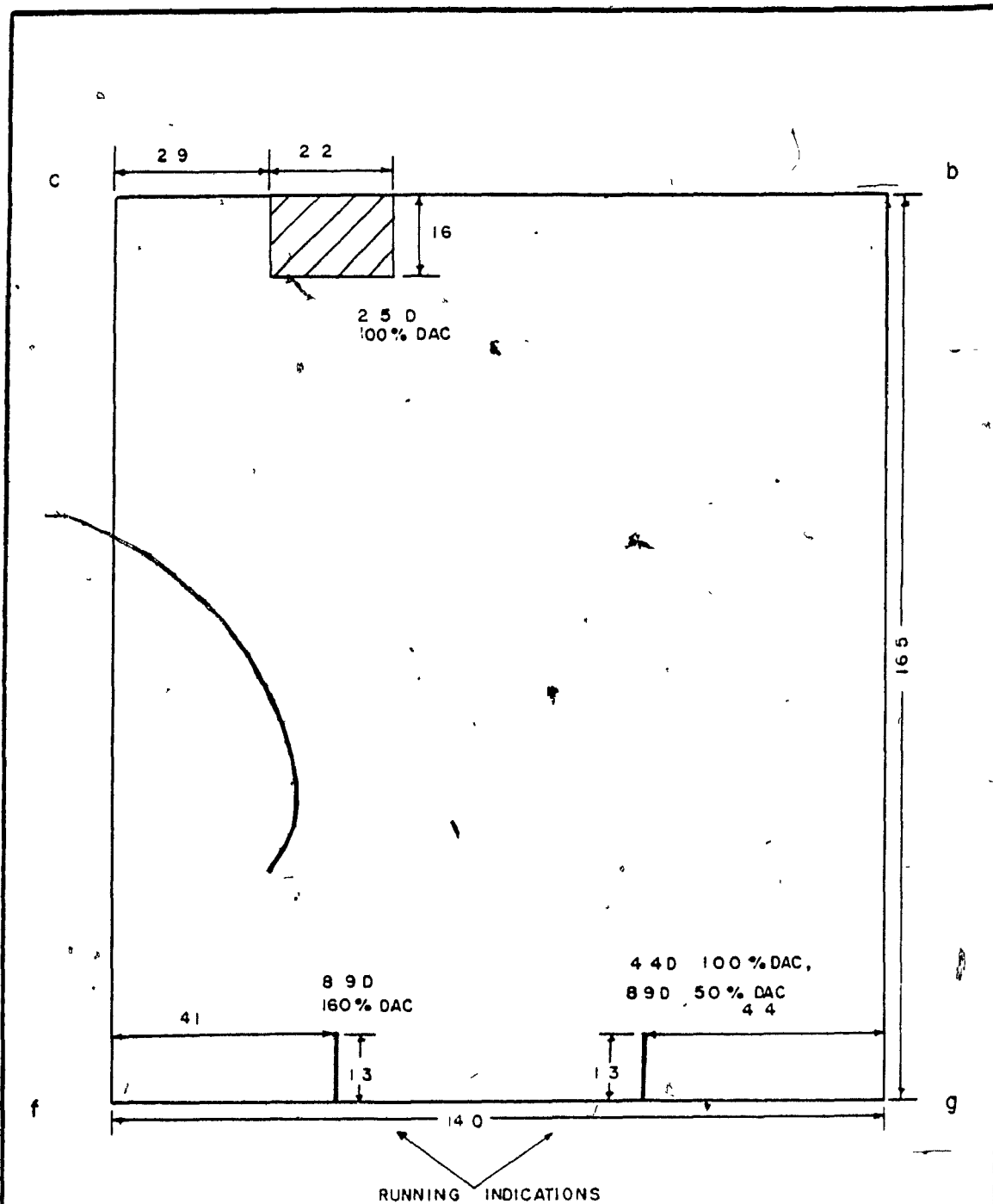TECHNICIAN M ESKAMEL DRAWN BY A KENDRICK

c   b

165

f |————————————— 15 9 ——————————————| g

NO DEFECTS INDICATED

ALL DIMENSIONS IN CM

BLOCK NO. 21	FACE B	DATE SEPT. 12, 1985
INSPECTION TECHNIQUE ASTM A 609-83 (⅛"ø FLAT BOTTOM HOLE)		
INSPECTION FIRM CRAWFORD McLEISH NDE. INC		
TECHNICIAN M ESK AMEL DRAWN BY A KENDRICK		

301

89

82

d   c

16

41

5 7D
40%
DAC

63

8.9

44D
40% DAC

86

48 D
150% DAC

41

41

2.2D
40% DAC

7 0 D
50 % DAC   6 0

165

3 5

3.8D
60% DAC

2 9 D
45%
DAC

73

13

2 2D
35% DAC

5.4 D
45%
DAC

44

3.8D
125%
DAC

25

6 0

6 3

67

41

35

e   15 9   f

ALL DIMENSIONS IN CM

BLOCK NO. 21	FACE C	DATE SEPT 12, 1985
INSPECTION TECHNIQUE ASTM A 609-83 (⅛" ∅ FLAT BOTTOM HOLE)		
INSPECTION FIRM CRAWFORD McLEISH NDE INC		
TECHNICIAN M ESKAMEL DRAWN BY A KENDRICK		

302

a   57   b

1.6

41 D
35% DAC

3 8

6 0

6 7

3 8 D   3.5
30% DAC

6 3

1.6   4 4 D
30% DAC

2 5 D   4 4
30% DAC

7.0   31 D
30% DAC

140

140

d   c

ALL DIMENSIONS IN CM

BLOCK NO. 2 2	FACE A	DATE SEPT. 12, 1985

INSPECTION TECHNIQUE   ASTM .A 609-83 (⅛"ø FLAT BOTTOM HOLE)

INSPECTION FIRM   CRAWFORD McLEISH NDE INC
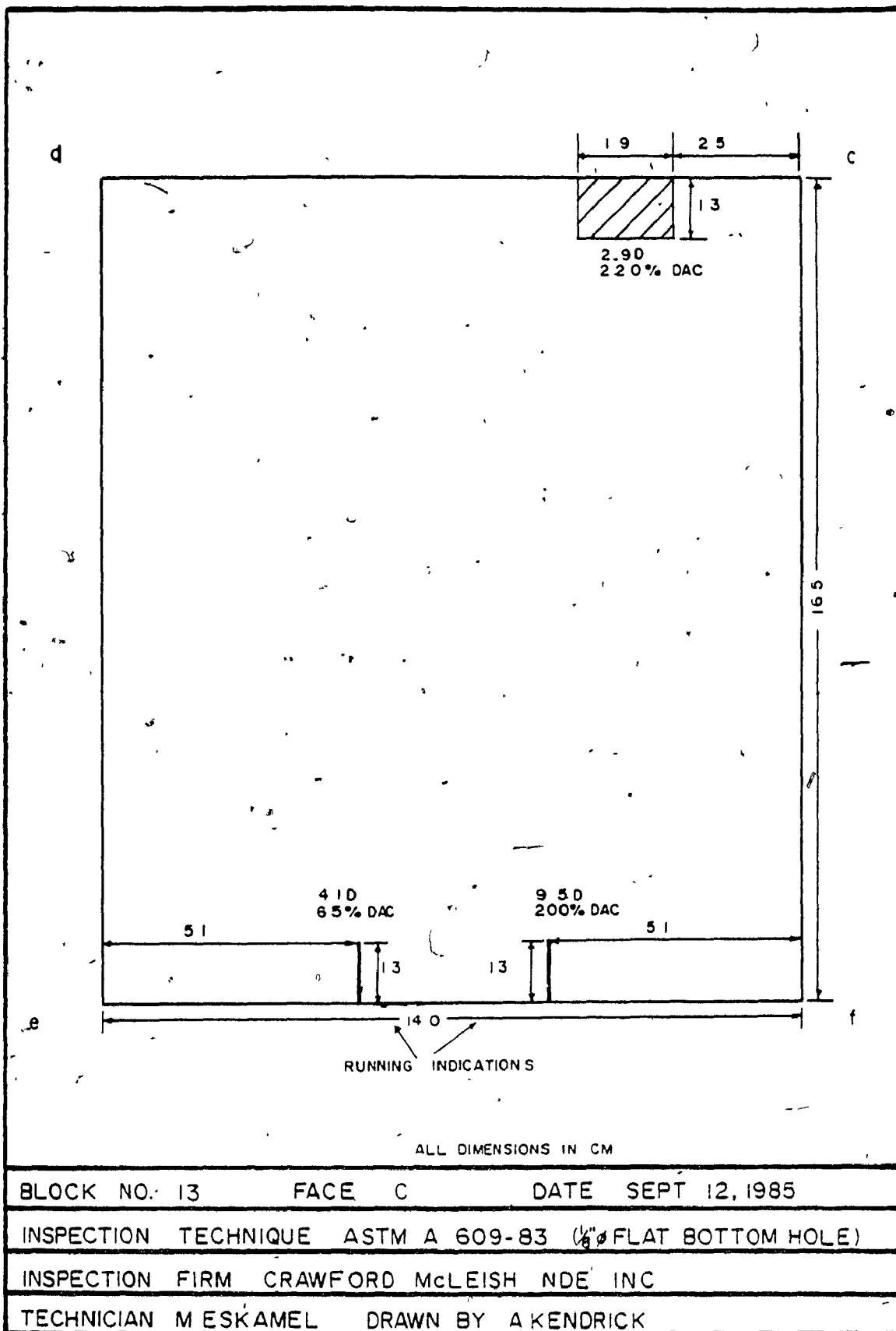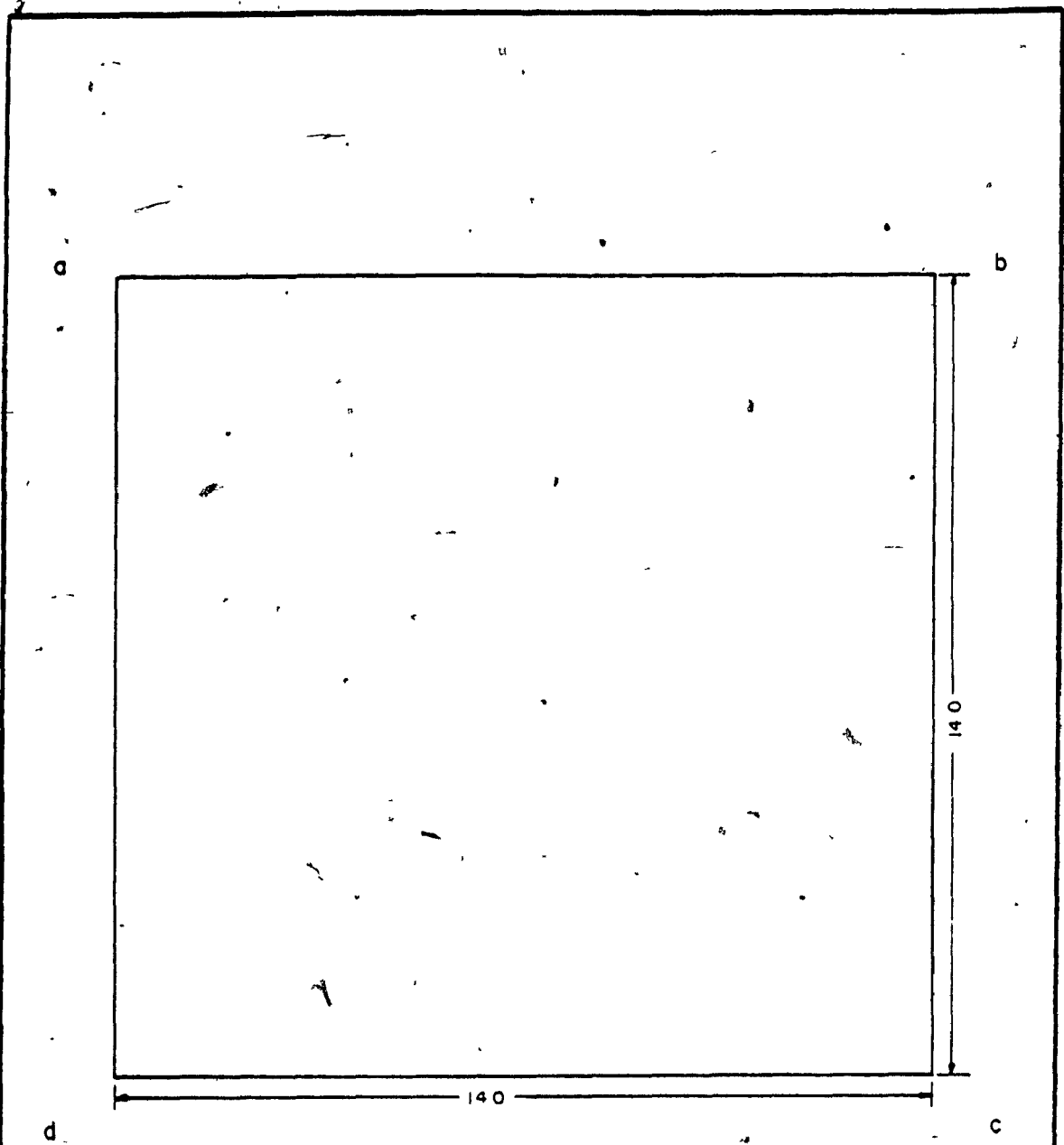
TECHNICIAN M ESKAMEL   DRAWN BY A KENDRICK

ALL DIMENSIONS IN CM

| BLOCK NO. 22 | FACE B | DATE SEPT 12, 985 |

INSPECTION TECHNIQUE ASTM A 609-83 (⅛"∅ FLAT BOTTOM HOLE)

INSPECTION FIRM CRAWFORD McLEISH NDE INC

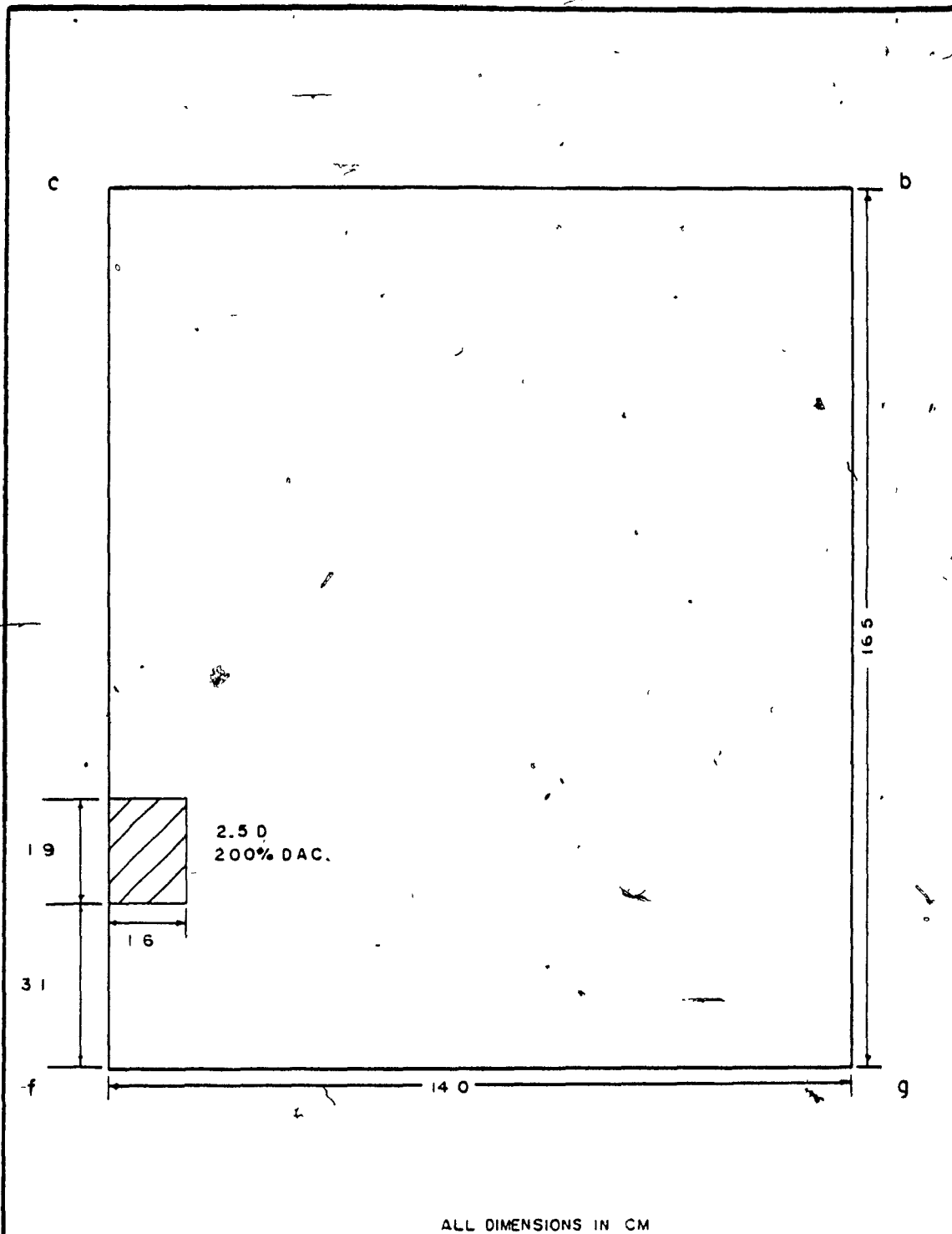TECHNICIAN M ESKAMEL DRAWN BY A KENDRICK

ALL DIMENSIONS IN CM
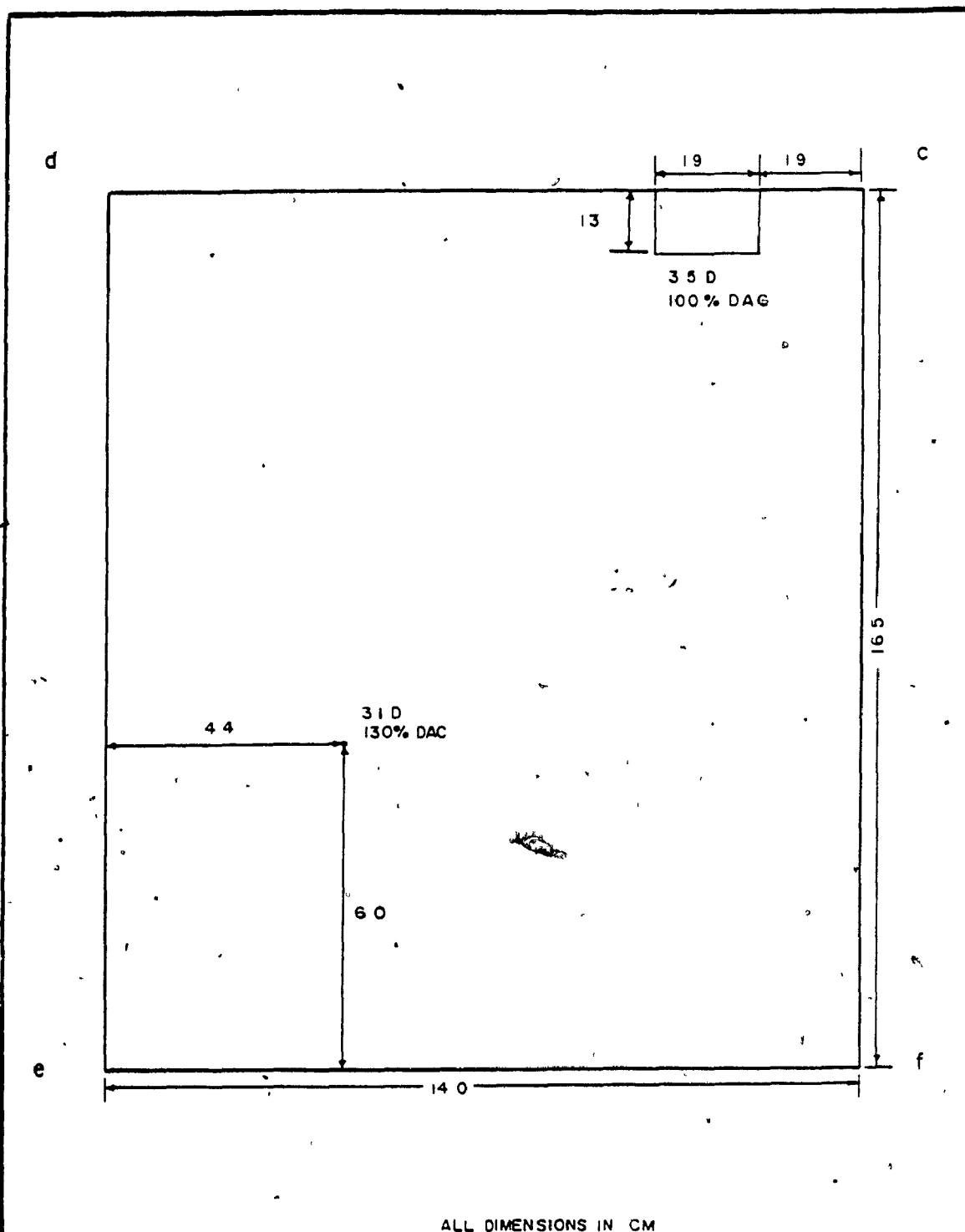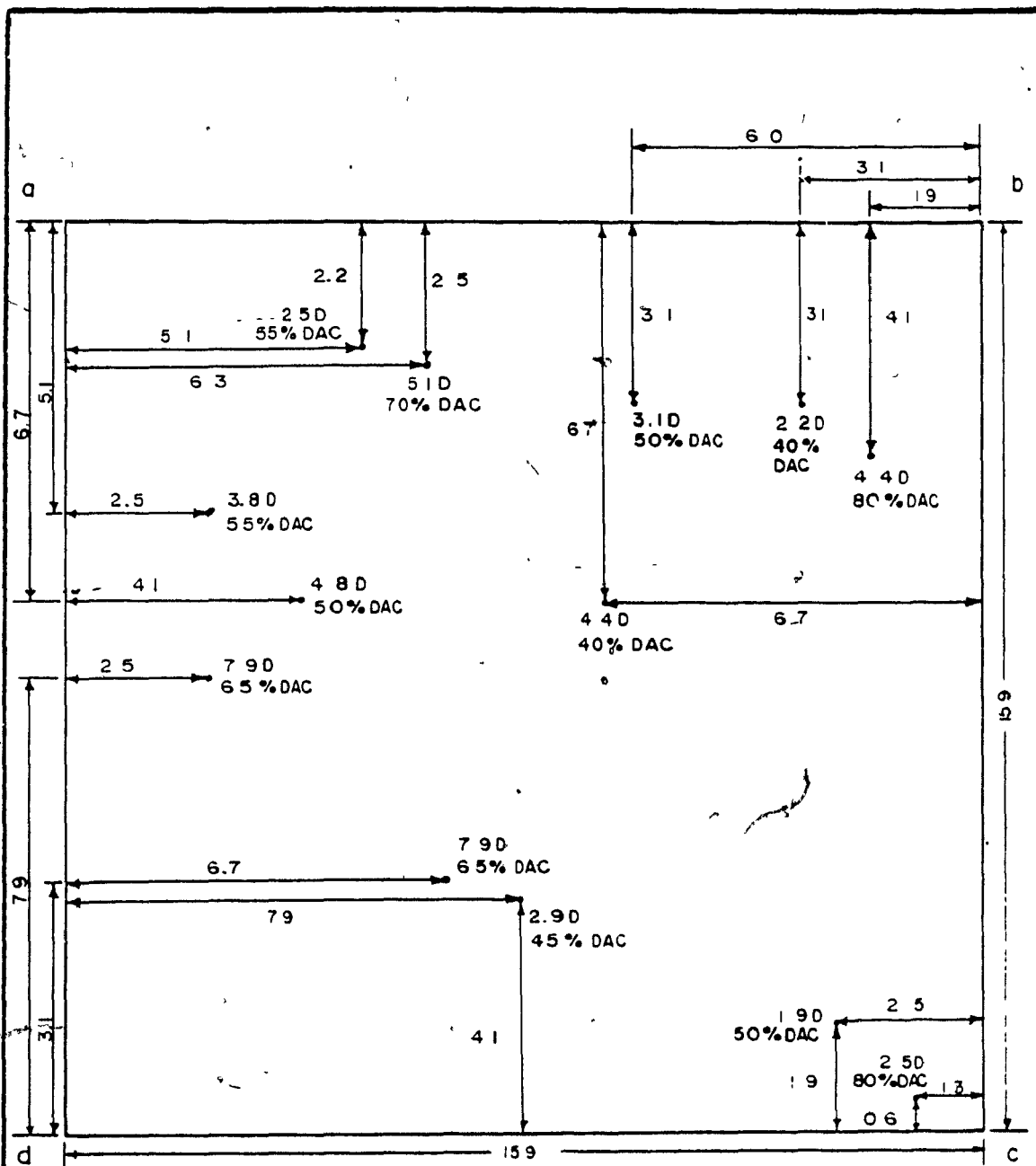
BLOCK NO. 22	FACE C	DATE SEPT 12, 1985

INSPECTION TECHNIQUE ASTM A 609-83 (⅛"ø FLAT BOTTOM HOLE)

INSPECTION FIRM CRAWFORD McLEISH NDE INC

TECHNICIAN M ESKAMEL DRAWN BY A KENDRICK

305

DRILLED IDENTIFICATION NUMBER

FACE B

FACE C

FACE A

BLOCK 23

c d

b a

f

g h

DRILLED IDENTIFICATION HOLES

FACE B

FACE A

FACE C

FACE D

BLOCK 23L

FACE E

c d

b a

f

g

h

e

n

m

k l

j i

IDENTIFICATION AND ORIENTATION OF THE FACES OF BLOCKS 23 &
23L FOR THE ULTRASONIC PULSE-ECHO, STRAIGHT-BEAM INSPECTION
(A-SCAN)   DRAWN BY· A. KENDRICK   DATE· SEPT. 6, 1985

a   b

1 6

6 3   5 I D
35% DAC

5.0

3.5

5 I D
35% DAC   5 4

1.0

7.5

4 4 D
150% DAC

7 6   3 8 D
120% DAC

7.9

8.2   2.9 D
150% DAC

5.4

16 3

16.4

d   c

ALL DIMENSIONS IN CM

| BLOCK NO. 23 | FACE A | DATE SEPT. 12, 1985 |

INSPECTION TECHNIQUE   ASTM A 609-83 (⅛"ø FLAT BOTTOM HOLE)

INSPECTION FIRM   CRAWFORD McLEISH NDE INC

TECHNICIAN M ESKAMEL   DRAWN BY A KENDRICK

51

→ | 1 0 |←

2 9 D
65 % DAC | ← 1 3

1 2 2

5 4 D   1 3 0 % DAC

57

1. 0 LONG

2 9

16. 3

c   b

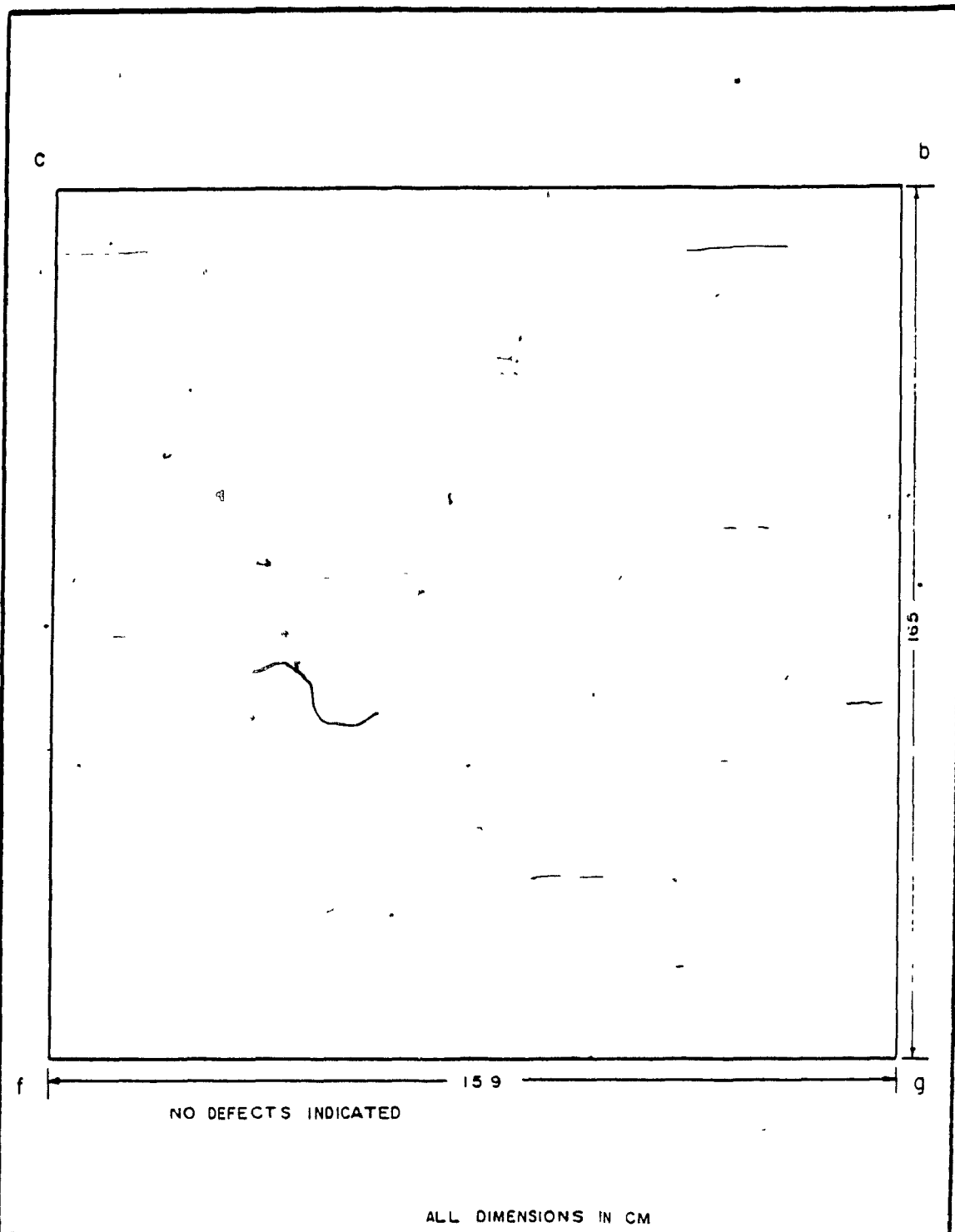f   g

ALL DIMENSIONS IN CM

BLOCK NO. 2 3   FACE B   DATE SEPT 12, 1985

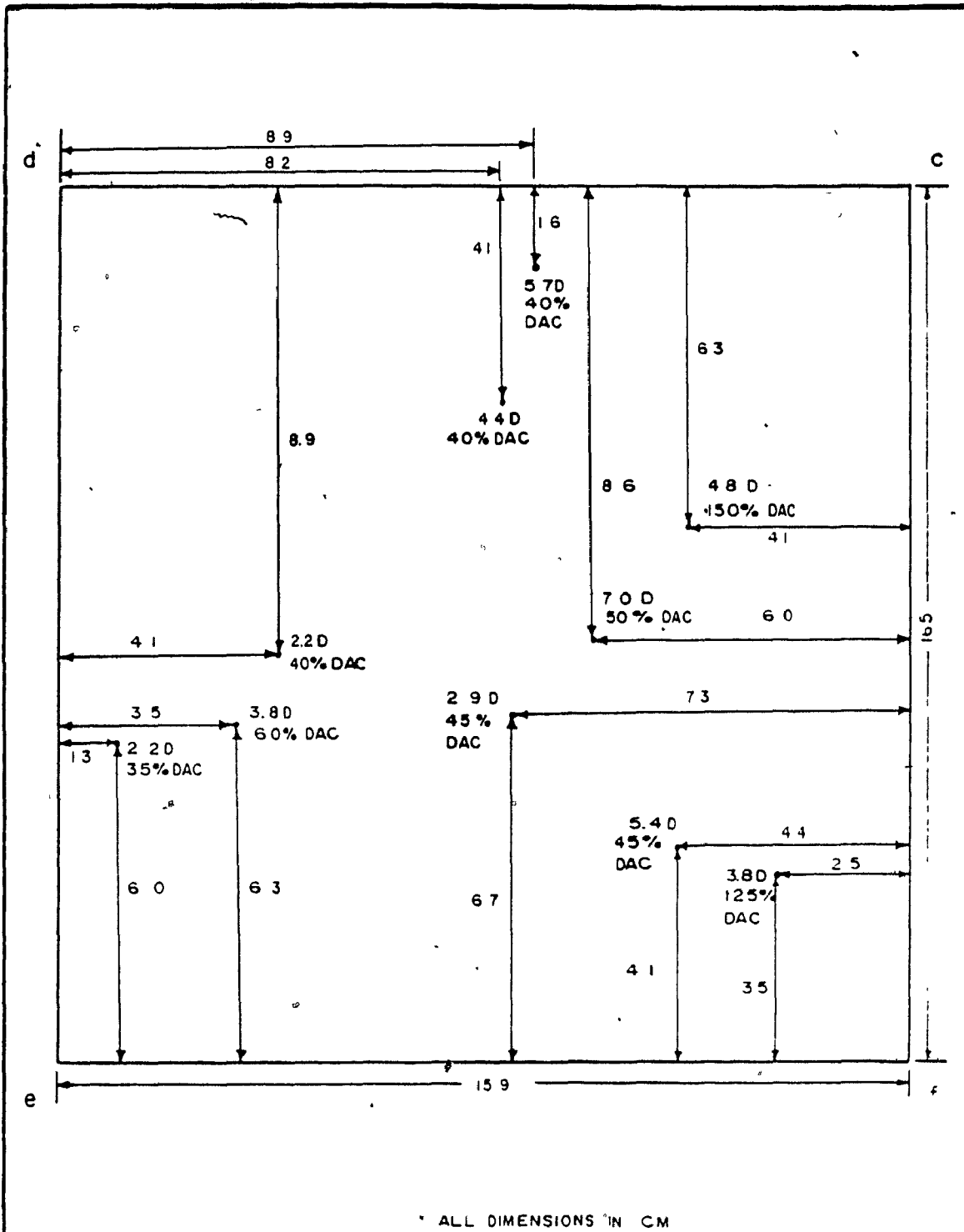INSPECTION TECHNIQUE ASTM A 609-83 (1/8"∅ FLAT BOTTOM HOLE)

INSPECTION FIRM CRAWFORD McLEISH NDE INC

TECHNICIAN M ESKAMEL   DRAWN BY A KENDRICK

308

d   c

|‹———————————————— 16 4 ————————————————›| 122

NO DEFECTS INDICATED

e   f

ALL DIMENSIONS IN CM.

BLOCK NO. 23   FACE C   DATE SEPT. 12, 1985

INSPECTION TECHNIQUE   ASTM A 609-83 (⅛"∅ FLAT BOTTOM HOLE)

INSPECTION FIRM   CRAWFORD McLEISH NDE INC
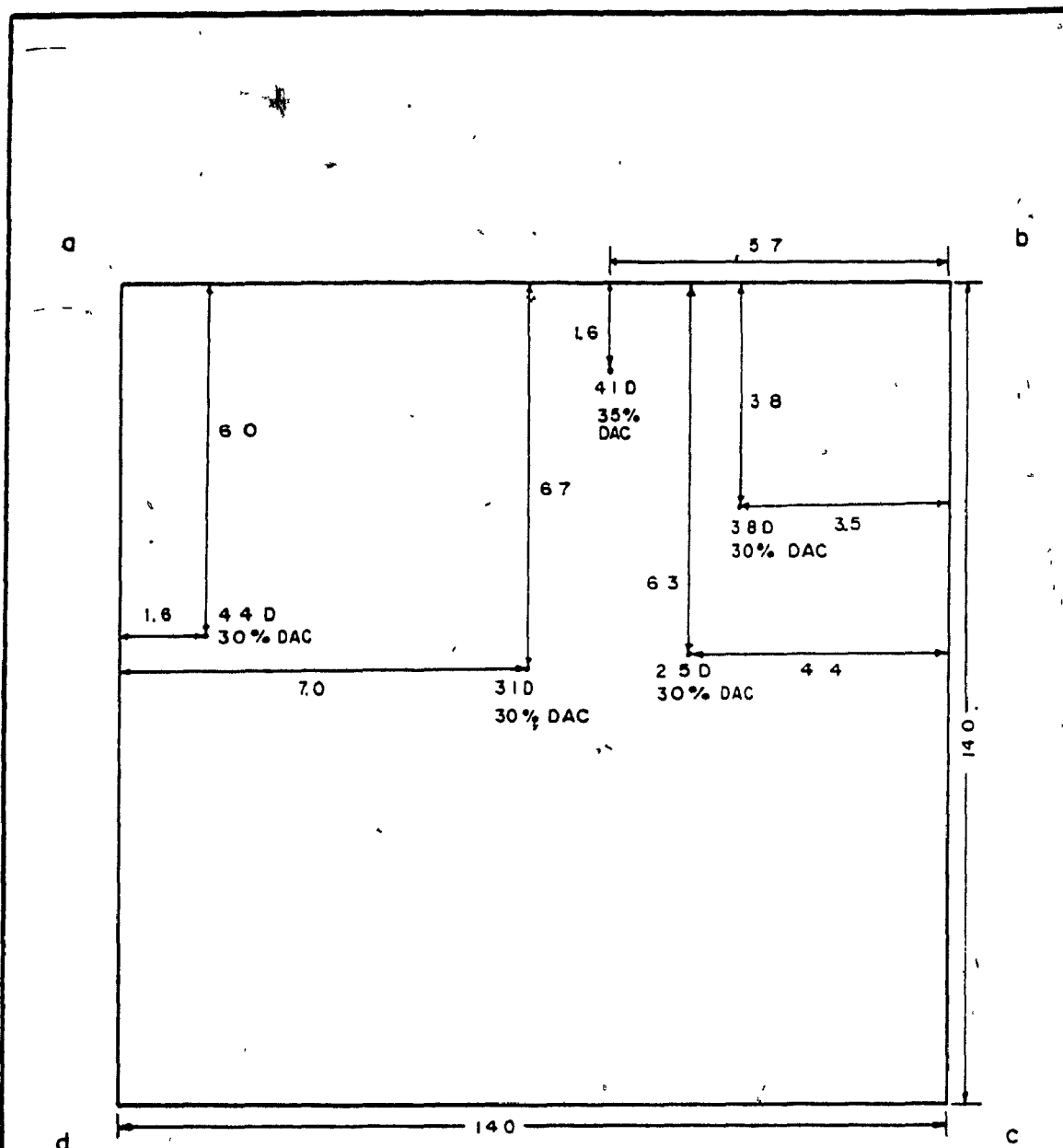
TECHNICIAN M ESKAMEL   DRAWN BY A KENDRICK

309

c | d

1.6

6.0 D
90%DAC

8 8

4.4

5.7

8.6 D
75% DAC

1 9 D
40%
DAC

1 9

15 8

4 4

6.3 D
60%DAC

9 5

7.0

5.1 D
75% DAC

1 9

0 9

15 8

b | a

ALL DIMENSIONS N CM

| BLOCK NO. 23L | FACE A | DATE SEPT 12, 1985 |

INSPECTION TECHNIQUE ASTM A 609-83 (⅛"ø FLAT BOTTOM HOLE)
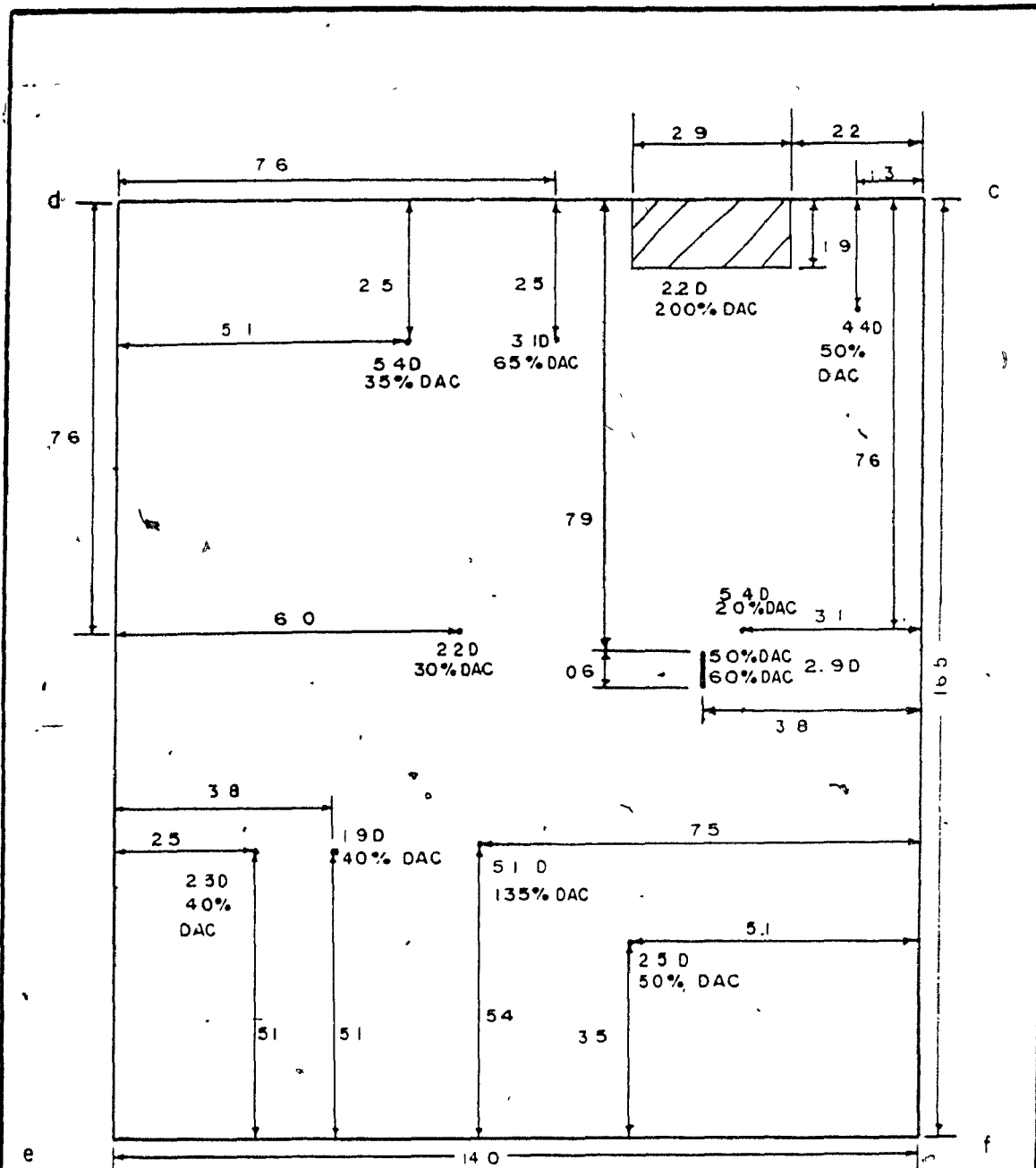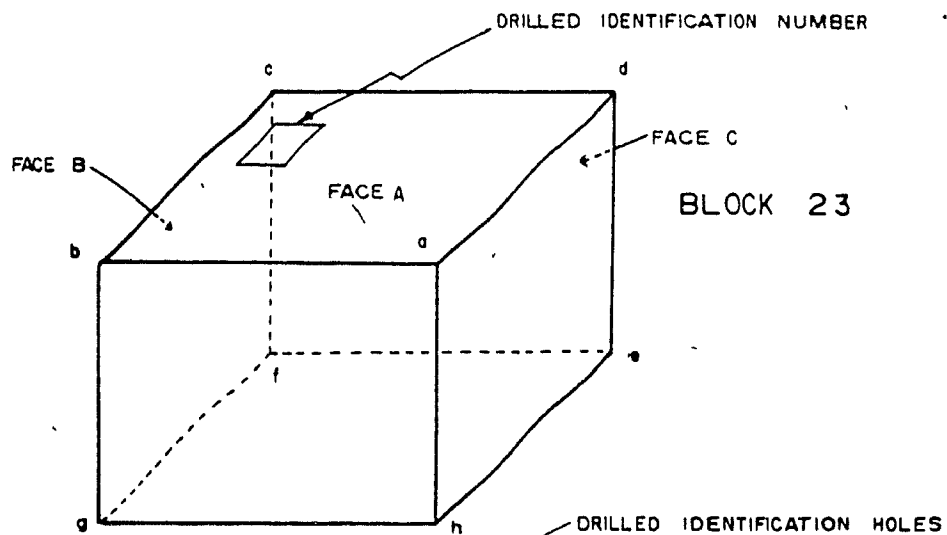
INSPECTION FIRM CRAWFORD McLEISH NDE INC

TECHNICIAN M ESKAMEL DRAWN BY A KENDRICK

310

d   c

15.8

7.0

6.3   6.3   9.2

12.6

5.4   3.8 D
55% DAC

1.6 D
50% DAC

e

1 3 D 60% DAC
4 4 D 55% DAC

2 9

75°

f

ALL DIMENSIONS IN CM

BLOCK NO. 23L	FACE C	DATE SEPT. 12, 1985

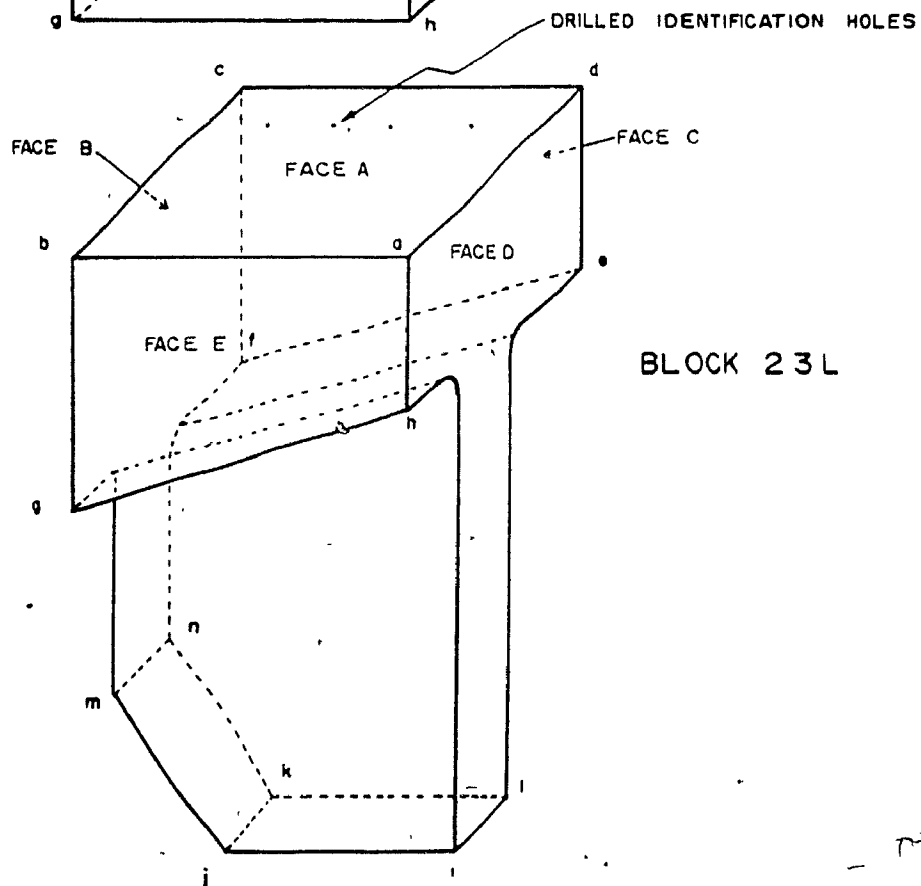INSPECTION TECHNIQUE ASTM A 609-83 (⅛"ø FLAT BOTTOM HOLE)

INSPECTION FIRM CRAWFORD McLEISH NDE. INC

TECHNICIAN M ESKAMEL   DRAWN BY A KENDRICK
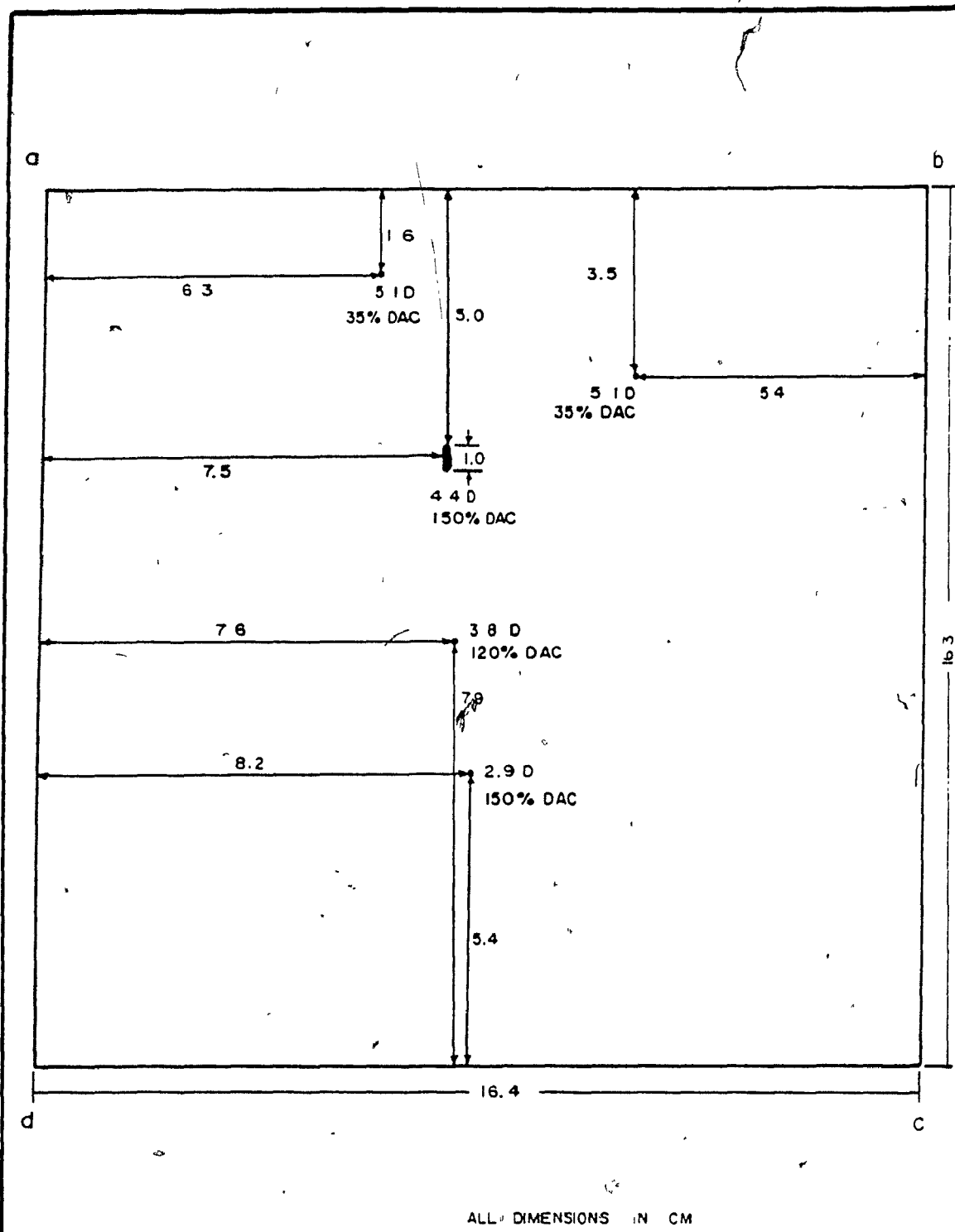
311

15 8

5 7

a · · · · d

2.2 · 0 7

1 3 · 2 5D · 3 · 1 3
90%DAC

3 1

4 4D · 38D
70%DAC · 50% · 2.5D
DAC · 30%DAC

7 2

51

7.4 · 1.90 · 6 0 · 7.2
35% DAC · 2.9D · 8.4
45%DAC

3 8

4 8 · 2.9D
50% DAC

3 3

h · · · · e

5 8

1.3 · 6.3 D
65%DAC

21.9

14.1

i · l

5 6
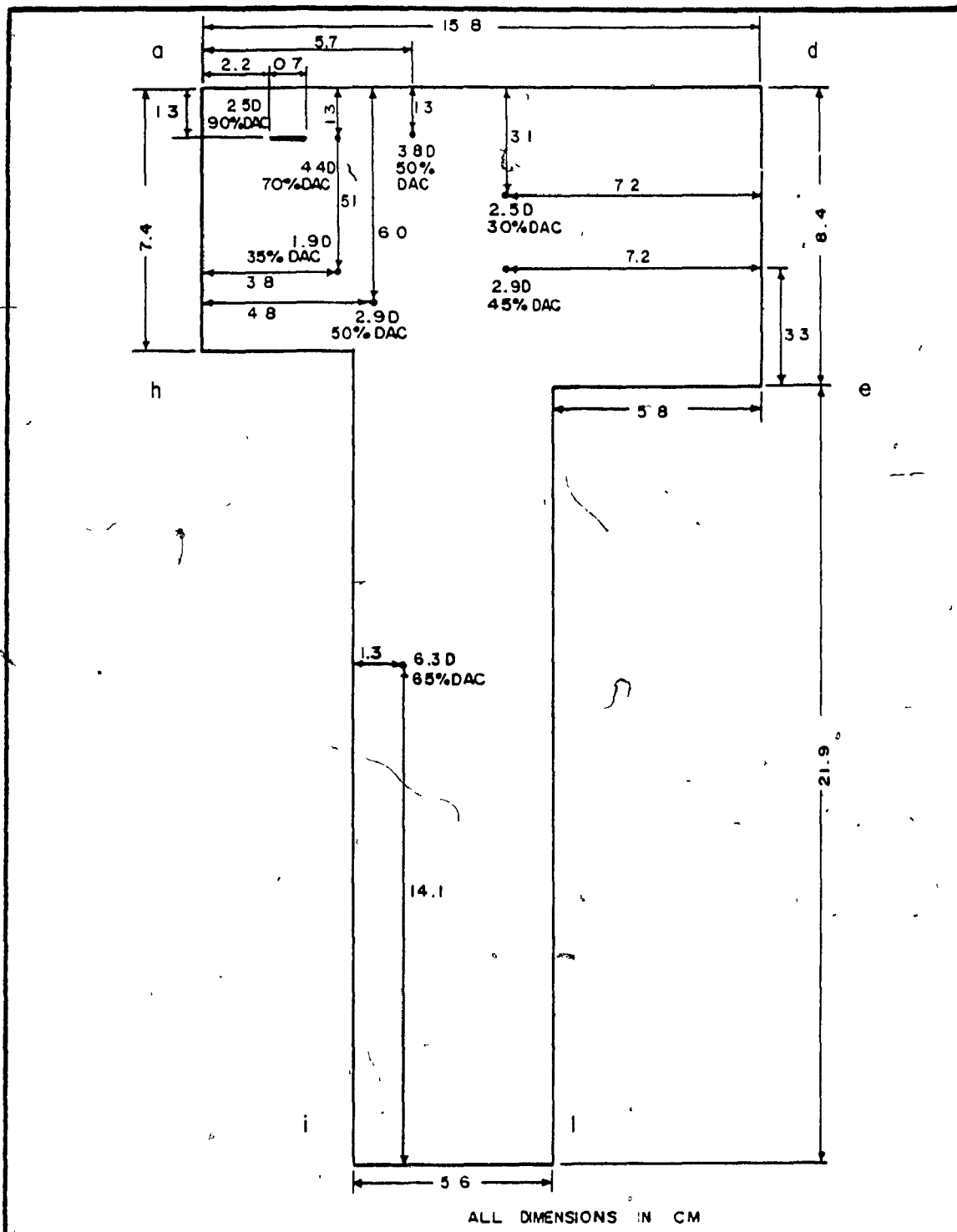
ALL DIMENSIONS IN CM

BLOCK NO. 23L	FACE D	DATE SEPT 12, 1985

INSPECTION TECHNIQUE ASTM A 609-83 (⅛"ø FLAT BOTTOM HOLE)

INSPECTION FIRM CRAWFORD McLEISH NDE INC

TECHNICIAN M. ESKAMEL DRAWN BY A KENDRICK

312
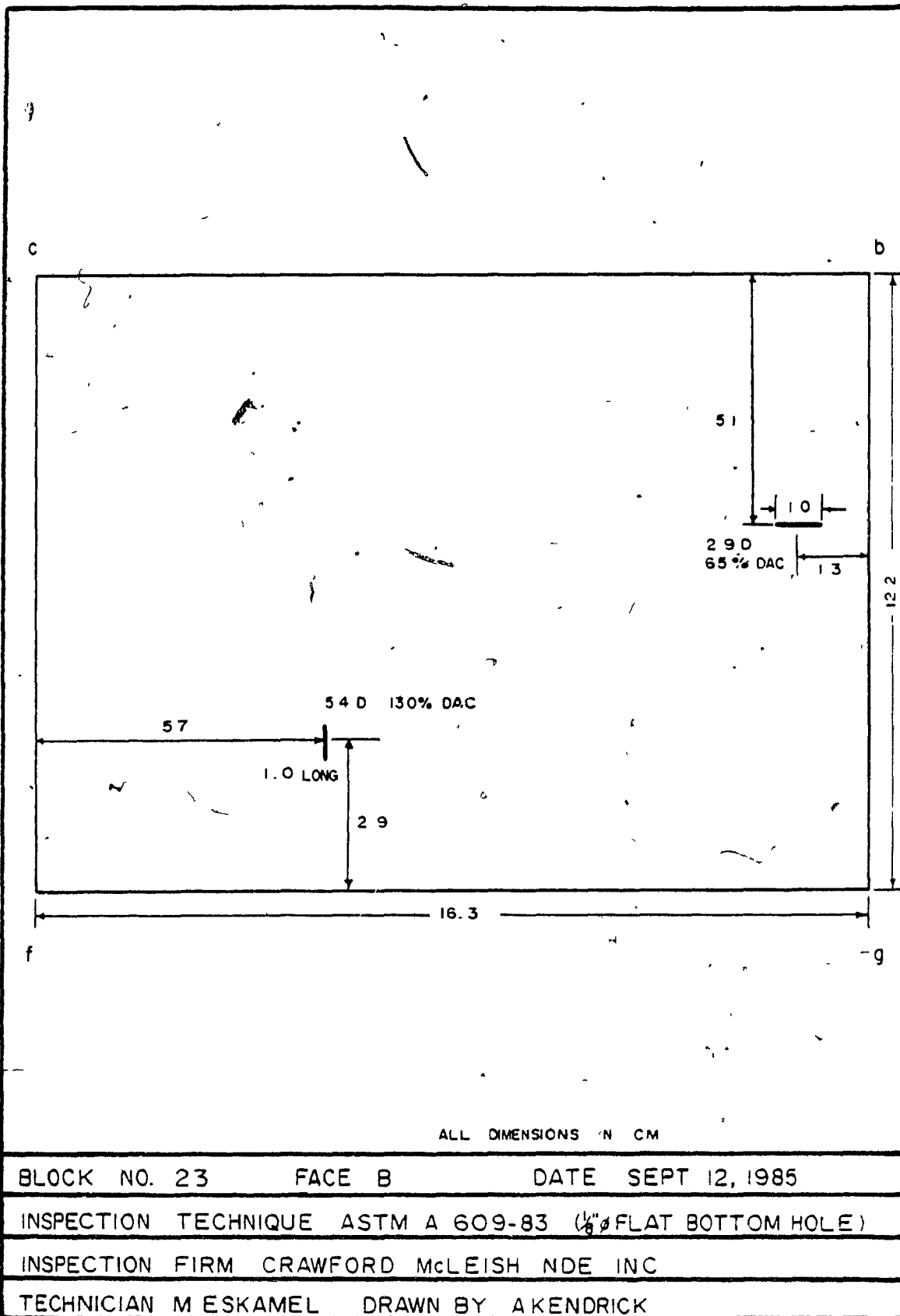
ALL DIMENSIONS IN CM

| BLOCK NO. 23L | FACE E | DATE SEPT. 12, 1985 |

INSPECTION TECHNIQUE ASTM A 609-83 (⅛"ø FLAT BOTTOM HOLE)

INSPECTION FIRM CRAWFORD McLEISH NDE. INC
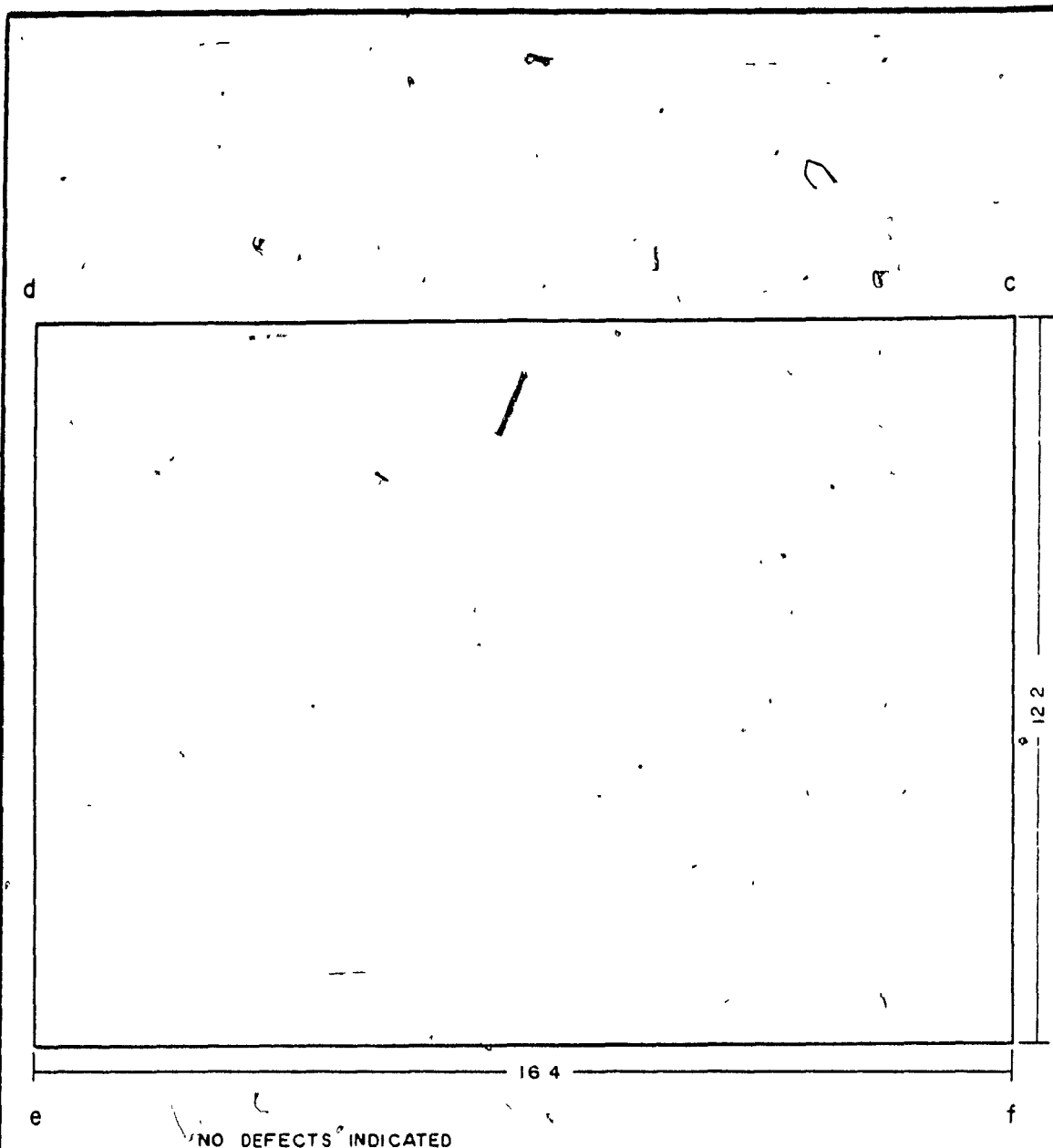
TECHNICIAN M.ESKAMEL DRAWN BY A KENDRICK

313

a   b

! 9

! 3

0 9

3 8 D
40% DAC

! 9

2 9 D
30% DAC

4 1

7 9

4 3 D
40% DAC   4 1

7 0

5.1 D
40% DAC

! 3

4 4 D
65% DAC   4 1

5.1   3.8 D
35% DAC

5 7

16 5

5 1 D
40% DAC

7 3

· 76

! 0   5 4

3 8 D
160% DAC

! 9

4 1

5 1 D
130% DAC

19

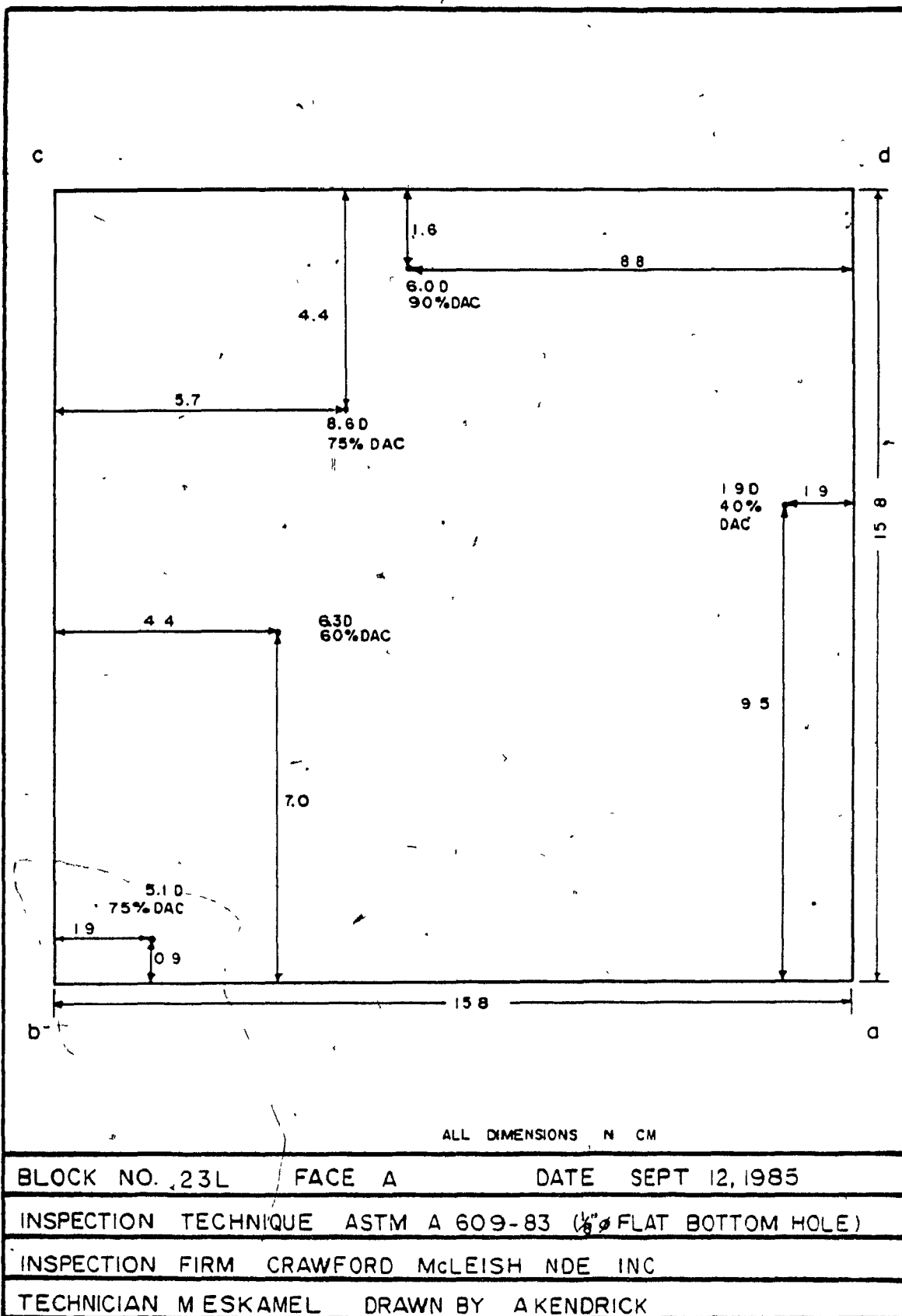d   16.5   c

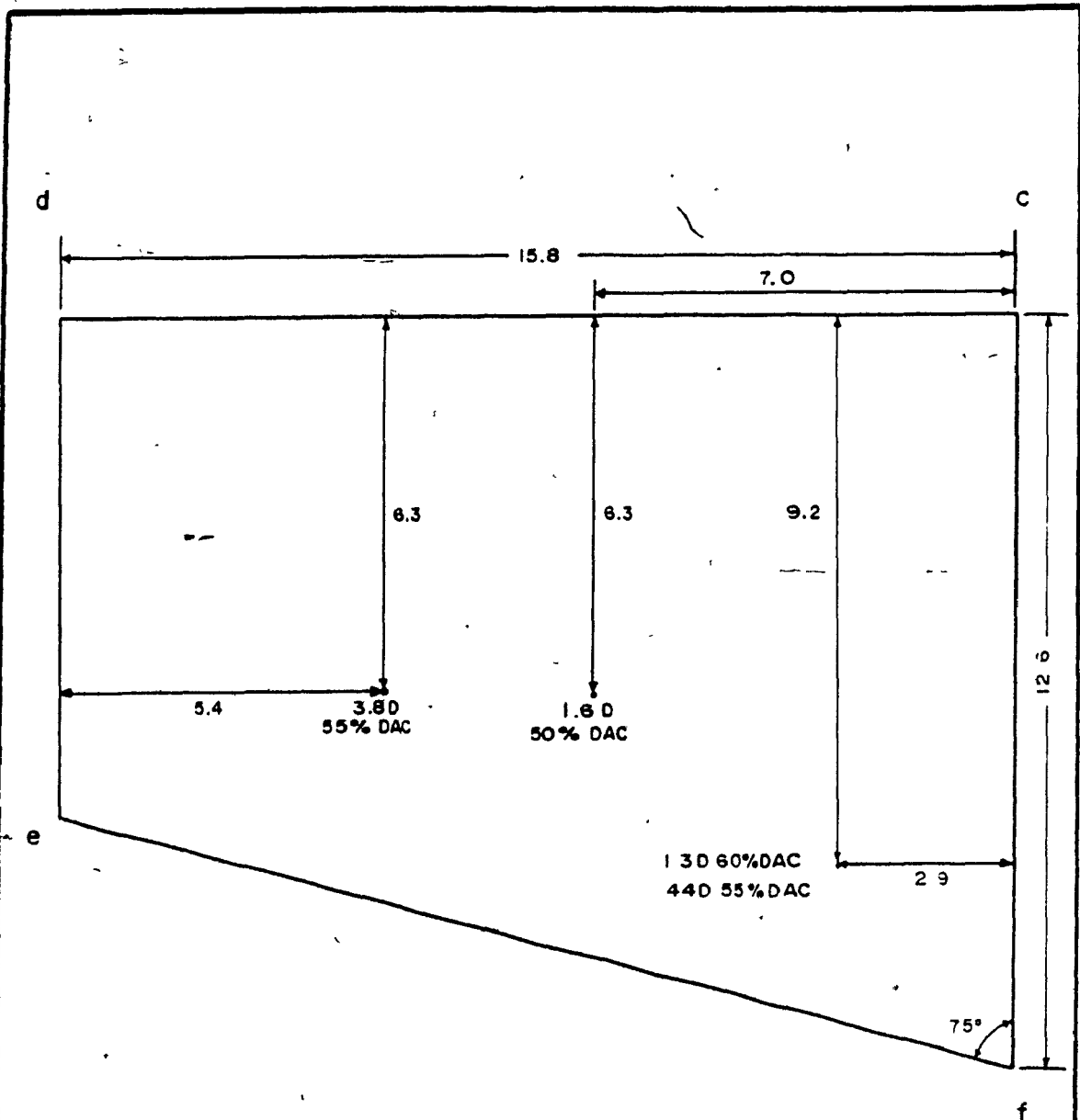ALL DIMENSIONS N CM

| BLOCK NO . 24 | FACE A | DATE SEPT. 12, 1985 |

INSPECTION TECHNIQUE ASTM A 609-83 (⅛"ø FLAT BOTTOM HOLE)

INSPECTION FIRM CRAWFORD McLEISH NDE INC

TECHNICIAN M ESKAMEL   DRAWN BY A KENDRICK

314
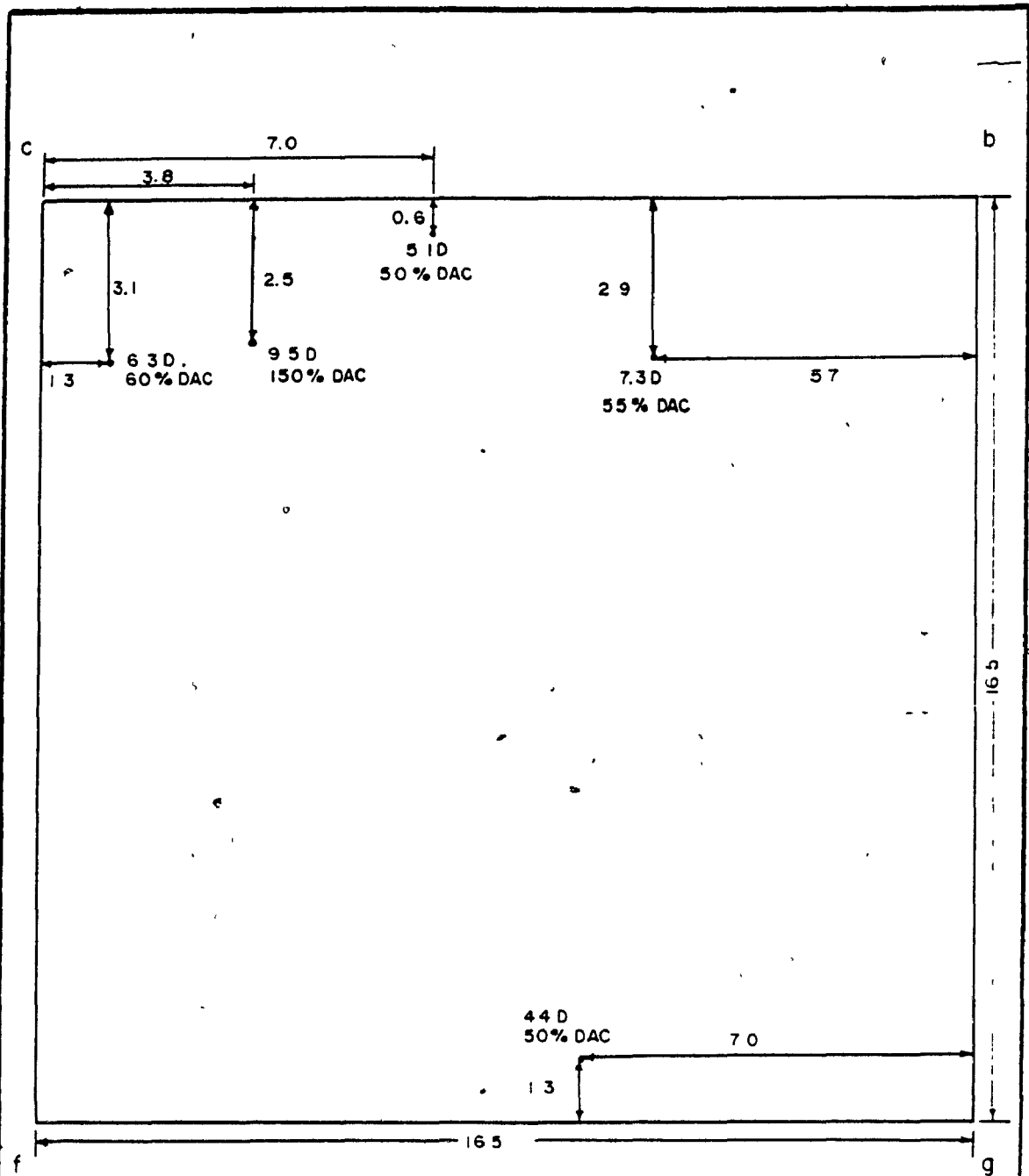
ALL DIMENSIONS IN CM

BLOCK NO. 24	FACE B	DATE SEPT. 12, 1985

INSPECTION TECHNIQUE ASTM A 609-83 (⅛"⌀ FLAT BOTTOM HOLE)

INSPECTION FIRM CRAWFORD McLEISH NDE INC

TECHNICIAN M ESKAMEL   DRAWN BY A KENDRICK

d

7 0

6 3

C

1.9

0.9   0 9

114 D
50% DAC

4 4

4.4 D
35% DAC

51

2.5 D
130% DAC

4 1

16 5

2 2

19

2.9 D
40% DAC

41

4 1 D
35% DAC

31

3.1   2 5

165

e

f

ALL DIMENSIONS N CM

BLOCK NO. 2 4	FACE C	DATE SEPT. 12,1985

INSPECTION   TECHNIQUE   ASTM A 609-83 (⅛"ø FLAT BOTTOM HOLE)
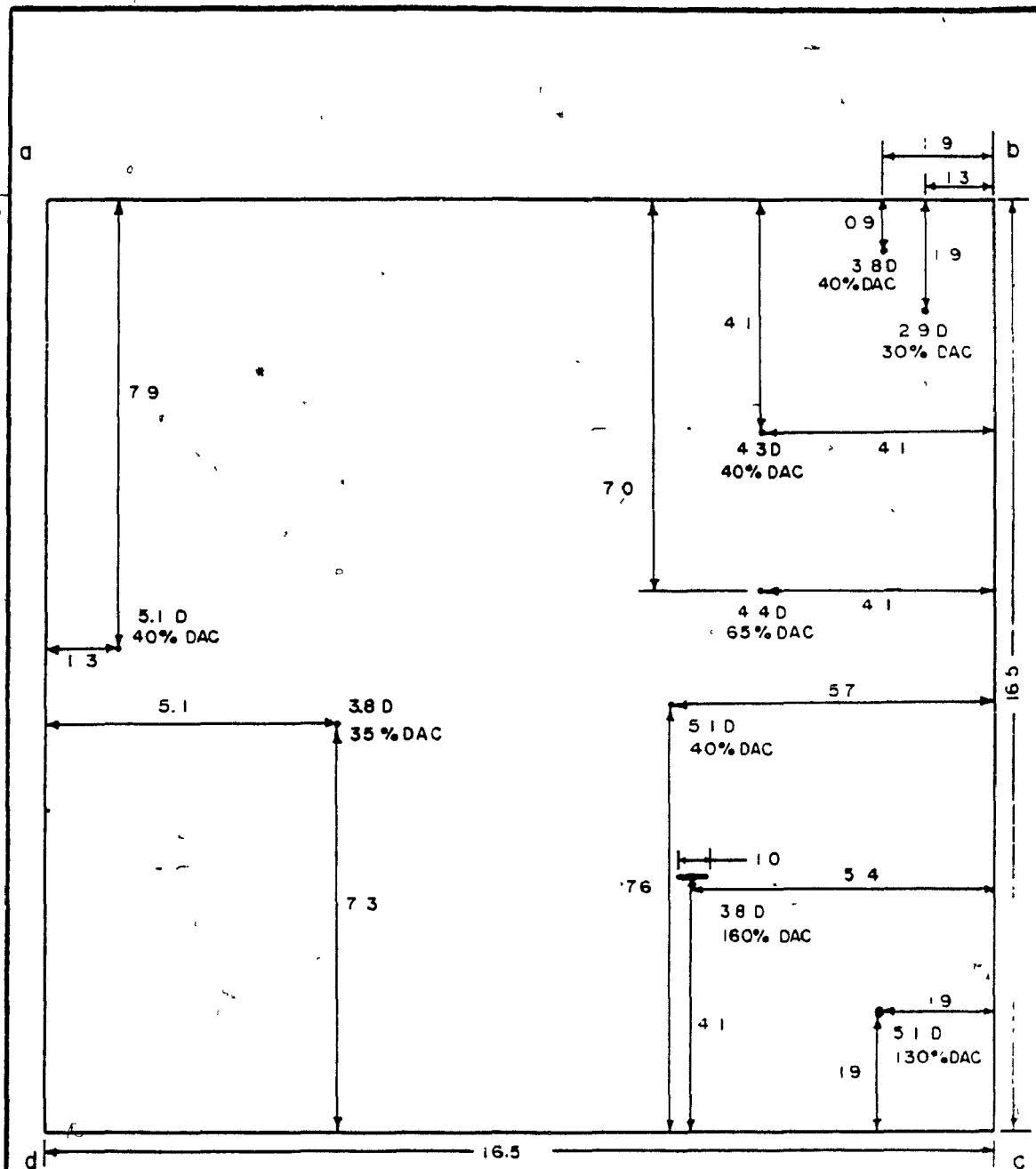
INSPECTION   FIRM   CRAWFORD McLEISH NDE INC

TECHNICIAN M ESKAMEL   DRAWN BY   A KENDRICK

316

a

79

3.8

D

19

16

44   29 D
30% DAC

41

2.5 D
70%
DAC

51

51

54

60

48 D
55% DAC

31

25 D
40% DAC

44 D
85% DAC

60

25 D
50% DAC

44 D
40% DAC

67

29

165

31 D
50% DAC

89

76

51

63

70

2 5 D
60% DAC

3.1

31

38 D
50%
DAC

4 1 D
60%
DAC

48 D
100%
DAC

38

3 8 D
60%
DAC

44

31

2.5

d   165   C

ALL DIMENSIONS IN CM

| BLOCK NO. 2 5 | FACE A | DATE SEPT 12, 1985 |

INSPECTION TECHNIQUE ASTM A 609-83 (⅛"∅ FLAT BOTTOM HOLE)

INSPECTION FIRM CRAWFORD McLEISH NDE INC

TECHNICIAN M ESKAMEL   DRAWN BY A KENDRICK

c   b

8 6   12 1D
                             75 % DAC

                                              16 5

                             5 7

                                                    115 D
                                                    120% DAC
                                                              0 7
                                                         0 5
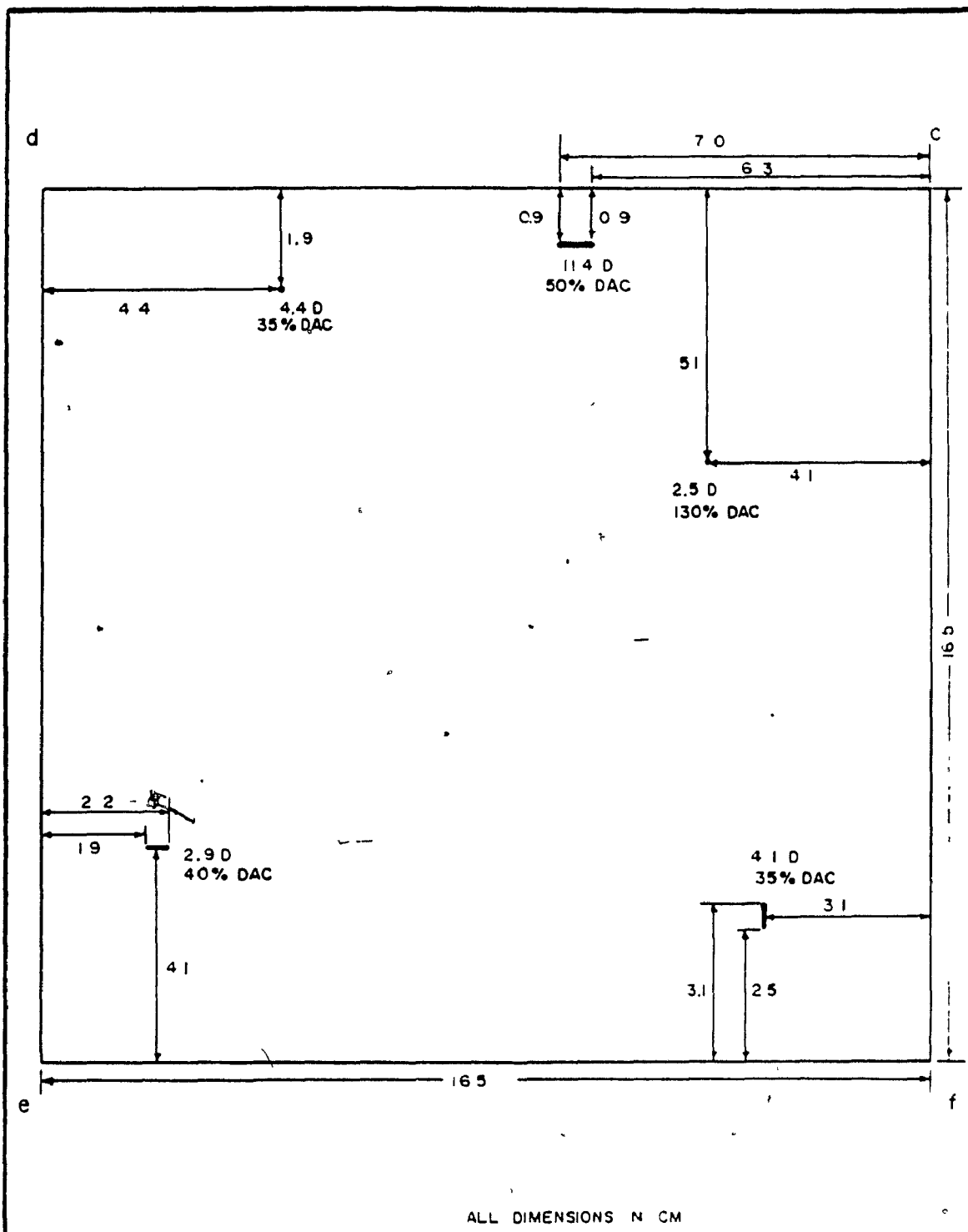
f   16 5   g
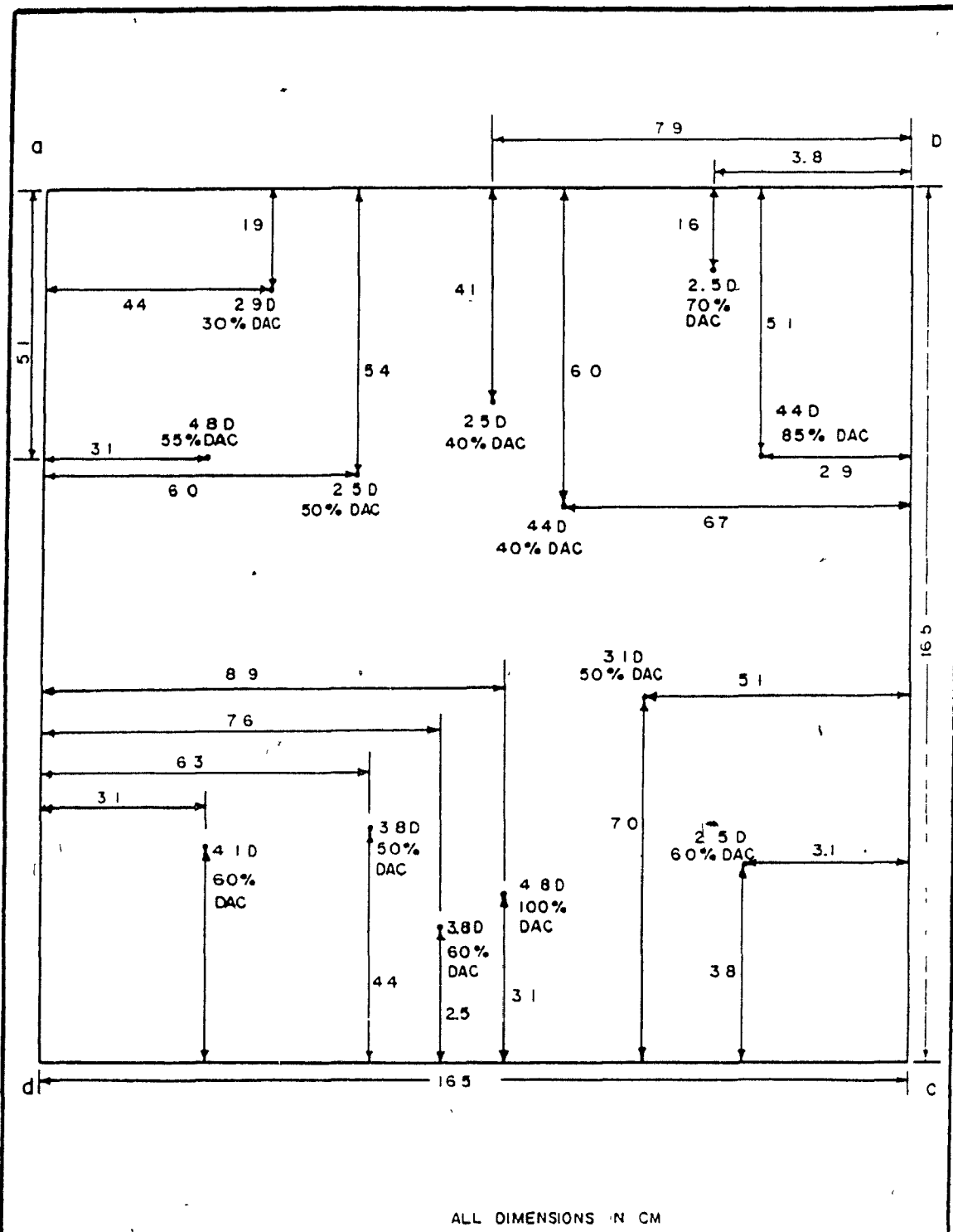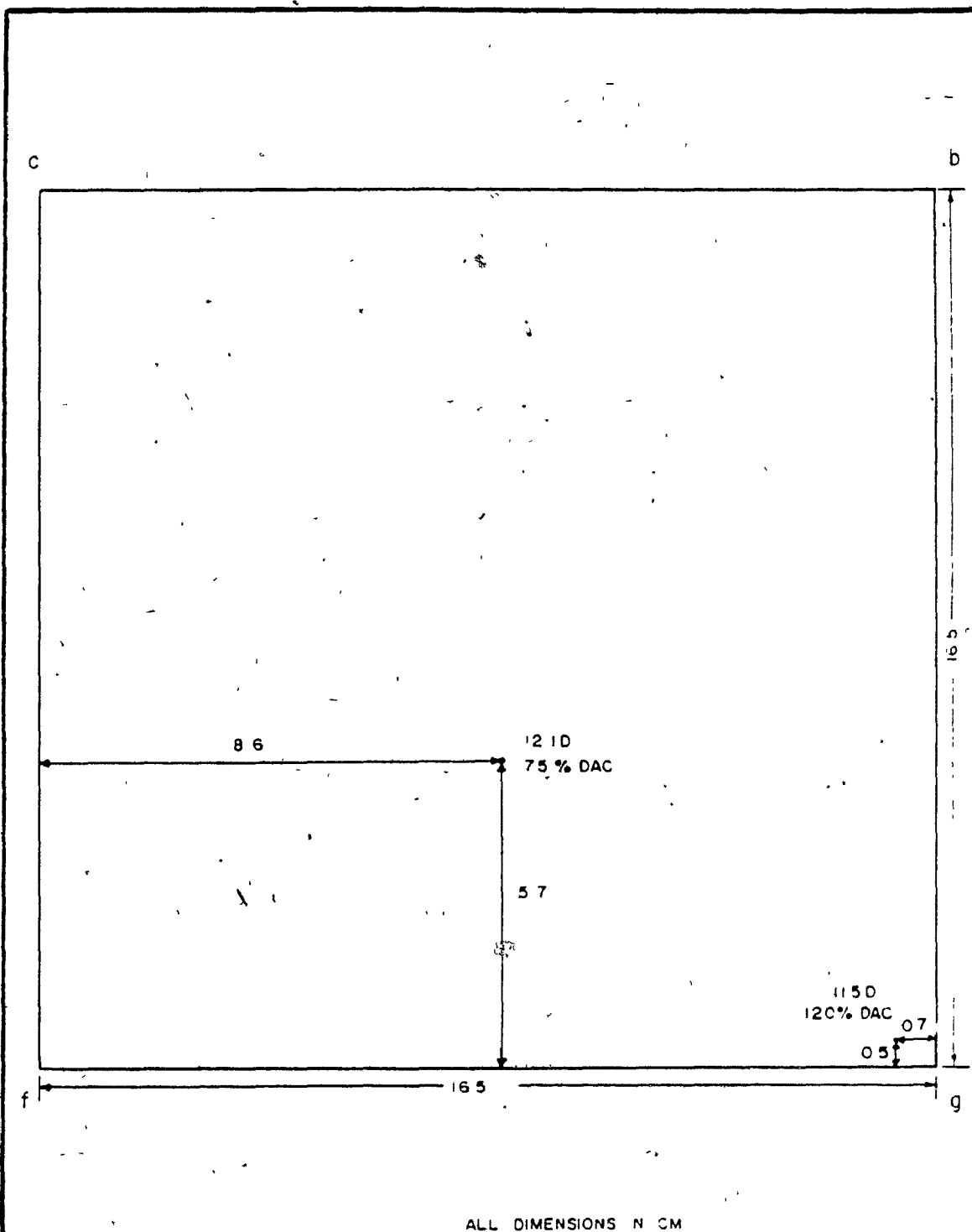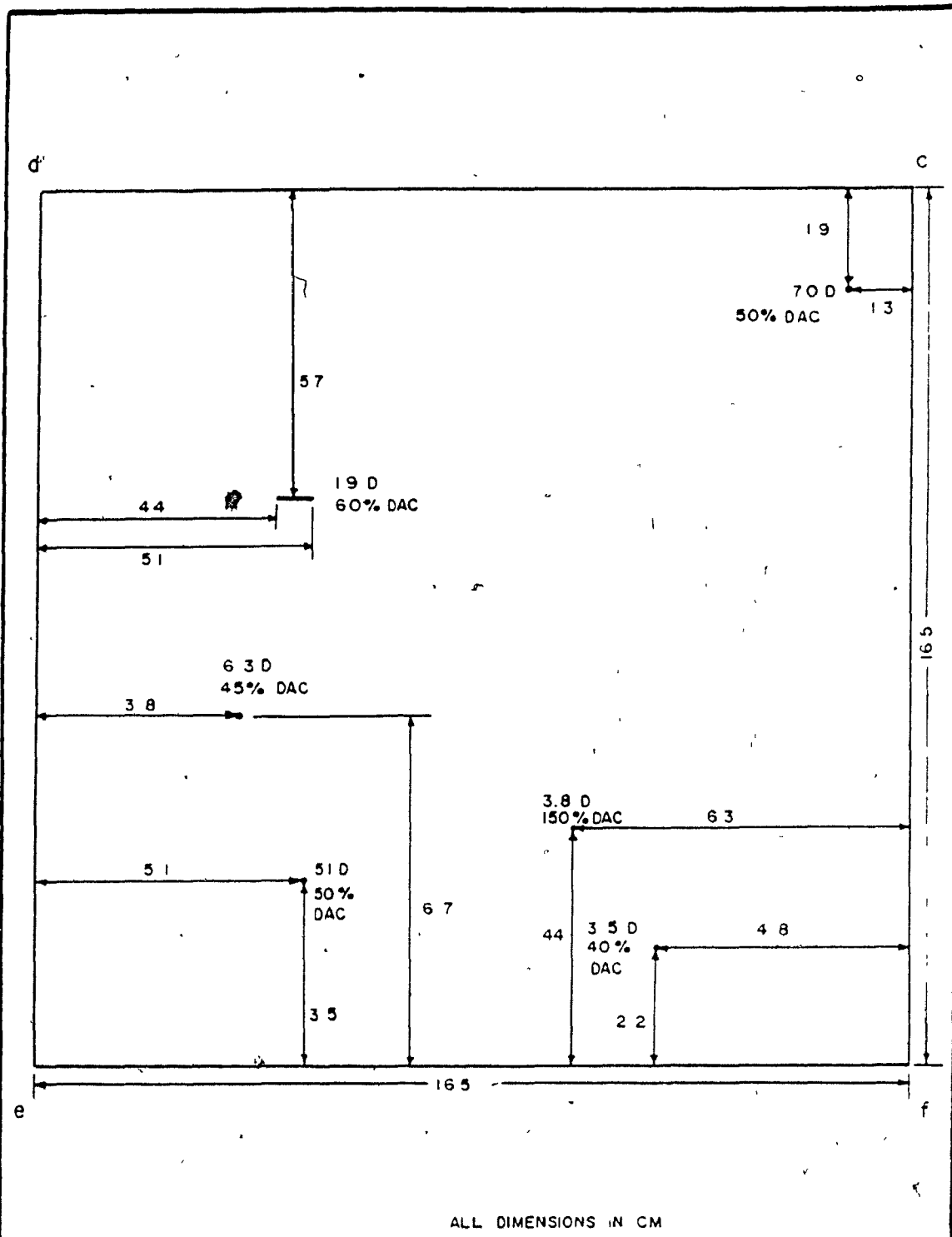
ALL DIMENSIONS N CM

BLOCK NO. 25   FACE B   DATE   SEPT 12, 1985

INSPECTION TECHNIQUE ASTM A 609-83 (⅛"ø FLAT BOTTOM HOLE)

INSPECTION FIRM CRAWFORD McLEISH NDE INC

TECHNICIAN M ESKAMEL   DRAWN BY A KENDRICK

318

ALL DIMENSIONS IN CM

BLOCK NO. 25 FACE C	DATE SEPT 12, 1985

INSPECTION TECHNIQUE ASTM A 609-83 (⅛"∅ FLAT BOTTOM HOLE)

INSPECTION FIRM CRAWFORD McLEISH NDE INC

TECHNICIAN M ESKAMEL DRAWN BY A KENDRICK

319

ALL DIMENSIONS IN CM

BLOCK NO. 26	FACE A	DATE SEPT 12, 1985

INSPECTION TECHNIQUE ASTM A 609-83 (⅛"∅ FLAT BOTTOM HOLE)

INSPECTION FIRM CRAWFORD McLEISH NDE INC

TECHNICIAN M ESKAMEL DRAWN BY A KENDRICK

320

c   b

                                                    19D
                                      19   13   120% DAC
                                                         4 8
                                                    6 0
              4 0   57 D
                                     150% DAC

    3 5   1.3D
               110% DAC

                                                                         16.5

f   16.5   g

                    ALL DIMENSIONS N CM
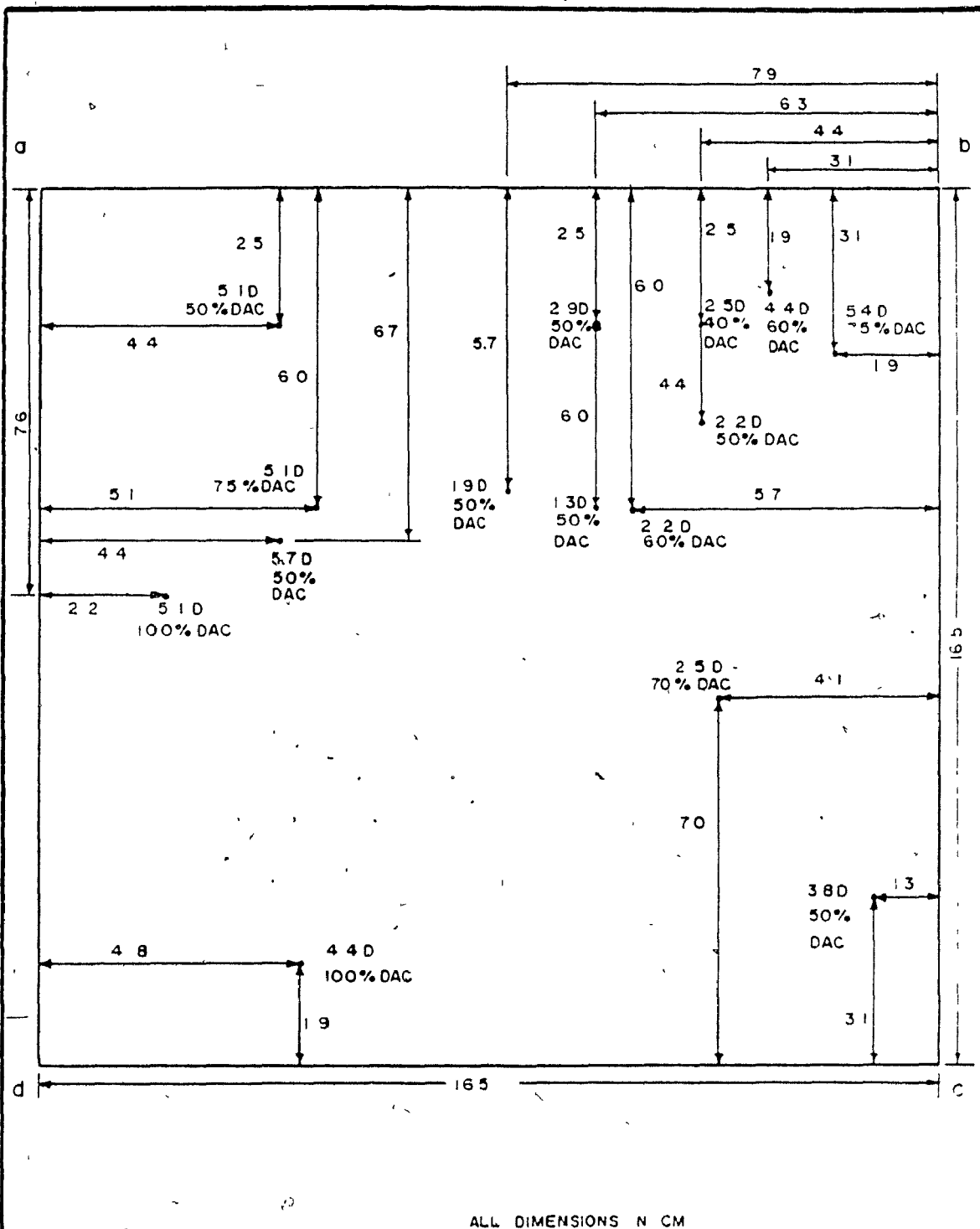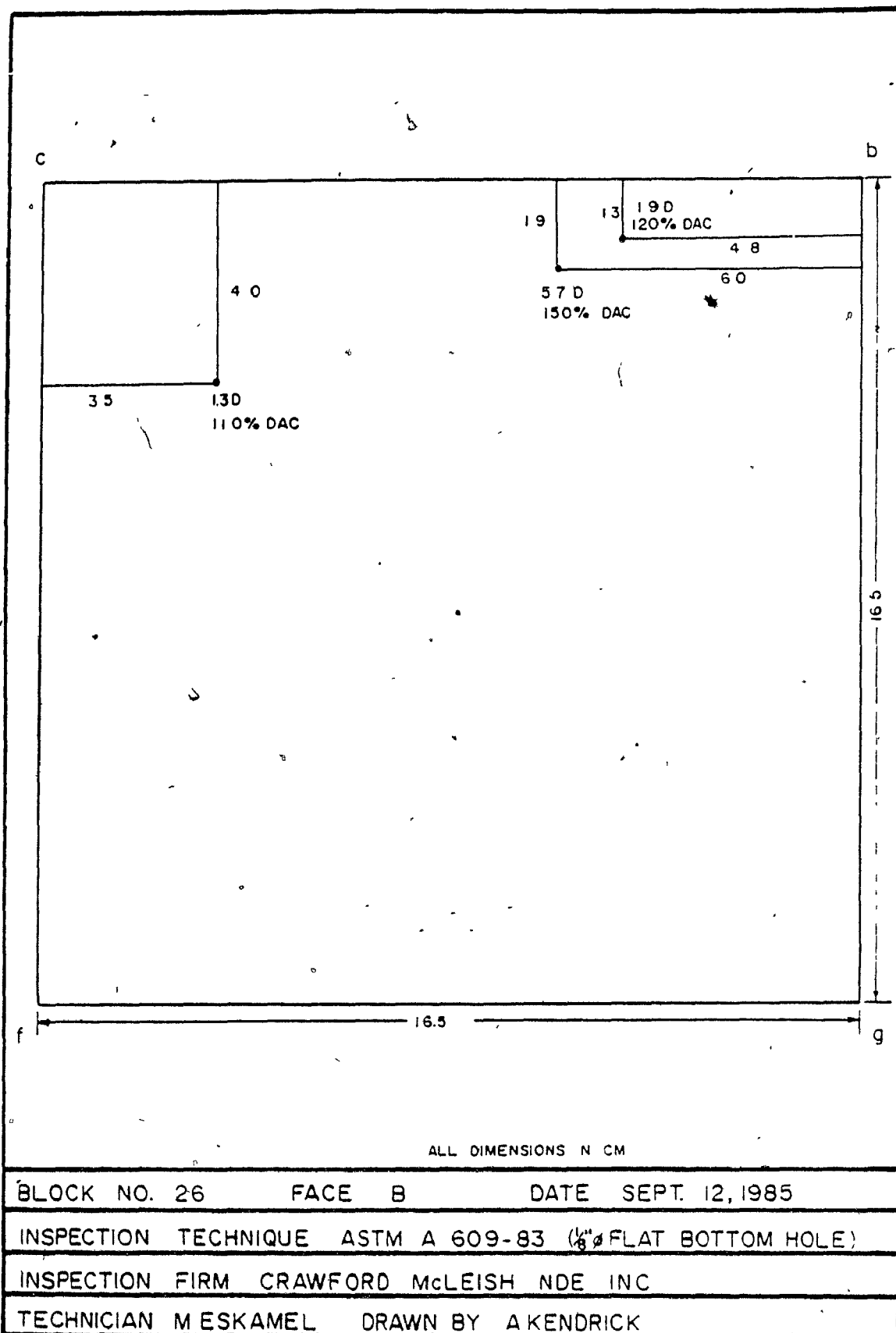
BLOCK NO. 26   FACE   B   DATE   SEPT. 12, 1985

INSPECTION   TECHNIQUE   ASTM A 609-83 (⅛"ø FLAT BOTTOM HOLE)

INSPECTION   FIRM   CRAWFORD   McLEISH   NDE   INC
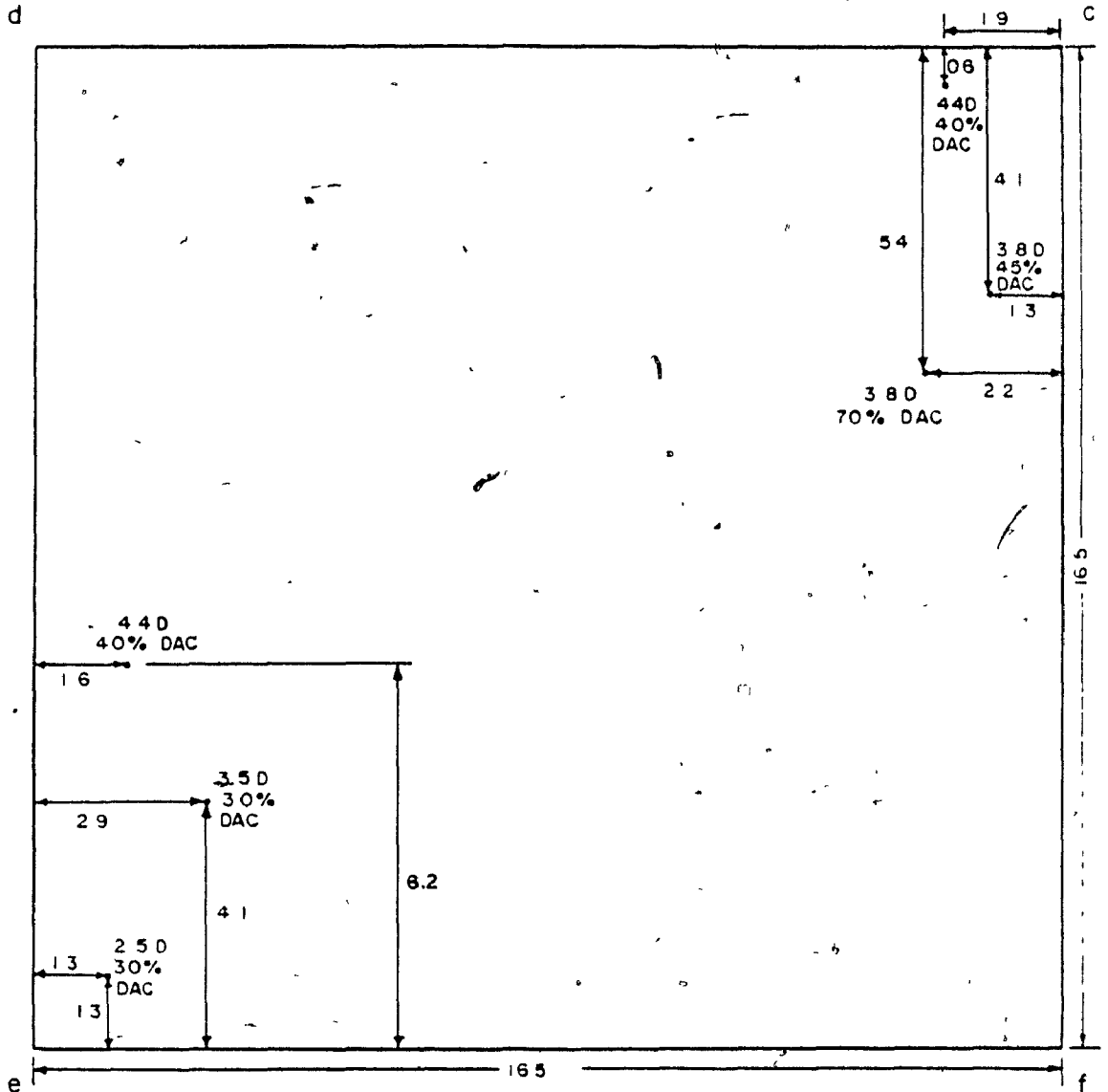
TECHNICIAN M ESKAMEL   DRAWN BY   A KENDRICK

321

ALL DIMENSIONS IN CM

BLOCK NO 26	FACE C	DATE SEPT 12, 1985

INSPECTION TECHNIQUE ASTM A 609-83 (⅛"ø FLAT BOTTOM HOLE)

INSPECTION FIRM CRAWFORD McLEISH NDE INC

TECHNICIAN M ESKAMEL   DRAWN BY A KENDRICK

ALL DIMENSIONS IN CM

| BLOCK NO. 31 | FACE A | DATE SEPT. 12, 1985 |

BLOCK NO.   31   FACE   A   DATE   SEPT. 12, 1985

INSPECTION   TECHNIQUE   ASTM A 609-83 (⅛"⌀ FLAT BOTTOM HOLE)

INSPECTION   FIRM   CRAWFORD McLEISH NDE INC

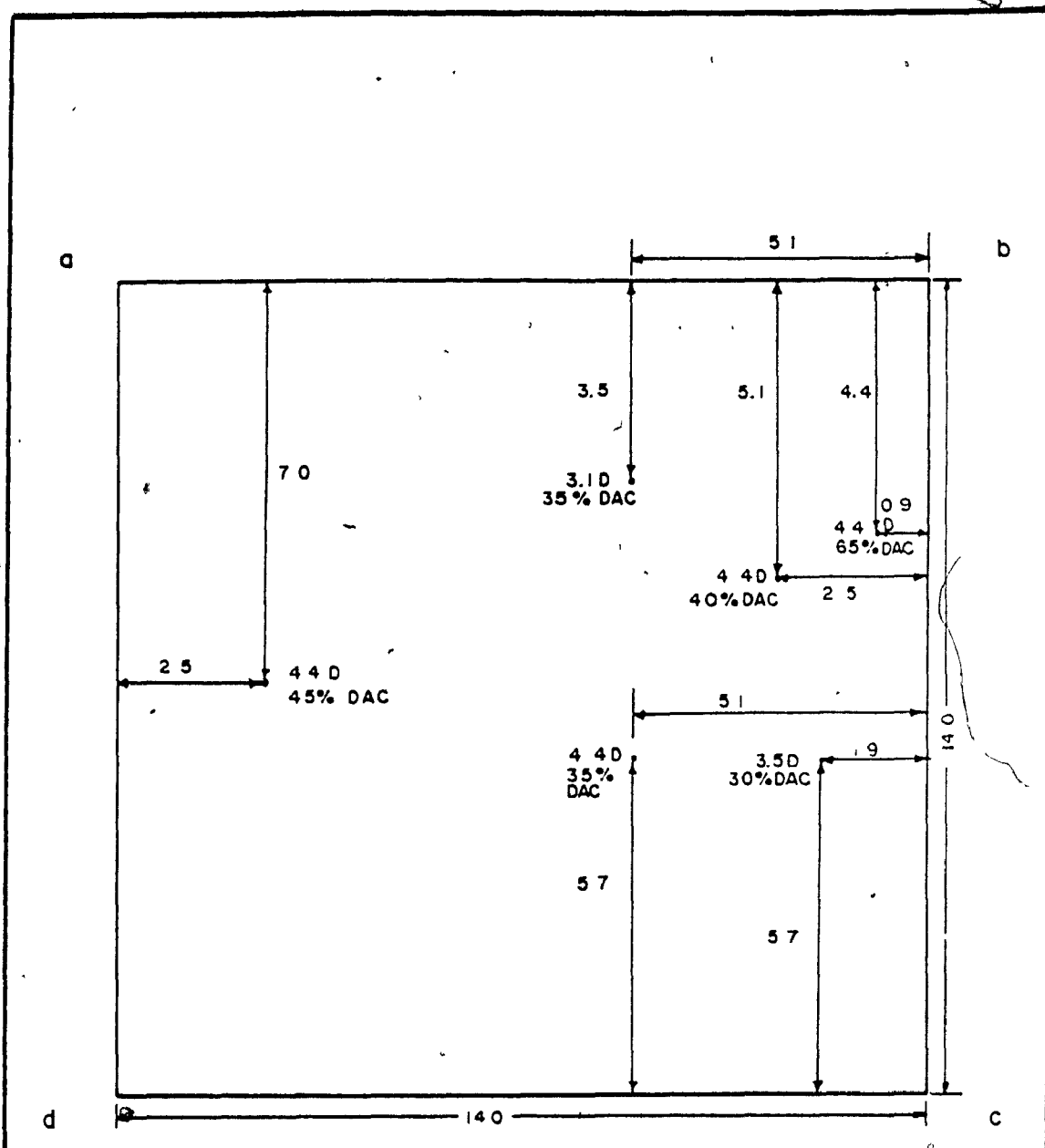TECHNICIAN M. ESKAMEL   DRAWN BY A. KENDRICK

323

ALL DIMENSIONS IN CM

BLOCK NO. 31	FACE B	DATE SEPT 12, 1985

INSPECTION TECHNIQUE ASTM A 609-83 (⅛" FLAT BOTTOM HOLE)

INSPECTION FIRM CRAWFORD McLEISH NDE INC

TECHNICIAN M ESKAMEL DRAWN BY A KENDRICK

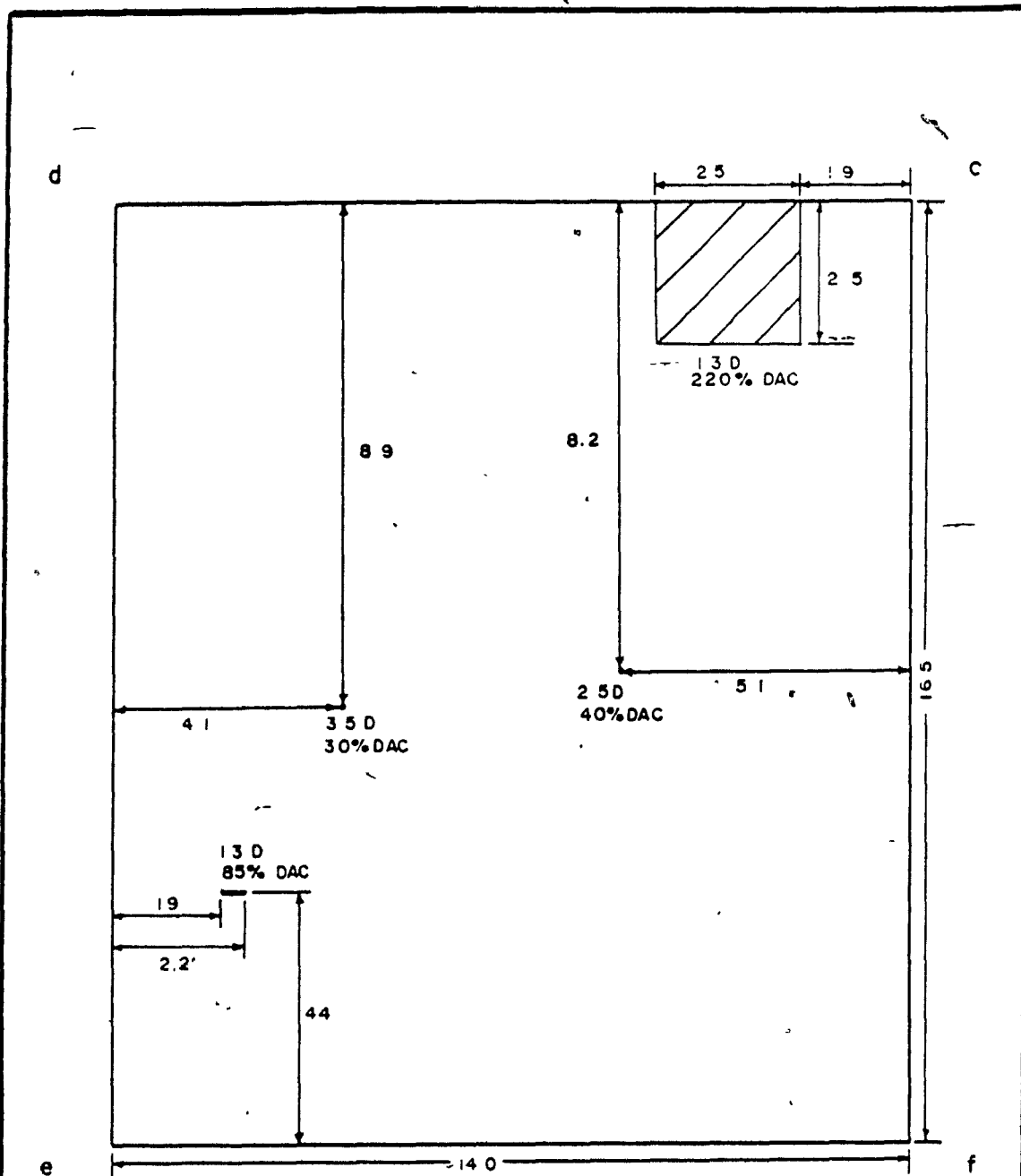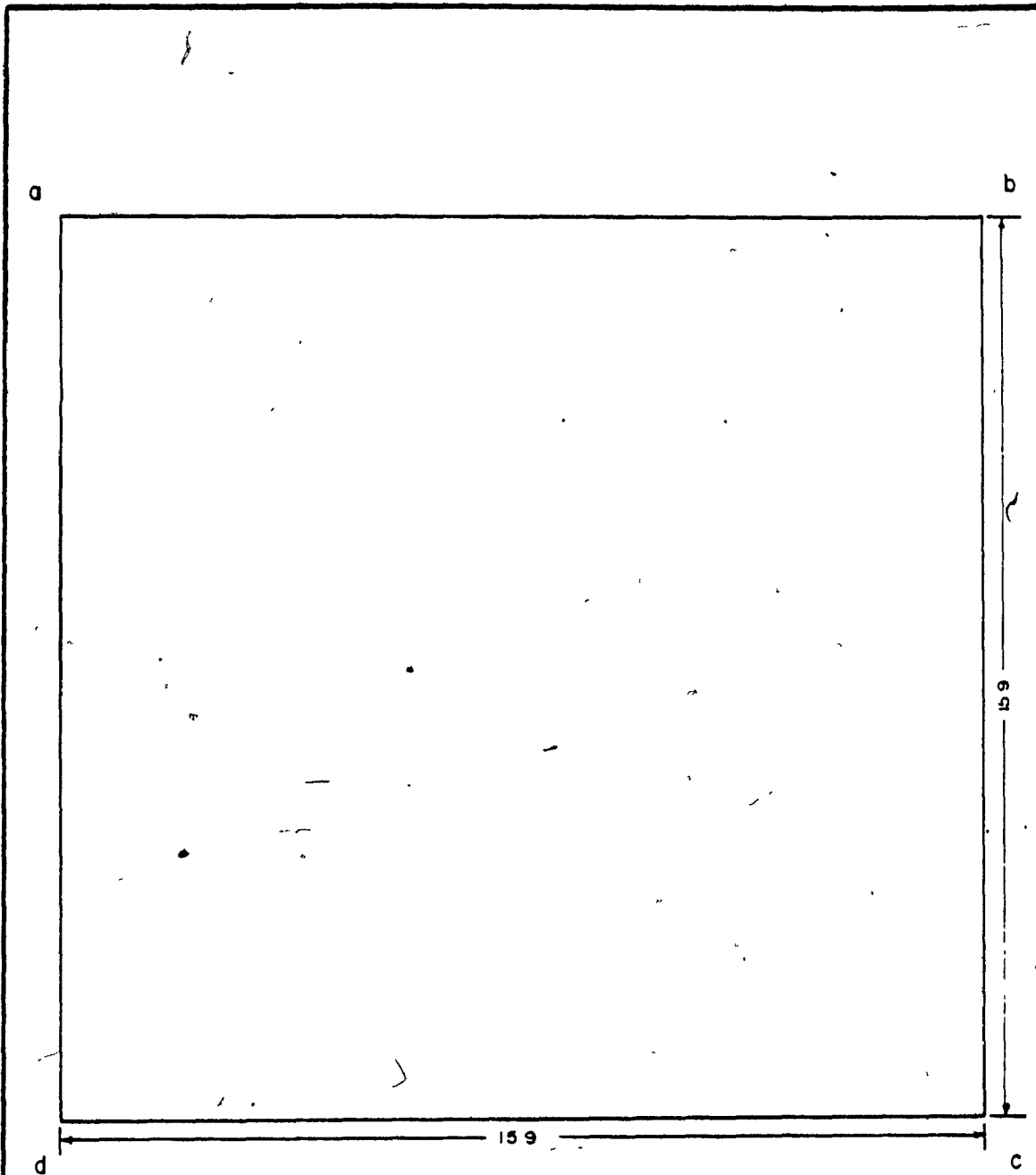ALL DIMENSIONS IN CM

| BLOCK NO. 31 | FACE C | DATE SEPT. 12, 1985 |
| INSPECTION TECHNIQUE ASTM A 609-83 (⅛"ø FLAT BOTTOM HOLE) |
| INSPECTION FIRM CRAWFORD McLEISH NDE. INC |
| TECHNICIAN M ESKAMEL DRAWN BY A KENDRICK |

a ⌐   ⌐ b

|← 69 →|

|← 159 →|

d ⌐   ⌐ c

NO DEFECTS INDICATED.

ALL DIMENSIONS IN CM

BLOCK NO. 32	FACE A	DATE SEPT. 12, 1985

INSPECTION TECHNIQUE ASTM A 609-83 (1/8"⌀ FLAT BOTTOM HOLE)

INSPECTION FIRM CRAWFORD McLEISH NDE. INC

TECHNICIAN M ESKAMEL   DRAWN BY A KENDRICK

c   b

165

3 5 C
30% DAC   0 9

3 8   5.1 0
30 % DAC

3 5

2 5

15 9

f   g

ALL DIMENSIONS IN CM

BLOCK NO. 32	FACE 8	DATE SEPT. 12, 1985

INSPECTION TECHNIQUE ASTM A 609-83 (⅛"ø FLAT BOTTOM HOLE)

INSPECTION FIRM CRAWFORD McLEISH NDE INC
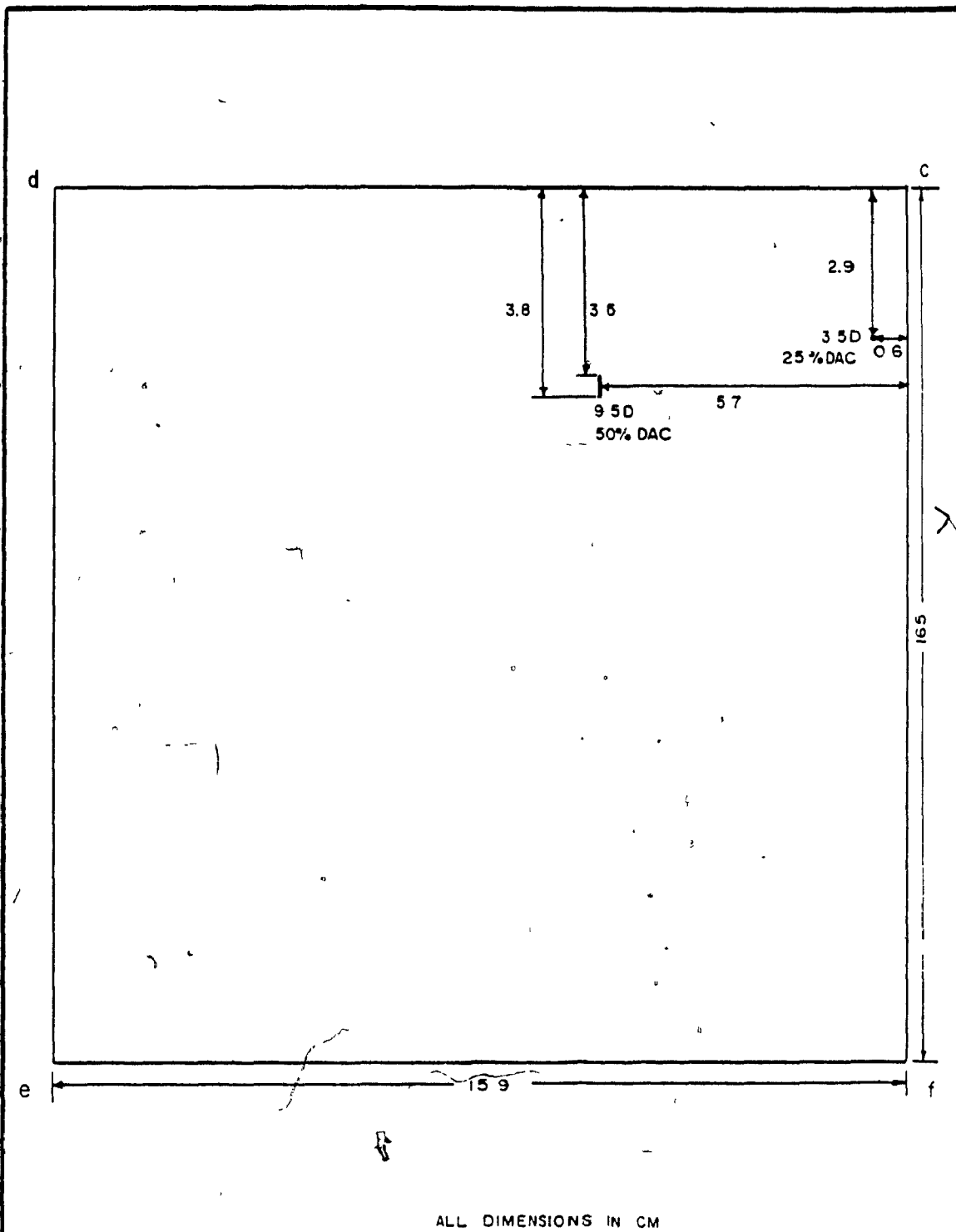
TECHNICIAN M ESKAMEL   DRAWN BY A KENDRICK

327

d c

2.9

3.8 3 6

3 5D
25 % DAC O 6

9 5D
50% DAC

5 7

165

e |————————— 15 9 ———————————| f

ALL DIMENSIONS IN CM
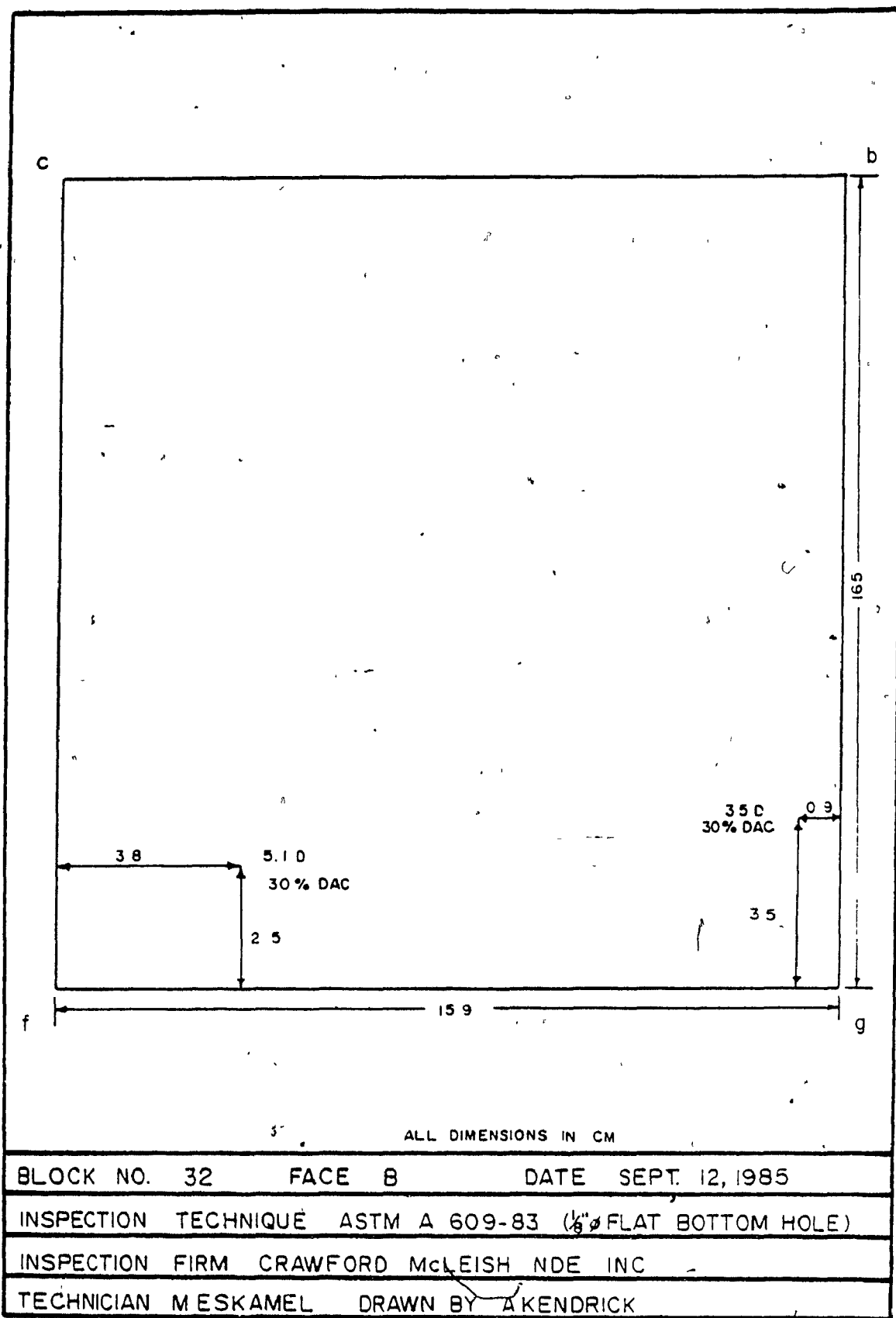
BLOCK NO. 32	FACE C	DATE SEPT 12, 1985

INSPECTION TECHNIQUE ASTM A 609-83 (⅛"∅ FLAT BOTTOM HOLE)

INSPECTION FIRM CRAWFORD McLEISH NDE INC
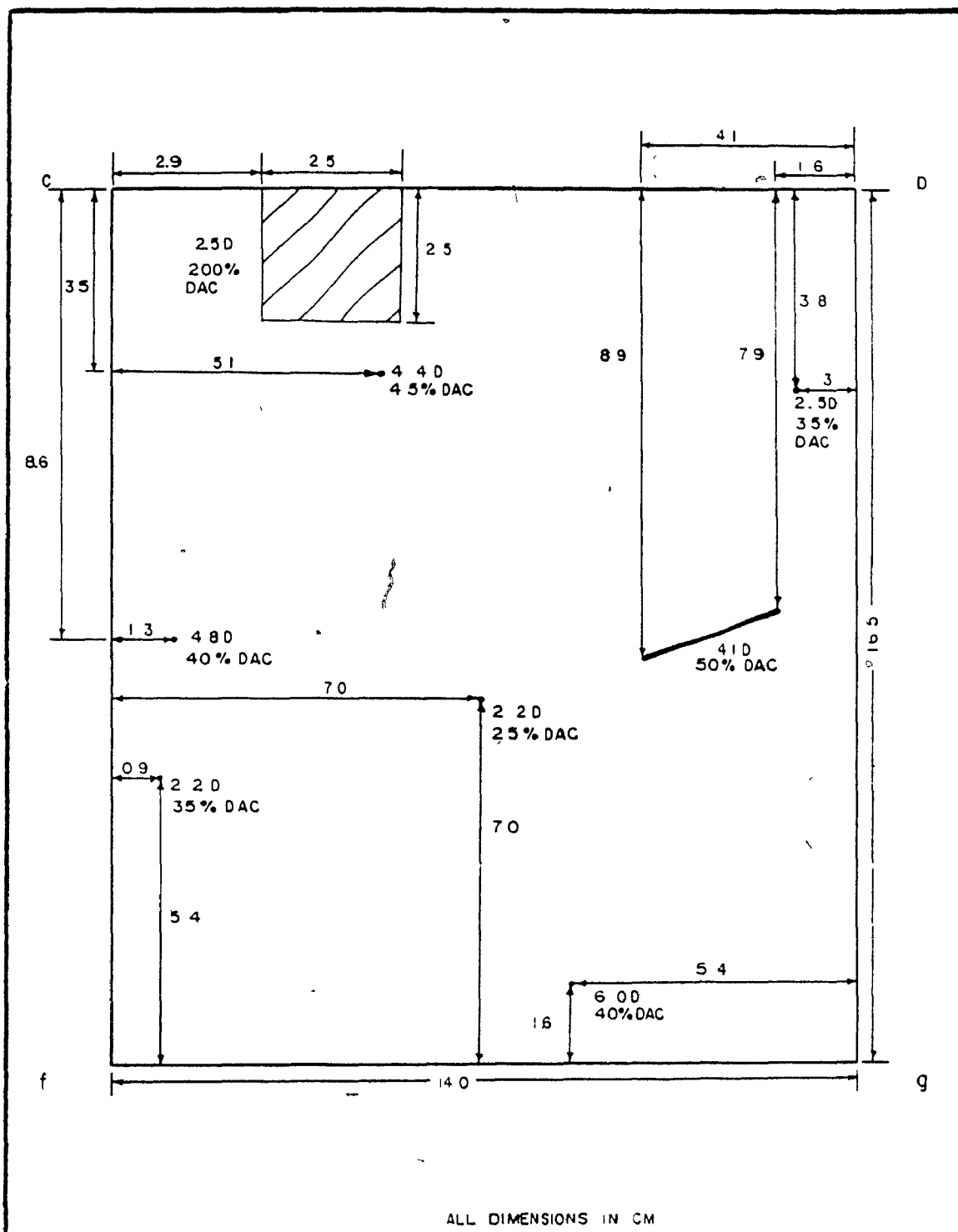
TECHNICIAN M ESKAMEL DRAWN BY A KENDRICK

ALL DIMENSIONS IN CM

BLOCK NO. 33	FACE A	DATE SEPT. 12, 1985
INSPECTION TECHNIQUE ASTM A 609-83 (⅛"ø FLAT BOTTOM HOLE)		
INSPECTION FIRM CRAWFORD McLEISH NDE INC		
TECHNICIAN M.ESKAMEL DRAWN BY A KENDRICK		

329

ALL DIMENSIONS IN CM

| BLOCK NO 33 | FACE B | DATE SEPT. 12, 1985 |

INSPECTION   TECHNIQUE   ASTM A 609-83   (⅛"⌀FLAT BOTTOM HOLE)

INSPECTION   FIRM   CRAWFORD McLEISH NDE INC

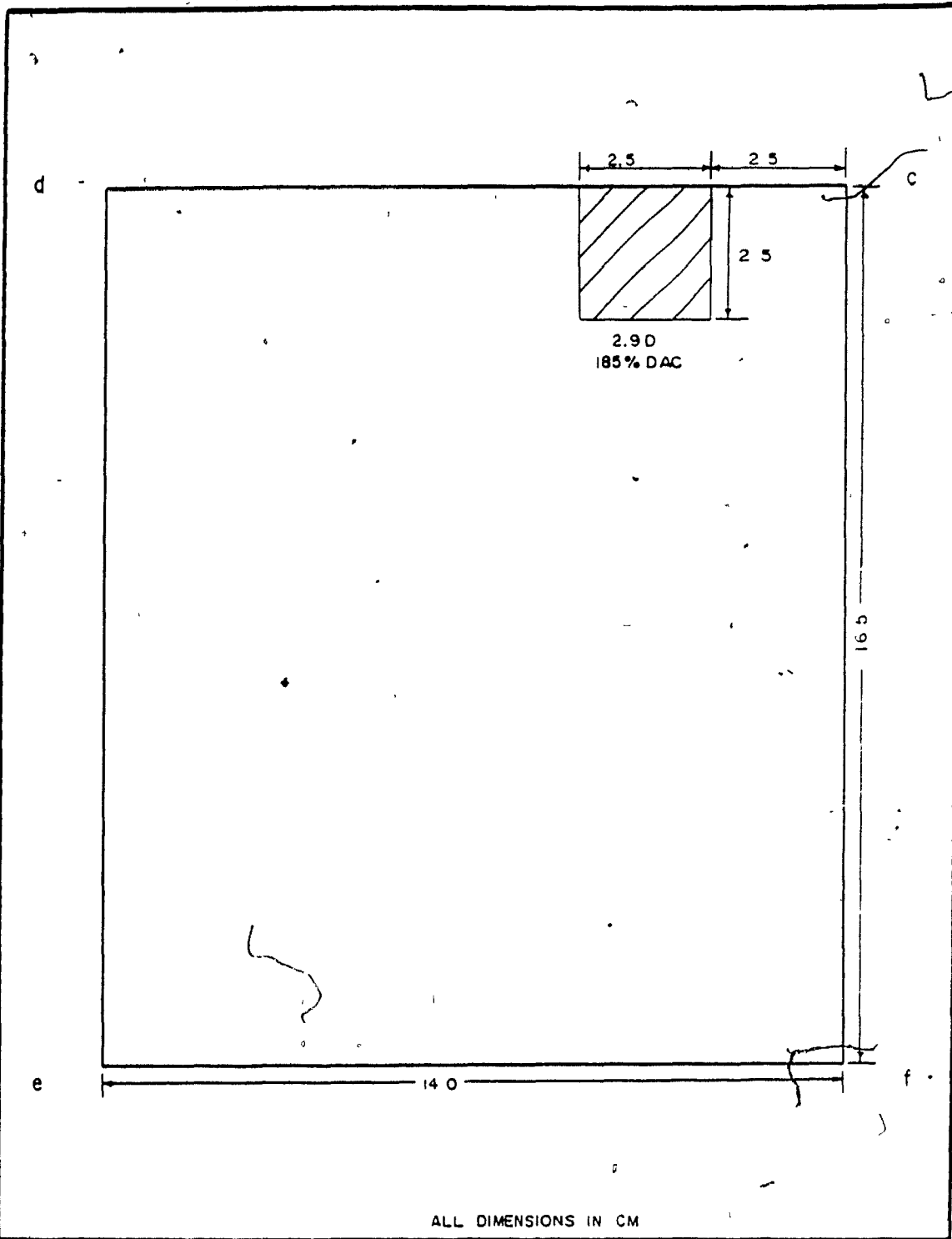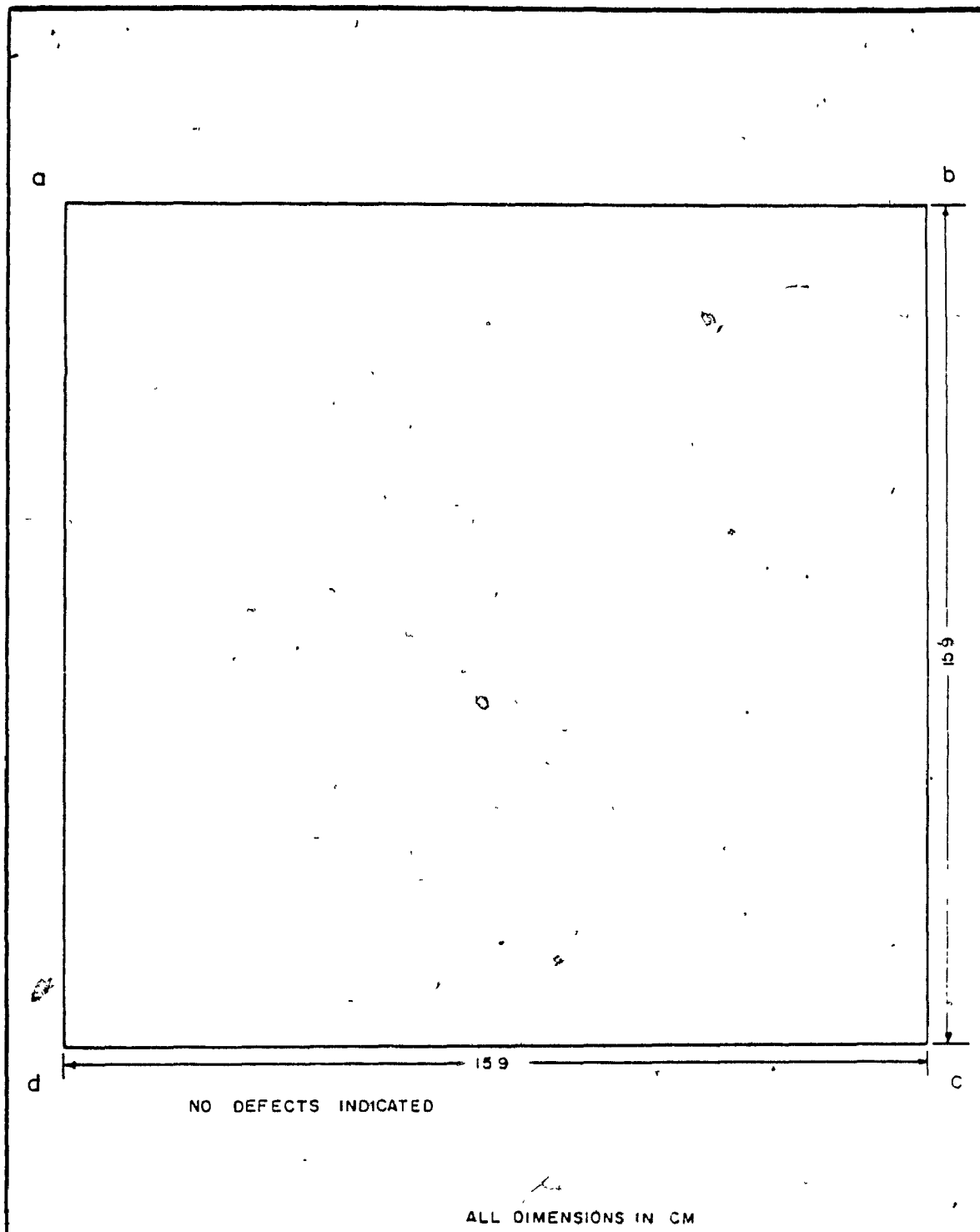TECHNICIAN M ESKAMEL   DRAWN BY A KENDRICK

ALL DIMENSIONS IN CM

BLOCK NO. 33	FACE C	DATE SEPT 12, 1985

INSPECTION TECHNIQUE ASTM A 609-83 (⅛"ø FLAT BOTTOM HOLE)

INSPECTION FIRM CRAWFORD McLEISH NDE INC

TECHNICIAN M ESKAMEL DRAWN BY A KENDRICK

a   b

159

d   159   c

NO DEFECTS INDICATED

ALL DIMENSIONS IN CM

| BLOCK NO. 34 | FACE A | DATE SEPT. 12, 1985 |

INSPECTION TECHNIQUE ASTM A 609-83 (⅛"∅ FLAT BOTTOM HOLE)

INSPECTION FIRM CRAWFORD McLEISH NDE INC

TECHNICIAN M ESKAMEL   DRAWN BY A KENDRICK

332

c   b

165

159

f   g

NO DEFECTS INDICATED

ALL DIMENSIONS IN CM

BLOCK NO. 34   FACE B   DATE SEPT 12, 1985

INSPECTION TECHNIQUE ASTM A 609-83 (1/8"Ø FLAT BOTTOM HOLE)

INSPECTION FIRM CRAWFORD McLEISH NDE. INC

TECHNICIAN M ESKAMEL   DRAWN BY A KENDRICK

d   c
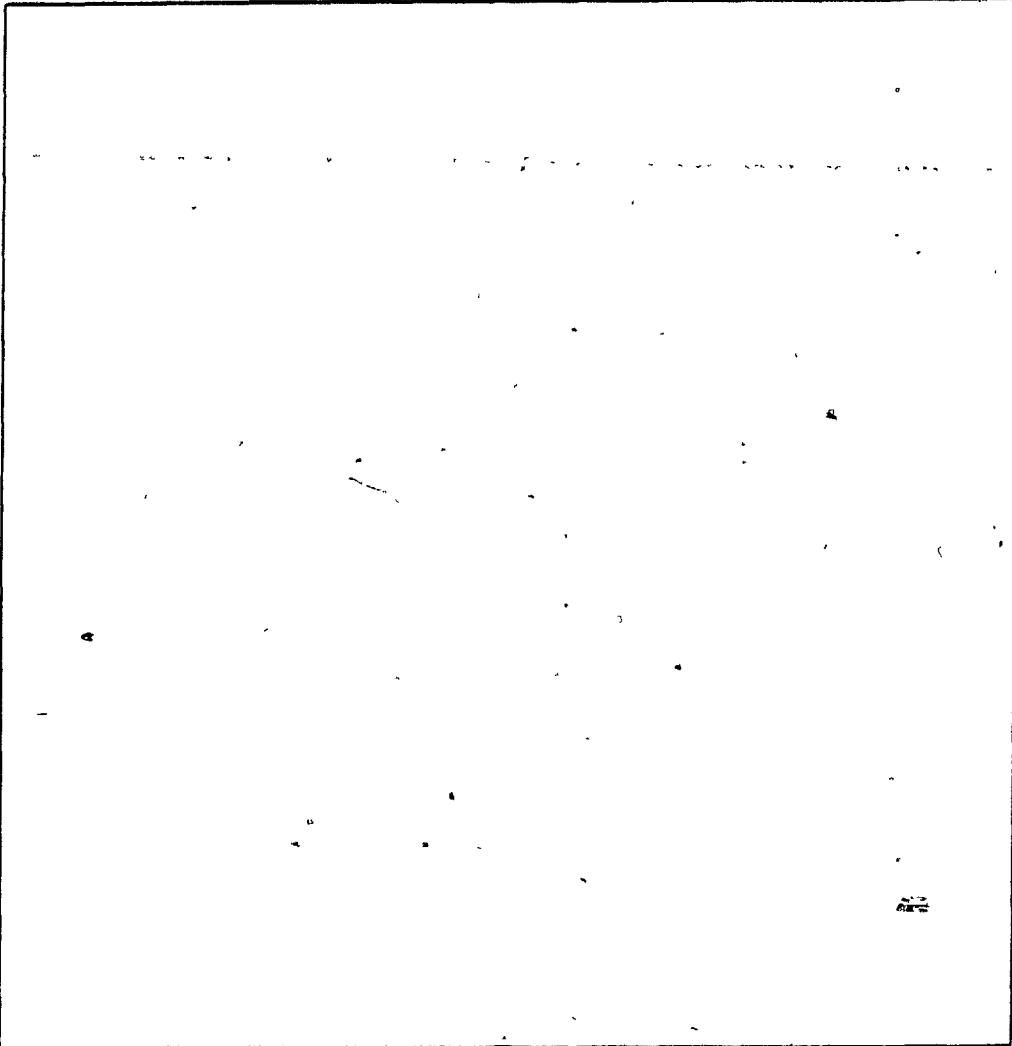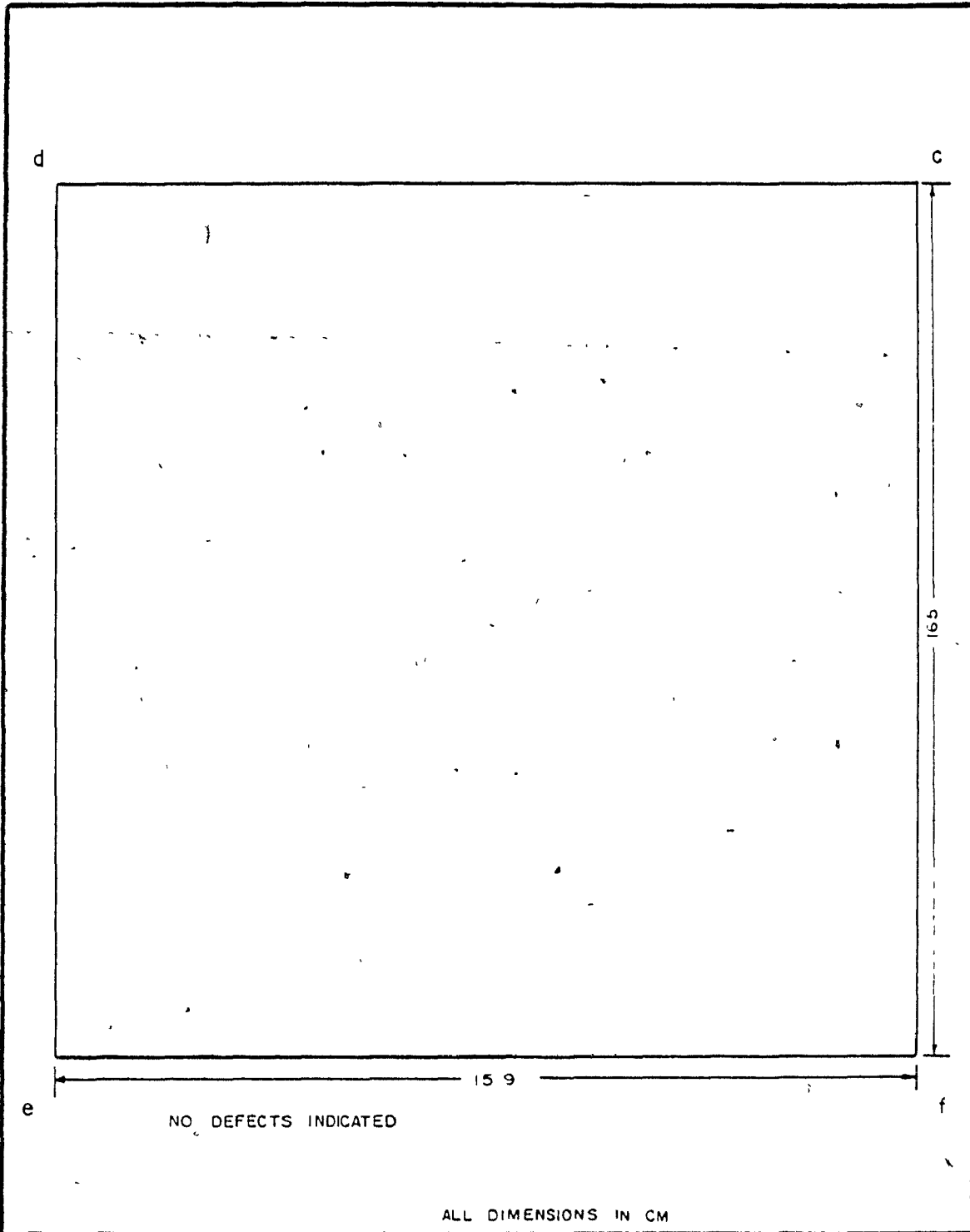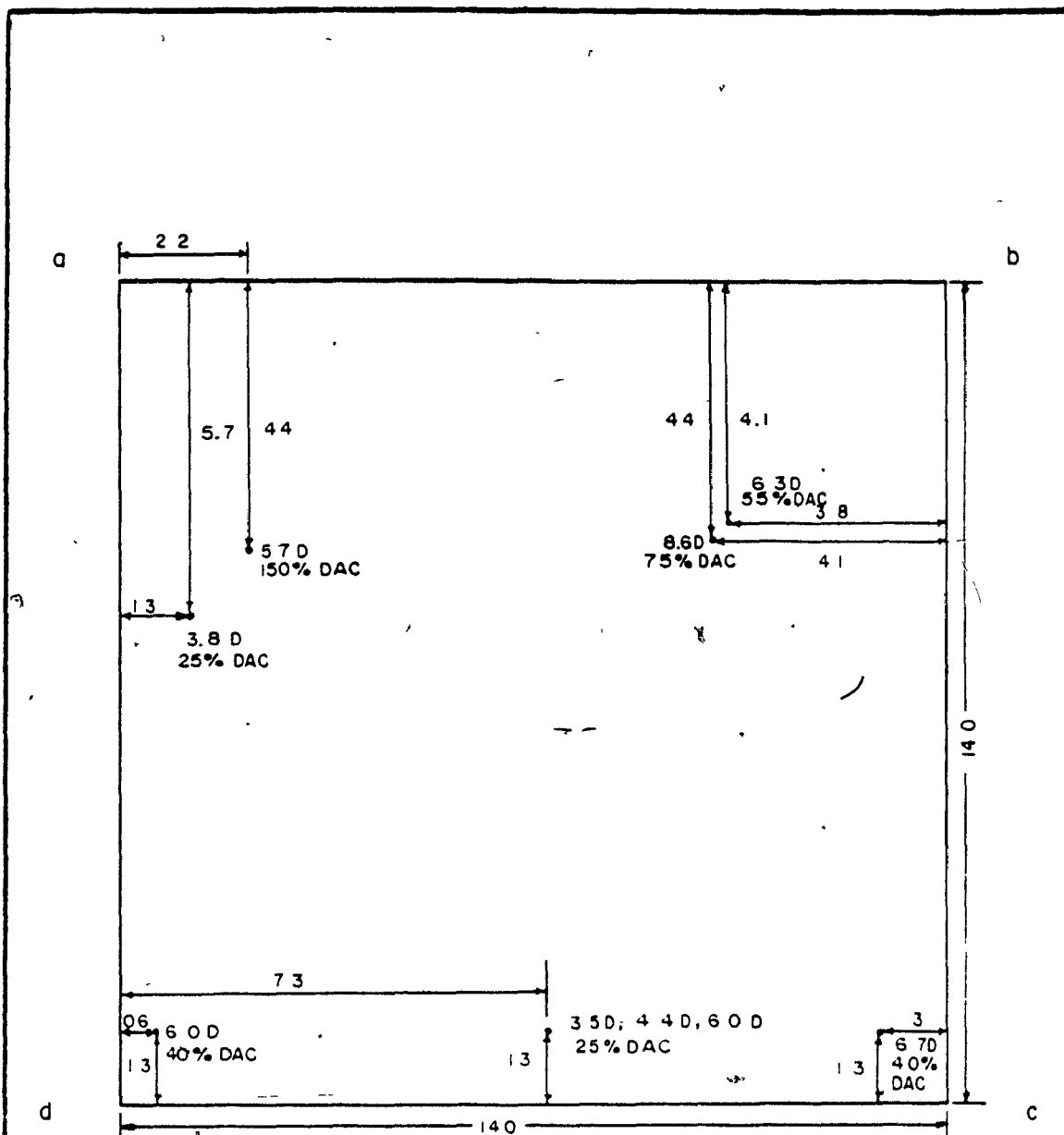
                                                                         |
                                                                        165

                                  NO DEFECTS INDICATED

|—————————————— 15 9 ——————————————|

e   f

                          ALL DIMENSIONS IN CM

BLOCK NO 34	FACE C	DATE SEPT 12, 1985

INSPECTION TECHNIQUE ASTM A 609-83 (⅛"∅ FLAT BOTTOM HOLE)

INSPECTION FIRM CRAWFORD McLEISH NDE INC

TECHNICIAN M ESKAMEL   DRAWN BY A KENDRICK

334

ALL DIMENSIONS IN CM

BLOCK NO. 41	FACE A	DATE SEPT 12, 1985

INSPECTION TECHNIQUE ASTM A 609-83 (⅛"ø FLAT BOTTOM HOLE)

INSPECTION FIRM CRAWFORD McLEISH NDE INC

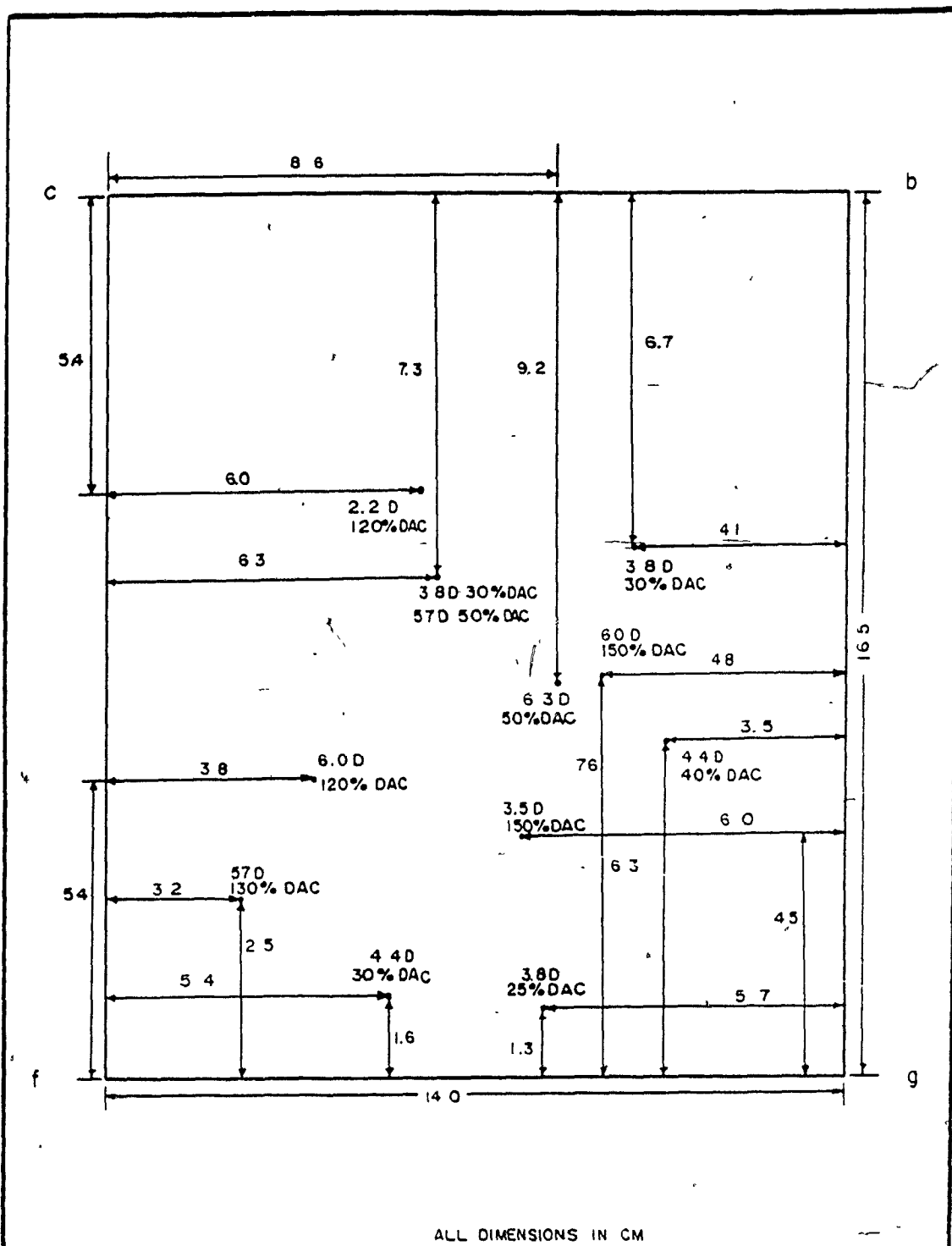TECHNICIAN M ESKAMEL   DRAWN BY A KENDRICK

335

ALL DIMENSIONS IN CM
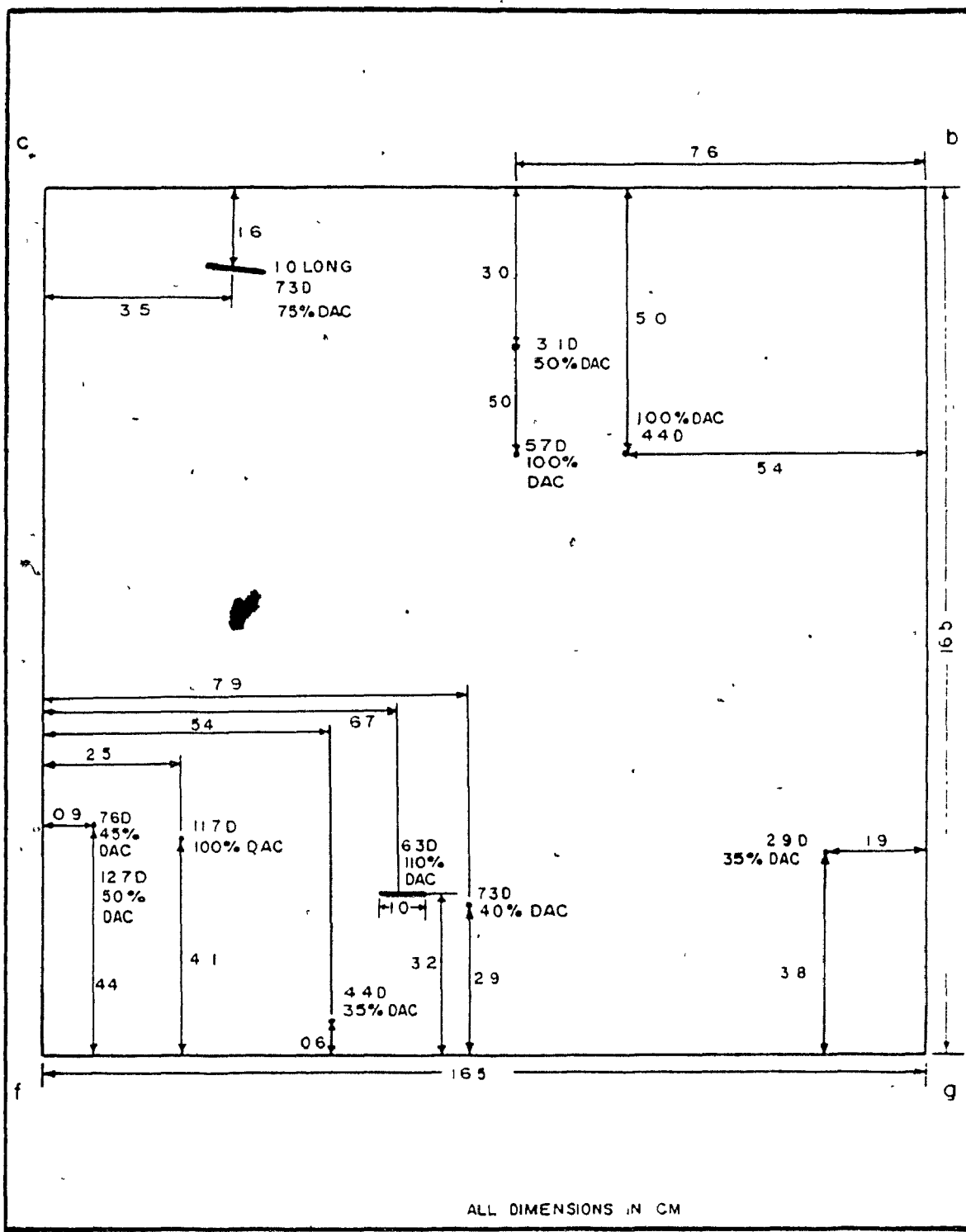
| BLOCK NO. 41 | FACE B | DATE SEPT 12, 1985 |

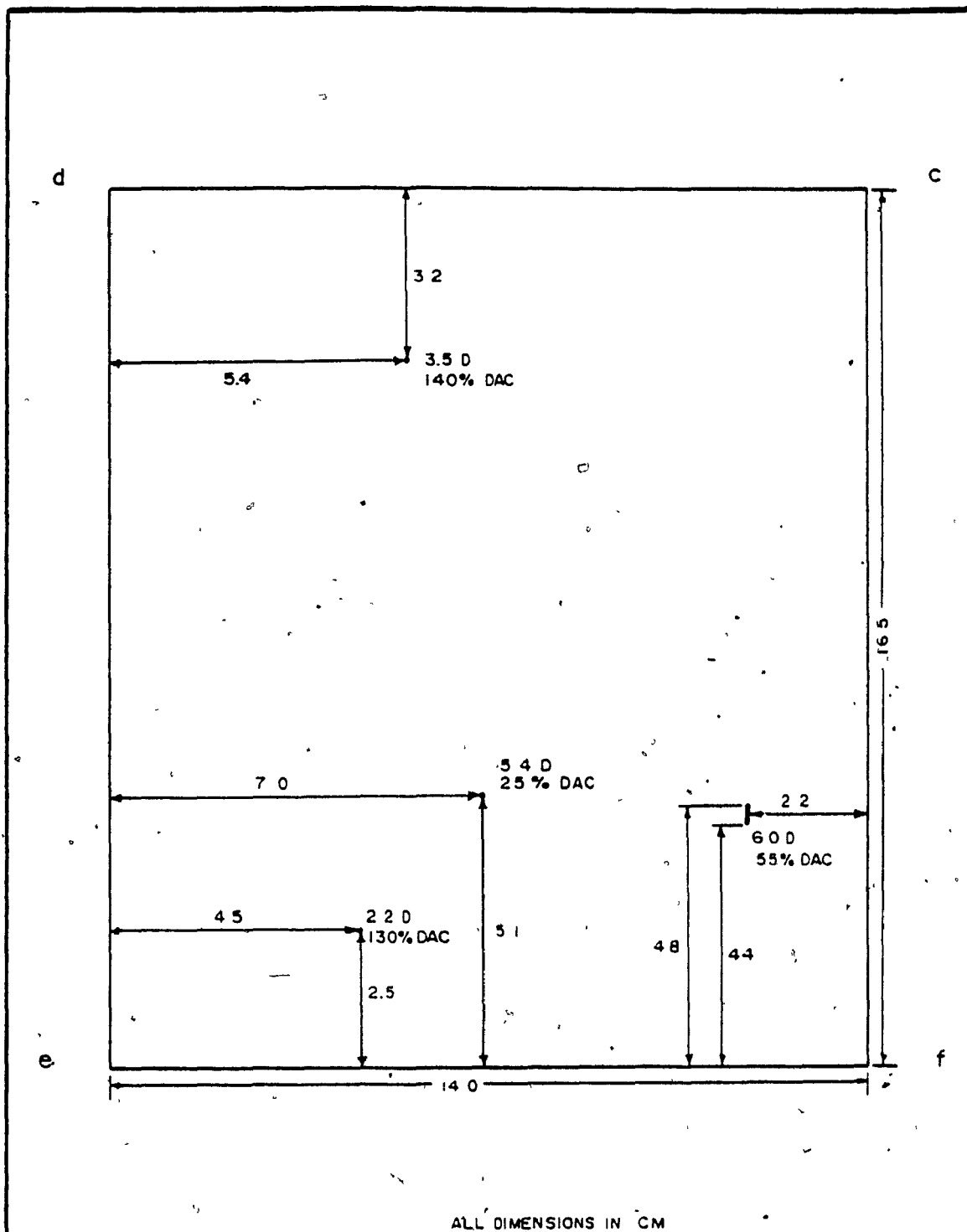INSPECTION TECHNIQUE ASTM A 609-83 (⅛"⌀ FLAT BOTTOM HOLE)

INSPECTION FIRM CRAWFORD McLEISH NDE INC

TECHNICIAN M ESKAMEL DRAWN BY A KENDRICK

336

d   c

3 I

5.4

0.6
114 D
50%
DAC
0.9

3 8 D
0 6 30 % DAC

3 8

4 4 D
155% DAC

6 7

5.7

16 5

5 I

19 D
50%
DAC

13 D
45%
DAC

44 D
45%
DAC

0 6

4 I

57 D
140%
DAC

7.6 0
55%
DAC

5 I

5 I

4 8

3 5

4 4

e   f

16 5

ALL DIMENSIONS N CM

BLOCK NO. 41	FACE C	DATE SEPT 12,1985

INSPECTION TECHNIQUE ASTM A 609-83 (⅛"ø FLAT BOTTOM HOLE)

INSPECTION FIRM CRAWFORD McLEISH NDE INC
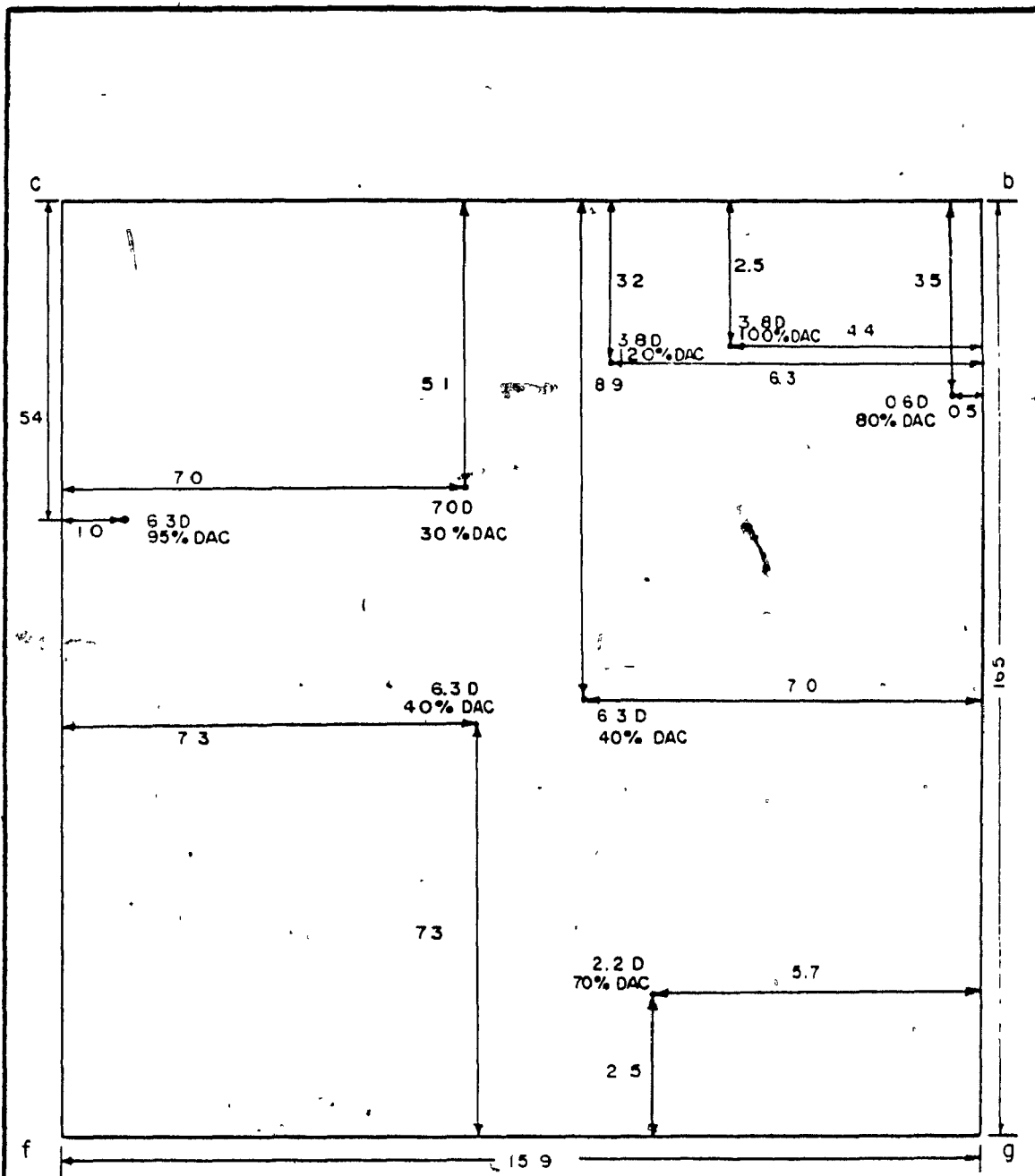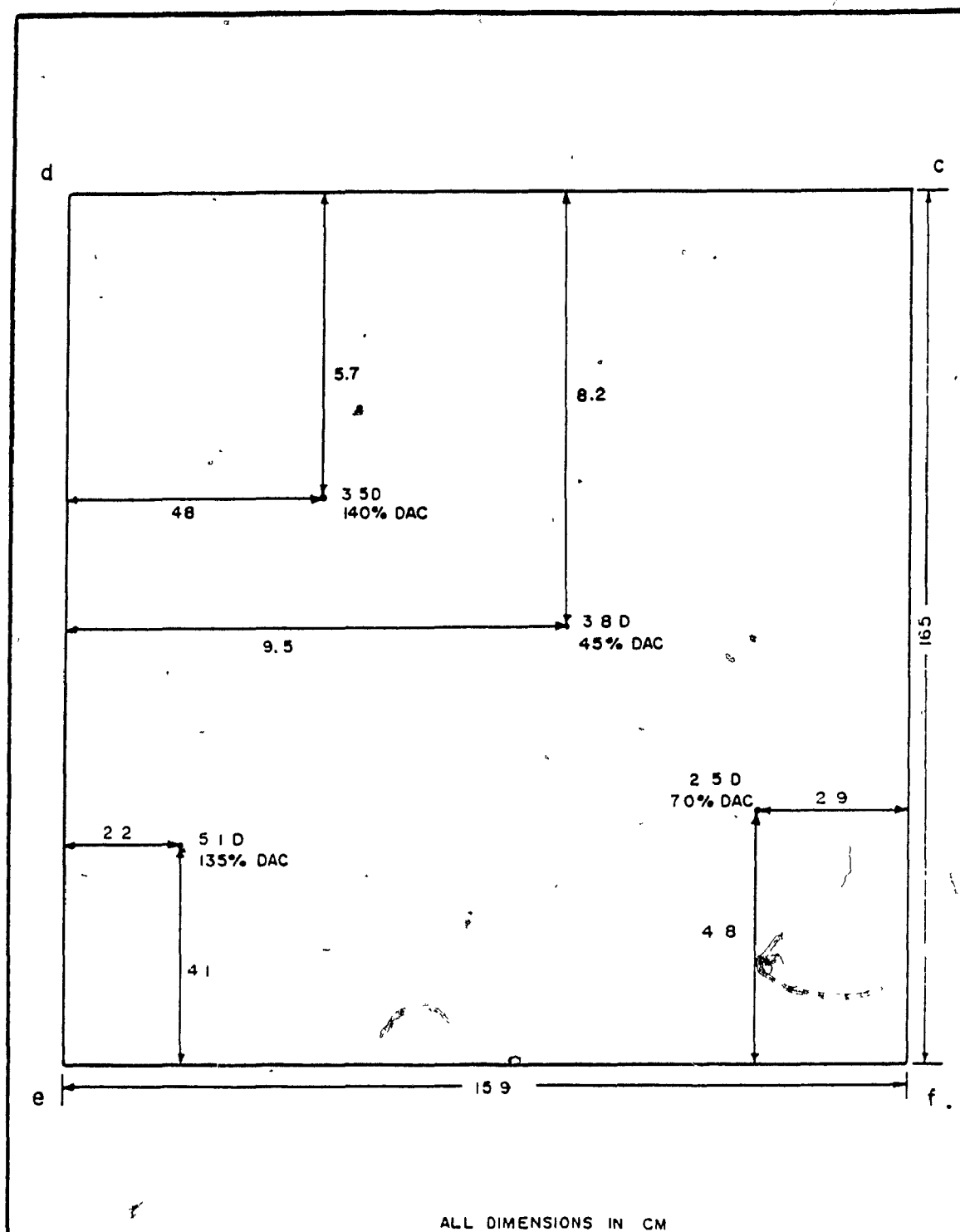
TECHNICIAN M ESKAMEL   DRAWN BY A KENDRICK

337

a   2 2   b

5.7   4 4   4 4   4.1

6 3D
55% DAC
3 8

5 7 D   8.6 D
150% DAC   75% DAC   4 1

1 3

3.8 D
25% DAC

140

7 3   3

06   6 0 D   3 5 D; 4 4 D, 6 0 D   6 7D
1 3   40% DAC   1 3   25% DAC   1 3   40%
                                                      DAC

d   1 4 0   c

ALL DIMENSIONS IN CM

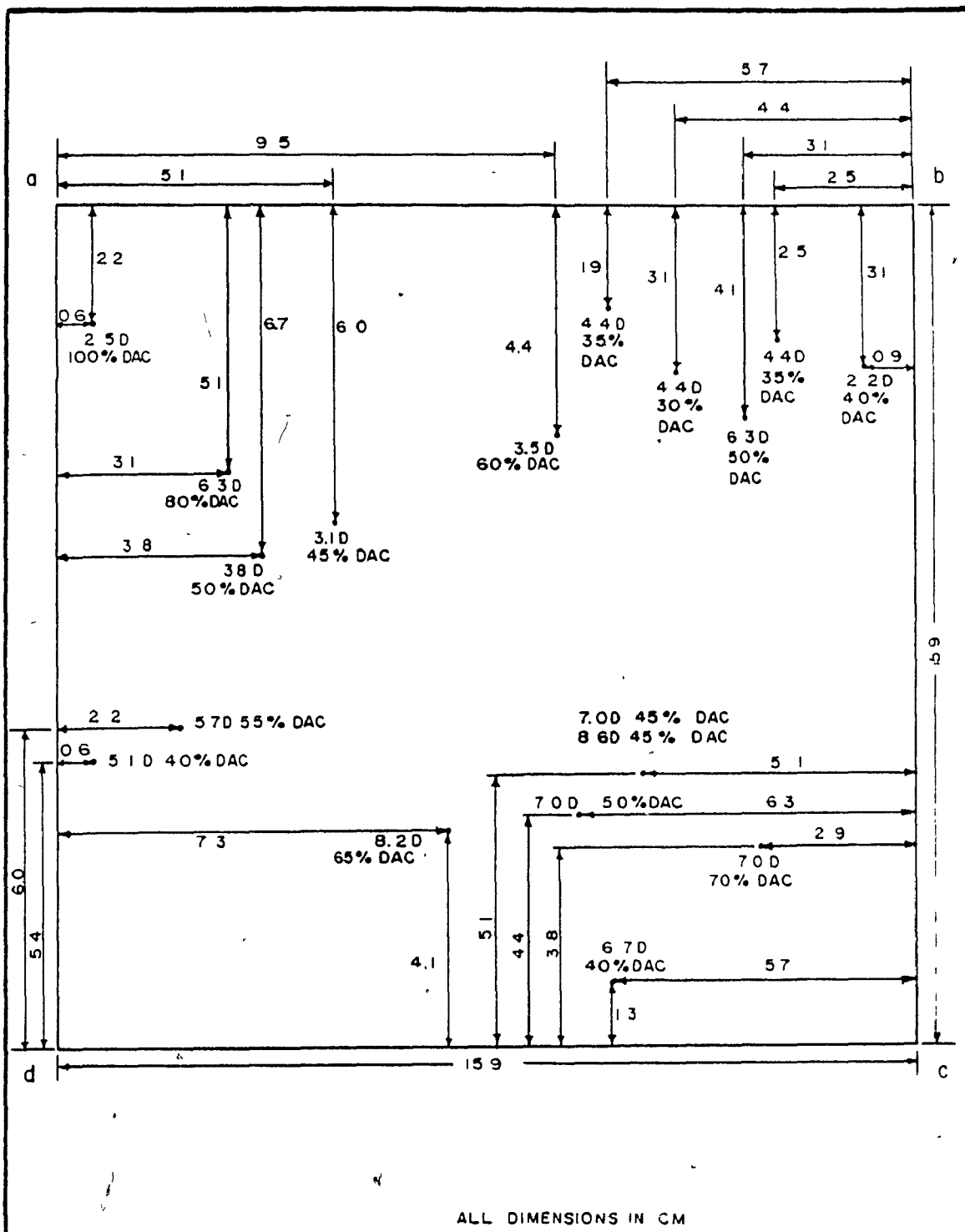| BLOCK NO. 42	FACE A	DATE SEPT 12, 1985
INSPECTION TECHNIQUE ASTM A 609-83 (⅛"⌀ FLAT BOTTOM HOLE)		
INSPECTION FIRM CRAWFORD McLEISH NDE INC		
TECHNICIAN M ESKAMEL DRAWN BY A KENDRICK		

8 6

c

b

54

7.3

9.2

6.7

6.0

2.2 D
120% DAC

4 1

3 8 D
30% DAC

6 3

3 8D 30%DAC
57D 50%DAC

6 0 D
150% DAC

48

6 3 D
50%DAC

3.5

3 8

6.0 D
120% DAC

76

4 4 D
40% DAC

3.5 D
150%DAC

6 0

54

3 2

57D
130% DAC

6 3

2 5

4 5

5 4

4 4 D
30% DAC

3.8D
25%DAC

5 7

1.6

1.3

16.5

f

g

14 0

ALL DIMENSIONS IN CM

BLOCK NO. 42	FACE B	DATE SEPT. 12, 1985
INSPECTION TECHNIQUE ASTM. A 609-83 (⅛"∅ FLAT BOTTOM HOLE)		
INSPECTION FIRM CRAWFORD McLEISH NDE INC		
TECHNICIAN M ESKAMEL DRAWN BY A KENDRICK		

339

ALL DIMENSIONS IN CM

BLOCK NO. 42	FACE C	DATE SEPT. 12, 1985
INSPECTION TECHNIQUE ASTM A 609-83 (⅛"ø FLAT BOTTOM HOLE)		
INSPECTION FIRM CRAWFORD McLEISH NDE INC		
TECHNICIAN M ESKAMEL DRAWN BY A KENDRICK		

340

ALL DIMENSIONS IN CM

| BLOCK NO. 43 | FACE A | DATE SEPT 12, 1985 |

INSPECTION TECHNIQUE ASTM A 609-83 (⅛"ø FLAT BOTTOM HOLE)

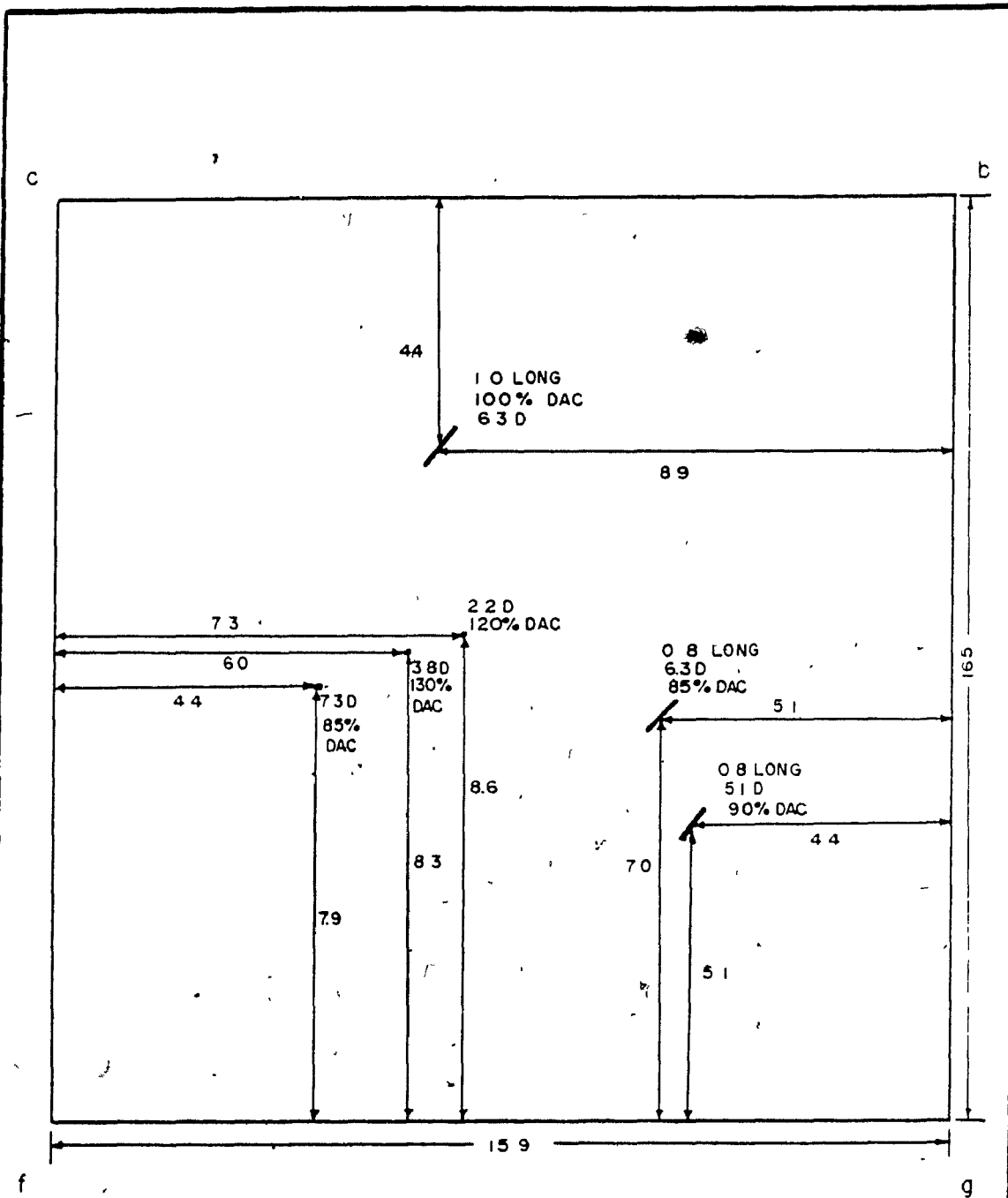INSPECTION FIRM CRAWFORD McLEISH NDE. INC

TECHNICIAN M ESKAMEL   DRAWN BY A KENDRICK

341

ALL DIMENSIONS IN CM

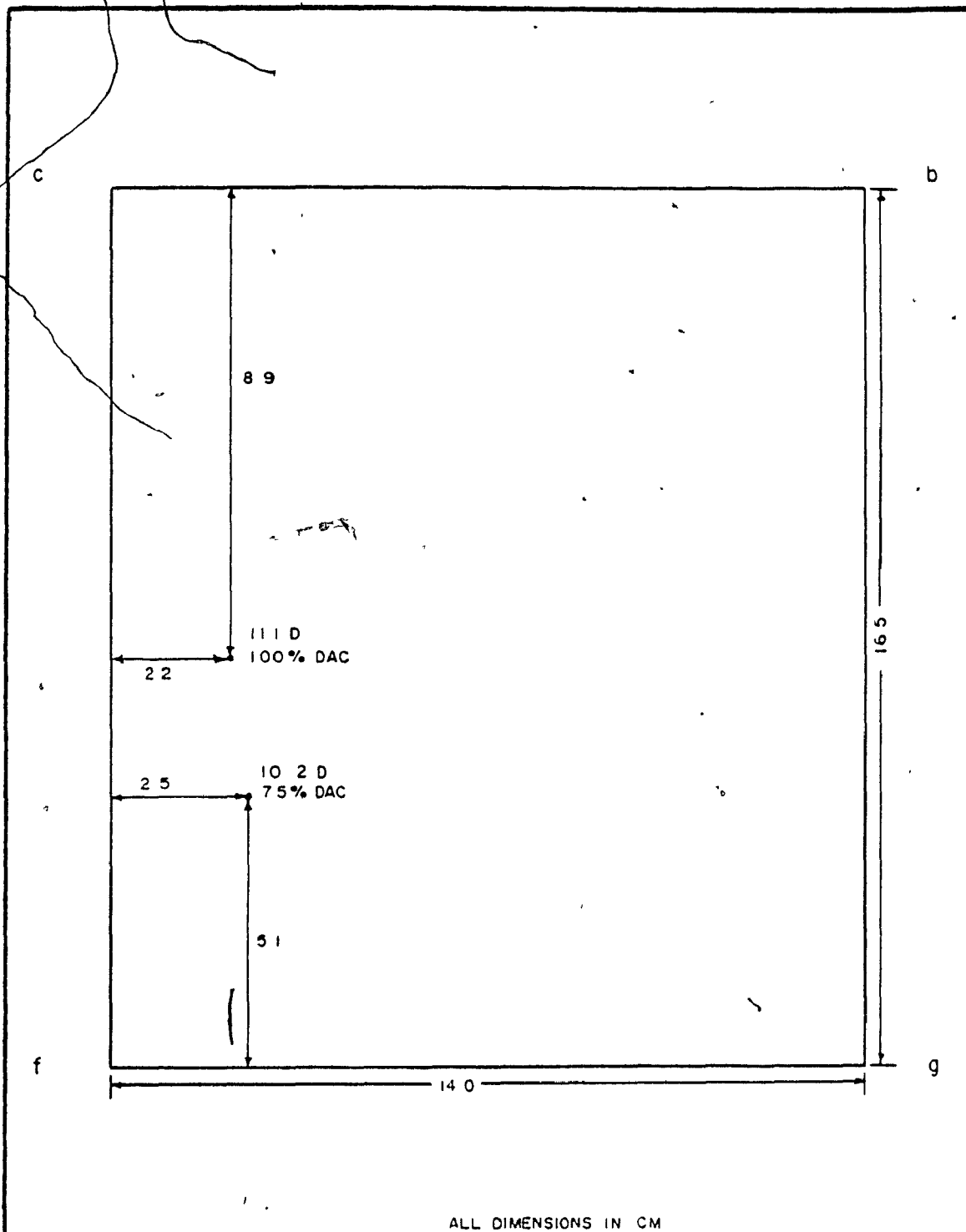| BLOCK NO. 43 | FACE B | DATE SEPT. 12, 1985 |

INSPECTION TECHNIQUE ASTM A 609-83 (⅛"ø FLAT BOTTOM HOLE)

INSPECTION FIRM CRAWFORD McLEISH NDE. INC

TECHNICIAN M ESKAMEL DRAWN BY A KENDRICK

ALL DIMENSIONS IN CM

BLOCK NO. 43	FACE C		DATE SEPT. 12, 1985	

INSPECTION TECHNIQUE ASTM A 609-83 (⅛"⌀ FLAT BOTTOM HOLE)

INSPECTION FIRM CRAWFORD McLEISH NDE INC
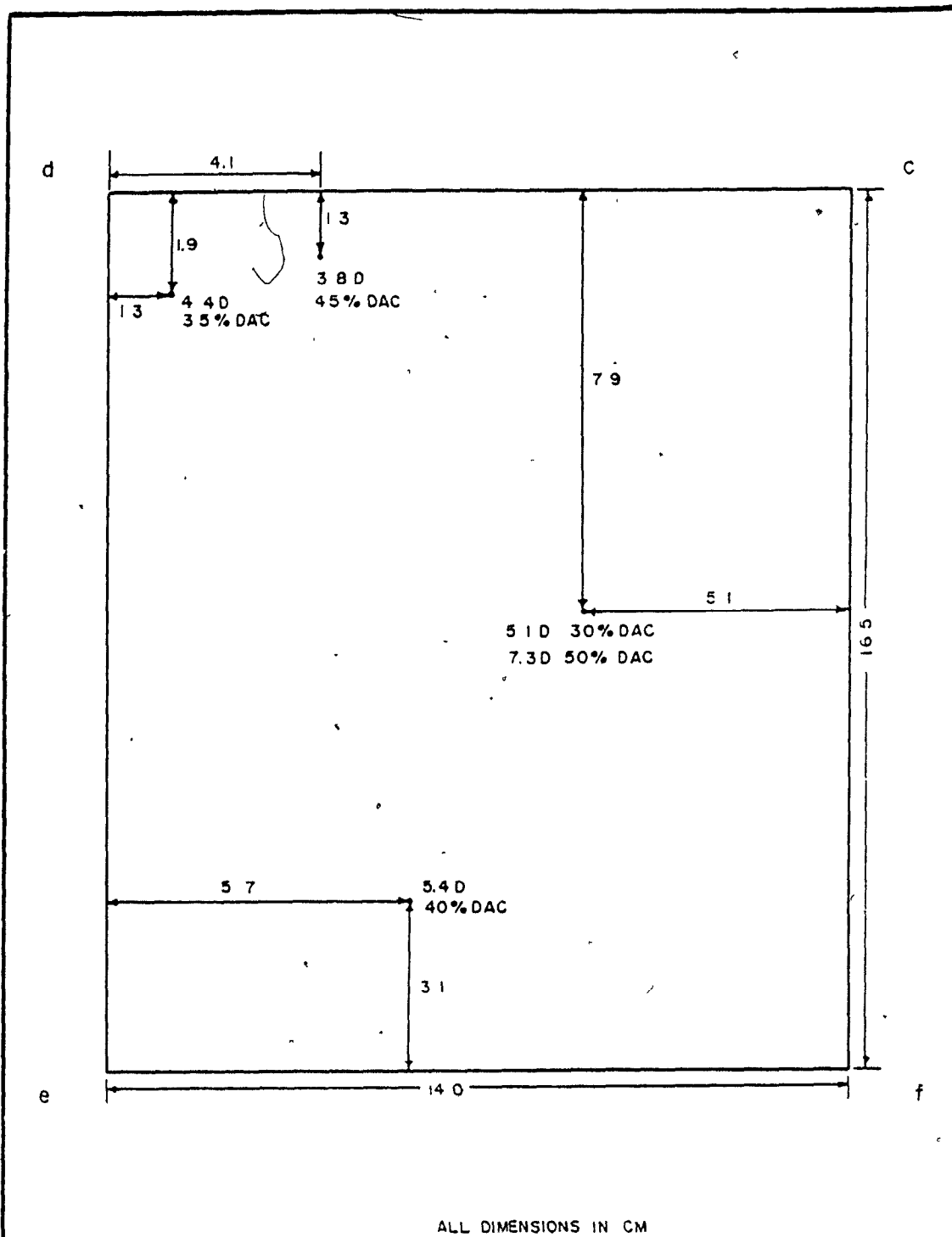
TECHNICIAN M ESKAMEL DRAWN BY A KENDRICK

ALL DIMENSIONS IN CM

| BLOCK NO. 44 | FACE A | DATE SEPT. 12, 1985 |

INSPECTION TECHNIQUE ASTM A 609-83 (⅛"∅ FLAT BOTTOM HOLE)

INSPECTION FIRM CRAWFORD McLEISH NDE INC

TECHNICIAN M ESKAMEL DRAWN BY A KENDRICK

344

c · b

44

I O LONG
100% DAC
6 3 D

8 9

165

7 3
60
44

2 2 D
120% DAC

3 8 D
130%
DAC

7 3 D
85%
DAC

O 8 LONG
6.3 D
85% DAC

51

8.6

O 8 LONG
51 D
90% DAC

8 3

4 4

7.9

70

51

f · g

15 9

ALL DIMENSIONS IN CM

BLOCK NO. 44	FACE B	DATE SEPT 12, 1985

INSPECTION TECHNIQUE ASTM A 609-83 (⅛"⌀ FLAT BOTTOM HOLE)

INSPECTION FIRM: CRAWFORD McLEISH NDE INC
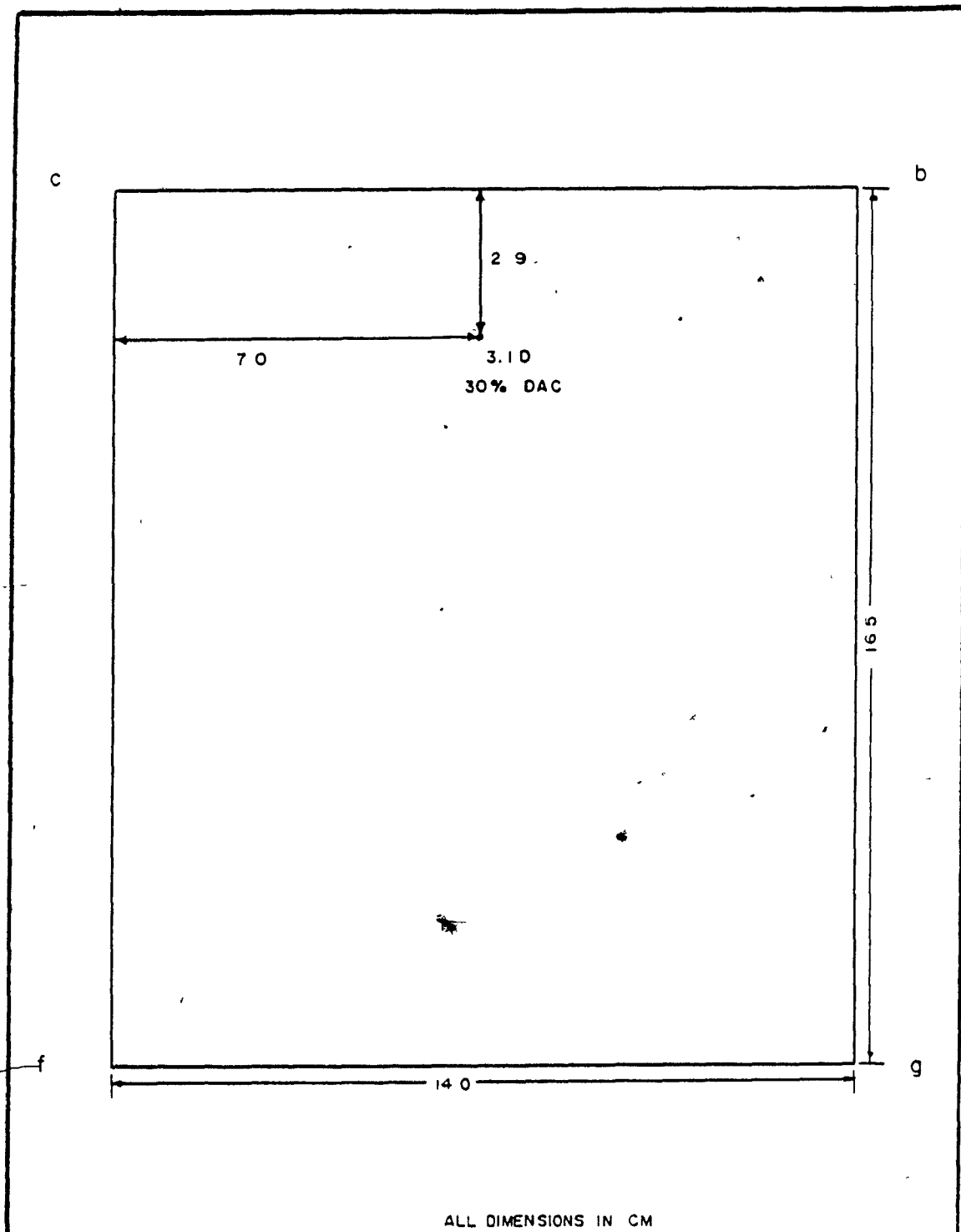
TECHNICIAN M ESKAMEL DRAWN BY A KENDRICK
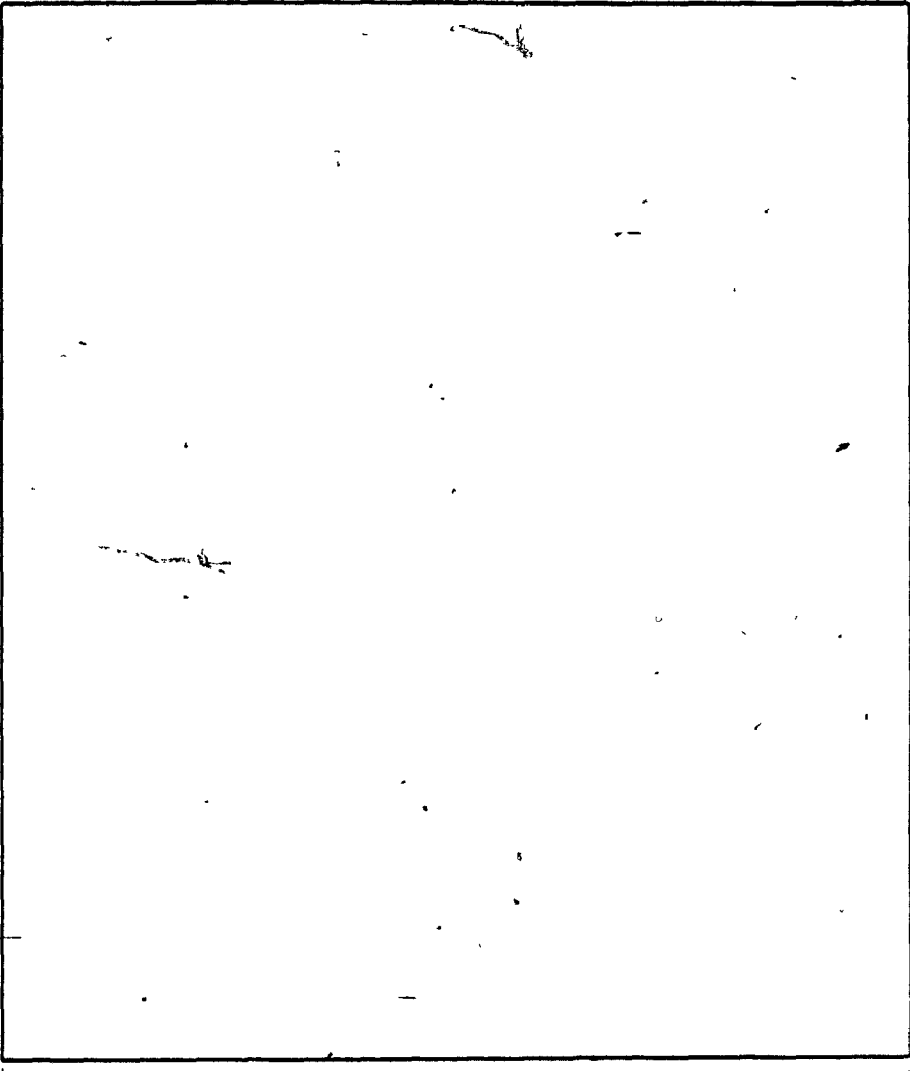
345

ALL DIMENSIONS IN CM

| BLOCK NO. 44 | FACE C | DATE SEPT. 12, 1985 |

INSPECTION TECHNIQUE ASTM A 609-83 (⅛"∅ FLAT BOTTOM HOLE)

INSPECTION FIRM CRAWFORD McLEISH NDE INC

TECHNICIAN M ESKAMEL DRAWN BY A KENDRICK

a

60

b

25

38

19

3.8D
50%DAC

16

6.3

4.4 D
70% DAC

67

3.8

51D
45% DAC

13

70D
60%DAC

6 3

5 7

8 9

29

4 4D
50%DAC

29

3.5 D
50% DAC

79D
40% DAC

51

140

29

06

35D
30% DAC

19

2 5D
30% DAC

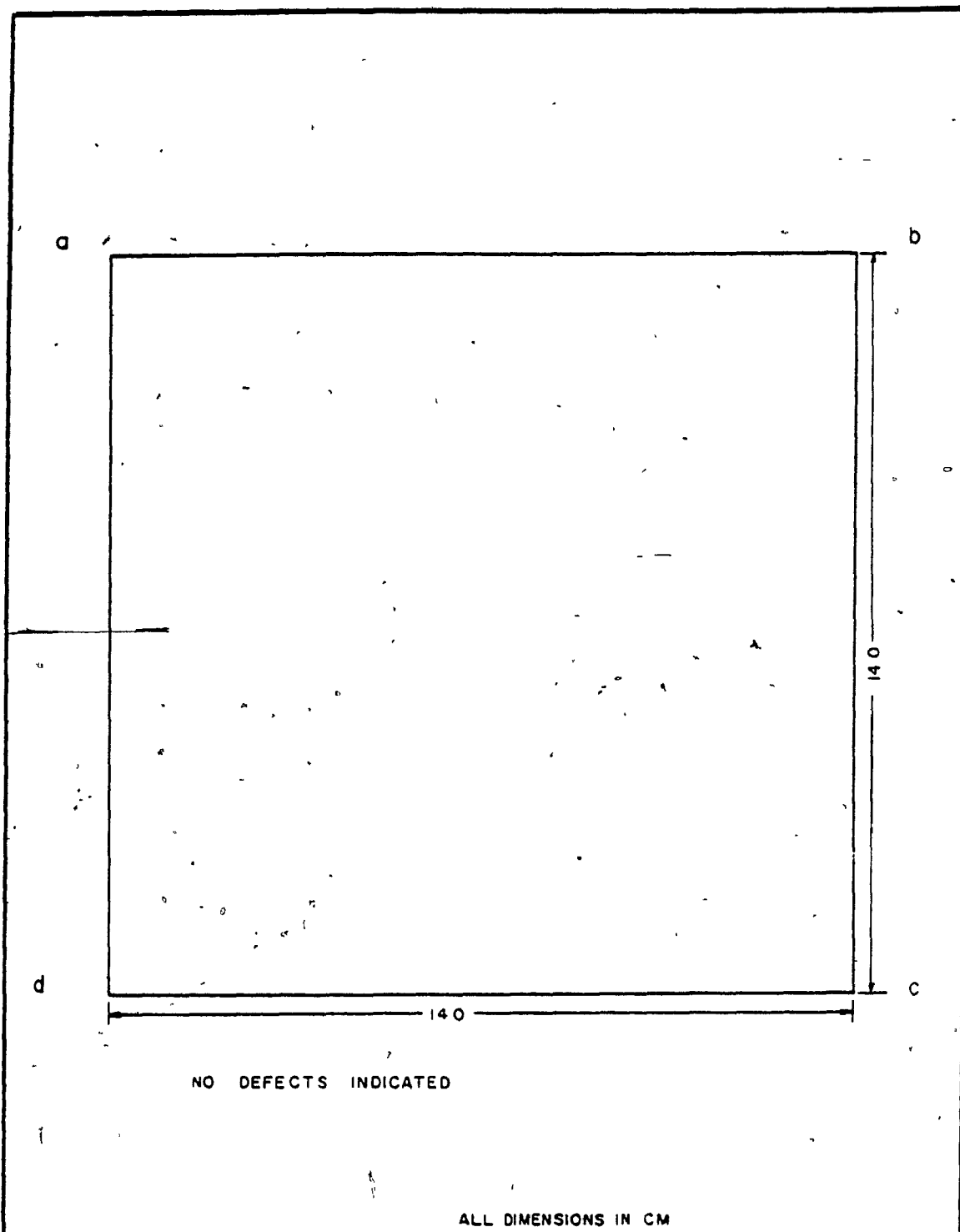19

13

d

140

c

ALL DIMENSIONS IN CM

| BLOCK NO. 61 | FACE A | DATE SEPT. 12, 1985 |

INSPECTION TECHNIQUE ASTM A 609-83 (⅛"∅ FLAT BOTTOM HOLE)

INSPECTION FIRM CRAWFORD McLEISH NDE INC

TECHNICIAN M ESKAMEL DRAWN BY A KENDRICK

347

ALL DIMENSIONS IN CM

BLOCK NO. 61	FACE B	DATE SEPT 12, 1985	

INSPECTION TECHNIQUE ASTM A 609-83 (⅛"∅ FLAT BOTTOM HOLE)

INSPECTION FIRM CRAWFORD McLEISH NDE INC

TECHNICIAN M ESKAMEL DRAWN BY A KENDRICK

348

ALL DIMENSIONS IN CM

BLOCK NO. 61	FACE C	DATE SEPT. 12, 1985

INSPECTION TECHNIQUE ASTM A 609-83 (⅛"∅ FLAT BOTTOM HOLE)

INSPECTION FIRM CRAWFORD·McLEISH NDE INC
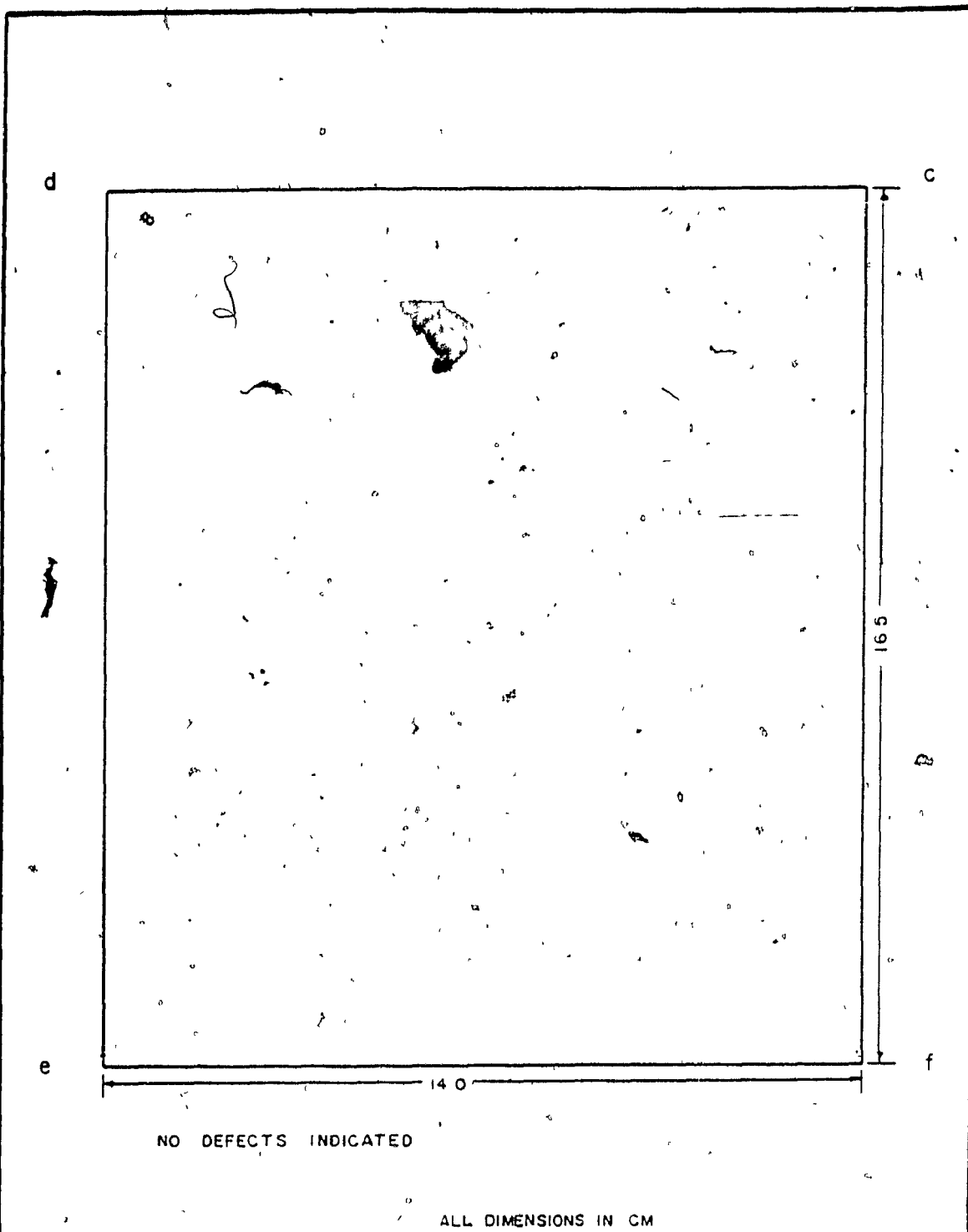
TECHNICIAN M ESKAMEL DRAWN BY A KENDRICK
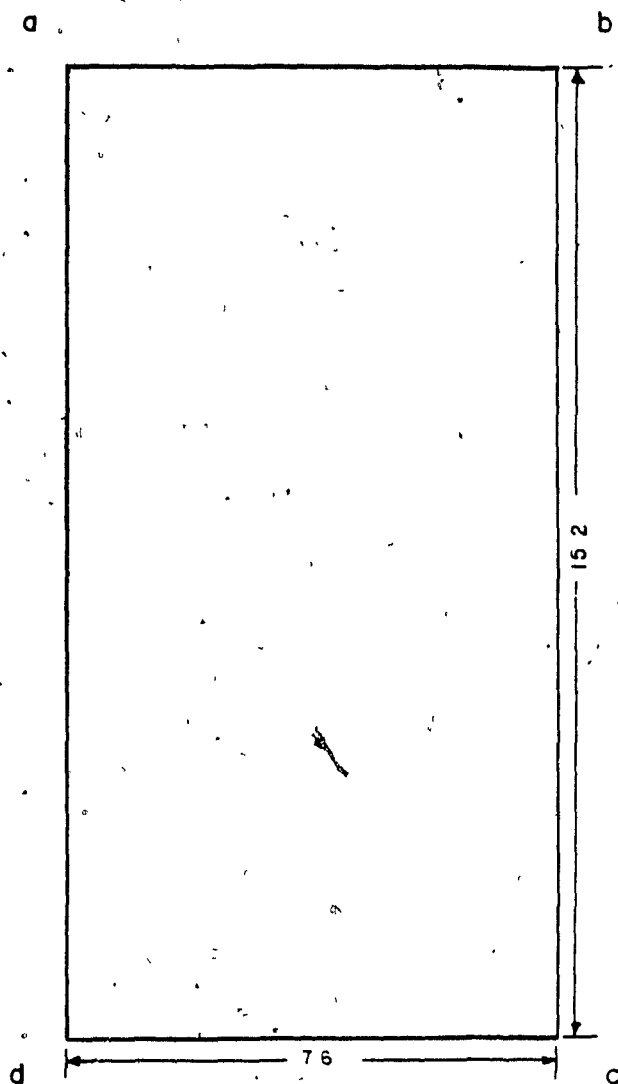
NO DEFECTS INDICATED

ALL DIMENSIONS IN CM

BLOCK NO. 62	FACE A	DATE SEPT 12, 1985

INSPECTION TECHNIQUE ASTM A 609-83 (⅛"ø FLAT BOTTOM HOLE)

INSPECTION FIRM CRAWFORD McLEISH NDE. INC

TECHNICIAN M ESKAMEL   DRAWN BY A KENDRICK

350

2 9

7 0   3.1 0

30% DAC

c

b

165

f

140

g

ALL DIMENSIONS IN CM

BLOCK NO. 62   FACE B   DATE SEPT. 12, 1985

INSPECTION TECHNIQUE ASTM A 609-83 (⅛"ø FLAT BOTTOM HOLE)

INSPECTION FIRM CRAWFORD McLEISH NDE INC

TECHNICIAN M ESKAMEL   DRAWN BY A KENDRICK

d ⌐ c

|←———————— 14 0 ————————→| (e to f)

16 5 (c to f)

e └ f

NO DEFECTS INDICATED

ALL DIMENSIONS IN CM

BLOCK NO. 62 FACE C	DATE SEPT 12, 1985

INSPECTION TECHNIQUE ASTM A 609-83 (⅛"ø FLAT BOTTOM HOLE)

INSPECTION FIRM CRAWFORD McLEISH NDE INC

TECHNICIAN M ESKAMEL DRAWN BY A KENDRICK

NO DEFECTS INDICATED

ALL DIMENSIONS IN CM

BLOCK NO. 63 FACE A	DATE SEPT 12, 1985

INSPECTION TECHNIQUE ASTM A 609-83 (⅛" FLAT BOTTOM HOLE)

INSPECTION FIRM CRAWFORD McLEISH NDE INC
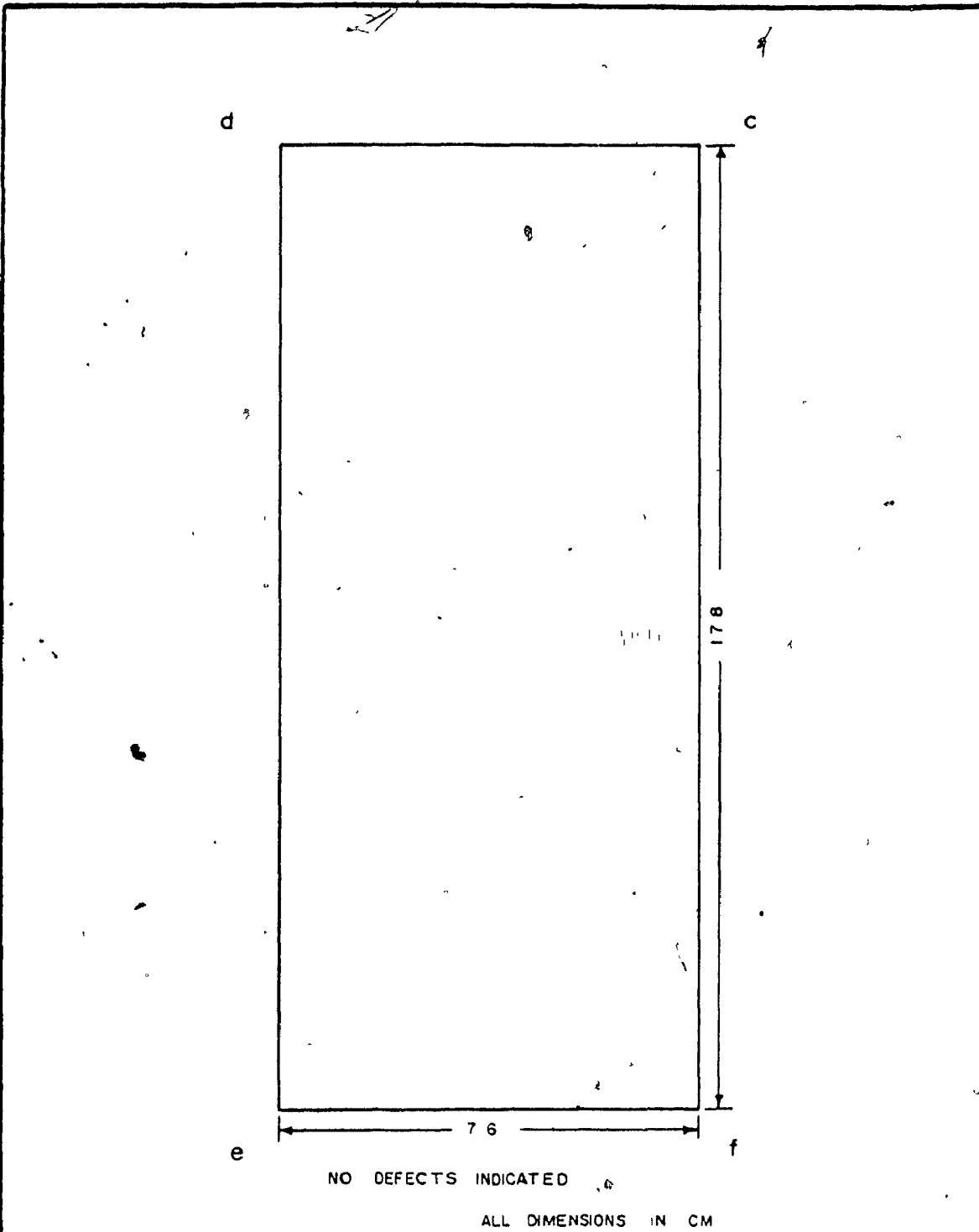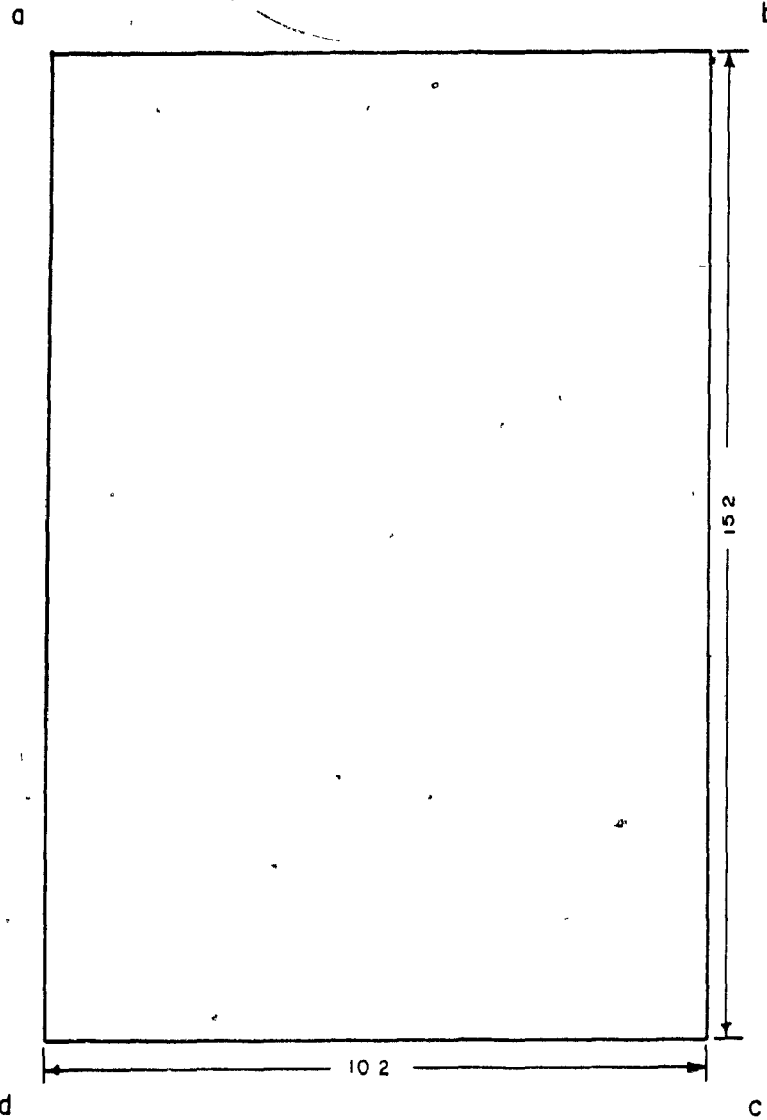
TECHNICIAN M. ESKAMEL   DRAWN BY A KENDRICK

c   b

165

f   g

14 0

NO DEFECTS INDICATED

ALL DIMENSIONS IN CM.

BLOCK NO. 63	FACE B	DATE SEPT. 12, 1985

INSPECTION TECHNIQUE ASTM A 609-83 (⅛"ø FLAT BOTTOM HOLE)

INSPECTION FIRM CRAWFORD McLEISH NDE. INC.

TECHNICIAN M ESKAMEL DRAWN BY A KENDRICK

354

NO DEFECTS INDICATED

ALL DIMENSIONS IN CM

BLOCK NO. 63	FACE C	DATE SEPT 12, 1985

INSPECTION TECHNIQUE ASTM A 609-83 (⅛"∅ FLAT BOTTOM HOLE)

INSPECTION FIRM CRAWFORD McLEISH NDE INC

TECHNICIAN M. ESKAMEL   DRAWN BY A KENDRICK

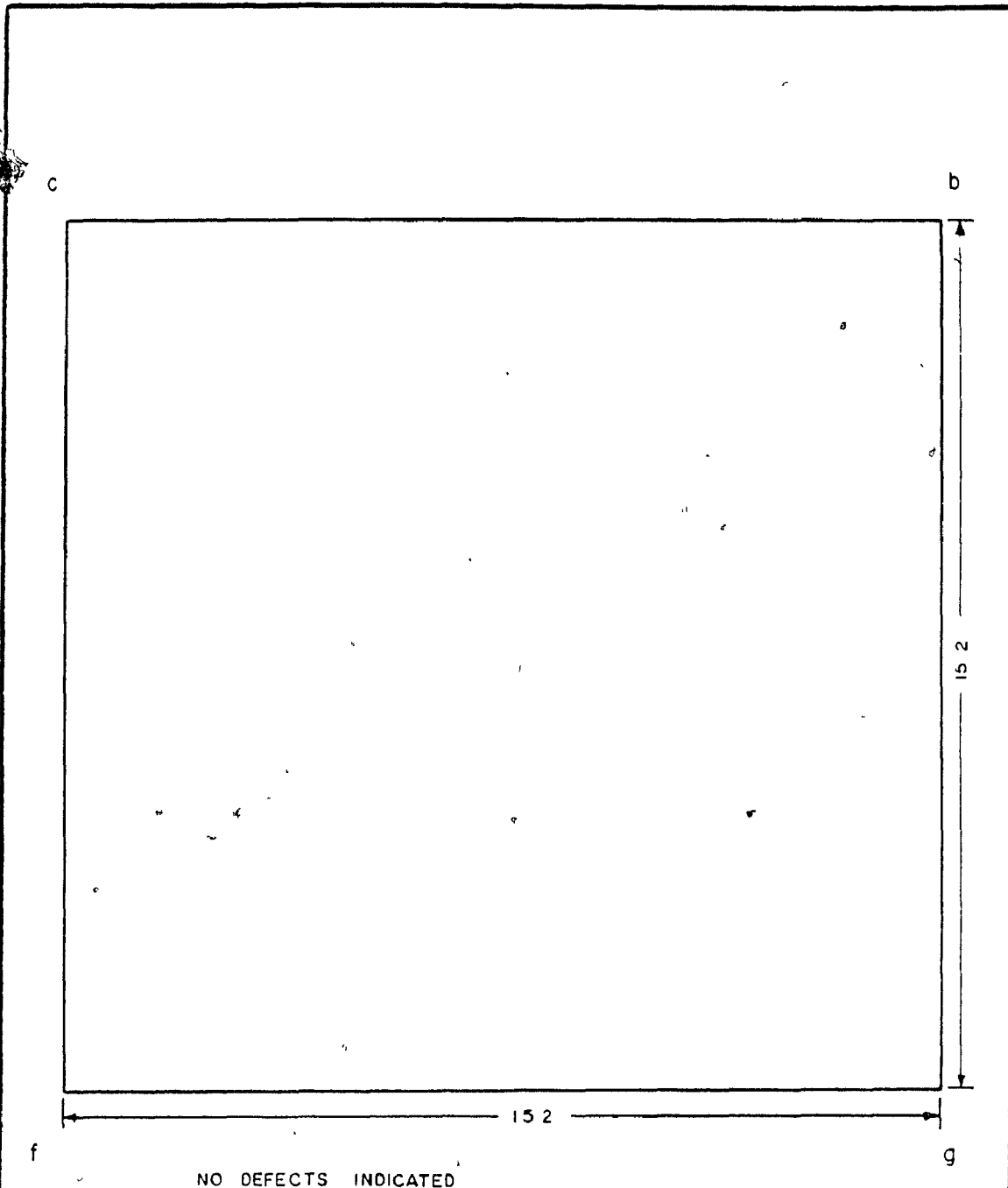355

NO DEFECTS INDICATED

ALL DIMENSIONS IN CM

BLOCK NO. 64	FACE A	DATE SEPT. 12, 1985

INSPECTION TECHNIQUE ASTM A 609-83 (⅛"∅ FLAT BOTTOM HOLE)

INSPECTION FIRM CRAWFORD McLEISH NDE INC

TECHNICIAN M ESKAMEL DRAWN BY A KENDRICK

NO DEFECTS INDICATED

ALL DIMENSIONS IN CM

| BLOCK NO. 64 | FACE B | DATE SEPT 12, 1985 |

INSPECTION TECHNIQUE ASTM A 609-83 (⅛"ø FLAT BOTTOM HOLE)

INSPECTION FIRM CRAWFORD McLEISH NDE INC

TECHNICIAN M ESKAMEL   DRAWN BY A KENDRICK

357

NO DEFECTS INDICATED

ALL DIMENSIONS IN CM
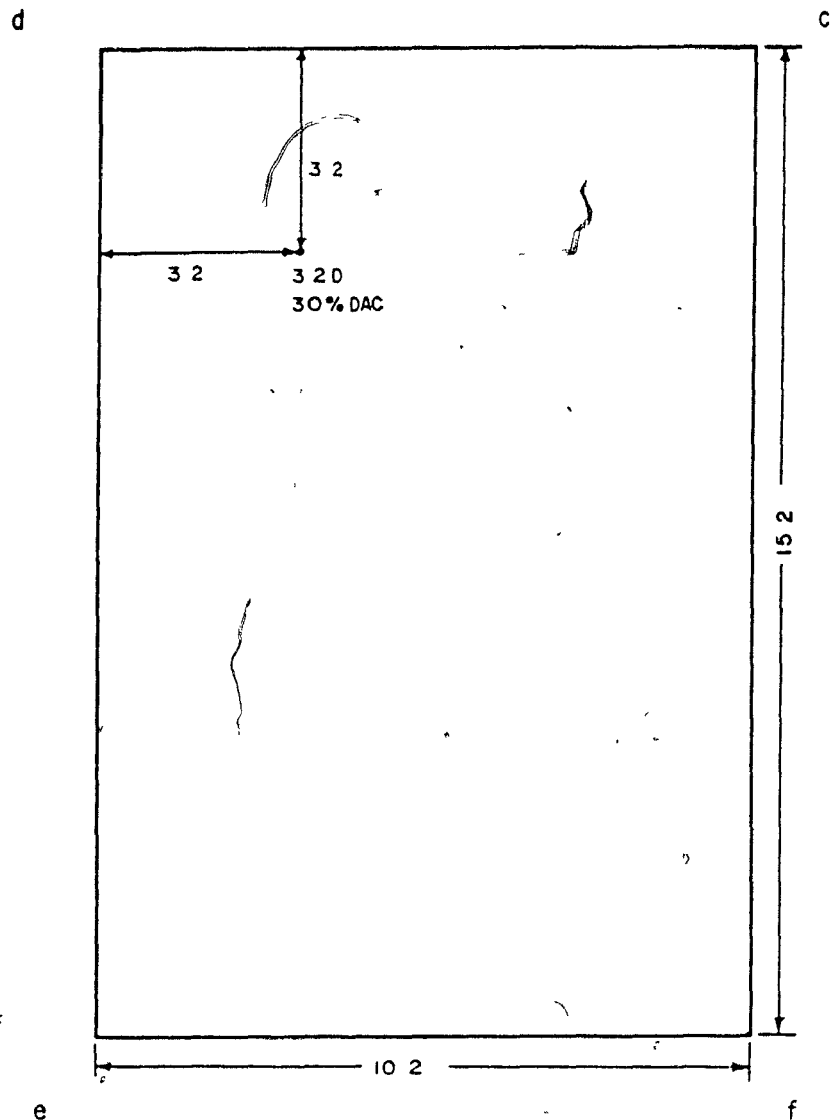
BLOCK NO 64	FACE C	DATE SEPT. 12, 1985

INSPECTION TECHNIQUE ASTM A 609-83 (⅛"⌀ FLAT BOTTOM HOLE)

INSPECTION FIRM CRAWFORD McLEISH NDE INC

TECHNICIAN M ESKAMEL   DRAWN BY A KENDRICK

a   b

152

102

d   c

NO DEFECTS INDICATED

ALL DIMENSIONS N CM

| BLOCK NO. 66 FACE A DATE SEPT. 12,1985 |
| INSPECTION TECHNIQUE ASTM A 609-83 ($\frac{1}{8}$"ø FLAT BOTTOM HOLE) |
| INSPECTION FIRM CRAWFORD McLEISH NDE. INC |
| TECHNICIAN M ESKAMEL DRAWN BY A KENDRICK |

c   b

a

d

15 2

15 2

f   g

NO DEFECTS INDICATED

ALL DIMENSIONS N CM

BLOCK NO. 66   FACE B   DATE SEPT 12, 1985
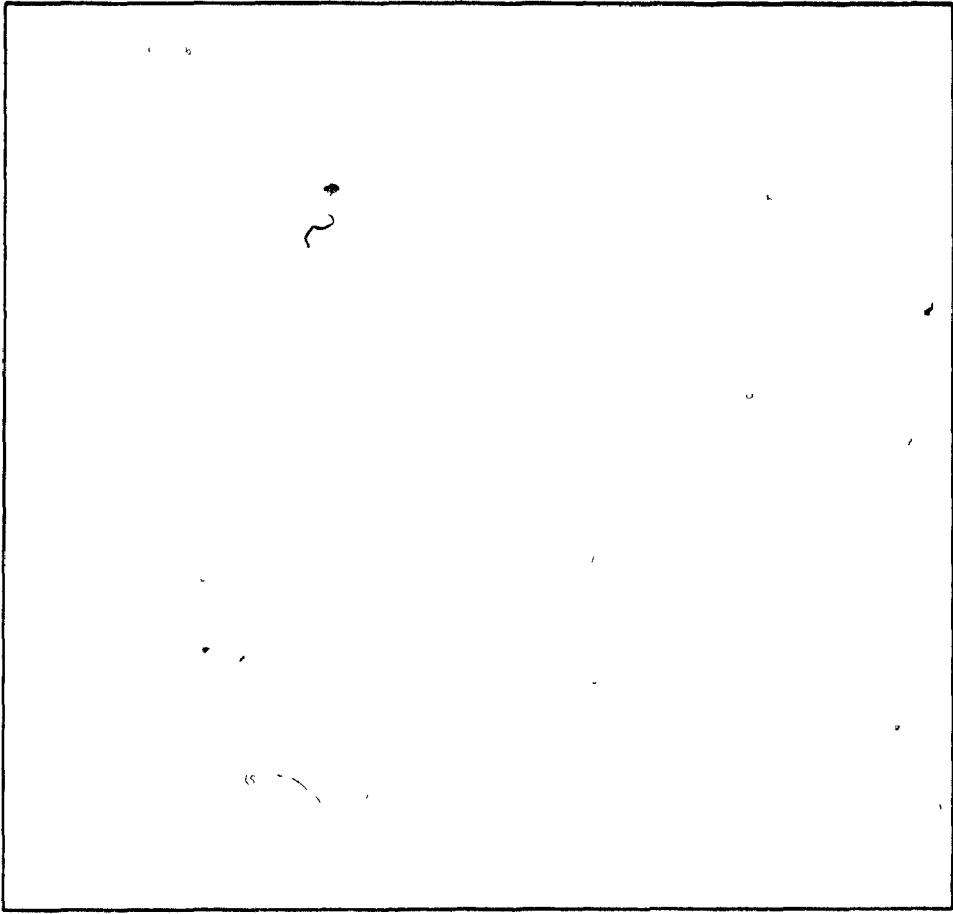
INSPECTION TECHNIQUE ASTM A 609-83 (⅛"∅FLAT BOTTOM HOLE)

INSPECTION FIRM CRAWFORD McLEISH NDE INC
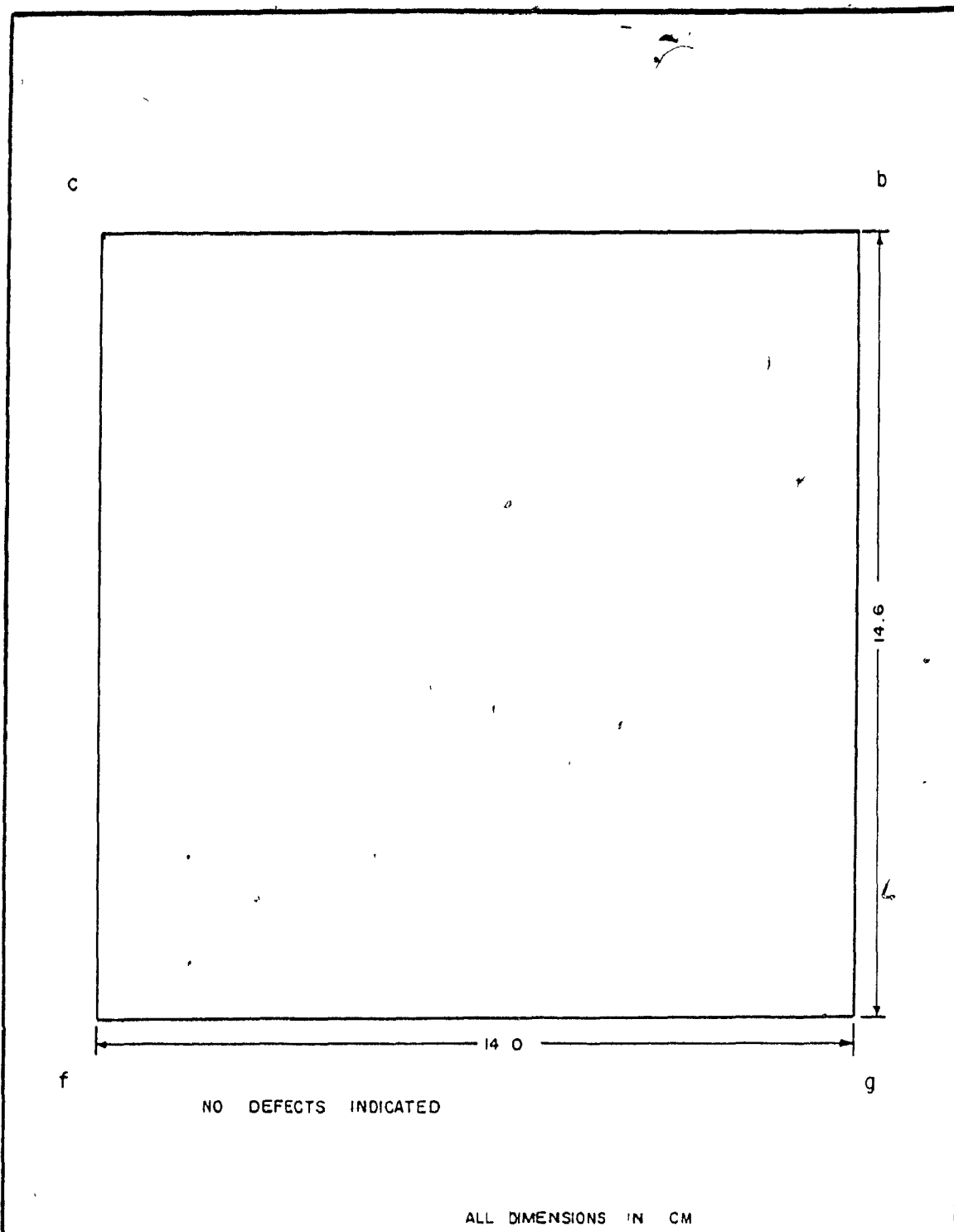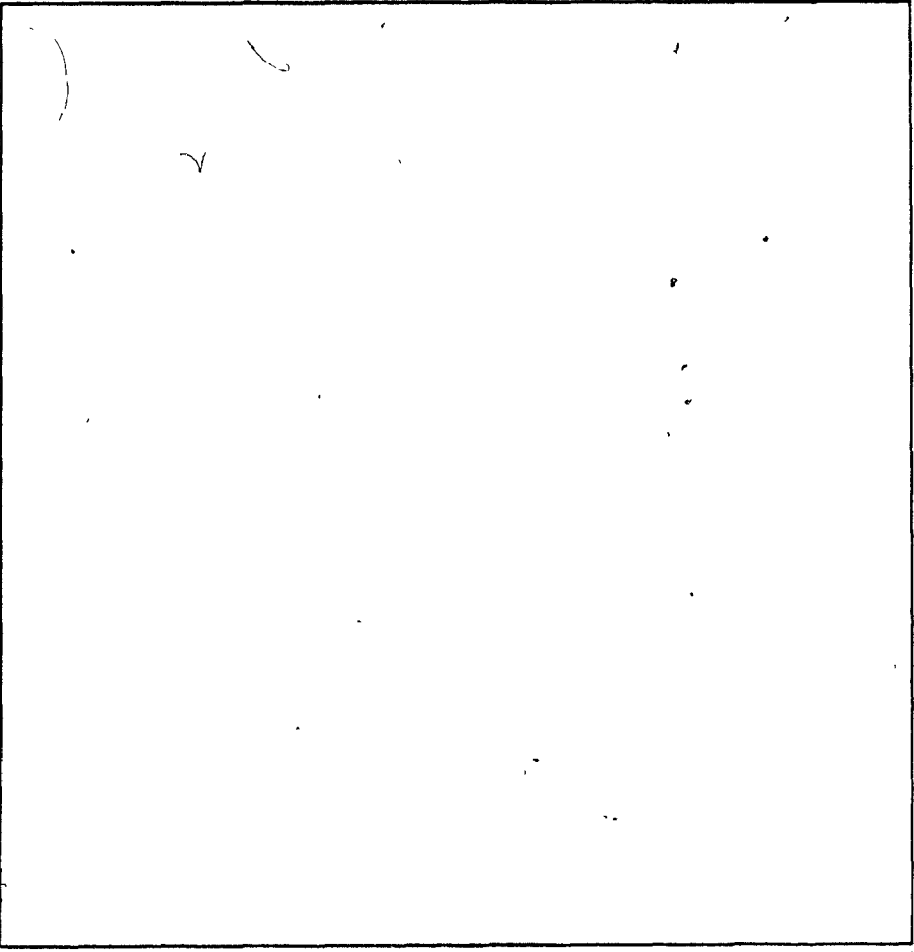
TECHNICIAN M ESKAMEL   DRAWN BY A KENDRICK

d

c

3 2

3 2

3 2 D
30% DAC

15 2

10 2

e

f

ALL DIMENSIONS IN CM

| BLOCK NO. 66 | FACE C | DATE SEPT 12, 1985 |

INSPECTION TECHNIQUE ASTM A 609-83 (⅛"ø FLAT BOTTOM HOLE)

INSPECTION FIRM CRAWFORD McLEISH NDE INC

TECHNICIAN M ESKAMEL DRAWN BY A KENDRICK

361

NO DEFECTS INDICATED

ALL DIMENSIONS IN CM

BLOCK NO. 67	FACE A	DATE SEPT. 12, 1985

INSPECTION TECHNIQUE ASTM A 609-83 ($\frac{1}{8}$"ø FLAT BOTTOM HOLE)

INSPECTION FIRM CRAWFORD McLEISH NDE INC

TECHNICIAN M ESKAMEL DRAWN BY A KENDRICK

c   b

14.6

14 0

f   g

NO   DEFECTS   INDICATED

ALL DIMENSIONS IN   CM

BLOCK NO. 67   FACE B   DATE   SEPT. 12, 1985

INSPECTION   TECHNIQUE   ASTM A 609-83 (1/8"ø FLAT BOTTOM HOLE)

INSPECTION   FIRM   CRAWFORD McLEISH   NDE. INC

TECHNICIAN M ESKAMEL   DRAWN BY   A KENDRICK

363

d   c
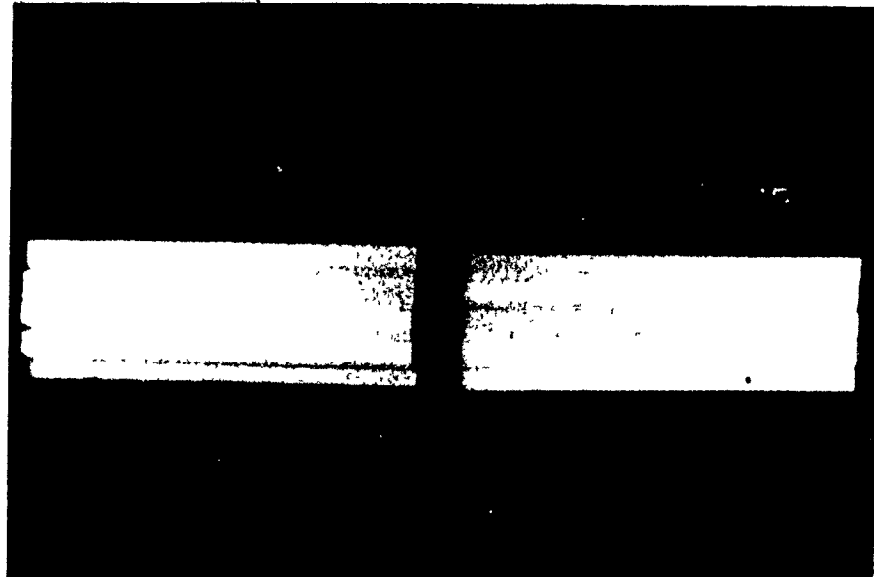
```
                                                        |
                                                        |
                                                       14 6
                                                        |
                                                        |
```

|← 14 6 →|

e   f

NO   DEFECTS   INDICATED

ALL   DIMENSIONS   N   CM

BLOCK NO. 67   FACE   C   DATE   SEPT 12, 1985

INSPECTION   TECHNIQUE   ASTM A 609-83   (⅛"ø FLAT BOTTOM HOLE)

INSPECTION FIRM   CRAWFORD McLEISH NDE. INC

TECHNICIAN M ESKAMEL   DRAWN BY   A KENDRICK

364

FRACTURE SPECIMEN RADIOGRAPHIC INSPECTION RESULTS

Fig. H.1 Direction 1 X-ray results of
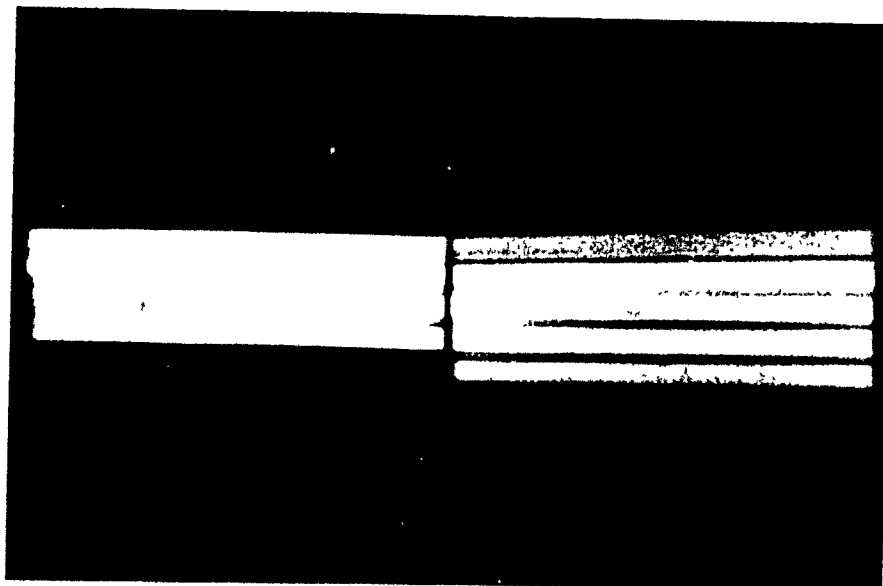type A fracture specimens.

Fig. H.2 Direction 2 X-ray results of
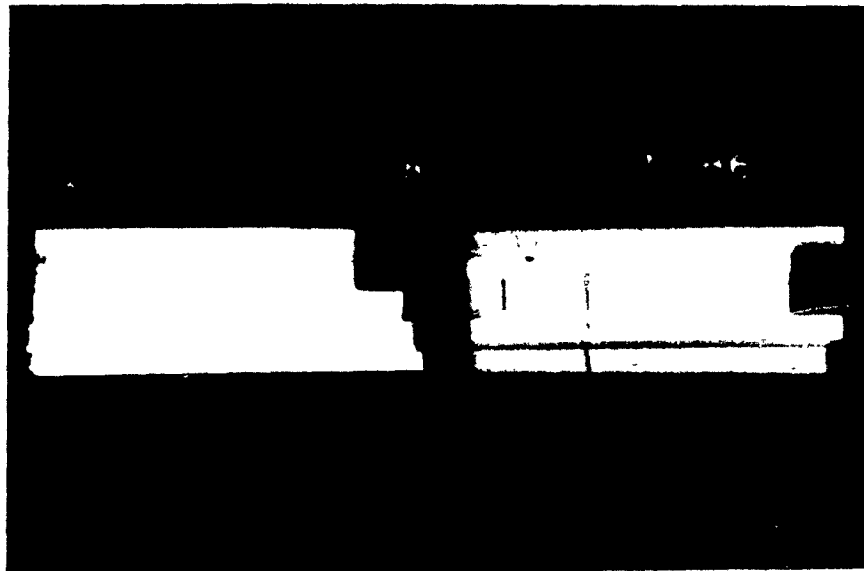Type A fracture specimens.

365

Fig. H.3   Direction 1 X-ray results of
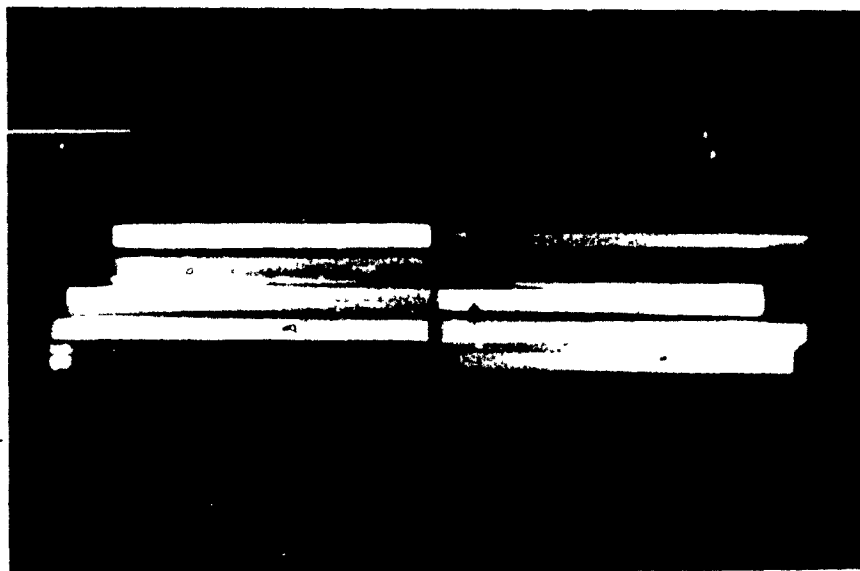type B fracture specimens.

Fig. H.4   Direction 2 X-ray results of
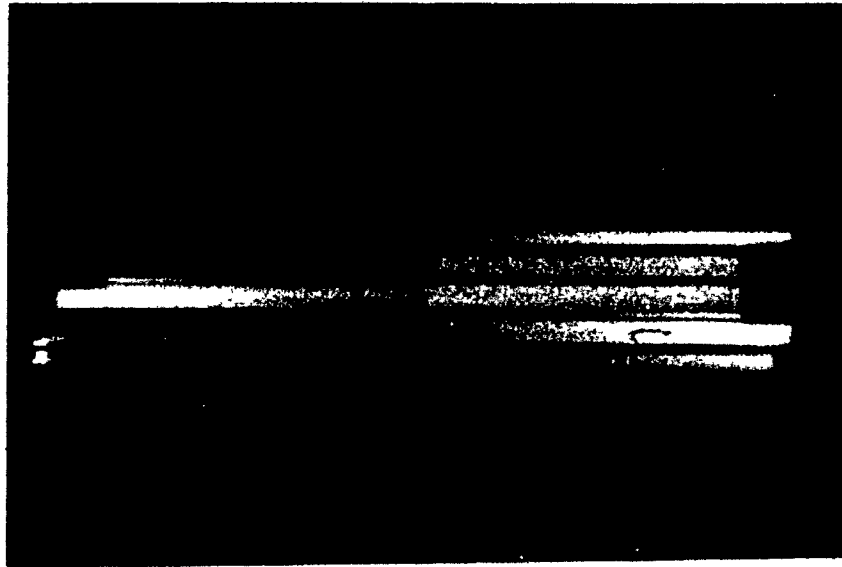type B fracture specimens.

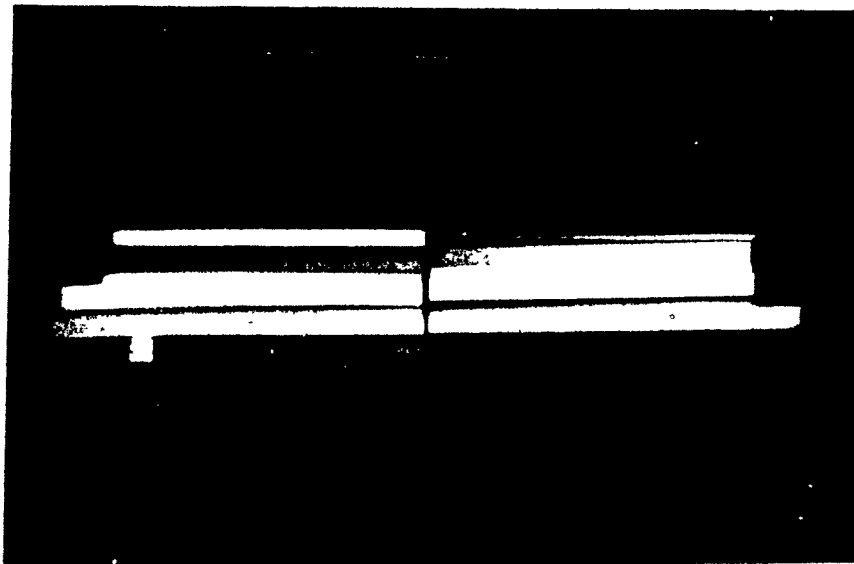Fig. H.5 Direction 1 X-ray results of
type C fracture specimens.

Fig. H.6 Direction 2 X-ray results of
type C fracture specimens